

Barium Sulphate Surface Deposition Kinetics and Inhibition in Dynamic Flow Systems

Benissa Mohamed Ali Tolaieb

Submitted in accordance with the requirements for the degree of
Doctor of Philosophy

The University of Leeds
Institute of Engineering, Thermofluids, Surfaces and Interfaces
School of Mechanical Engineering

July, 2014

The candidate confirms that the work submitted is his own. The contribution of the candidate and the other authors to this work has been explicitly indicated below. The candidate confirms that appropriate credit has been given within the thesis where reference has been made to the work of others.

In all the papers and presentations listed below, the primary author completed all the experimental data, paper drafting and presentation slide. All authors contributed to proof reading of the papers and presentation with advised before publication and presentation.

This copy has been supplied on the understanding that it is copyright material and that no quotation from the thesis may be published without proper acknowledgement.

© 2014 The University of Leeds and Benissa Mohamed Ali Tolaieb.

THESIS RELATED PUBLICATIONS AND PRESENTATIONS

Conference Papers:

Benissa Tolaieb, Ruth Bingham, Anne Neville. *Barium Sulphate Kinetics on Steel Surfaces at Different Supersaturation Ratios*. 2013, NACE International 2751, 17-21 March 2013.

Journal Papers:

Benissa Tolaieb, Eleftheria Mavredaki, Anne Neville. *The role of barium content on surface crystallization from oilfield real brine at 75 °C*, Journal of Petroleum Science and Engineering, submitted.

Oral Presentation:

Benissa Tolaieb, Anne Neville, *Barium Sulphate Formation in Bulk Phase and in a Modified Capillary Tube - Surface Kinetic Assessments*. 2011, Eurocorr international, Stockholm, Sweden.

Poster Presentation

Benissa Tolaieb, Anne Neville, Poster presentation at the Royal Academy of Engineering (RAE), May 2010, Sheffield, UK.

DEDICATION

I dedicate this work in loving memory of my father Mohamed Ali Tolaieb who left us and rest in heaven eighteen years ago. I also dedicate it to my mother Fatima Nouah who is waiting for me to finish, and my wife Amna Ahmad and my sons Mohamed, Mahir, and Motaz and also my daughters Fatima, Fattin and Farah who encourage and support me in this work from the beginning and I am proud to have my great lovely family. I here extend my dedication to my older brothers Abdusalam and Ali Tolaieb as well as my nephew Mohamed Tolaieb and my sister Khadija Tolaieb.

ACKNOWLEDGEMENTS

I would like to thank my Almighty God for being with me in every successful step I make and through my health hardship. I would like to thank my unique academic supervisor, Professor Anne Neville for all her continuous support, encouragement, advice, guidance endurance and moral boost throughout this studies. I really do appreciate all her effort, that without it, I would not be at this stage. Thank you a lot Professor Anne. I would like to extend this acknowledgment to the Libyan Higher Education, specifically the University of Sebha for giving me this chance to finish my doctorate degree.

I here thank my research group mate Benjamin Pickles for his help with proof reading and all the group members who supported me throughout this work.

ABSTRACT

This research work focuses on scale kinetics in real field complex brines using two complementary laboratory techniques; static bulk precipitation tests and dynamic surface deposition capillary cell tests. All experimental results are backed up by theoretical scale predictions.

This study focuses on the barium sulphate system in complex solutions. It explores the effect of temperature (25 °C, 50 °C and 75 °C), and the resulting saturation ratio (SR) of barium species active concentration on the barium sulphate formation. The effect involves both static bulk precipitation and surface deposition using a dynamic flow system.

This work systematically shows that the predicted saturation ratios, at different temperatures, do not seem to control the surface crystallization in a barium sulphate system once heat is applied. At room temperature, the saturation ratio was predicted to be the highest while the observed bulk and surface induction periods are largest. On the other hand, at 75 °C when the saturation ratio was predicted to be the lowest, the observed bulk and surface crystallization induction periods were shortest. The surface morphology of scale crystals is also affected by the saturation ratios resulting from temperature differences rather than the smaller differences in SR due to mixing ratios within each temperature applied.

The novelty of this research work is primarily around the detailed investigation of the surface nucleation/scaling period, and the mechanism of growth. In addition, the barite/scale surface kinetic investigations supported by thermodynamic theoretical calculations and static bulk tests to explain surface kinetics.

The advantage of this setup facilitates a uniform development of scale thickness along a test capillary with respect to the differential pressure drop across it. A mathematical relation (Hagen–Poiseuille) which links the average flow velocity in

the pipe (Q) to the pressure drop Δp across a circular pipe of length (L) was used. The results show the scale thickness increase rate.

In addition to assessing the barium content, this work is also focused on the effect of other different variables (saturation ratio (SR), mixing ratio, temperature, flow rate, residence time, and surface condition) on the scaling kinetics and final crystal surface conformations.

As the main precipitate, on stainless steel surface substrate, the effect of free active barium cations was successfully studied across a wide range of saturation ratios using the dynamic flow loop rig. In this regard, the barium content was varied from 0 ppm - 150 ppm through 20 ppm, 50 ppm, 80 ppm and 100 ppm at 75 °C. The surface induction period and the total cell blockage time were used to assess the effect of barium ions in real field brines.

The data analysis show that the surface induction time is proportional to barium content (SR); it increases with the increase of barium species activities. The surface growth factor was also found to be proportional to the saturation ratio which results from the increase of barium content in the brine mixture.

The figures were used as a reference when similar brine formulation mixtures were used to scale chemically manipulated steel surfaces with a water soluble anti-nucleation phosphonate scale inhibitor called diethylene tri amine penta phosphonic acid (DETPMP).

Almost all of the scaled surfaces (resulting from the dynamic tests) were analysed using different surface integration techniques; surface topography and chemical composition using SEM and EDX respectively. Multiphase crystal composition and alignments were investigated using *ex-situ* X-Ray diffraction apparatus.

TABLE OF CONTENTS

THESIS RELATED PUBLICATIONS AND PRESENTATIONS	iii
DEDICATION	iv
ABSTRACT	vi
TABLE OF CONTENTS	viii
LIST OF FIGURES	15
LIST OF TABLES	22
NOMENCLATURES.....	23
Chapter 1. INTRODUCTION TO SCALE FORMATION AND MANAGEMENT	28
1.1. CONCEPTS AND OVERVIEW	28
1.2. SULPHATE SCALE FORMATION	29
1.2.1. Barite Production and Synthesis	31
1.2.2. Physical Properties of Barium Sulphate.....	31
1.2.3. Solubility and Reactions	33
1.2.4. Stability of Mineral Barite Crystal	33
1.2.5. Oilfield Inorganic Scale Formation.....	33
1.2.6. The Aims and Objectives	34
1.2.7. THESIS CONTRIBUTIONS	35
1.3. STRUCTURE OF THESIS.....	36
1.4. SUMMARY OF SCALE FORMATION AND MANAGEMENT	37
Chapter 2. GENERAL ASPECTS OF SCALING PROCESS.....	38
2.1. SCALE DEPOSITION REQUIRMENETS.....	38
2.1.1. Saturation Ratio (SR)	39
2.1.2. Saturation Index (SI)	41
2.1.3. Sulphate Scales (Ca^{2+} , Ba^{2+} , Mg^{2+} and Sr^{2+}) - SO_4^{2-}	42
2.1.4. Prediction of Barium Sulphate Solubility	43
2.1.5. Solubility	43
2.1.6. Transient Period	46
2.1.7. Factors Affecting Sulphate Scaling.....	48
2.1.8. Surface Nature.....	48
2.2. MINERAL SCALE (UNDERSTANDING AND MITIGATION)	49

2.3. SUMMARY OF INTRODUCTION.....	50
Chapter 3. THEORY	51
3.1. NUCLEATION THEORY	51
3.2. NUCLEATION KINETICS AND TERMINOLOGY	51
3.2.1. Primary Nucleation	52
3.2.2. Secondary Nucleation	56
3.2.3. Factors Affecting the Nucleation Process	59
3.2.4. Nucleation Rate Concept.....	59
3.2.5. Nucleation Induction Time	62
3.2.6. Crystal Growth	63
3.2.7. Induction Period.....	64
3.3. SUMMARY OF THEORY	65
Chapter 4. LITERATURE REVIEW.....	67
4.1. DYNAMIC TUBE BLOCKING	67
4.1.1. Tube Blocking Technique Review	71
4.2. ROLE OF IONS IN COMPLEX BRINES	75
4.3. INDUCTION TIME AND SR AT CONSTANT TEMPERATURE	77
4.4. SURFACE DEPOSITION AND BULK PRECIPITATION – EARLY NUCLEATION.....	78
4.5. TEMPERATURE FACTOR ON BARITE FORMATION KINETICS	79
4.6. DYNAMIC FLOW AND ITS INFLUENCE ON CRYSTALLIZATION.....	81
4.7. SCALE SURFACE DEPOSITION THICKNESS	83
4.8. SEEDING (BULK OR SURFACE)	83
4.9. CHEMICAL APPLICATION AND TREATMENT.....	84
4.9.1. Inhibition Mechanisms.....	85
4.9.2. Inhibitor Efficiency (IE).....	89
4.9.3. Inhibitor Thermal Stability.....	90
4.9.4. Surface Reactions.....	91
4.9.5. Inhibition and Critical Supersaturation Ratio (CSSR).....	93
4.9.6. Barium Sulphate Chemical Inhibition and Temperature	94
4.10. OPTICAL SURFACE CHARACTERIZATION	94
4.10.1. X-Ray Diffraction (XRD)	95
4.11. LITERATURE CONTRIBUTION	97

4.12. SUMMARY OF LITERATURE REVIEW	99
Chapter 5. EXPERIMENTAL METHODOLOGY.....	101
5.1. INTRODUCTION	101
5.1.1. Outlines	101
5.1.2. Brines Composition.....	103
5.2. DYNAMIC FLOW TEST.....	104
5.2.1. Hydraulic design and flow calculation.....	105
5.2.2. Flow Rig Description	105
5.2.3. Capillary Cell Design	109
5.2.4. Specimen Surface Scaling for Optical Analysis	110
5.2.5. Sampling During Flow Test	111
5.2.6. Inductively Coupled Plasma (ICP).....	112
5.2.7. Scale Surface Kinetic (Barium Varies 20 – 150 ppm).....	113
5.2.8. Dynamic Test – Flow Effect	113
5.3. CHEMICAL TREATMENT (DYNAMIC).....	114
5.3.1. Barite Scaling Treatment Test.....	114
5.3.2. Diethylene Triamine Penta Methylene Phosphonic Acid ...	115
5.3.3. DETPMP Identification	115
5.3.4. Physical and Chemical Properties.....	116
5.3.5. DETPMP Applications	116
5.3.6. Inhibitor Preparation and Treatment	116
5.3.7. Surface Pre-treatment (chemically pre - coated).....	118
5.3.8. Surface Pre-scaling (surface seeding)	118
5.3.9. Surface Pre-scaling Steps.....	119
5.4. BULK PRECIPITATION TEST	119
5.4.1. Turbidity Measurements	120
5.4.2. Sampling During Bulk Test	123
5.4.3. Conductivity Measurements	123
5.4.4. Ion Selectivity for Barium as a Main Variable	125
5.4.5. Turbidity Measurements for Scale Particles	126
5.5. THERMODYNAMIC SCALE PREDICTION	127
5.5.1. Predicted SR at Different Temperature/Mixing Ratios.....	129
5.5.2. Scale Prediction at 25 °C, 50 °C and 75 °C.....	129
5.6. SURFACE ANALYSIS	130

5.6.1.	Scanning Electron Microscope (SEM).....	130
5.6.2.	Energy Dispersive X – Ray (EDX) Analysis	134
5.6.3.	Surface Deposit Analysis Using EDX	134
5.6.4.	X-Ray Diffraction Analysis	134
5.6.5.	Raman Surface Analysis and Observation.....	138
5.6.6.	Fourier Transform Infrared (FT-IR) Surface Analysis	139
Chapter 6. RESULTS: THEORETICAL, BULK AND DYNAMIC TESTS (PART 1)..... 141		
6.1.	INTRODUCTION	141
6.1.1.	Result Outlines	142
6.2.	MODEL PREDICTIONS	142
6.2.1.	Thermodynamic Scale Predictions.....	142
6.2.2.	Scale Prediction at 25 °C, 50 °C and 75 °C.....	143
6.2.3.	Actual Mass Precipitated in Bulk.....	145
6.2.4.	Thermodynamic Predictions at Different Ba ²⁺ Contents	147
6.3.	BULK SCALING ASSESSMENT.....	148
6.3.1.	Turbidity Bulk Assessments	148
6.3.2.	Effect of Barium Content on Bulk Kinetic	151
6.3.3.	Conductivity at Different Ba ²⁺ Content (75 °C)	152
6.3.4.	Ion Selective for Ba ²⁺ Concentrations at 50 °C	153
6.3.5.	Turbidity Assessments at Different Barium Contents	154
6.4.	DYNAMIC FLOW: SURFACE SCALING KINETIC ASSESSMENT	155
6.4.1.	Effect of Different Temperature and Mixing Ratios.....	155
6.4.2.	Scale Surface Deposition Kinetics at 25 °C	156
6.4.3.	Scale Surface Deposition Kinetics at 50 °C	157
6.4.4.	Scale Surface Deposition Kinetics at 75 °C	159
6.4.5.	Surface Kinetic Data Versus Prediction.....	162
6.4.6.	Prediction Versus Observed Induction Period	163
6.4.7.	Average Rate of Deposition and Seawater Fraction	163
6.4.8.	Mass Percentage Deposited on Surface	164
6.4.9.	Total Scale Mass Deposited in Capillary	165
6.4.10.	Total Surface Mass Gained at Different Saturations.....	166
6.4.11.	ICP Analysis of Rig Waste During Surface Deposition	167

6.4.12.	Scale Surface Kinetics at Fixed Mixing Ratio (50:50)	168
6.4.13.	Effect of Flow Rate on Surface Deposition	168
6.4.14.	Surface Deposition at 10 ml/min Flow Rate	170
6.5.	EFFECT OF Ba ²⁺ CONTENT ON SURFACE DEPOSITION	173
6.5.1.	Scale Surface Kinetics at Different SR and Barium Contents	173
6.5.2.	Observed t_{ind} and Predicted Saturation Ratios	174
6.5.3.	Surface Scale Growth Period at Different Barium Content	175
6.5.4.	Scale Mass Deposited at Different Barium Contents.....	177
6.5.5.	Surface Mass gained Correlation to Observed t_{ind}	177
6.5.6.	Scale Thickness growth with Time	178
6.5.7.	Surface Deposition at Zero Barium Content at	180
6.6.	RESIDENCE TIME IN DYNAMIC SYSTEM.....	182
6.6.1.	Modified Mixing Part (Shorter Residence Time)	182
6.7.	INHIBITION OF GROWTH STAGE (DYNAMIC)	183
6.7.1.	Surface Deposition Treatment with DETPMP.....	184
6.8.	EFFECT OF SURFACE CONDITION ON SURFACE DEPOSITION	187
6.8.1.	Surface Pre-Scaling.....	187
6.8.2.	Surface Pre-Treatment	188
6.9.	SUMMARY OF RESULTS.....	190
Chapter 7.	SURFACE ANALYSIS RESULTS (PART 2).....	191
7.1.	INTRODUCTION	191
7.2.	SURFACE ANALYSIS	191
7.2.1.	Surface Analysis at Different Variables.....	192
7.2.2.	The Surface Scale Topography - Effect of Early Surface Nucleation	192
7.2.3.	Scanning Electron Microscope Analysis at Different Temperatures & Mixing Ratio	194
7.2.4.	Scanning Electron Microscope Analysis - Surface Pre- Scaling (Seeding)	196
7.2.5.	SEM Analysis of the Pre-scaled Surface with Odd Mixing Ratio	197
7.2.6.	SEM Surface Analysis of Treated Deposit in Dynamic Condition.....	199

7.2.7.	Raman Analysis	201
7.2.8.	Effect of Flow Rate (10 ml/min) on Surface Alignment.....	202
7.2.9.	Crystal Morphology on SS 316L Substrate at 20 – 150 ppm Ba ²⁺ and 75 °C	204
7.2.10.	Scale Deposition on Pre-treated Steel 316L Surface Substrate.....	206
7.2.11.	EDX Elemental Analysis of Scale/Barite Deposited on a Pre – Chemically Treated Stainless Steel 316L Substrate.....	207
7.2.12.	<i>Ex – Situ</i> X-Ray Diffraction Analysis.....	211
7.2.13.	Single Phase Barite Crystal on SS 316L Substrate – Surface Background.....	211
7.2.14.	<i>Ex –Situ</i> X-Ray Analysis of Multiphase Scale/Barite Crystals.....	213
7.2.15.	Multiphase Scale Deposited on Untreated SS 316L Substrates as a Function of Barium Content (flow).....	213
7.2.16.	Phase Analysis of Multiphase Crystal Deposit.....	215
7.2.17.	Multiphase Scale Deposited on Treated SS 316L Substrates (Flow).	216
7.2.18.	FT-IR Surface Characterization of DETPMP.....	216
Chapter 8.	DISCUSSION	219
8.1.	INTRODUCTION	219
8.2.	PREDICTED SATURATION RATIO – BULK PRECIPITATION VERSUS SURFACE DEPOSITION.....	220
8.3.	SCALE SURFACE GROWTH AND ΔP MEASUREMENTS	223
8.3.1.	Theoretical Calculation and Surface Kinetic Agreement....	227
8.4.	SURFACE PRE – TREATMENT – INHIBITION OR CRYSTALLIZATION INITIATOR.....	230
Chapter 9.	CONCLUSIONS	233
9.1.	EFFECT OF THE FLOW RATE ON MASS AND SURFACE MORPHOLOGY	235
9.2.	EFFECT OF BARIUM CONTENTS IN COMPLEX BRINE.....	236
9.3.	BULK PRECIPITATION IN FAVOUR OF SURFACE DEPOSITION	236
9.4.	PREDICTED SATURATION RATIOS AND BULK KINETICS CORRELATION	237
9.5.	TECHNIQUES OVERLAP (THEORETICAL, BULK AND SURFACE)	237

9.6. THE FINGER PRINTS OF INITIAL NUCLEATION AND ITS EFFECT ON SURFACE MORPHOLOGY	238
9.7. THE CORRELATION BETWEEN PREDICTED AND SURFACE DATA.....	238
Chapter 10. FUTURE WORK.....	240
REFERENCES.....	242

LIST OF FIGURES

Figure 1-1 : The secondary oil recovery (SOR) process and the possible mixing of active ions in the formation with sea water [1].	30
Figure 1-2 : The mechanism of the mineral scale deposit formation [2].	31
Figure 1-3 : Three dimensional barite crystal model [5].	32
Figure 2-1 : The scale crystallization kinetics from a super saturated solution.	39
Figure 2-2 : The three zones of saturation [19].	45
Figure 2-3 : The course of supersaturation ratio (S) through the precipitation process [24].	47
Figure 2-4 : The schematic diagram of scale prediction, experimental investigations and preventions.	50
Figure 3-1 : Heterogeneous nucleation model in presence of trace foreign particles [38].	54
Figure 3-2 : The reduction of the energy barrier needed for heterogeneous nucleation [38].	55
Figure 3-3 : Interfacial tensions at the boundaries between three phases γ_{sl} , γ_{cl} , γ_{cs} .	56
Figure 3-4 : Schematic diagram of the proposed growth mechanism [57].	64
Figure 4-1 : Typical tube blocking test rig with coil using differential pressure tool, Dyre [60].	68
Figure 4-2 : Inhibitor ranking under influence of pre-scaled surfaces using TBT and real field brine [64].	69
Figure 4-3 : Pressure drop across a porous media as a function of time in calcium sulphate system [74].	70
Figure 4-4 : The influence of Mg^{2+} and Ca^{2+} ions on scale thickness growth of barium – strontium system [80].	72
Figure 4-5 : Linear relationship between lattice dimensions and calcium content for the a-axis of barium sulphate [91].	76

Figure 4-6 : Surface deposition coverage (%) with respect to time using their different solution composition [96].	78
Figure 4-7 : Predicted barium sulphate nucleation time as a function of temperature [83].	79
Figure 4-8 : Size distribution of BaSO ₄ particles prepared at different flow rates of BaCl ₂ and Na ₂ SO ₄ solutions [72].	82
Figure 4-9 : Schematic diagram for crystals inhibition mechanisms [115].	86
Figure 4-10 : The chemical structure of commercial scale inhibitors with different functional group as anti-nucleation (PPCA, PVS) and anti-growth (DETPMP).	88
Figure 4-11 : Barium sulphate particles obtained in the presence of (a) no additives (control), (b) 0.026 mM of nitrile tri acetic acid (NTA) [124].	90
Figure 4-12 : Schematic representation of the main bonding modes of diethyl phosphonate molecules on a TiO ₂ surface [143].	92
Figure 4-13 : Concentration of BaSO ₄ precipitates as a function of the supersaturation ratio [151].	93
Figure 4-14 : Variation of output voltage (reflecting turbidity) vs time [155].	95
Figure 4-15 : The coverage % of the treated polarized steel metal surface [166].	97
Figure 5-1 : Surface deposition components.	102
Figure 5-2 : Schematic diagram of the turbidity measurements [168].	102
Figure 5-3 : Dynamic flow rig in use for surface deposition.	107
Figure 5-4 : Dynamic flow scale rig in use for surface deposition.	108
Figure 5-5 : The scale rig's cell compartment including the capillary cell.	110
Figure 5-6 : ICP unit used for water analysis.	112
Figure 5-7 : The structural formula of Diethylene tri amine Penta (Methylene Phosphonic Acid - DETPMP) used as anti-scaling agent.	115
Figure 5-8 : HACH colorimeter DR/890 turbidity meter [168].	120

Figure 5-9 : A typical bulk measurement using the turbidity with phase change assigned (t_{ind}) at 25 °C and 50:50 SW:FW mixing ratio.	121
Figure 5-10 : The Mettler Toledo combined conductivity/ion selectivity probe setup used in the bulk measurements and pH meter.	124
Figure 5-11 : New Carl Zeiss EVO MA15 SEM apparatus.	131
Figure 5-12 : The ¼”stainless extension tube and the plate for the surface analysis.	132
Figure 5-13 : The simple goniometer image shows details of the Philips Analytical diffractometer [175].	135
Figure 5-14 : Sample holders for XRD powder diffraction [175].	137
Figure 5-15 : Diagram of the external reflection spectroscopy.	140
Figure 6-1 : Predicted supersaturation ratio (SR) at different temperature sea water % values.	144
Figure 6-2 : The barite mass predicted at different temperature versus sea water %.	146
Figure 6-3 : The actual scale mass precipitated during bulk jar tests at 25 °C, 50 °C & 75 °C.	146
Figure 6-4 : The linear increase of the SR versus the actual Ba ²⁺ (at 75 °C) in the final mix at equilibrium.	148
Figure 6-5 : Turbidity of formed scale vs. time at 50:50 mixing ratio at three temperatures (25 °C, 50 °C and 75 °C).	149
Figure 6-6 : Scale bulk precipitation tests – turbidity versus time at 25 °C.	150
Figure 6-7 : Scale bulk precipitation tests – turbidity versus time at 50 °C.	150
Figure 6-8 : Scale bulk precipitation tests – turbidity versus time at 75 °C.	151
Figure 6-9 : Barium Ions Conductivity Measurements at 50 °C.	152
Figure 6-10 : Barium Ions Selectivity Measurements at 50 °C and the Induction Period Marked at About Five Seconds.	153

Figure 6-11 : The Observed Turbidity Using Bulk Measurements at 50 °C and 75 °C at 22 Seconds.	154
Figure 6-12 : Shows differential pressure as a function of time at 25 °C at five mixing ratios.	156
Figure 6-13 : Shows scale surface deposition at different mixing ratios at 50 °C. .	158
Figure 6-14 : The observed surface scaling film induction time at different mixing ratios and 75 °C.	160
Figure 6-15 : Observed surface scale filming induction times vs. predicted saturation ratios at different SW: FW mixing ratios.	163
Figure 6-16 : Measured average surface deposition rate at 25 °C, 50 °C & 75 °C and five mixing ratios.	164
Figure 6-17 : The mass % deposited on the capillary surface from the total mass precipitated at different temperatures and sea water percentage.	165
Figure 6-18 : Total barite mass deposited in capillaries at different temperatures and seawater percentage.	166
Figure 6-19 : The ICP elemental analysis of the brine mixture waste at 20:80 FW: SW and 50 °C.	167
Figure 6-20 : Observed differential pressure values vs. time at 50:50 mixing ratio and 25 °C, 50 °C and 75 °C.	168
Figure 6-21 : The reproducible recoded differential pressure versus time at 10 ml/min flow rate.	170
Figure 6-22 : Barite scale mass deposited in capillary at 10 ml/min flow and 50:50 mixing ratio.	172
Figure 6-23 : The relation between the 5 & 10 ml/min flow rate and the recorded induction time (hrs).	173
Figure 6-24 : The surface dynamic flow test at different barium contents.	174
Figure 6-25 : The relation between the predicted saturation ratios, actual Ba ²⁺ concentration and experimentally observed surface scaling induction time (hrs). .	175

Figure 6-26 : The Growth period on surface at 150 ppm barium concentration at 75 °C.....	176
Figure 6-27 : The growth factor increases as a function of the barium content increase.....	176
Figure 6-28 : The scale deposited in the capillary cell with respect to the barium concentrations.	177
Figure 6-29 : The relation between barium concentrations and both the surface induction period and the gained scale mass as a function of the barium content. ..	178
Figure 6-30 : Surface scale thickness (mm) development with time at different barium content and SR values.....	179
Figure 6-31 : Capillary radius reduction with respect to time.	180
Figure 6-32 : Surface deposition at zero barium content at 75 °C and 10 ml/min flow.	181
Figure 6-33 : Scale/barite surface deposition at 50 ppm barium in the final mixture at 2 – 3 seconds residence time.....	183
Figure 6-34 : Differential pressure versus time for surface deposition treatments with 10 ppm DETPMP at 25 °C, 50 °C & 75 °C and 50:50 mixing ratio.	184
Figure 6-35 : Differential pressure versus time for surface deposition treatments with 5 ppm DETPMP at 25 °C, 50 °C & 75 °C and 50:50 mixing ratio.	185
Figure 6-36 : Scale and scale – DETPMP complex mass deposited in capillary during treatments with 5 ppm DETPMP.....	185
Figure 6-37 : The pre-scaling surface effect on surface deposition.....	188
Figure 6-38 : The effect of surface pre-treatment using 1000 ppm DETPMP on surface scaling film induction time.	189
Figure 6-39 : The comparison between the total blockage time during pre-treatment using 1000 ppm DETPMP and no treatment.	189
Figure 7-1 : Surface nucleation period at 50:50 mixing ratio and 25 °C.....	193
Figure 7-2 : Surface nucleation period at 40:60 SW: FW mixing ratio and 50 °C..	193

Figure 7-3 : Surface nucleation period at 20:80 SW: FW mixing ratio and 75 °C..	194
Figure 7-4 : SEM images of final barite deposit surface growth at 25 °C & 50 °C.	196
Figure 7-5 : SEM images of deposited barite at 25 °C (a) 50:50, (b) 70:30 and (c) 90:10.....	198
Figure 7-6 : EDX quantitative analysis of barite deposited at 90:10 FW:SW at 25 °C.	198
Figure 7-7 : SEM images of untreated barite deposit at 5 ml/min flow (bottom row) and treated barite deposit with 10 ppm DETPMP (top row) at specified temperatures and mixing.....	200
Figure 7-8 : SEM images of treated barite surface with 5 ppm DETPMP at specified temperatures and mixing.....	201
Figure 7-9 : Raman spectra of treated barite with 10 ppm DETPMP deposit on steel surface at 25 °C, 50 °C and 75 °C.	202
Figure 7-10 : Barite crystallization on steel surface at 10 ml/min flow and 50:50 mixing ratio (temperatures from left to right 25 °C, 50 °C & 75 °C) – no treatment.	203
Figure 7-11 : Scale barite deposition on a bare 316L steel surface substrate at 50 – 150 ppm Ba ²⁺ and 75 °C.	205
Figure 7-12 : Scale barite deposition on bare 316L steel surface substrate at the lowest 20 ppm Ba ²⁺ and 75 °C.....	205
Figure 7-13 : SEM image of scale barite deposition morphology on pre – treated SS 316L in dynamic flow system at 75 °C.....	207
Figure 7-14 : EDX elemental analyses (selected area) of scale barite deposit on the pre-treated surface at different barium concentration and 75 °C.....	209
Figure 7-15 : EDX elemental analyses of complex scale barite deposit on pre-treated surface at different barium concentration 50 – 150 ppm at 75 °C.....	210
Figure 7-16 : <i>Ex – situ</i> X-Ray spectrum of single barite crystal deposited on steel surface used as a background.....	212

Figure 7-17 : The multiphase X-Ray spectrum of scale/barite deposition on SS 316 substrate.....	214
Figure 7-18 : The effect of barium content on (122), (113), and (401) crystal faces in terms of the orientation and positions.	214
Figure 7-19 : The phase analysis of the multiphase scale deposit at 20 ppm Ba ²⁺ content.....	215
Figure 7-20 : FT- IR spectrum of DETPMP on SS 316 surface substrate.....	217
Figure 7-21 : <i>Ex – situ</i> X – Ray analysis of multiphase crystallization on pre - treated steel surfaces.	218
Figure 7-22 : <i>Ex – situ</i> X – Ray analysis of multiphase crystallization on pre - treated steel surfaces.	218
Figure 8-1 : The early and secondary crystal growth and induction time at high temperature [176].	221
Figure 8-2 : Predicted masses with respect to the predicted SR.	222
Figure 8-3 : The rapid variation of barium species concentration with time in a non-nucleated system [59].	223
Figure 8-4 : Measured and calculated ΔP between the inlet and outlet of a one meter long tube, 3.04 mm ID tube at same flow rate used in this work (10 ml/min) [81].	224
Figure 8-5 : (a) Effect of flow rate on deposition with respect to the capillary-volume injected (CVI) as a measure of the elapsed time, Lawal [180], and (b) the effect of SR, this work.	226
Figure 8-6 : The effect of flow rate on the uniformity of surface deposit (no homogeneity [181].	227
Figure 8-7 : Effect of temperature on the induction period at different supersaturations [92].	228
Figure 8-8 : The untreated barite scale crystals at 100 and 150 ppm (a,b) and effect of the surface pre-treatment on crystal morphology (c,d) at 75 °C.	231
Figure 8-9 : The DETPMP expected alignment on steel surface prior to scaling. .	232

LIST OF TABLES

Table 4-1 : Dynamic flow technique statistics.....	74
Table 4-2 : The dimensions of the cells used based on Table 4.1.....	75
Table 5-1 : Synthetic formation and sea water used in this part.	104
Table 5-2 : Calculated residence time at the two selected flow rates (5 ml/min and 10 ml/min).....	105
Table 5-3 : DETPMP specification	116
Table 5-4 : Formation and sea water brines formulation used.....	125
Table 6-1 : Formation and sea water brines formulation used.....	144
Table 6-2 : Bulk precipitation and dynamic surface deposition data at 25 °C.	157
Table 6-3 : Bulk precipitation and dynamic surface deposition data at 50 °C.	159
Table 6-4 : Bulk precipitation and dynamic surface deposition data at 75 °C.	160
Table 6-5 : The observed surface deposition induction time using tube capillary at 25 °C, 50 °C & 75 °C.	162
Table 6-6 : Reproducibility of dynamic surface deposition data of barite at 25 °C, 50 °C & 75 °C at 10 ml/min flow rate.	171
Table 6-7 : ICP analysis of the treated brine mixture waste for Ba & P residuals..	187
Table 7-1 : EDX analysis of the surface complex deposit treated with 5 ppm DETPMP at 75 °C in Figure 7-7.	202
Table 7-2 : The elemental analysis of the main precipitant at different Ba ²⁺ contents.	210
Table 8-1 : Calculated saturation ratios (SR) and the saturation indices of the brine mixture.	229

NOMENCLATURES

γ_{\pm}	Activity coefficient.
$\Delta G_{\text{heterogeneous}}$	The free energy for heterogeneous nucleation.
$\Delta G_{\text{homogeneous}}$	The free energy for homogeneous nucleation.
ΔG_{crit}	The change of the free energy at critical size of a particle.
ΔG_{crit}	The actual critical free energy of formation.
\emptyset	The reaction affinity.
ΔG	Overall excess free energy.
ΔG_s	Surface excess free energy.
ΔG_v	Volume excess free energy.
ΔP	Differential pressure.
γ	Interfacial tension.
γ_{cl}	Solid crystalline – liquid interfacial tension.
γ_{cs}	Solid crystalline - foreign solid surface interfacial tension.
γ_{sl}	Solid surface – liquid interfacial tension.
ΔG°_f	Gibbs free formation energy.
ΔH°_f	Formation energy.
ΔH_{fus}	Energy of fusion.
ΔP_i	Pressure drop at time zero.
σ	Surface tension.
θ	Theta – contact angle.
μ	Dynamic viscosity.
ρ	The density of the solid.
A	Pre exponential factor, efficiency of ions collision.
a	Activity of the solute in solution.
A	Surface area of the crystal.

a^*	Activity of the pure solute in a macroscopic crystal.
$A_{het/hom}$	Kinetic factor in nucleation rate expression.
BHPMP acid.	Bis-hexamethylene triamine-penta methylene phosphonic acid.
$C_{(r)}$	The solubility of a particle size of radius (r).
r_{crit}	Critical size of a particle.
C^*	The normal equilibrium solubility of a substance.
CGR	Crystal growth retardation.
CSSR	The critical supersaturation ratio.
CVI	Capillary-volume injected.
DETPMP	diethylene triamine penta methylene phosphonic acid.
DRIFT	Diffuse reflectance IR Fourier transform.
DTB	Dynamic tube blocking.
EDTA	Ethylene diamine tetra acetic acid.
EDTP	Ethylene diamine tetra phosphonic acid.
EDX	Energy dispersive X-Ray.
EM	Electronic microscope.
ERS	External reflection spectroscopy.
ESEM	Environmental scanning electron microscope.
FT-IR	Fourier transform infrared spectroscopy.
FW	Formation water.
HMDP	hydroxyl methylene diphosphonate.
IAP	Ion activity product.
ICP	Inductively Coupled Plasma.
ID	Internal diameter of capillary.
ISAB	Ionic strength adjustment buffer.
ISE	Ion-Selective Electrode.

$J_{het/hom}$	Heterogeneous/homogeneous nucleation rate (nuclei/cm ³ .s).
J	The rate of nucleation (nuclei/cm ³ .s).
$J_{max,het/hom}$	Pre-exponential factor.
K	Boltzmann's constant ($K = 1.3805 \times 10^{-23} \text{ JK}^{-1}$).
K_B	Boltzmann constant (J/Kmol).
KDP	Potassium dihydrogen orthophosphate.
K_{sp}	Solubility product.
L	Length (m).
LSI	Langelier saturation index.
M	The molar mass of the solid in solution.
$M.Wt$	Molecular weight.
M_0	The mass of the metal plate when $T_{dep} = 0$.
MEG	Methylene ethylene glycol.
MIC	Minimum inhibitor concentration.
IE	Inhibitor efficiency.
mmol	millimole.
MPa	Mega Pascal
mS	Micro Siemens.
MT_{dep}	Mass of the metal plate at the time of deposition.
N	Avogadro's number ($N = 6.023 \times 10^{23} \text{ mol}^{-1}$).
N	The number of nuclei emerging in a time period.
N	Number of ions or molecules in the crystal.
NACE	National association of corrosion engineering.
NI	Nucleation inhibition.
NTA	Nitrilo tri acetic acid.
OD	Outer diameter.

PAA	Poly acrylic acid polymer.
PLGA	Pteroyl-L- glutamic acid.
PPCA	Phosphino poly carboxylic acid.
ppm	Part per million.
PSD	Power spectral density.
Psid	Pound per square inch - differential.
Psig	Pound per square inch – line pressure.
P_t	Pressure drop after time (t).
PVS	Polyvinyl sulphonate.
Q	Flow rate (m^3/s).
QCM	Quartz crystal microbalance.
R	The gas constant (R) = $8.314 \text{ JK}^{-1} \text{ mol}^{-1}$.
r	The radius of capillary after time t.
R	Initial radius of a capillary.
r_c	The critical size of a particle to the free energy.
$S. R_{\text{offline}}$	Scaling rate offline.
S	Equilibrium saturation value.
S°	Enthalpy.
S_a	Activity based on the supersaturation.
S_c	Concentration based supersaturation.
SE	Secondary electron.
SEM	Scanning electron microscope.
SI	Scale inhibitor.
SI	Saturation Index.
SOR	Secondary Oil Recovery.
SR	Saturation Ratio.

SR-GIXRD	Synchrotron radiation grazing incidence X-Ray diffraction technique.
SS316L	Stainless steel - low carbon
SW	Sea water.
SXRD	Synchrotron X-Ray diffraction technique.
τ	Thickness (mm).
T	Residence time (s).
T	Temperature in Kelvin.
TBT	Tube blocking test technique.
T_{dep}	T_{dep} is the time of deposition.
TDS	Total dissolved solids.
t_g	The time nucleus needs to grow to a visible size.
t_{ind}	The induction time.
TISAB	Total ionic strength adjuster and buffer.
TM	Test method.
t_n	The time necessary for the critical nucleus to be formed.
t_n	The formation time of the critical nucleus.
t_r	Relaxation time.
v	Volume of solution (m^3).
v	The molecular volume.
VS-Co	Vinyl sulphonate co-polymer.
WAXS	Wide angle X-Ray scattering.
WD	Working distance.
WDS	Wavelength-dispersive spectroscopy.
XRD	X-Ray Diffraction.
ZTS	Zinc tris(thiourea) sulphate.

Chapter 1. INTRODUCTION TO SCALE FORMATION AND MANAGEMENT

The mechanisms of inorganic mineral scale deposition and precipitation kinetics are still an important topic in the oil industry and desalination units. Much still remains unknown around the kinetics of scale formation in both bulk solution and particularly at surfaces. Once the solution mixture is supersaturated with the divalent alkaline earth metal cations (Ca^{2+} , Ba^{2+} , Sr^{2+} and Mg^{2+}) and optimum reaction conditions are met, these inorganic salts can form deposits on a surface or in the reservoir formation as sulphate or carbonate deposits. The prediction, evaluation and mitigation of such deposits is still the focus of many research groups around the globe.

1.1. CONCEPTS AND OVERVIEW

Inorganic mineral deposits/precipitates on surfaces and in underground water reservoirs are common and are problematic in the oil industry. They arise from simple chemical reactions based on the level of saturation of reacted species (anions and cations) in a media, temperature, and also pressure in some cases. These inorganic mineral deposits or precipitates are called “mineral scale” in the oil and gas industry or may be called ‘scale’ as a single term.

Mineral scales fall into different categories, which are directly related to the type of reactants, such as carbonate (calcium carbonate CaCO_3 , magnesium carbonate MgCO_3 and iron carbonate FeCO_3). The other common type of scale is sulphate; it deposits as barium sulphate BaSO_4 , strontium sulphate SrSO_4 and calcium sulphate CaSO_4 . In addition to the previously mentioned scales, there are others such as hydroxides and silicates. Three questions often arise in relation to particular scales; when, where, and at what rate are they formed? It is clear that the former is related to thermodynamic conditions while the latter is related to the kinetics. In the literature, it is fair to say that most of the work is focused on different aspects

relating to thermodynamics. Most experimental techniques assess the mechanisms of different crystal formation in the bulk solution. Thermodynamic data are explored in terms of solution properties, the rate of formation, effect of different components, and the morphology of the resulting surface crystal (shape and size).

In this work, the focus is to investigate the kinetics of surface deposition/bulk precipitation of one persistent scale mentioned earlier, namely barium sulphate or barite in real oilfield complex brines. There is a vast amount of research work done to investigate the mechanism of insoluble mineral formation in the oil industry. However, there is still a lack of knowledge in understanding the crystallization kinetics in static conditions (bulk) and dynamic conditions (flow) at variable conditions in real complex brines. The use of the two combined techniques has been proven useful to link the bulk thermodynamic properties to the surface kinetics. The techniques are always supported with theoretical calculations around scaling tendency by considering thermodynamics. Much less is published around the kinetics although papers are now emerging.

1.2. SULPHATE SCALE FORMATION

In the oil industry, sulphate scales are usually produced in the secondary oil recovery (SOR) in the later stages. The different types of such insoluble scale formations are directly related to the mixing of incompatible sea/produced water rich in sulphate anions ($-\text{SO}_4^{2-}$) with formation water rich in the divalent cations (Ba^{2+} , Sr^{2+} , Ca^{2+} , and Mg^{2+}). Figure 1-1 shows the enhanced oil recovery process and the possible mixing of cationic and anionic solution phases in underground reservoirs and equipment surfaces. The scaling mechanism of the process is shown in Figure 1-2.

Sulphate scale is not as complicated as the carbonate type scales in terms of phase formation or transformation, but it is considered worse in terms of removal once formed. Kinetically, the challenge was always when and how fast it forms, and the

mitigation. For barium sulphate for instance, its severity is related to the temperature variation, which causes the solubility to vary across different stages in one system. The lower solubility alkaline earth sulphate scales (BaSO_4 , SrSO_4) precipitate as non-hydrated products which makes it difficult to dissolve once formed. On the other hand, some sulphates do tend to re-dissolve in water.

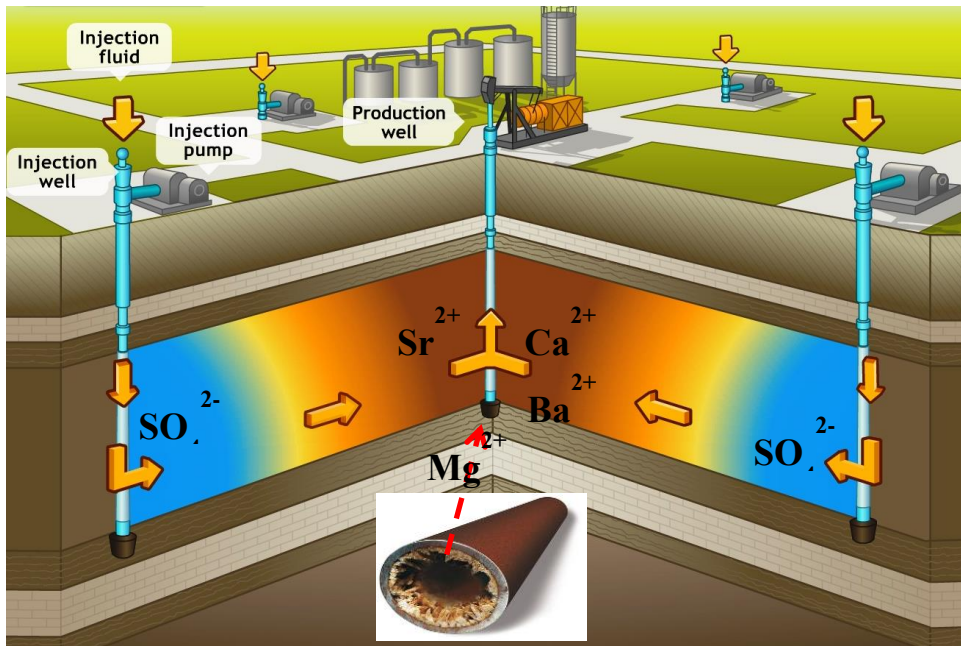


Figure 1-1 : The secondary oil recovery (SOR) process and the possible mixing of active ions in the formation with sea water [1].

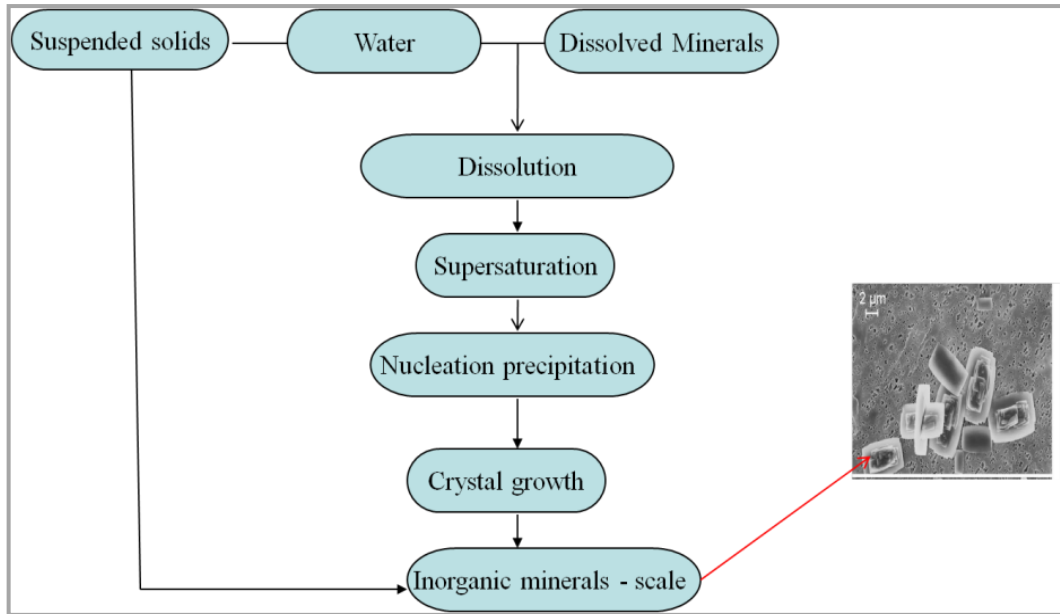


Figure 1-2 : The mechanism of the mineral scale deposit formation [2].

1.2.1. Barite Production and Synthesis

Naturally, barium sulphate or barite is widely distributed. There are different impurities which do commonly exist in natural barite salt. These foreign impurities are, for example, silica as a prime impurity, ferric oxide and fluoride impurities. The highly purified barium sulphate is produced by the precipitation method; it is precipitated as a result of treating an aqueous solution of barium chloride salt with the solution of sodium sulphate at desired concentration and ratios of both reactants.



1.2.2. Physical Properties of Barium Sulphate

Barium sulphate, or barite as it is commonly known, is a soft crystalline solid, with rhombic crystal shape. The pure barium sulphate salt is usually white, but because of the impurities which may exist as co-precipitants, the colour may vary. The density of barite is 4.50 g/cm^3 , and the calculated density is 4.48 g/cm^3 . Its melting point is $1,580^\circ \text{C}$ and it decomposes above $1,600^\circ \text{C}$. BaSO_4 is insoluble in both water (about

285 mg/L at 30 °C) and alcohols as well, its solubility product (K_{sp}) is 1.1×10^{-10} , but it is actually soluble in concentrated sulphuric acid. Barite crystal cell has dimensions of: $a = 8.878$, $b = 5.45$, $c = 7.152$, which forms: [001] [011] [101] faces. The three dimensional barite crystal model is shown in Figure 1-3 [2].

It is well-known that barite, BaSO_4 , is one of the most widely distributed sulphate compounds in the world. It was reported in the literature that barite has the structure of orthorhombic system with space group of Pnma. In the barite structure, each S atom coordinates with four oxygen atoms and forms the SO_4 tetrahedron while the cation, Ba^{2+} , coordinates with 12 oxygen atoms. The structure of barite is found to be close or similar to that of olivine, $(\text{Mg}, \text{Fe})_2\text{SiO}_4$. It is also recognised as one of the most predominant minerals in the earth's interior crust [3]. The thermochemical properties of barite can be listed as:

$$\Delta H_f^\circ = -352.3 \text{ kcal/mol.}$$

$$\Delta G_f^\circ = -325.7 \text{ kcal/mol.}$$

$$S^\circ = 31.6 \text{ cal/degree mol.}$$

$$\Delta H_{\text{fus}} = 9.71 \text{ kcal/mol [4].}$$

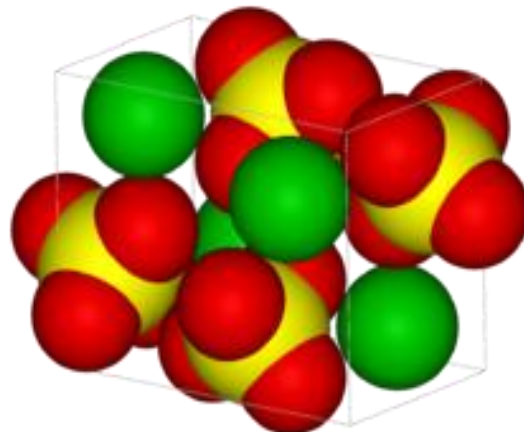
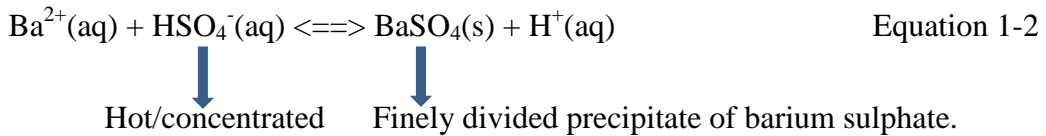


Figure 1-3 : Three dimensional barite crystal model [5].

1.2.3. Solubility and Reactions

Barium sulphate is one of the most insoluble salts of barium. The double decomposition reactions in aqueous phases are unlikely to take place. It dissolves and decomposes in concentrated H₂SO₄ to form an acid sulphate, when diluted with distilled water. It then breaks down and returns to the original BaSO₄ form.



1.2.4. Stability of Mineral Barite Crystal

The barite (BaSO₄) crystals exhibit a pseudomorphic replacement, which means that at certain conditions a mineral could have the crystalline form of another mineral rather than keep its own original crystalline form. So barite crystal is replaced into barium carbonate by using carbonated alkaline hydrothermal fluids over the temperature range from 150 up to 250 °C. The chemical reactivity of mineral barite crystals was limited to temperatures below 200 °C [6].

1.2.5. Oilfield Inorganic Scale Formation

The precipitation or deposition of the insoluble mineral scale deposits (scaling) is a common cause of formation damage resulting in flow restrictions and lost production. Two mechanisms of scale formation commonly occur; carbonate scales (calcite CaCO₃, siderite FeCO₃) can be formed when pressure and/or temperature change in produced flow and release carbon dioxide (change in partial pressure). The other mechanism is a result of incompatible brines mixing leading to sulphate scales e.g. barite BaSO₄, celestite SrSO₄, anhydride calcium sulphate CaSO₄ and hydrated calcium sulphate CaSO₄.2H₂O (gypsum). Barium sulphate is the least soluble mineral and attracts more attention and is a major concerns (the subject of this work) [7].

This research work was carried out at atmospheric pressure using a modified tube blocking test apparatus. It was used to investigate the kinetics of barium sulphate formed on the stainless steel surface, at two different elevated temperatures at atmospheric pressure [8]. Finally, the scale kinetics were investigated when barium (Ba^{2+}) species were the only variable in mixed brines. It was to reveal their role in the scale deposition/precipitation processes as the BaSO_4 is the lowest predicted solubility component.

1.2.6. The Aims and Objectives

The aims and objectives of this work are as follows:

- To investigate, for the first time, different kinetic data with a new dynamic system setup (combination of differential pressure tool and stainless steel capillary at specified dimensions, 1mm ID and 10 mm length) that facilitates:
 - Surface nucleation patterns (fingerprint of surface scaling process) which highlights various kinetic aspects, surface scale filming induction time, rate of surface deposition per a unit of time.
 - Scale mass quantifications.
- To investigate with a real complex brine the barite surface deposition using the data correlation between the theoretical, bulk and dynamic surface flow system.
- To systematically explore the effect of temperature and to understand the surface kinetics of scale formation.
- To investigate the role of barium content as the main variant on surface and bulk crystallization.

- To investigate the time and location of crystal birth in both bulk precipitation and surface deposition. If it is determined, would it be possible to finalize the crystallization process whether it is deposition, adhesion or combined?
- To explore the inhibition of different brine mixtures with different predicted saturation ratio and surface mass. The correlation between scale – inhibitor complex mass formed on surface at different temperature and untreated deposit case .
- To investigate the role of surface conditions (pre-scaled or pre-nucleated surfaces and chemically modified surface) on surface deposition kinetics and final alignment.

1.2.7. THESIS CONTRIBUTIONS

- This work shows another investigation of bulk and surface scaling mechanism, based on the maximum SR, to show and agree with previous study that exhibits a complete different scaling mechanism.
- This is the first work to show an agreement between the theoretical thermodynamic calculation and surface observation (based on barium content) in assessing the rate of surface scaling.
- The nature of the setup and novel use of such cell facilitates surface scaling quantification to assess more parameters which are related to surface scaling.
- Unlike coils, the used cell provides long duration scaling condition to explore the early and latest surface scaling scheme (pattern) to the final growth.
- Chemically pre-treated steel surface with DETPMP could generate a centre of crystallization on surface and may speed/slow surface deposition.

1.3. STRUCTURE OF THESIS

The thesis structure is as follows:

Chapter 1: Introduction (*Section 1*): Scale formation principles and background. It gives an overview about the scale processes, concepts and mechanisms.

Chapter 2: This part shows general aspects of the scaling process as well as the factors that may affect scaling.

Chapter 3: Introduction (*Section 2*): Theory. This section focuses on the mechanism and kinetic aspects of scaling phenomenon (prediction and thermodynamic).

Chapter 4: Literature review: This section deals with the review of previous work using dynamic techniques including some statistics. It also includes different aspects in relation to scale surface thickness propagation, temperature effect, flow, and different roles of ions on scale kinetics. Chemical applications were included.

Chapter 5: This part shows the experimental setup and methodology. It explains what this upgraded setup facilitates differently and the new parameters to consider in scale kinetic studies.

Chapter 6: Results are divided into two chapters as well: Part 1 contains the collected data from the three applied techniques, namely; theoretical, bulk and dynamic flow tests.

Chapter 7: Part 2 contains the optical surface analysis which resulted from the previous dynamic flow tests data.

Chapter 8: It gives the results discussion in a flow in which all of the different data collected from different techniques and variable conditions are interpreted to give the idea behind this research work.

Chapter 9: Conclusions. These summarize the important parts of the thesis and present the highlights.

Chapter 10: Future work, new ideas are presented to continue with this research work.

1.4. SUMMARY OF SCALE FORMATION AND MANAGEMENT

The scale formation and management section summarizes the simple mechanism of barium sulphate scale formation from complex brines. Since the focus was on barite formation, the synthesis and physical properties of barium sulphate were explored. The mechanism of underground/formation brine mixing due to breakthrough of different supersaturated brines was revealed. The management of such a natural persistent problem in oilfield formation is far from clearly understood and resolved.

The aim of this research work, which is focused on the kinetics of surface scale kinetics, was outlined. In this section, the thesis structure was also stated to cover important scale kinetic aspects.

Chapter 2. GENERAL ASPECTS OF SCALING PROCESS

This introduction chapter focuses on the main aspects of the scaling process and the conditions required in order for it to take place. Apart from the solution factors, other controlling parameters that may affect the scaling precipitation and deposition processes are explored.

2.1. SCALE DEPOSITION REQUIRMENETS

In the early stages of surface scaling kinetics studies, the impingement of formed solid particles on a metal surface, particularly heated surfaces, was expected to be the primary cause of scale deposition. It has been shown that the precipitates and/or crystals, which are formed in one part of a system and then transported to another part, are less adhered than those crystals formed on site. Furthermore, the impingement of solids has little effect on scale deposition [2]. As a matter of fact, and according to the literature, the three essential requirement factors for scale deposition (on surface) or precipitation (in bulk) to take place have to be met. The scale crystallization kinetics from a solution, for instance, onto a surface site (see the nucleation model in Figure 2-1) may require three factors [9]:

- 1) Supersaturation condition.
- 2) Nucleation.
- 3) Contact time elapsed.

The number of initial crystal sites may have a major impact on the growth of these sites and the final amount of scale deposition formed.

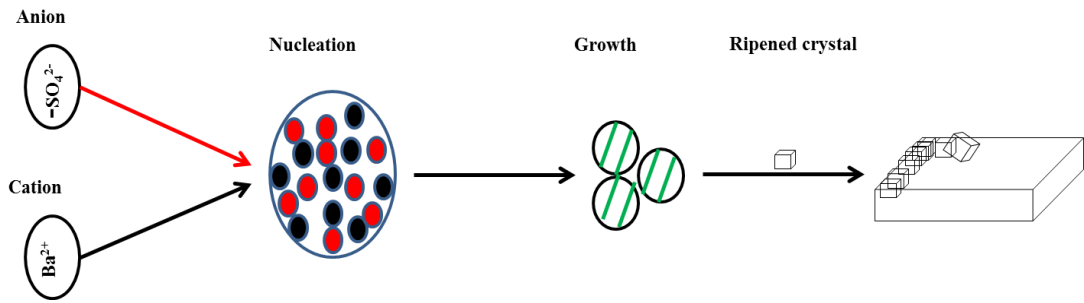
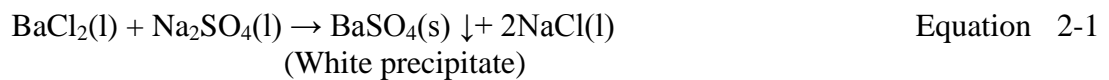


Figure 2-1 : The scale crystallization kinetics from a super saturated solution.

2.1.1. Saturation Ratio (SR)

Saturation ratio is defined as the ratio between the product of ions molar concentration of the reactants to the solubility product. In the case of barium sulphate formations;



Will a barite substance dissolve or precipitate? In this case, ion activity product (IAP) is considered.



Equilibrium constant (K) in terms of activities of reactants & products at equilibrium is;

$$K = \left(a_{\text{Ba}^{2+}_{free}} \right)_{equil} \cdot \left(a_{\text{SO}_4^{2-}_{free}} \right)_{equil} \quad \text{Equation 2-3}$$

However, a real solution may or may not be in equilibrium. The ion activity product (IAP) has the same form as the equilibrium constant, but involves the actual activities. So the IAP can be;

$$IAP = \left(a_{Ba^{2+}}\right)_{actual} \cdot \left(a_{SO_4^{2-}}\right)_{actual} \quad \text{Equation 2-4}$$

According to equation 2-2;

If $IAP = K$, the solution is in equilibrium with barite.

if $IAP < K$, the reaction will proceed to the right (dissolution).

if $IAP > K$, the reaction will proceed to the left (precipitation).

The saturation ratio (SR) is usually written as the product of the barium and sulphate species concentrations in molal units to the solubility product, K_{sp} .

$$SR = \frac{(Ba^{++})(SO_4^{--})}{K_{sp}} \quad \text{Equation 2-5}$$

Solutions with dissolved solutes fall into three different categories:

- Under - saturated solutions are those which have less soluble solutes and in this case precipitation is unlikely.
- Saturated solutions are those which are in equilibrium with their solute; it is the critical stage before any precipitation occurs.
- Supersaturated solutions contain higher concentrations of dissolved solute than their equilibrium concentration.

Supersaturation can occur for many reasons. One is the fact that sub microscopic crystals, which normally precipitate first, have a higher solubility than larger particles. This prevents the crystallization process from starting easily [10]. Thermodynamically, it is known that not all of the cations/anions species in solutions are active and the activity coefficient (a) considers only those species which are actually taking part in the reaction; the actual free ions. So, most of the modern prediction software take into consideration the activity based on the supersaturation (S_a) and not the concentration based supersaturation (S_c). The activity is affected by the ionic strength which is related to the mixed brines composition.

2.1.2. Saturation Index (SI)

The inability to predict exactly where and to what extent (location & the severity) scale deposits will form might pose a question as to whether scaling tendency calculations are worthwhile. Scale prediction calculations are important in water injection operations, when two or more waters are mixed either in the formation or prior to injection. Due to the supersaturation with cations and anions species, the mixtures of incompatible waters are scale forming even though the individual waters do not tend to scale. The mix of formation water with producing water (source wells) or sea water in water flooding systems is the best example.

Saturation index (SI) indicates whether a substance dissolves or precipitates based on the saturation index, it is also referred to as the logarithm of the saturation ratio (SR).

$$SI = \log_{10} SR \quad \text{Equation 2-6}$$

$$SI = \log \left(\frac{(Ba^{++})(SO_4^{--})}{K_{sp}} \right) \quad \text{Equation 2-7}$$

The saturation index (SI) is defined as:

$IAP = K_{SP}$, $SI = 0$ water is saturated with the mineral

$IAP < K_{SP}$, $SI < 0$ water is under saturated with the mineral, and reaction is proceeding from left to right (dissolution).

$IAP > K_{SP}$, $SI > 0$ water is supersaturated with the mineral, and Reaction is proceeding from right to left (precipitation).

In the case of the carbonate scale, an index for fresh waters was developed earlier by Langelier [11], in the pH range 6.5 – 9.5, and with the help of this index, it becomes possible to predict whether a given water will deposit or dissolve formed scale. This is called the saturation index (SI), and it can be calculated and predicted.

Field brine water analysis, in many cases, shows a high total dissolved solids (TDS) 5000 mg/L. It is used to describe the inorganic salts and small amounts of organic

matter present in water solution. These constituents are usually calcium, magnesium, sodium, potassium, carbonate, hydrogen carbonate, chloride, sulphate, and nitrate anions. The total dissolved solids has an influence on the validity of the Langelier saturation index (LSI) and as a result of the calculation. As a result of the restriction on LSI, the empirical calculation was simplified by Stiff and Davis [12] for application to oilfield brines.

2.1.3. Sulphate Scales (Ca^{2+} , Ba^{2+} , Mg^{2+} and Sr^{2+}) - SO_4^{2-}

In general, precipitation of calcium, barium and strontium sulphate scales is usually caused when all of the following conditions are met or sometimes one of them:

- 1) Pressure reduction at the well bore in the formation causing liberation of CO_2 gas.
- 2) Mixing of incompatible waters (high sulphate waters such as sea water or flooding water system mixed with brines containing high concentration of divalent sulphate cations of (Ca^{2+} , Ba^{2+} , and Sr^{2+}) in the reservoir formation water.
- 3) Evaporation and concentration of brines by gas evolution in wellbores or by heating in surface equipment.
- 4) Temperature fluctuations through the system.

The solubility of BaSO_4 and SrSO_4 decreases with the reduction in pressure, at high pressure, the pressure effect could shift solubility of the sulphate salts sufficiently to cause a saturated water solution to become supersaturated. This situation can occur when the formation water reaches the wellbore, for example. However, it is unlikely that the pressure drop alone can account for the heavy scaling that often occurs in wells producing from low pressure (> 35 MPa or 5000 psig) reservoirs. Supersaturation is the result of previous mixing of incompatible waters and pressure reduction probably contributes in accelerating precipitation [13]. Moreover, as the

solubility decreases, it was suggested that a drop in pressure, at well bores for instance, can cause and promote barium sulphate scale deposition [14].

2.1.4. Prediction of Barium Sulphate Solubility

In oilfield brines, the barium sulphate solubility increases with the increase of sodium chloride solutions was predicted [15]. The solubility product, K_{sp} , of barium sulphate is the product of the barium and sulphate concentrations in molal units (as shown below).



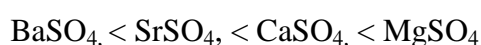
If the product of barium cation and sulphate anion concentrations in an oilfield water of specified sodium chloride concentration is less than K'_{sp} , the water is not saturated with barium sulphate. As a result of supersaturation, if the product $(Ba^{++})(SO_4^{--})$ is more than K'_{sp} for a specified sodium chloride concentration, barium sulphate will precipitate. When one atom of barium precipitates, then it is possible that, one atom of sulphate must also precipitate, and the amount precipitated or oversaturated can be estimated.

The solubility of barium sulphate in distilled water at 25 °C is as low as 0.0023 g/l and starts to increase with temperature and NaCl content; it is less soluble than calcium sulphate of 2.08 g/l and calcium carbonate of 0.053 g/l [16].

2.1.5. Solubility

The solubility of the produced sulphate mineral salts in water (their media of reaction) is the major determination of scaling. As the sulphate salts in complex brine water mixture is the main subject of this work, it is important to understand the solubility effect on their scaling regime at different temperatures. Beside the barite ($BaSO_4$), the solubility of hydrated $CaSO_4 \cdot 2H_2O$ and anhydrite $CaSO_4$ sulphate salt were investigated [17]. The solubility is found to differ but the reason is still not

clearly understood. It was related to the crystal structure and the effect of larger sulphate anion causing a distortion in the complex coordination [18]. This deformation of the complex reduces its ability to accept water at the open ligand site. The inability to coordinate with water changes the solubility property of the formed complex salt. So the increase in solubility is related to the increase in the number of coordination formed between water and ligand sites available in the metallic complex. In addition, the nature of such a complex is also affected by the electronic effects from ionic groups of formed ligands, which bond to metal cations. In terms of solubility, metal salt complexes in oil production are put in order as follows;



Solubility-super solubility diagram, see Figure 2-2, are given elsewhere in literature [19] to show the three zones/states of supersaturation named as stable, metastable and labile. In the stable region (unsaturated) crystallization is unlikely to occur at lower saturation conditions even at higher temperature; in the metastable region, spontaneous crystallization is not likely to take place; and in the unstable, or labile region, spontaneous crystallization is probable and most likely. The growth rate of a crystal depends on the different parameters such as temperature, the solution pH, the degree of supersaturation of the solution and also the concentration of the impurities in the solution. The metastable zone or transient region for sulphate compound (Zinc tris(thiourea) sulphate ZTS was studied [20]. In addition, the pH was found to have a significant effect on this transient state zone, solubility and the induction period, and that was in the presence and absence of phosphate substitutions.

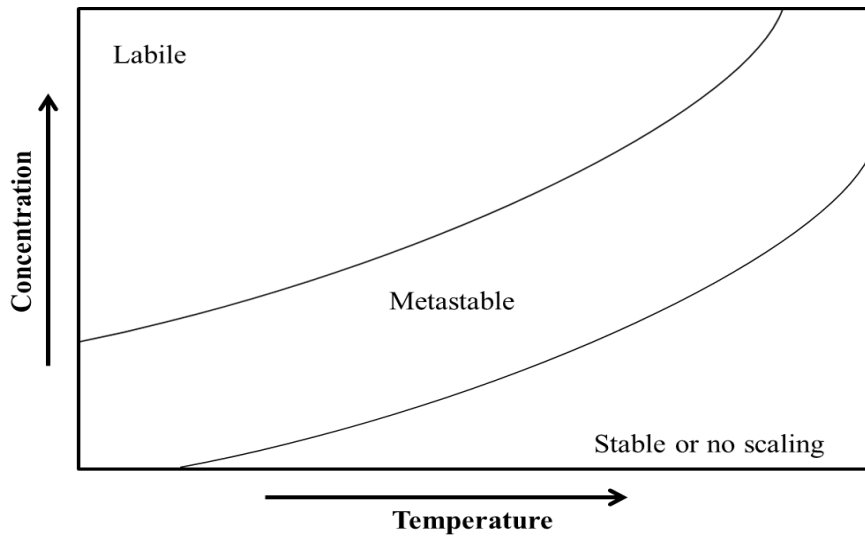


Figure 2-2 : The three zones of saturation [19].

The thermodynamic driving force for the primary crystallization processes, nucleation and growth, is supersaturation level of the reactant species. In the cases of very low solubility of the precipitated substances and for economic reasons, highly supersaturated solutions are used so that the precipitation processes can progress faster. Because of these high supersaturation levels, the associated primary processes nucleation and crystal growth proceed very quickly, at timescales probably below or less than a second. These challenging short timescales are the reason behind why particle formation processes during the early stages of precipitation. Crystallization of sparingly soluble substances are still insufficiently studied and comprehensive studies are undertaken by many research groups.

Due to the relatively high ionic strength in supersaturated solutions which may reach up to 0.5 mol/l, ion activities of the free species instead of concentrations can be used for the calculation of the supersaturation. The activity-based supersaturation (S_a) is defined as follows,

$$S_a = \sqrt{\frac{a_{Ba_{free}^{2+}} \cdot a_{SO_4^{2-}_{free}}}{K_{sp}}} = \gamma_{\pm} \sqrt{\frac{C_{Ba_{free}^{2+}} \cdot C_{SO_4^{2-}_{free}}}{K_{sp}}} \quad \text{Equation 2-9}$$

When $a_{Ba^{2+}_{free}}$ is the activity of free barium cations, an $a_{SO_4^{2-}_{free}}$ is the activity of free sulphate anions and K_{sp} is the solubility product of $BaSO_4$.

Using the given solubility product [21], the mean activity coefficient γ_{\pm} can be calculated as a function of ionic strength.

2.1.6. Transient Period

There must be some time elapsing between the creation of supersaturation and the appearance or detection of a new phase in the system. This is called the nucleation induction period and it is based on the initial supersaturation. During many crystallization processes, the nucleation process is progressing by either primary or secondary nucleation mechanisms. The primary nucleation is referred to as homogenous or spontaneous if the new solid phase is formed without a foreign body or crystallizing material. But when the foreign solid phase is intentionally introduced as an impurity or initial site, the process is called heterogeneous primary nucleation. The width of the metastable (transient period, see Figure 2-3) region decreases in the presence of crystals of the crystallizing material. Such crystals, which are implanted in the system as seeds, are sometimes added intentionally as desired to induce nucleation in highly supersaturated solutions. In such cases, the nuclei are formed due to the secondary nucleation mechanism. Once the nuclei are formed, part of them grow under supersaturation conditions. The others may gradually dissolve via an Ostwald ripening mechanism creating supersaturation which then becomes a source of solute for the growth of the nuclei [22].

The classical theory of nucleation which developed for homogenous nucleation from gaseous and liquid phases is assumed to be applicable also for nucleation from a supersaturated solution. The Gibbs free energy change, ΔG , to form crystal from homogenous supersaturated solution was studied [23].

$$\Delta G = -N\phi + A\sigma$$

Equation 2-10

N is the number of ions or molecules in the crystal, ϕ is the reaction affinity, A is the surface area of the crystal ($A \sim N^{2/3}$) and σ is the surface tension.

The general expression for affinity ϕ is given by

$$\phi = KT \ln\left(\frac{a}{a^*}\right) \quad \text{Equation 2-11}$$

When, K is the Boltzmann's constant, T is temperature, a is the activity of the solute in solution, a^* is the activity of the pure solute in a macroscopic crystal.

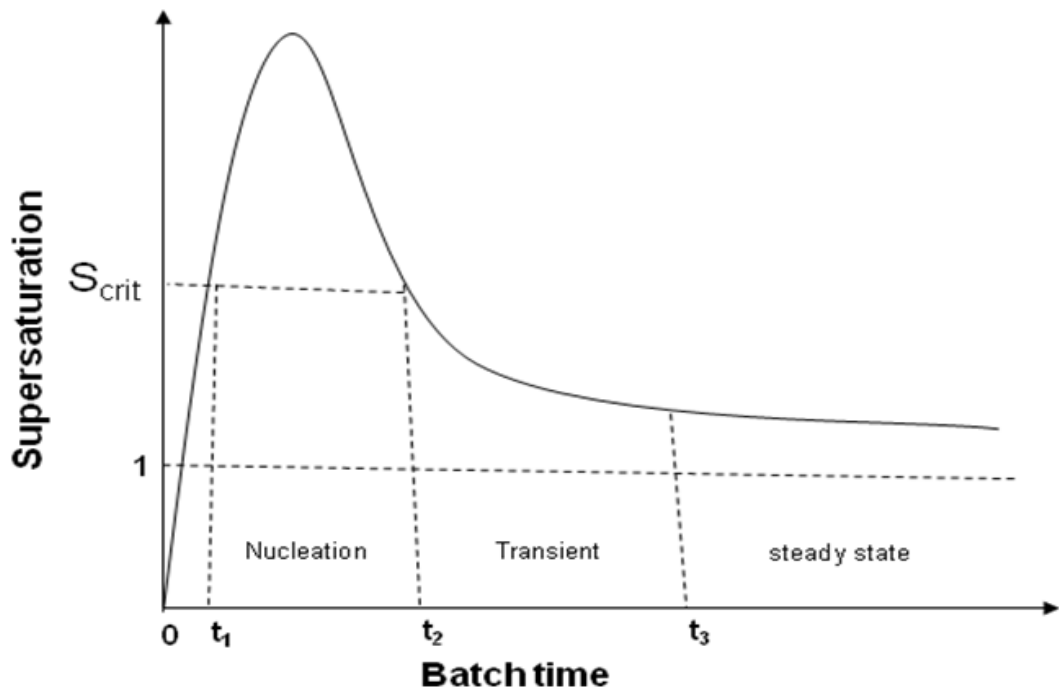


Figure 2-3 : The course of supersaturation ratio (S) through the precipitation process [24].

2.1.7. Factors Affecting Sulphate Scaling

In general, the type of process makes a significant difference in scale deposition requirements. For instance, mixing different waters in the oilfield formations at different conditions, the makeup process in boilers, and membrane processes in desalination involve wide temperature ranges and different water chemistry. On the other hand, there are other processes which involve mineral scale formation with only one type of water such as the evaporation process in seawater distillation. But all of the mentioned processes agree to have a certain level of supersaturation of the reactive particles (free ions). In order for the scaling or precipitation process to take place, the saturation level condition must be reached. This means the equilibrium between the reacted species and the formed solid solutions of a product is exceeded. Thermodynamically, it is referred to as solubility product (K_{sp}).

Since the supersaturation is known to be the primary factor or the driving force for scaling deposition/precipitation, there are other secondary factors that play a major role and contribute in controlling the process rate, contact time...etc. These are temperature, pressure, flow velocity, surface engineering geometry, surface/bulk seeding, pH alterations increases or decreases and probably the chemical properties of the solutes.

2.1.8. Surface Nature

Barite surface deposits are affected by the nature of the surface on which it is deposited. The morphology of the scale formed on different surfaces becomes a focus of active research. The surface scaling kinetics, surface chemical composition, and probably the surface roughness, flow velocity are important factors that affect the crystal's surface alignment and the final arrangements. The surface can either be nucleated to speed the scaling or pre-coated/inhibited by which the nucleation is altered. There are some other factors that can affect the amount of scale formed such as flow rate and temperature. The barite formation is a temperature dependent process and the solubility increases with temperature.

In real oilfield conditions, when a carryover is possible, laboratory work shows that suspended sand particles in a flow stream may introduce a seeding environment (naturally) or crystallization sites. This will not only start the scaling deposition but also speed up the growth rate. The induction time was found to be shorter at elevated temperature in the case of CaCO_3 [25]. When different salts are predicted as a co-deposit, such as magnesium sulphate, it was found that it blocks and retards the possible active sites and may increase the induction period.

2.2. MINERAL SCALE (UNDERSTANDING AND MITIGATION)

Initially, proper scaling assessment starts from the well and involves understanding of the solutions ion composition, properties and reaction conditions. This leads to an accurate thermodynamic scaling tendency prediction and evaluation in terms of its occurrence or not and severity.

The second step focuses on the scale crystal kinetic evaluation in different static and dynamic conditions, followed by the data correlations which result from the three techniques. Once the mineral deposit or/and the precipitate are confirmed, it is important that the scale crystal and its growth are retarded using different available methods, e.g. different types of chemical treatments and/or surface engineering. Figure 2-4 shows the schematic diagram of scale prediction, experimental investigations and prevention schemes in relation to oilfield scale mitigation.

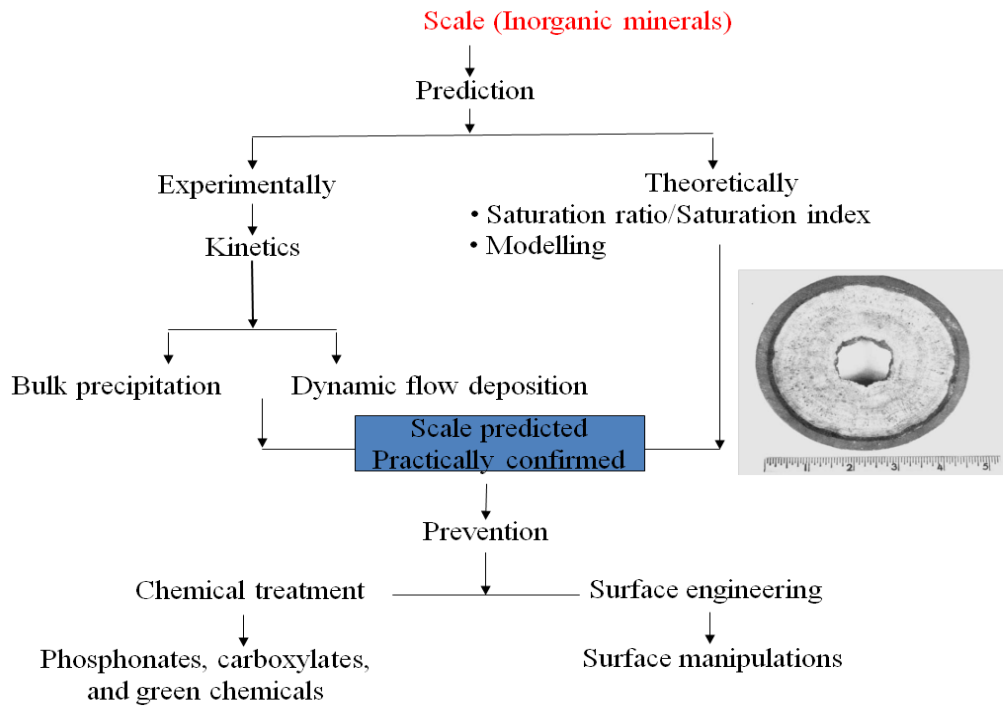


Figure 2-4 : The schematic diagram of scale prediction, experimental investigations and preventions.

2.3. SUMMARY OF INTRODUCTION

The introduction highlights the persistent problem of in oil field formations. It shows that it occurs naturally due to the difference in brine chemistry composition of mixed water. The prediction of common sulphate deposits which exist in the oil field were also explored, and the focus is given to the targeted mineral of barium sulphate. In this part, it is understood that a certain level of saturation conditions must be reached in the brine mixture before solid phase appears. The course of supersaturation change with respect to time through the crystallization process was simplified at the three zones of saturation. The role of solubility as a factor in scaling process was also identified. Other secondary factors that play a major role and contribute in controlling the scaling process rate were also clarified. The steps by which the scale is predicted and the practically confirmed (lab level) followed by its control with chemical products is shown in a chart Figure 2-4.

Chapter 3. THEORY

3.1. NUCLEATION THEORY

In principle, and as a solo parameter, the supersaturation condition is not enough cause for a supersaturated system to begin to crystallize. So this means that none of the supersaturated solutions of barium chloride or and sodium sulphate will induce crystallization in separate form (before mixing). In this case, the condition of crystallization must be fulfilled before crystals can develop; it is simply represented in invisible embryos/nuclei which act as centres of crystallization. The construction process, which occurs very rapidly, can only continue (to a stable phase) in local regions of very high supersaturation. Many of the embryos or 'sub-nuclei' fail to achieve maturity. They simply redissolve back into the solution as they are extremely unstable. So it is vital that the born nuclei grow beyond the critical size to become stable and grow to its final shape.

In general, a crystallization process can spontaneously take place as in some chemical reactions. But on the other hand, it can also be induced and stimulated artificially as in the case of solution seeding or using external influences. The latest was first implemented by Yong in 1911 [26]. Fifty years later, incident light (with energetic waves) was also used to stimulate the crystallization as an influenced external simulators e.g. ultra-violet light, X-Rays, sonic and ultrasonic irradiations [27].

3.2. NUCLEATION KINETICS AND TERMINOLOGY

The understanding of the terms which are used to explain different concepts of kinetics are very important. In this regard, the nucleation nomenclatures are set into two initial categories to simply avoid the confusion in terms:

- Primary nucleation; this is related to nucleation in systems that do not contain crystalline matter.

- Secondary nucleation; this is related to the creation and formation of nuclei in the vicinity of crystals present, induced on purpose, in a supersaturated solution.

3.2.1. Primary Nucleation

Primary nucleation is considered the first step in the crystallization process in systems that do not contain crystalline matter (spontaneous crystal formation). It can be simplified as an *instantaneous* formation of a new crystal. On an industrial scale, a large supersaturation driving force is necessary to initiate primary nucleation. The initiation of primary nucleation via this driving force is not fully understood, which makes it difficult to model. Practically, experiments are still the best guide. In crystallization kinetics, the primary nucleation is divided into two categories namely; homogeneous and heterogeneous nucleation.

3.2.1.1. Homogeneous Nucleation

In practice, the kinetic investigation studies of homogeneous nucleation were done earlier in the bulk solution [28]. However, the main difficulties were the preparation of a system free from impurities, which might act as nucleation centres, and these centres behave as catalysts to speed up the process. This intervention may also be expected from the reactor smooth surface which is hard to eliminate.

The empirical approach could assume the homogenous nucleation as the presence of impurities cannot be accurately estimated, but that is not the case in experimental practice when an impurity-free system is virtually impossible. Besides, this discrepancy is extended to include the dependability of formed particle size on the supersaturation level in the case of the classical theory. So far these differences have not been resolved due to the fact that the experimental investigation of true homogenous nucleation is difficult and far from reality. Extensive work in this regard has been done to overview the different types of nucleation kinetic processes [29-35].

Besides the presence and absence of foreign matter in the crystallizing solution, agitation is frequently used to induce crystallization. This factor is known to influence the whole process in bulk precipitation or in the case of turbulent flow for surface deposition. Most agitated solutions nucleate spontaneously at lower degrees of supersaturation due to the expected super solubility; this means that the width of the metastable zone is reduced.

However, the influence of agitation on the nucleation process is probably very complex. It is generally agreed that mechanical disturbances can enhance nucleation, but it has been shown that an increase in the intensity of agitation does not always lead to an increase in nucleation [36, 37]. As a matter of fact, gentle or mild agitation causes nucleation in solutions that are stable, and vigorous agitation considerably enhances nucleation.

3.2.1.2. Heterogeneous nucleation

Heterogeneous nucleation occurs much more often than homogeneous nucleation. It applies to the phase transformation between any two phases of gas, liquid, or solid, typically, solidification from liquid. Moreover, heterogeneous nucleation forms at preferential sites such as phase boundaries, surfaces (of capillaries, coils, container, bottles, etc.) or impurities. At such preferential sites, the effective surface energy is lower, thus diminishing the free energy barrier and facilitating nucleation. An example model is give in Figure 3-1.

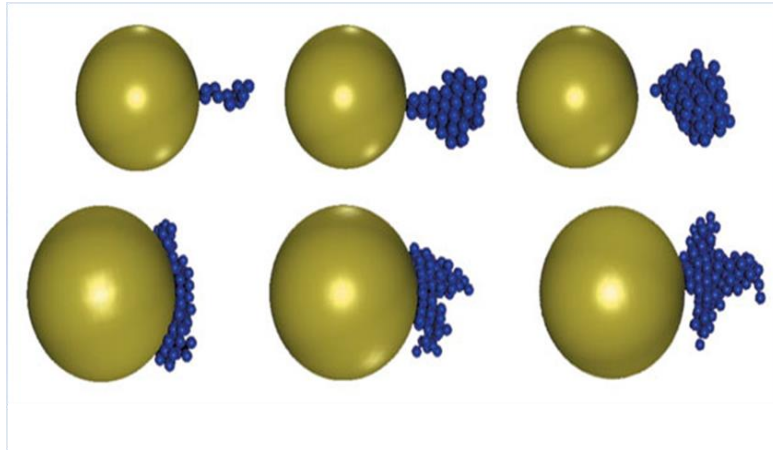


Figure 3-1 : Heterogeneous nucleation model in presence of trace foreign particles [38].

In this case, surfaces promote nucleation because of wetting – contact angles greater than zero between phases facilitate particles to nucleate. The free energy needed for heterogeneous nucleation is equal to the product of homogeneous nucleation and a function of the contact angle θ [39]:

$$\Delta G_{\text{heterogeneous}} = \Delta G_{\text{homogeneous}} * f(\theta) \quad \text{Equation 3-1}$$

The barrier energy needed for heterogeneous nucleation is reduced; Figure 3-2, the wetting angle determines the ease of nucleation by reducing the energy needed. The rate of nucleation of a solution is considerably affected by the presence of trace amount of impurities in the system. However, an impurity that may acts as a nucleation accelerator in one case may not necessarily be effective similarly in another.

Generally, solutions, which are normally prepared in the laboratory, may contain $>10^6$ solid particles per cm^3 of sizes $< 1 \mu\text{m}$. It is virtually impossible to achieve a solution completely free of foreign bodies. These active foreign particles are called heteronuclei, they may be reduced to almost a half by filtration but they cannot be completely eliminated from the media. So in this case, the homogeneous nucleation is not a common event.

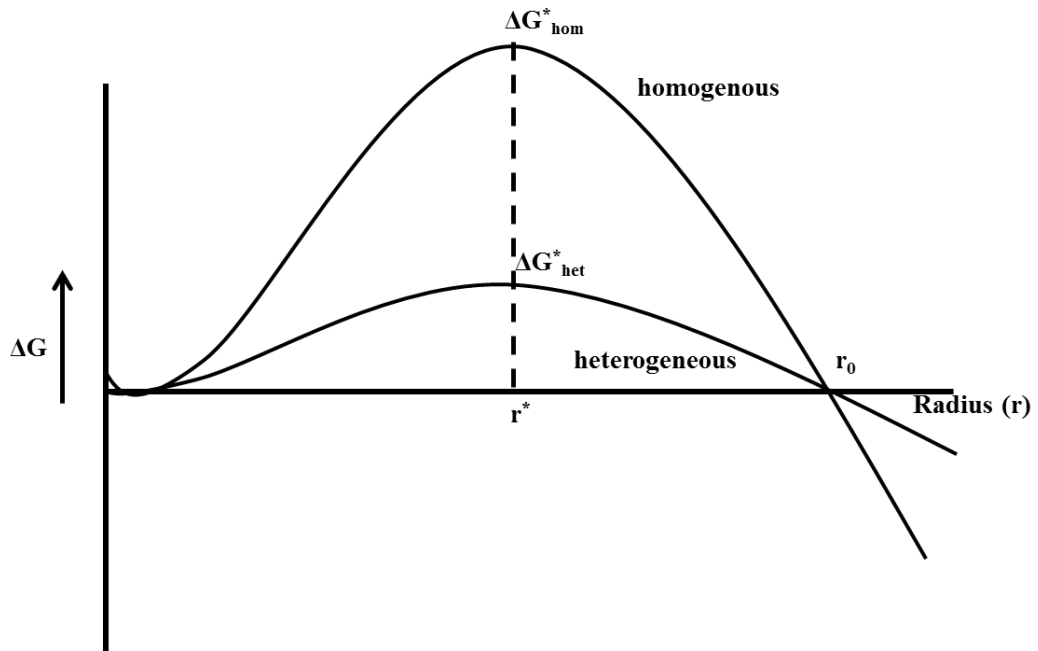


Figure 3-2 : The reduction of the energy barrier needed for heterogeneous nucleation [38].

Beside the absolute temperature and supersaturation. It was mentioned earlier that the energy as interfacial tension, (γ), is another important parameter which governs the nucleation process. Figure 3-3 shows an interfacial energy diagram for three phases in contact; foreign solid surface – liquid (γ_{sl}), solid crystalline – liquid (γ_{cl}), and the energy between the solid crystalline phase and the foreign solid surface (γ_{cs}). These energy forces can be represented as;

$$\gamma_{sl} = \gamma_{sc} + \gamma_{cl} \cos \theta \quad \text{Equation 3-2}$$

$$\cos \theta = \frac{\gamma_{sl} - \gamma_{sc}}{\gamma_{cl}} \quad \text{Equation 3-3}$$

So, the angle (θ), the angle of contact between the crystalline deposit (c) and the foreign solid surface (s), corresponds to the angle of wetting in liquid-solid system.

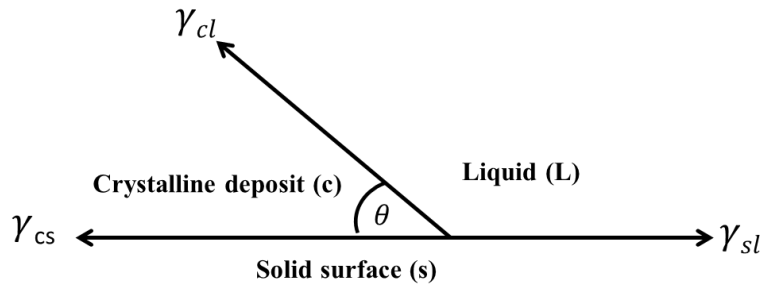


Figure 3-3 : Interfacial tensions at the boundaries between three phases (γ_{sl}), (γ_{cl}), (γ_{cs}).

3.2.2. Secondary Nucleation

Secondary nucleation is just another type of nucleation, which takes place in lower supersaturated solutions in the presence of crystals of the solute which are deliberately added. This terminology is found to distinguish it from the early explained *primary* nucleation. It has to be clearly stressed that the main difference is that the secondary nucleation involves the existence of foreign particles. They are to enhance the crystallization process or control the product shape and size.

Early work (1935) in this area was first to show a sulphate salt nucleation, at moderate supersaturation solutions, in the presence of seed crystals [40]. In flowing liquids, the fact that the transitional boundary layer in the integrated crystal units could be dethatched from the crystal surfaces is due to the flow dynamic [41]. This was later proven when a moving crystal in a stream of supersaturated solution passes in the vicinity of a proposed stationary crystal to create nuclei at a detectable size [42]. This work on the secondary nucleation was followed by several review studies in the literature [43, 44]. In the case of agitated bulk or static conditions, the fluid shear became a factor in the nucleation mechanism for generating embryos (sub-nuclei), which develop into stable nuclei with time when swept into regions of high supersaturation [45]. The contact of a stirrer, for instance, could also cause what is called a contact nucleation. Crystal-agitator contacts are also prime suspects for causing secondary nucleation in a crystallizer. This principle is related to the ability of crystals to penetrate the fluid boundary layer by the stirrer. So the crystals may

overcome these forces and come in direct contact with the stirring device. The probability of such an impact is directly proportional to the rotational speed of the agitator [46]. If the comparison is made, it was proven that the crystal-crystal contacts have five times nuclei in comparison with its contact with other objects during crystallization (stirring bar or vessel wall) [47]. Furthermore, statistically, the faster growing faces produced fewer nuclei than the slower growing faces; this was another indication of the connection between secondary nucleation and the crystal growth process [48].

Earlier, the classical theory of nucleation was extracted from research work which was done on vapour. The role of the total energy in micro and submicron of the molecular condensations were studied [49, 50]. The solid solution and crystal formations were also investigated.

Therefore, in the case of homogenous nucleation, the free energy changes associated is considered as follows;

$$\Delta G = \Delta G_s + \Delta G_v \quad \text{Equation 3-4}$$

$$\Delta G = 4\pi r^2 \gamma + \frac{3}{4} \pi r^3 \Delta G_v \quad \text{Equation 3-5}$$

The overall excess free energy, ΔG , between small solid particles of solute (spherical of radius r) and the solute in solution is equal to the sum of the surface excess free energy, ΔG_s , i.e. the excess free energy between the surface of the particle and the bulk of the particle, and the volume excess free energy, ΔG_v , i.e. the excess free energy between a very large particle ($r = \infty$) and the solute in solution. ΔG_s , is a positive quantity, the magnitude of which is proportional to r^2 . In a supersaturated solution ΔG_v is a negative quantity proportional to r^3 [51].

ΔG_v is the free energy change of the transformation per unit volume. γ is the interfacial surface tension, which is represented by the energy between the developing crystalline surface and the supersaturated solution in which it is located. The two terms in the previous relation depend on different values of radius r . The maximum value of ΔG - the formation free energy - will then vary with respect to the radius $\left(\frac{d\Delta G}{dr}\right)$ until it reaches to its critical value r_{crit} . It will result in nucleus for spherical cluster at critical size.

Once the value of $\left(\frac{d\Delta G}{dr}\right)$ is equal to zero at a maximum of the nuclei's critical size, the above relation can be written as

$$\left(\frac{d\Delta G}{dr}\right) = 8\pi r\gamma + 4\pi r^2\Delta G_v = 0 \quad \text{Equation 3-6}$$

The free energy diagram for crystal formation is similar to the molecular formation potential energy in nature, which explains the lowest energy and its stability. The energy of formation seems positive whereas the formed particles become only stable when the energy is at a minimum (negative). So the relation, which links the critical size r_c of a particle to the free energy change of the transformation per unit volume ΔG_v , becomes negative;

$$r_c = -\frac{2\gamma}{\Delta G_v} \quad \text{Equation 3-7}$$

When in stable conditions, ΔG is a negative quantity according to the free energy graph;

$$\Delta G_{crit} = \frac{16\pi\gamma^3}{3(\Delta G_v)^2} = \frac{4\pi\gamma r_c^2}{3} \quad \text{Equation 3-8}$$

Generally, in supersaturated solutions, the freshly formed/generated solid crystallites in solid solutions would act based on their size. This imposes a condition that the formed particles must exceed their critical size to reach the stability state and continue to grow. On the other hand, those particles or crystals may redissolve back into the solution if their size is smaller than the critical size. It was assumed that particles smaller than r_c will dissolve, or evaporate if the particle is a liquid supersaturated vapour. This is the only way the particle can achieve a reduction in its free energy. Similarly, the particles, which are larger than r_c , will continue to grow. The continuity of the growth involves the decrease in the free energy of the particle. The critical size r_c , therefore, represents the minimum size of a stable particle [51].

3.2.3. Factors Affecting the Nucleation Process

The actual critical free energy of formation (ΔG_{crit}) is elusive to be determined if other important parameters, such as temperature and pressure, are not considered. This energy is necessary to form a stable nucleus.

At constant temperature and pressure, the distributed energy level within a fluid system would not have to be constant in all parts of the system. The inconsistency of this energy level would result in energy fluctuation with higher and lower saturations. Moreover, in those supersaturated regions, where the energy level rises temporarily to a high value, nucleation will be favoured.

3.2.4. Nucleation Rate Concept

Nucleation rate is considered one of the most important terms in scale kinetics. The nucleation process, in some cases, is a thermally activated process. In this case, the rate of nucleation, J , e.g. the number of nuclei formed per unit time per unit volume, can be expressed in the form of the Arrhenius reaction equation. It is commonly used for the nucleation rate evaluation:

$$J = A \exp\left(-\frac{\Delta G}{KT}\right) \quad \text{Equation 3-9}$$

Where K is the Boltzmann constant, the gas constant per molecule ($1.3805 \times 10^{-23} \text{ JK}^{-1}$), it represents the value of the gas constant (R) divided by the Avogadro's number (N).

The gas constant (R) = $8.314 \text{ JK}^{-1} \text{ mol}^{-1}$.

Avogadro's number (N) = $6.023 \times 10^{23} \text{ mol}^{-1}$.

At this stage, the other important variable is introduced namely; the saturation ratio (S). As a result of the particle size solubility effect, solution compositions may exceed the normal equilibrium saturation value (S) and become supersaturated. So in this case, if the excess solute particles that are usually dispersed in the solution are thinnest or below the r_c in size, they tend to redissolve back into the solution. The relationship between particle size and solubility was originally derived for vapour pressures in liquid-vapour systems. Lately it was applied for the solid -liquid systems[52, 53], according to;

$$\ln \left[\frac{C(r)}{C^*} \right] = \frac{2M\gamma}{vRT\rho r} \quad \text{Equation 3-10}$$

Where $C(r)$ is the solubility of particle size of radius (r), C^* is the normal equilibrium solubility of the substance, R is the gas constant, T is the absolute temperature, ρ is the density of the solid, M is the molar mass of the solid in solution and γ is the interfacial tension (surface interfacial energy) between the solid particles in contact with the solution.

So, the Gibbs -Thomson relationship for a non-electrolyte may be written;

$$\ln S = \frac{2\gamma v}{kTr} \quad \text{Equation 3-11}$$

Where S is defined by the previous relation and v is the molecular volume; this gives the following value of the free energy change as a function of the particles volume.

$$-\Delta G_v = \frac{2\gamma}{r} = \frac{KT \ln S}{v} \quad \text{Equation 3-12}$$

From equation (3.8)

The change of the free energy at critical size of a particle can be;

$$\Delta G_{crit} = \frac{16\pi\gamma^3 v^2}{3(KT \ln S)^2} \quad \text{Equation 3-13}$$

According to equation (3.9), the rate of nucleation is;

$$J = A \exp \left[-\frac{16\pi\gamma^3 v^2}{3K^3 T^3 (\ln S)^2} \right] \quad \text{Equation 3-14}$$

Therefore, it can be concluded that, and according to this relation, there are three main variables which govern the rate of nucleation; absolute temperature, T , the degree of supersaturation, S , and interfacial tension, γ or the energy between the solid particles and the solvent.

The geometrical value $\frac{16\pi}{3}$, which represents the spherical shape is subjected to change based on the particle's shape and size.

Since earlier, the nucleation process has been studied and widely discussed in terms of classical theories of nucleation, which is based on Gibbs and Volmer

thermodynamic approaches. Although these approaches were subjected to further investigations later, the problem still arises since all of these theories depend on the interfacial tension (or surface energy, γ). This means that in the case of clusters near the critical size of a formed nucleus, the Gibbs-Thomson equation cannot be implemented as the relation takes into consideration the formation of an individual particle.

3.2.5. Nucleation Induction Time

Similar to the classical theories of homogeneous nucleation, the empirical findings facilitates the concept of a clustering mechanism of reacting molecules or ions. Theoretically, in order to understand the nucleation process, it is vital to explore the relationship between the induction period, t_{ind} , (the time interval between mixing two reacting solutions and the appearance of crystals) and the initial concentration, c , of the supersaturated solutions [23].

$$t_{ind} = KC^{1-\rho} \quad \text{Equation 3-15}$$

Where K is a constant, and ρ is the number of molecules in a critical nucleus. It was suggested that the induction period may range from microseconds to days depending on the supersaturation. It represents the time needed for the assembly of a critical nucleus.

As the nucleation rate J is defined as the number of nuclei N emerging in a time period t_n , which is the formation time of the critical nucleus.

$$J = \frac{N}{t_n} \quad \text{Equation 3-16}$$

The nucleation kinetics of barium sulphate has been the subject of different research groups [54, 55] under stoichiometric conditions when the free ion ratio ($R = 1$) when R is represented by the following relation.

$$R = \frac{C_{Ba^{2+}}^{free}}{C_{SO_4^{2-}}^{free}} \quad \text{Equation 3-17}$$

The nucleation rate equation for the heterogeneous and homogeneous regions is explained as;

$$J_{het/hom} = J_{max,het/hom} \cdot e^{\left(\frac{A_{het/hom}}{\ln^2 S_a}\right)} \quad \text{Equation 3-18}$$

When $A_{het/hom}$ = kinetic factor in nucleation rate expression, $J_{max,het/hom}$ = pre-exponential factor.

The ion activity was found more reliable for representing the supersaturation as the activity of ions is different depending on the surrounding environment. It is worth mentioning that the use of concentration-based S_c supersaturation instead of activity-based S_a supersaturation may lead to different slopes in the nucleation data due to different values expected for the interfacial energy γ_{cl} [56].

3.2.6. Crystal Growth

The crystal growth process is considered to take place within two steps: first, it is the diffusional transport of building units to the surface and the second is the integration of these units into the crystal lattice. Actually, the slower process of the two determines the overall kinetics of the precipitation. In this case the crystal growth of barium sulphate can be considered as diffusion or transport-controlled/diffusion at high supersaturation. Therefore the kinetic process expression for growth rate is given [10]. Figure 3-4 shows the proposed growth mechanism stages of crystals,

after nucleation, small nano-crystallites are produced which are responsible for the later aggregative growth.

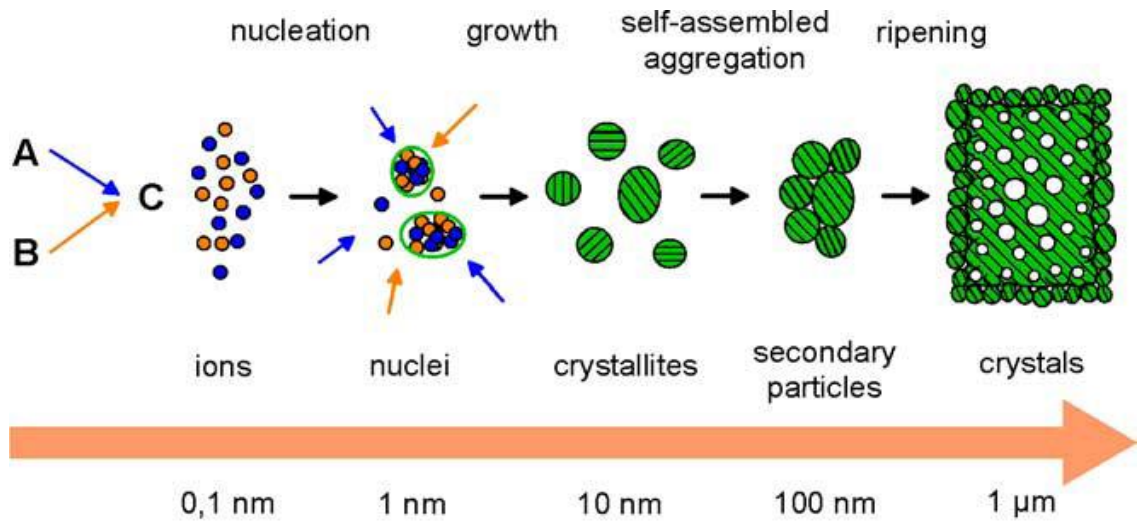


Figure 3-4 : Schematic diagram of the proposed growth mechanism [57].

3.2.7. Induction Period

During the past decade, measurements of the induction time have been used broadly to study the nucleation process. The induction time t_{ind} represents the sum of the time necessary for the critical nucleus to be formed, t_n , and the time this nucleus needs to grow to a visible size t_g .

$$t_{ind} = t_n + t_g \quad \text{Equation 3-19}$$

The term, t_r (relaxation time) is sometimes added to the right hand side of the above equation to achieve a quasi-steady state distribution of cluster structure in a system. The relaxation time depends on the system viscosity and diffusivity.

On the other hand, the induction time, t_{ind} , is frequently used to estimate the nucleation time either in the bulk or surface precipitation. It is defined as the time elapsed between the creation of a supersaturated solution and the first appearance of

a new crystalline solid phase. Ideally, it is a nuclei with the critical cluster size dimensions. In other words, it is a time delay between attainment or achievement of supersaturation and the detection of the newly created crystal or bigger clusters in a solution. It is a complex process which involves both the nucleation and growth components to be completed. However, as the induction time is determined experimentally, it may also include growth to a detectable size once the nuclei are formed. If it is assumed that the nucleation time is much greater than the time required for growth of crystal nuclei to a detectable size, then the induction period is inversely proportional to the primary nucleation rate (J) as shown in the following equation [58].

$$t_{ind} = \frac{1}{J} \quad \text{Equation 3-20}$$

So the primary nucleation rate (J in nuclei/cm³.s) is represented by the following;

$$J = A \exp \left[-\phi B \frac{\gamma^3 v^2}{(K_B T)^3 (\ln S^2)} \right] \quad \text{Equation 3-21}$$

When, A is the pre-exponential factor related to the efficiency of collision of the ions or molecules, K_B is Boltzmann constant (J/Kmol), T is absolute temperature (K), v is volume of solution (m³).

3.3. SUMMARY OF THEORY

This part summarizes the theory behind the scale precipitation and deposition kinetics concepts and terminologies. The main factors, which effect the deposition reaction kinetic, were highlighted. These include the main thermodynamic driving force of saturation ratio, temperature, agitation, solution/surface condition in order for the crystallization process to take place. It is now known that the nucleation process can be initialized by either a higher level of supersaturation or existence of foreign particles added deliberately (heterogeneous nucleation) to the system. The nucleation process is a thermally activated process. The rate of nucleation, J , is

considered as the number of nuclei formed per unit time per unit volume. It is also represented as the number of nuclei emerged in a time unit.

It is also important that the relationship between the induction period, t_{ind} , and the initial supersaturation of a solution is well understood. The induction period may range from microseconds or minutes to days depending on the level of supersaturation and other factors mentioned earlier.

Finally, the growth of the formed crystal is considered to take place either through the diffusional transport of building units to the surface or the integration of new formed units into the crystal lattice.

Chapter 4. LITERATURE REVIEW

This section highlights the contributions of other researchers in this area in relation to kinetic aspects of scaling. The dynamic technique of studying scale is also presented. This section may be simplified as follows;

- Dynamic techniques for scaling.
- Ions in complex brines.
- Induction time and SR.
- Early stages of crystal formation.
- Flow rate influences.
- pre crystallization of surfaces.

4.1. DYNAMIC TUBE BLOCKING

In the oil industry, inorganic mineral scale deposits such as barium sulphate BaSO_4 are considered a major and persistent problem. The frequent occurrence of barite can have an effect on the flow assurance during oil and gas production. It results in unscheduled shutdown of a system. In the aged oil reservoir, the water cut increases and oil percentage decreases. In order to enhance the oil productivity, the secondary oil recovery (SOR) process is implemented. During the SOR process, unavoidable mixing of supersaturated brines rich with divalent cations (Ba^{2+} , Ca^{2+} , Mg^{2+} , & Sr^{2+} - formation water) with surface or seawater brine (rich in anion radicals of $-\text{SO}_4^{2-}$) generates a highly supersaturated brine mixture. The generated supersaturated mixture is known as a driving force for barite formation process. Similarly, these types of inorganic scaling are widely acknowledged in the reverse osmosis units when this technology is applied to the surface, ground and sea water sources [10].

Earlier investigations on the barium sulphate system have shown that the crystal growth and dissolution of barite are surface controlled when the heterogeneous nucleation is avoided [17, 18]. It was also suggested that the barite kinetic is

influenced by both diffusion and surface integration processes [59]. In literature, there is considerable work, which was carried out using the tube blocking test technique (TBT), Figure 4-1, to assess the sulphate and carbonate scaling tendencies at higher temperature and pressure. Those investigations were done in the absence and the presence of chemical additives [60, 61]. As a matter of fact, there is still limited data available explaining systematically the effect of a wide range of temperatures on the barite surface deposition kinetics in dynamic flow systems. The mitigation of predicted formed scale is based on which phase formation (nucleation or growth) is to be retarded. Its determination has to be precise for proper selection of inhibitor.

Most of the work which was done in this regard basically relies on the change of the differential pressure across a long coil in the presence/absence of different scale inhibitor chemicals. Moreover, the quick change in the differential pressure may lead to a misleading kinetic assessment as the scale formed scattered along the longer capillary. In addition, in the previous dynamic investigation work, the surface profiles of the deposited scale crystals from dynamic flow were not broadly and properly investigated. Surface observation, which is difficult in the case of coils, has the potential to give information of what is happening on the surface in terms of the crystal shape, surface coverage as well as the final growth morphology. In addition, using coil, the effect of the additives on the crystal morphology could not be easily identified although the effect on the formation of scale can be assessed.

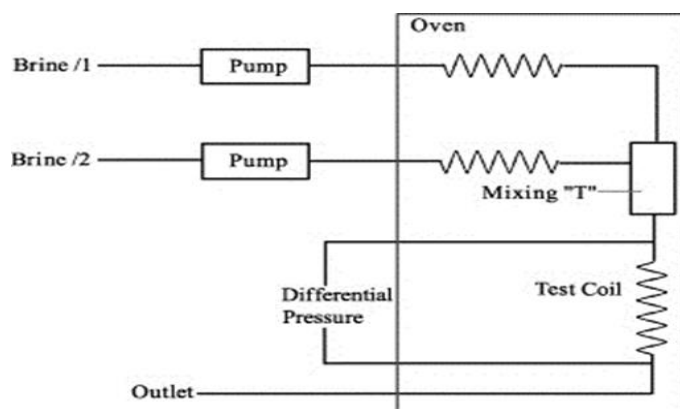


Figure 4-1 : Typical tube blocking test rig with coil using differential pressure tool, Dyre [60].

Dynamic tube blocking test (TBT) experiments actually examine and investigate the scale growth kinetics and inhibition mechanisms within micro-bore tube or a coil under dynamic flow conditions, Figure 4-2. An applied back pressure can be used in the experimental conditions [62-66]. This gives the dynamic tube blocking tests an advantage over conventional static bulk jar techniques, which are adapted and coded on the NACE standards TM 0197-97 [67] and TM 0374-2010 [68].

The dynamic tube blocking technique enables the study of scale growth and inhibition performance mechanisms in real field conditions at temperatures higher than 100 °C and also at higher pressures up to 5,000 psi. Intensive research work was carried out to rank different chemical inhibitors and/or explore the kinetic studies of different mineral scale deposits at different conditions [69, 70]. The TBT technique represents the field flow mixing condition, but this technique has no standard or NACE coded yet. This technique was criticized for having a very short residence time in coils (under 10 seconds). Moreover, the chance for scaling at the time of mixing is not enough for deposition to take place, while the bulk jar test can run for longer time. The bottle test has application limitations in pressure, temperature below 100 °C, and pH. The dynamic technique has advantages of controlling all the relevant parameters of pressure and temperature [71].

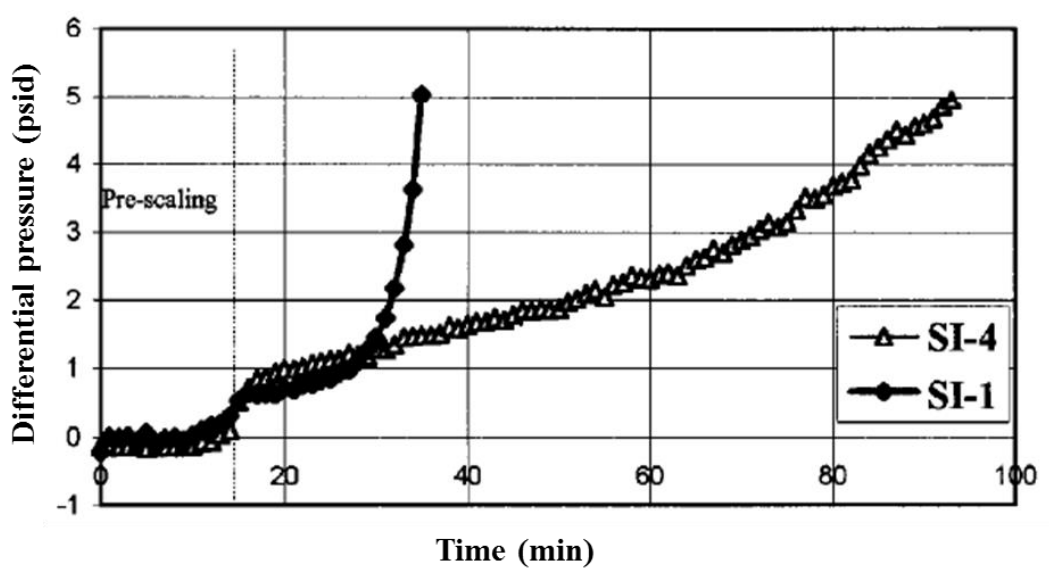


Figure 4-2 : Inhibitor ranking under influence of pre-scaled surfaces using TBT and real field brine [64].

In a dynamic system, it was reported that an average of 37 nm particle sizes were prepared using a developed micro channel reactor. The barite nanoparticle size, size distribution and morphology were investigated and found strongly dependent on the flow rate of the reactants solution into this reactor. It was also noticed that the average particle size decreases with the increase of the flow rate and reactant concentration [72].

The differential pressure measurement aspect has been used to investigate the mechanism of oilfield mineral scale deposition kinetics in a dynamic system. In addition, it is also used to rank different scale retardants and study their efficiency [73]. The dynamic technique is also used to estimate the blank time, which represents the ratio of the time needed to block the tube in the presence of an inhibitor to the time needed to block the tube in an inhibitor free system. The effectiveness of the fluid flow rate and the test tube dimensions were also explored.

Dynamic tube blocking tests were also used in terms of a core in order to study the permeability and the scaling tendencies of carbonate and sulphate. The reduction of the core pores as a function of time was monitored and evaluated by pressure drop across the testing sections [74], Figure 4-3 is shown as an example.

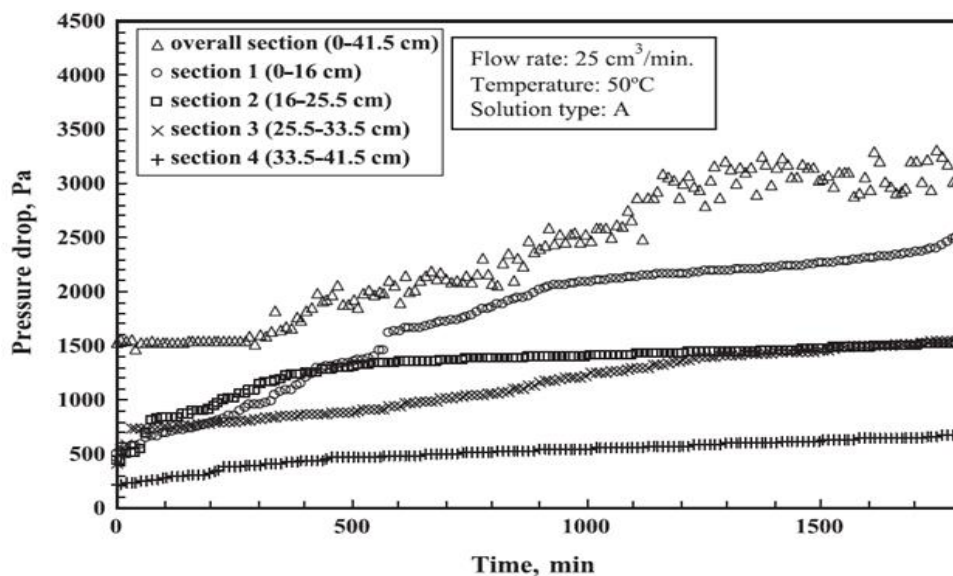


Figure 4-3 : Pressure drop across a porous media as a function of time in calcium sulphate system [74].

The technique was developed to simulate the subsea gas/condensate hydration using methylene ethylene glycol (MEG). The point was that the conventional dynamic tube blocking (DTB) does not allow the CO₂ gas to be present at the mixing point. This would result in higher pH and then higher scaling [71]. In 2010, Vishwanatham and co-workers [75] have studied a minimum concentration requirement of a green inhibitor (pteroyl-L- glutamic acid). The differential pressure technique was used at 1 ml/min flow, 50:50 mixing ratio and 110 °C. The inhibitor concentration was reduced stepwise while monitoring pressure changes. The performances of different phosphonate inhibitor were examined based on the differential pressure measurements in dynamic test. It was at high temperature and pressure in sulphate and carbonate rich environments [60]. The barite kinetics was studied at high temperature (0 - 200 °C) in presence and absence of inhibitors. It was done by monitoring the pressure change over a micrometre sized - inline filter and a reaction coil of 240 cm in length and 2.15 ml in volume. The aim was to develop a mathematical model to evaluate an inhibitor efficiency of bis-hexamethylene triamine-penta methylene phosphonic acid (BHPMP). This was in presence of hydrate inhibitors such as methylene ethylene glycol (MEG) for barite scale control. It was found that using the MEG may have a significant role in avoiding negative effects on the inhibition process. The consistencies of observed and calculated induction time were investigated and the relationship of precipitation kinetics of barite as a function of temperature and saturation index was established [76].

4.1.1. Tube Blocking Technique Review

In the literature, a wide range of studies have been performed using a dynamic flow technique (sometimes called tube blocking test method). Statistically, the coils or/and tubes are used based on the nature of the experiment and application. It facilitates the real field flow and mixing criterion systems on its own or when it is combined with other techniques. The dynamic system is combined with radiotracer technology to investigate the calcite CaCO₃ deposition kinetics in sand packs in terms of scale deposit distribution and induction time [77]. Moreover, various solid solution suspensions are used in dynamic flow phases to investigate the mechanisms by which a precipitate reduces permeability of porous medium [74].

The harsh reservoir conditions were modelled using a dynamic flow system to investigate the effect of increasing temperature and pressure on barium sulphate and calcium carbonate scale formation. The effect of temperature on scaling tendency was more significant than that of pressure [60].

The testing cell was modified to different materials and dimensions and has lead recently to novel *in-situ* studies of different mineral scale (sulphate and carbonate formation and inhibition) and its inhibition [78, 79]. A glass flow cell was used in conjunction with the Laser Raman Spectroscopy to record the *in-situ* growth of mixed barium and strontium sulphate scale on the 316 stainless steel surface. As a time dependent experiment, Raman spectroscopic measurements were recorded at 45 second intervals for 10 minutes [80]. The scale film thickness was also investigated in the presence of Ca^{2+} and Mg^{2+} in the barium - strontium system. Figure 4-4 shows the effect of these ions upon the uninhibited growth of scale. For Ba^{2+} and Sr^{2+} solutions, the most rapid scale growth occurred in the absence of Mg^{2+} and Ca^{2+} .

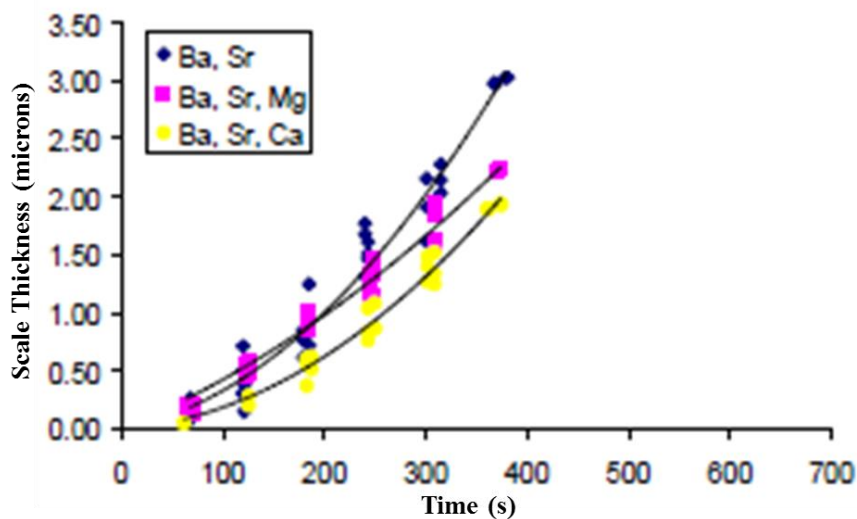


Figure 4-4 : The influence of Mg^{2+} and Ca^{2+} ions on scale thickness growth of barium – strontium system [80].

The kinetic scale prediction model was combined with results from a thermodynamic model to investigate the CaCO₃ influence in downhole scaling environment. The influence of flow velocity and pressure were also revealed. The results show that scaling rates decrease slightly with increasing pressure, but the differences are not significant. Results from the tube blocking tests performed at different flow velocity values, show that the calcium carbonate scaling rate sharply increases with increasing flow velocity [81]. The scaling rate in this study was determined from the time required to block the tube and the thickness of the scale. The time required to block the tube includes the combined time for nucleation and crystal growth.

Physically, scaling rate measurements using weight difference (immersed plate, in this work the capillary was part of the system) were used as an offline measurement to validate an inline scaling monitoring evaluation. The offline scaling rate was calculated, based on weight difference and deposition time, according to the following equation [82]:

$$S. R_{\text{offline}} = \frac{MT_{\text{dep}} - M_0}{T_{\text{dep}}} \quad \text{Equation 4-1}$$

where MT_{dep} is the mass of the metal plate at the time of deposition, T_{dep} and M_0 is the mass of the metal plate when $T_{\text{dep}} = 0$, T_{dep} is the time of deposition.

On the surface using a flow dynamic system, the early nucleation surface can be monitored using a differential pressure sensitive tool. The online scaling weight monitoring techniques, based on the piezo electric effect system namely a quartz crystal microbalance (QCM), was also used [83].

According to statistics through a decade, more than 70% of the scale kinetics studies on surfaces or in specified porous media were done using tubes/capillaries for different purposes. This may give an advantage over coil system. The scale quantification and uniformity build up on the internal surface of the specimen is

most likely to be evaluated more precisely in tubes. Some work, which was done with different testing cells and dimensions within the last 10 years, has been tabulated in Table 4-1 and Table 4-2.

Table 4-1 : Dynamic flow technique statistics.

Study S.No	Workers	Year	Type of cell		Differential pressure	Comment
			Tube	Coil		
1.	E. Stamatakis <i>et al.</i> [77]	2006	Sandpack	✗	✓	⁴⁷ Ca tracer
2.	J. Moghadasi <i>et al.</i> [74]	2004	SS porous media	✗	Pressure monitoring not ΔP	CaCO ₃ , SO ₄ kinetics
3.	G. M. Graham <i>et al.</i> [60]	2002	✗	✓	✓	SI vs. Bulk & Surface
4.	T. Chen <i>et al.</i> [78]	2006	✓	✗	<i>In-situ</i> X-Ray	Silicon cell
	T. Chen <i>et al.</i> [79]	2006	✓	✗	<i>In-situ</i> X-Ray	Scale kinetic
5.	E. Mavredaki <i>et al.</i> [84]	2011	✓	✗	<i>In-situ</i> X-Ray	SS cell
6.	S. Vishwanathan <i>et al.</i> [75]	2010	✗	✓	✓	Green inh. Evaluation
7.	Y. Zhang <i>et al.</i> [81]	2001	✗	✓	At room temp. & pressure	Flow velocity effect
8.	B. Tolaieb <i>et al.</i> [85]	2013	✓	✗	✓	BaSO ₄ Surface kinetic
9.	Wylde J. Jonathan <i>et al.</i> [80]	2001	✓	✗	<i>In - situ</i> Raman	Ba,SrSO ₄ kinetics

Table 4-2 : The dimensions of the cells used based on Table 4.1.

Study no.	Coil/Tube capillary dimensions		
	Length mm	ID mm	Comments
1.	600 (Tube capillary)	60	<i>Pressure drop along the tube.</i>
2.	580 (Tube capillary)	32	<i>Pressure drop along the tube.</i>
3	1000 (Coil)	0.85	<i>Differential pressure</i>
4. & 5.	9.4 (Tube capillary)	1	<i>Surface crystallization development</i>
6.	1000 (Coil)	1	<i>Differential pressure</i>
7.	1000 (Coil)	1	<i>Surface crystallization development</i>
8.	10 (Tube capillary)	1	<i>Differential pressure</i>
9.	(Tube capillary)	-	<i>Surface crystallization development</i>

4.2. ROLE OF IONS IN COMPLEX BRINES

Complex formation and sea water brines consist of multiple ions that co-precipitate or deposit with the lowest soluble components. This may also alter the course of the crystallization by inhibition or acceleration of the whole process.

In barium and strontium scaling systems. It was found the most rapid scale growth occurred in the absence of Mg^{2+} and Ca^{2+} . Although the addition of Mg^{2+} decreases the rate of growth, this observation was considered to be a consequence of Mg^{2+} and Ca^{2+} ions competing with the Ba^{2+} and Sr^{2+} ions for the free sulphate ($-SO_4^{2-}$) ions in the solution [80]. In the presence of a metal surface, the broad statement that Mg^{2+} ions poison inhibition whilst the Ca^{2+} ions enhance inhibition was confirmed. It has been shown that the formation of inhibitor-cation complexes leads to surface effects on deposition process.

In the same system (Ba, Sr) at room temperature, with an extended equilibration period (years), the precipitation reaches a reversible point with the aqueous solution. In addition, a single solid – solution phase does not actually control the aqueous Ba^{2+} and Sr^{2+} concentrations. The substitution of Sr^{2+} into a solid solution phase with the BaSO_4 components never allow the thermodynamic equilibrium with the aqueous phase [86].

In literature, it was found that the existence of foreign ions seems to affect both the scale formed on the metal surface and precipitation formed in the bulk solution. Mg^{2+} ions, for instance, were found to inhibit the bulk precipitations much greater than in the case of surface deposition. It shows that the bulk precipitation and surface deposition are two different processes with two different mechanisms [87, 88]. Alternatively, these Mg^{2+} ions may incorporate into a formed scale crystal causing a lattice strain and inhibit the crystal growth [89]. It was also found that the differences in the behaviour of barium sulphate precipitation occur depending on the cation present (sodium or calcium). It is believed to be due to calcium incorporation into the lattice, which increases the internal energy of the crystal. In addition, calcium adsorbs on the crystal surface and poisons BaSO_4 crystal growth [90]. Hennessey et al. [91] highlighted the effect of calcium at very high supersaturation. They also concluded that the presence of calcium cations increases the solubility of barium sulphate. The effect of calcium which is incorporated in barium sulphate crystal was confirmed, Figure 4-5.

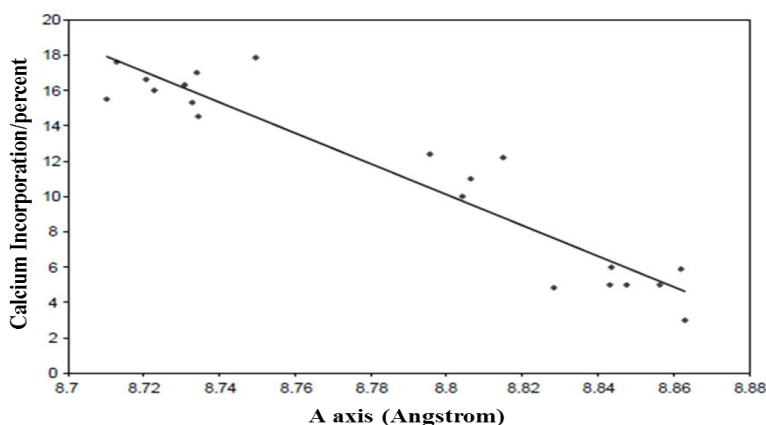


Figure 4-5 : Linear relationship between lattice dimensions and calcium content for the a-axis of barium sulphate [91].

4.3. INDUCTION TIME AND SR AT CONSTANT TEMPERATURE

A period of time usually elapses between the attainment of supersaturation and the appearance of crystals, this time lag, is generally referred to as the induction time, t_{ind} . It is considerably influenced by the level of supersaturation (SR). Moreover, the influences are extended to the state of agitation, presence of impurities, viscosity, flow, temperature and residence time in dynamic systems.

So this means that different external factors may have an effect on the induction period, it cannot be regarded as a fundamental property of a system. This complexity makes it difficult to be fully relied upon to give basic information on the process of nucleation. Nevertheless, the induction time has frequently been used as a measure of the nucleation event. It can be considered to be inversely proportional to the rate of nucleation (J) [51].

At constant temperature, which in this part of current research was lately fixed to 75 °C. Published experimental data show that the $\log t_{ind}$ vs. $(\log SR)^{-2}$ relation at constant temperature is linear for a large number of substances. These data vary from a readily soluble crystallites, when the rates of nucleation in supersaturated aqueous solutions, of potassium dihydrogen orthophosphate (KDP) was investigated [92]. It was found that the nucleation rate increases with supersaturation, temperature and agitation. In 1971, Kirkova [93] studied the crystallization kinetics of moderately soluble zinc oxalate crystal ($ZnC_2O_4 \cdot 2H_2O$) at 25 °C and at different super saturations. The specific surface energy at the crystal-solution interface critical nuclei dimension were investigated. The sparingly soluble, e.g. $BaSO_4$, $SrSO_4$, $BaCO_3$ and $PbSO_4$, were also studied when homogeneous nucleation followed by diffusion controlled crystal growth. It was observed in a range of highly supersaturated solutions. The induction period decreases from 1 to 10^{-4} second, and the number of particles found per cm^3 increases from 10^7 to 10^{12} with increasing concentration [94, 95].

4.4. SURFACE DEPOSITION AND BULK PRECIPITATION – EARLY NUCLEATION

Once the reacted solutions are carefully filtered prior to mixing, the resulted bulk precipitation solution is considered a homogenous process (foreign body free system). On the other hand, the surface deposition counterpart process, formed on the metal surface, is regarded as a heterogeneous crystallization process. The metal surface may introduce foreign solid and affect the rate of deposition, shape and size of deposited crystals.

Scale crystallizations kinetics of surface deposition and bulk precipitation are known to have completely different mechanisms. In bulk as well as on surfaces, initial nucleation assessment is taken place at very early stages with sub micro size crystals, which develop to the growth size. This can be performed differently based on the technique in use. In combined bulk and surface for instance, the surface scale coverage percentage can be assessed, and the deposited elements are quantified with time intervals [96]. Chen has shown the relation between three different saturation ratios of calcium carbonate system. It was found that the SR has a huge effect on the surface coverage in the early stages of surface nucleation using rotating disk, Figure 4-6.

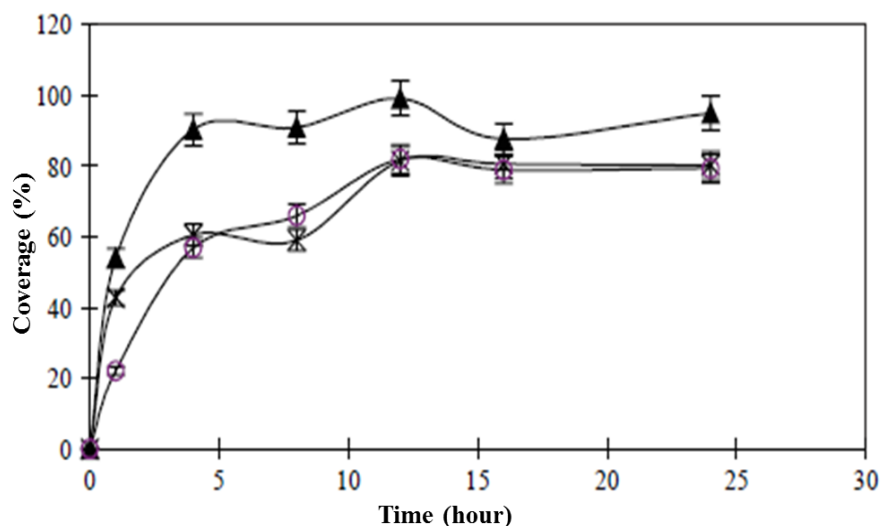


Figure 4-6 : Surface deposition coverage (%) with respect to time using their different solution composition [96].

4.5. TEMPERATURE FACTOR ON BARITE FORMATION KINETICS

Various work focuses on investigating surface nucleation and growth on metal surfaces. It was carried out in order to investigate and understand the relationship between crystal heterogeneous nucleation and its growth on surfaces.

In the oil industry, the mineral scale formation and deposition on downhole and surface production equipment takes place at two different environments of solutions thermodynamic properties. This is in terms of changeable saturation ratios, temperature, pH, pressure and the partial pressure of CO₂. So the location and time at which the scale is deposited/precipitated in any system must be kinetically predicted and practically determined [83]. Collins has shown the predicted barium sulphate nucleation time as a function of temperature, Figure 4-7. It was noticed that the barium sulphate nucleation should occur within a time frame of one to few second.

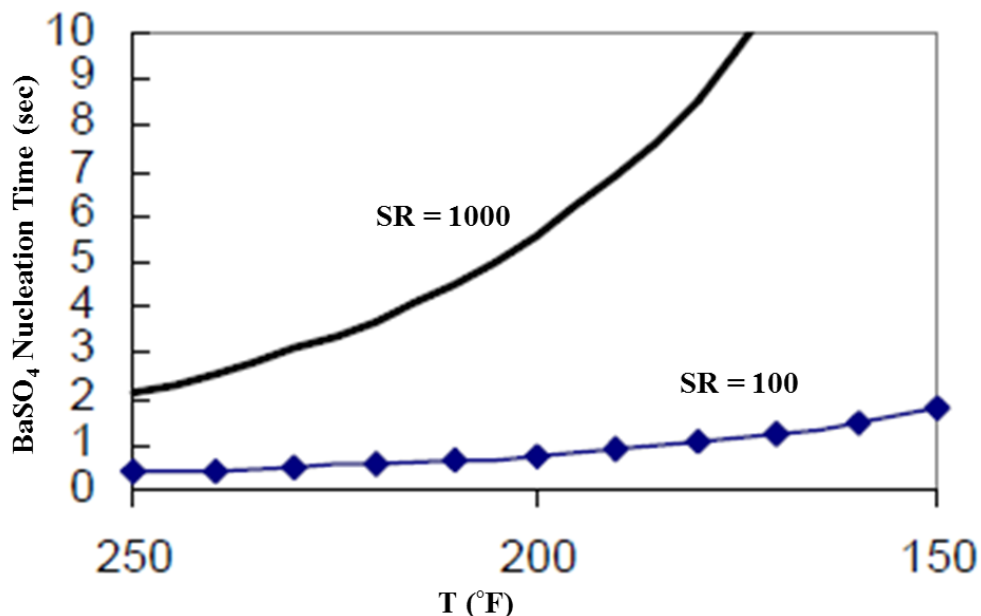


Figure 4-7 : Predicted barium sulphate nucleation time as a function of temperature [83].

In principle, once the supersaturation level is reached in the brine mixture, it is thought that the scale surface deposition in dynamic flow takes place due to a combination of both bulk precipitation and surface deposition. So as the flow propagates with time, the nucleation and growth may occur in the bulk solution stream (homogenous). The formed crystals increase in size then transfer to the surface to commence a further growth in heterogeneous form.

Besides the supersaturation, the crystal growth and nucleation rates can depend on a number of factors including static/dynamic conditions and temperature. The temperature varies as high as 95 °C - 75 °C in the reservoir through 50 °C – 40 °C at the topside production facilities. The scaling environment may become cooler at deep water reservoirs (3 °C – 5 °C at seabed). This, in fact, may help the design and setup of a lab experiment modelling the actual practice. At elevated temperature, the reservoir rock permeability damage and scaling crystal morphology were found to be influenced by sulfate supersaturation and scaling ion concentration in the brines [97]. In the presence of solid surfaces, the flux of barium ions (Ba^{2+}) can be calculated based on the difference between the actual ions concentration and their concentration at equilibrium [98].

The barium sulphate scale formation and inhibition as a function of temperature, ranging from 95 °C to 23 °C was investigated. It was found that, for a given brine, barium sulphate scaling tendency increases significantly as temperature decreases. The much lower barium solubility at 5 °C, subsea environment for instance, suggests that a produced water may become oversaturated with barium sulphate as temperature cools (SR is higher).

4.6. DYNAMIC FLOW AND ITS INFLUENCE ON CRYSTALLIZATION

Inorganic scale (carbonate, sulphate and sulphides) formation can be predicted from thermodynamic models which have been developed over recent years. However these models have not been able to predict the possible location of scale deposition (in field condition) in a system. The brine flow conditions vary in terms of it being turbulent or laminar [99, 100].

Only a few studies can be found that take into account the effect of the flow regime and velocity on the precipitation process [101-103]. However, all those studies focus mostly on the kinetics of the precipitation process and not on the induction time itself. For instance, frequent flow pulsation was applied for the placement of calcium phosphate (through the *in-situ* precipitation within the granular stratum or sand layers) to consolidation the formation. It was obtained by alternating injection and mixing of two aqueous solutions of calcium chloride and potassium phosphate [104].

Recently, at two different temperatures and therefore different supersaturation using static tests, it was found that the turbulence at certain locations in a system increases the likelihood of scale barium sulphate scale formation. It was also proven experimentally that the increased turbulence also has an impact on the minimum scale inhibitor concentration required to prevent scale [105].

In porous media, the flow rate variations may compare the precipitation, which results from the supersaturated solution, with the deposition/precipitation induced by the pressure decay through the dynamic flow [106]. Based on the mass conservation of both barium and sulphate species, it was assumed that each species is advected with the flow. The interface between the two fluid components (dispersive and diffusive mixing) of fluids leads to *in-situ* precipitation [107].

Similar applications of dynamic tube blocking tests (using 1 meter coil) performed at different flow velocities show that the calcium carbonate (CaCO_3) scaling rate sharply increases with increasing flow velocity. The low flow velocity range shows a relative stability [72]. The particle size distributions of the BaSO_4 nanoparticles are given in Figure 4-8. It can be found that the average particle size decreased with the increase of the flow rate. The possible reason is that an increase of the flow rate results in both the increase of the supersaturation (responsible for smaller average size) and improvement the mixing (responsible for uniform size distribution).

In the case of inhibited flow targeting calcite deposition retardation, the complexes of physico-chemical effects occur in the presence of additives in the flow. The influence of the flow configuration on the inhibitory effect of an additive was revealed [108]. The enhancement of precipitation under mixed flow conditions at relatively low residence times is due to the shorter induction period occurring under mixed flow conditions. When the induction period is not taken into account, plug flow conditions are shown to provide more rapid precipitation at practically all levels of flow [109].

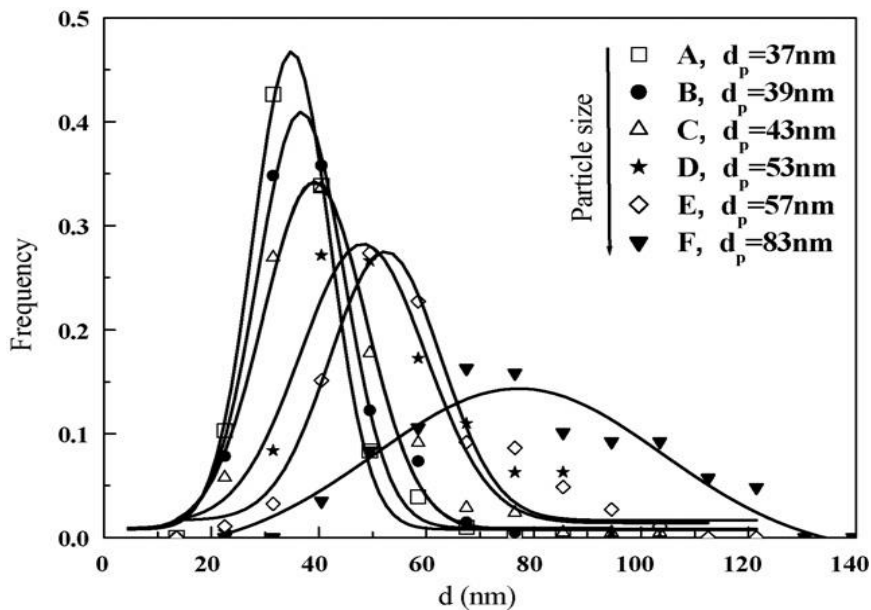


Figure 4-8 : Size distribution of BaSO_4 particles prepared at different flow rates of BaCl_2 and Na_2SO_4 solutions [72].

4.7. SCALE SURFACE DEPOSITION THICKNESS

In this area of scale studies, a model was developed to gain a better understanding about wall deposit thickness development in a capillary with respect to the pressure drop across it. A well-known Hagen–Poiseuille equation was used. The deposition of asphaltene was monitored by imaging the capillary tube and by measuring the pressure drop across it. A model was developed to relate the pressure drop to the change in the thickness of the deposited layer and subsequently to the change in radius r .

$$r = R \left(\frac{\Delta p_i}{\Delta p_t} \right)^{0.25} \quad \text{Equation 4-2}$$

When r is the radius after time t .

R initial radius of a capillary.

ΔP_i and ΔP_t are the pressure drop at 0 time and after time (t).

The model indicates that the thickness varies as one over the fourth power of the pressure drop [110]. In 2000, Broseta et al. investigated the deposition rate of asphaltene as a function of pressure, temperature and different fluid compositions by measuring the pressure drop over the length of a stainless steel capillary [111]. It is assumed a homogeneous layer of deposits.

4.8. SEEDING (BULK OR SURFACE)

Seeding is one of the best methods to induce crystallization in supersaturated solutions. It takes place mainly in bulk precipitation by the addition of small particles of the material to be crystallized. Deliberate/or intentional seeding is frequently employed in industrial crystallization to effect a control over the product yield, size and size distribution. Seed crystals, however, do not necessarily have to consist of the material being crystallized in order to be effective. In open to air industrial vessels, particles are unintentionally found in the system. They may serve

to prevent the crystallization of thermodynamic unstable phases, e.g., hydrates. Thus it was reported that the nucleation rate is independent on the number of the seeded particles added to the solution [69].

Regarding the nuclei critical size (the size that the nuclei must reach to grow further), It was reported by different scientists that the crystal size had to reach 220 μm [112] and others estimated it to be 200 μm [113].

The impurities could work as foreign body (initiators) for the secondary nucleation. It is not only the solution that can be nucleated but also the surface in a dynamic process. Graham and co-workers [60], used the tube blocking technique for the scale deposition process using lower sulphate brine. The nucleation was indicated by the differential pressure measurements up to 0.5 psid to give a desired surface nucleation. In other words, it is called pre-scaling and can be the key to evaluating the scaling kinetics process on nucleated and non-nucleated surfaces.

4.9. CHEMICAL APPLICATION AND TREATMENT

The control and inhibition of crystal growth are a major concern in several contemporary technologies. It is well-known that the oil formation rocks frequently contain alkaline earth metal ions, such as barium, calcium and in some cases strontium. During chemical treatment, these cations comes in contact with chemical additives to scale-inhibitor complex. In this process, inhibitor's phosphonate groups complex with cations to minimize the chance to complex sulphate ions and form mineral scales.

4.9.1. Inhibition Mechanisms

Scale inhibitors (SI) which are used in the oil and gas industry do function by many different mechanisms under certain conditions. Various chemical products are used either to reduce, delay, and even retard/eliminate the risk of scale forming within the production facilities. The two main classes of SIs are Polymeric species (e.g. PPCA, PVS, VS-Co etc..) and smaller phosphonate molecules (e.g DETPMP, NTP, HMDP, HMTMPMP etc.). Polymeric scale inhibitors usually function *mainly* through nucleation stage for nucleation inhibition (NI) mechanism, and perform best over short residence times. Phosphonates, on the other hand, function as a crystal growth retardation (CGR) mechanism and perform best over longer residence times. No scale inhibitor functions exclusively through only one type of mechanism – both mechanisms are always involved but to different extents [114]. There are many ways which have been proposed and experimentally proven for the inhibition mechanism, Figure 4-9. Generally, the inhibitors have the ability to act as:

- Anti – precipitants such as phosphonates.
- Sequesterants.
- Dispersants.
- Chelating agents e.g. EDTA.
- Crystal modifier, such as Nitrilo tri acetic acid (NTA).

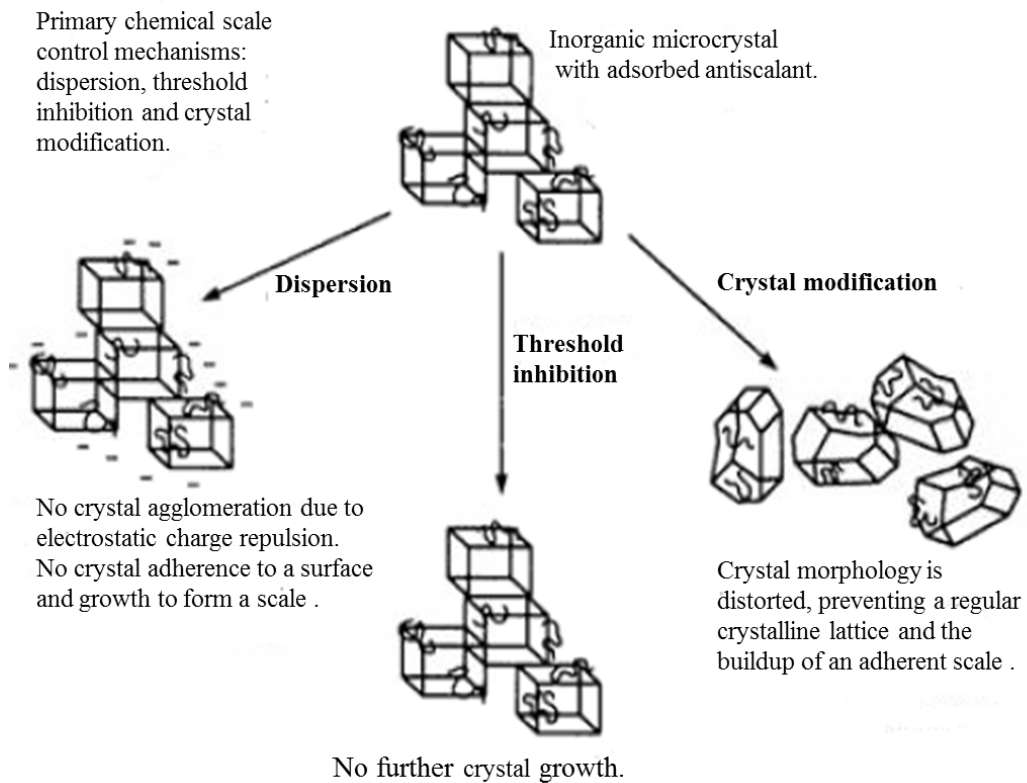


Figure 4-9 : Schematic diagram for crystals inhibition mechanisms [115].

Moreover, most of the recognized scale retardants are thought to alter the crystal morphology with the exception of some sequesterants, such as ethylene diamine tetra acetic acid (EDTA) and Nitrilo tri acetic acid (NTA). Although there was a lot of work undergone in this area, the question is how this alteration in crystal size and shape affects the over whole adhesion of barite to surface? This mechanism is not well-understood yet.

In general, scale inhibitors, based on their functionality and inhibition mechanism performance within the environment, can be characterized into two categories; thermodynamic inhibitors and kinetic inhibitors. The thermodynamic inhibitors are known to act either to decrease the ionic activity product by lowering the pH of the solution. They also chelate with the positively charged metal ions existing in the media such as Ca^{2+} , Ba^{2+} , Sr^{2+} and Mg^{2+} . Ethylene diamine tetra acetic acid (EDTA), for instance, is a well-known thermodynamic inhibitor for barite. So in this

case, EDTA will work as a chelating agent to reduce the Ba^{2+} cations concentration in a solution ready to precipitate in the crystallization process. The solution supersaturation decreases as a result of forming an EDTA complex with barium free cations.

On the other hand, kinetic inhibitors work differently. These inhibitors adsorb onto a crystal surface and prevent the lattice ion incorporation into the growing lattice to form a final crystal. For the sake of comparison, the kinetic inhibitors do have an advantage over the thermodynamic ones; which is the amount needed for the inhibition process. Very small amount of the kinetic inhibitor is needed to block the growing surface of a crystal, the kinetic inhibitor is also called threshold inhibitor. It is related to the amount needed of the retardant to inhibit scaling process mechanism.

The threshold scale inhibitors are phosphonates e.g. diethylene triamine penta methylene phosphonic acid (DETPMP), poly acrylates, and poly maleates. In addition, polymeric scale inhibitors are long chain polymers e.g. poly acrylic acid polymer (PAA), polyvinyl sulphonate (PVS), and phosphino poly carboxylic acid (PPCA). The two mentioned types of scale inhibitors have been used to control the scale deposition and precipitation since 1936 [116]. In the solution (in which the anti-scalant and divalent alkali earth metal cations are present) complexes can be formed between the free radicals of the positive and negative species. In the case of Ca^{2+} or Ba^{2+} , metal ions act as central atoms of a ligand. Coordination stability between the Ca^{2+} , Ba^{2+} cations radicals, compared to the commonly used ligands of transition metals, are much lower. This is because these species provide no outer free shell electrons for the split d-orbital. So, instead of coordination, an interaction between the adsorbed anti-scalants and the surface of metal ions are dominated by the electrostatic force [117].

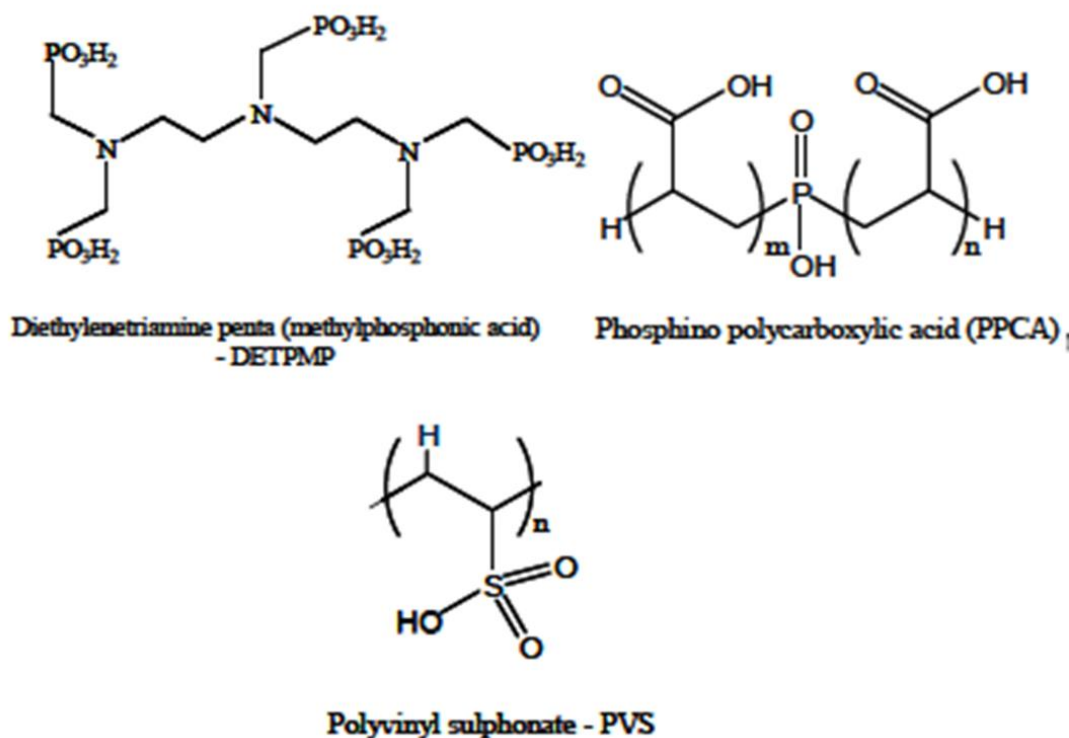


Figure 4-10 : The chemical structure of commercial scale inhibitors with different functional group as anti-nucleation (PPCA, PVS) and anti-growth (DETPMP).

The most commonly used anti-growth inhibitors of the sulphate or carbonate crystals are poly phosphonates, Figure 4-10, of which the most widely studied are diphosphonates [118, 119]. Phosphorous-containing derivatives are sometimes used in higher concentration to act as sequesterants for potential scale forming cations. It is thought that it takes place through the replacement of the sulphate group by phosphonate groups in the barium sulphate crystal. The inhibition prevents further deposition of inorganic material on the particular face. Both barium sulphate BaSO_4 and calcium carbonate CaCO_3 scales may be prevented using different products of inhibitors.

Both of these mechanisms are consistent with the inhibition of mineral scale at “threshold” levels, typically at (minimum inhibitor concentration (MIC) = (0.5 – 20 ppm) [120]. It was proven in detail that the inhibitors can be used as blend inhibitors when PPCA and DETPMP were studied as individual inhibitors and combined

[121]. It was noticed that the blend inhibitors of both products have a greater inhibition efficiency and induction time. Scale inhibitors can reduce the tendency for crystallization or completely prevent scale formation and growth by disrupting the thermodynamic stability of growing nuclei. It causes the dissolution of the nucleated scale and/or interferes with the crystal growth process, resulting in blocking of the growing sites [122].

4.9.2. Inhibitor Efficiency (IE)

There are well-known numbers of factors that affect the inhibitor efficiency (IE) of scale inhibitor against barite (BaSO_4) formation; the main factors are pH, temperature and the calcium/ magnesium levels in the brine mixture. The inhibitor efficiency determinations, by which the inhibitors are ranked, usually fall under two well-recognized categories and are described in details elsewhere [123]; static inhibition (bottle or jar) test and dynamic (tube blocking) test.

Barium sulphate growth modifier using tri functional group molecules varying from the tri phosphonate to the tri carboxylate were studied. The purpose was to substitute one functional group of phosphonate ($-\text{PO}_3^{2-}$) with another functional group of carboxylate ($-\text{COOH}$). This helps minimize the overall changes of the additives. It was concluded that the nitrile tri acetic acid (NTA) in which the three phosphonic groups were replaced by carboxylate groups, for instance, shows an inhibition of barium sulphate precipitation. But only at much higher concentrations. In addition, the resulted barite spherical crystal particle suggest that the morphology control is due to some surface adsorption process, and gives the uniformity of the particles. it further suggests that this adsorption *is equal on all faces*. Moreover, it was noticed that the nature of the particles was mono-disperse, once again implying a uniform surface interaction.

The NTA is said to behave as a ‘universal face-binding agent [124], Figure 4-11. Coveney *et al*, 2000 has used the term ‘coined’ to describe the phenomenon [125]. A series of aromatic carboxylate of benzoic acid were used as a crystal growth inhibitor or modifier to investigate their effect on both calcite and barite

precipitation. In general, additives on barite are assumed to act via the so-called “lattice matching” effect, [118], [125], [126], while recently, it was suggested that a simple charge density correlation exists with calcite inhibition or modification [127-130].

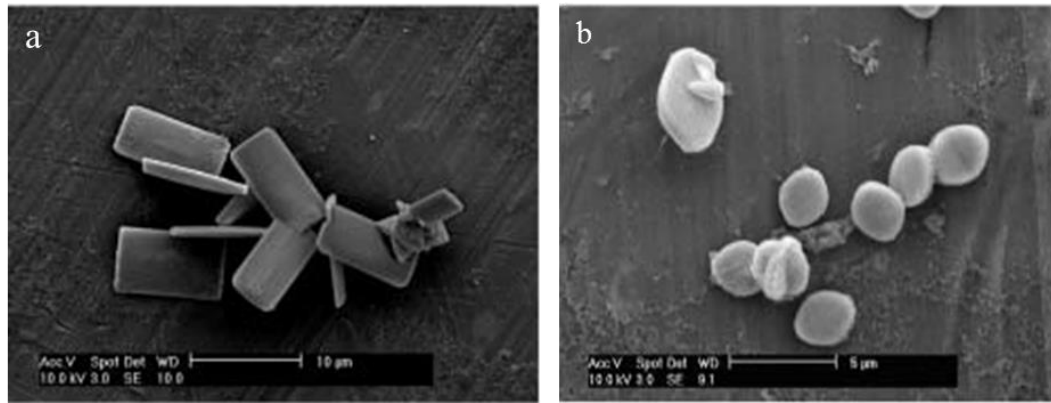


Figure 4-11 : Barium sulphate particles obtained in the presence of (a) no additives (control), (b) 0.026 mM of nitrile tri acetic acid (NTA) [124].

4.9.3. Inhibitor Thermal Stability

The additional factor for the scale inhibitors evaluation is the thermal stability of these products at high temperature and pressure of harsh formation conditions. The possible thermal decomposition of scale inhibitor chemical chains significantly reduces the inhibition efficiency, as the polymer would break to smaller molecular weight molecules [131], [132]. The degradation and hydrolysis could happen in the functional group itself, which is supposed to be responsible for binding. The above mentioned types of thermal degradation will reduce the adsorptivity of the inhibitor onto reservoir rocks. In 2003, A review shows that PVS was the most thermally stable inhibitor product and was not degraded at 200 °C. It was stable at different pH values while DETPMP was rapidly degraded at lower temperature of 175 °C, whereas the stability of PPCA was dependant on the solution pH [133].

4.9.4. Surface Reactions

Phosphonates are known as effective chelating agents, which are used in different industrial applications. Phosphonates are broadly used to minimize and control the corrosion process in water purification systems [134-136]. As surface active lubricants, they are also used in rolling steel and in polymer mixes to improve and enhance the adhesion of plastics and rubber materials to steel [137]. In addition, self-assembly monolayer technique is used to study the phosphonates behaviour on oxide surface of SS 316L. The acids of alkyl phosphonic acid are covalently bound to the surface as phosphonates in a bidentate manner. It was determined by diffuse reflectance Fourier transform infrared spectroscopy (FT-IR) and X-Ray photoelectron spectroscopy [138].

Phosphonate-metal oxide interactions have been studied on surfaces other than steel and the interaction or bonding mode varies among different surfaces studied. The interaction was reported to be monodentate [139-141], and the possible bidentate interaction was also investigated [136], [142]. Furthermore, phosphonate-metal interactions were confirmed in tridentate manner [136], [143, 144], Figure 4-12. The bonding of silicon with surface active phosphonates was also studied [136], [145, 146].

The effect of the number of carboxyl groups on the adsorption behaviour of low-molecular-weight substances on a stainless steel surface were investigated as a function of pH and the ionic strength of the solution. The temperature condition was just 5 degrees above the room temperature. It was concluded that the carboxylic acids having plural carboxyl groups had much higher affinity to the surface. They were adsorbed in both reversible and irreversible modes, while the monocarboxylic acids such as benzoic acid and *n*-butyric acid were reversibly adsorbed on the stainless steel particles. Both reversible and irreversible adsorptions were considered to occur through the electrostatic interaction between negatively charged carboxyl groups and the positively charged sites on the surface [147].

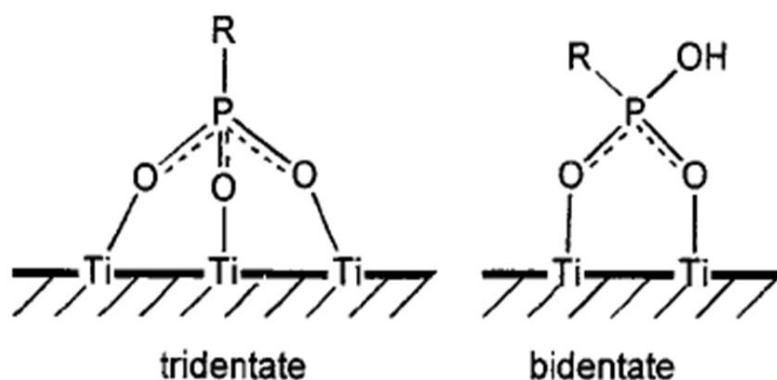


Figure 4-12 : Schematic representation of the main bonding modes of diethyl phosphonate molecules on a TiO_2 surface [143].

According to IUPAC definition, the chelating involves coordination of more than one sigma-electron pair donor group from the same ligand to the same central atom. Their adsorptions are described to be very strong to most of the mineral surfaces. This behaviour distinguishes them from the corresponding amino carboxylate, which shows a weaker interaction with mineral surfaces, especially near a neutral pH of 7 [148]. Different adsorbent interactions were investigated using phosphonates such as with calcite [149] and with barite crystals [118]. One of the trends of this study is to investigate the behaviour and BaSO_4 kinetics on a chemically pre-treated steel/carbon steel surfaces. As these phosphonates or inhibitors dissociate in water by hydrolysis, part of the molecules chelate with the early stages of formed crystals or even at ion level. These ripen crystals have also advantages to bind to the surfaces with the negative charge of carboxylic group. Although the phosphonate - steel interaction has been immensely important in industry, the nature as well as the details of that interaction is not well- recognized and characterized.

Generally, the effect of a series of phosphonate molecules on barium sulphate precipitation have been investigated in terms of the degree of inhibition. It was found that not only the number of phosphonate group results in increasing the inhibition of barite. In returns, the low number of the phosphonate groups does not imply inhibition at all. It was also found that there are other factors to effect the inhibition such as inhibitor structure matching the crystal lattice. This is in addition to how easy to remove the hydration layer on the barite crystal, degree of

dissociation of subjected inhibitor, complexation with ions in solution and the ability to hydrogen bond.

The increase of the pH up to pH = 8, shows an increase of inhibitors dissociation and inhibition efficiency. Ethylene diamine tetra phosphonic acid (EDTP) was found to be very effective in inhibiting barium sulphate precipitation. It is assumed that only 0.5 ppm (0.1×10^{-5} mol/l) is required to effectively suppress the precipitation process (this corresponds to roughly 1 phosphonate molecule per 200 barium atoms). Even if each of the phosphonate molecules were able to complex 4 barium atoms this is still a ratio of 1:50 for complete inhibition [150].

4.9.5. Inhibition and Critical Supersaturation Ratio (CSSR)

The critical supersaturation ratio (CSSR) concept is used to characterize the effectiveness of different types of scale inhibitors (SI), inhibitor concentration, and precipitation solution pH. The critical supersaturation ratio at which barium sulphate precipitates was obtained as a function of time for different precipitation condition, later, it was used to evaluate the effect of the precipitation conditions. It was proven that the CSSR decreases with increase of the time elapsed after mixing while it increases with the increase of scale inhibitor concentration and the solution pH [151], Figure 4-13.

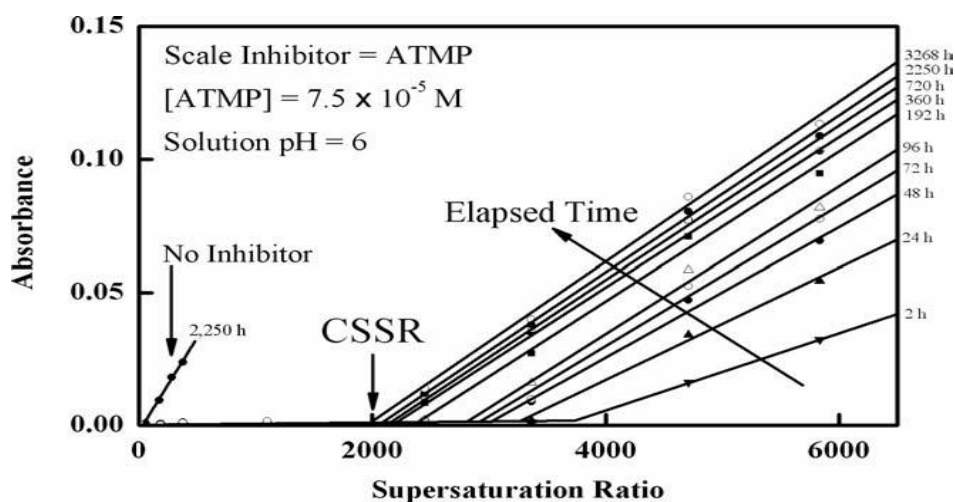


Figure 4-13 : Concentration of BaSO₄ precipitates as a function of the supersaturation ratio [151].

4.9.6. Barium Sulphate Chemical Inhibition and Temperature

In literature, DETPMP is used vastly as an anti-crystal growth retardant. It was found that at a constant supersaturation and as temperature increases from room temperature of 25 °C to 60 °C, barium sulphate inhibition efficiency of DETPMP decreases considerably. However, as temperature increases further from 60 °C to 95 °C, the performance of DETPMP remains constant. Moreover, DETPMP adsorption on barium sulphate reagent powder show that adsorption on barium sulphate continuously increases as temperature rises [152].

4.10. OPTICAL SURFACE CHARACTERIZATION

It was more than sixty years ago when the first Raman spectra for barium sulphate (BaSO_4) was collected [153]. The Raman bands for the synthetic barite were assigned with the use of 514.5 nm laser line and power of (4 mW). The experimentally observed Raman bands were 453 medium intensity, 461 weak shoulder, 616 weak intensity, 647 weak intensity and 988 very strong.

The light scattering method was also used in the mid-eighties to investigate the induction period of the nucleation process of barium sulphate under different values of the initial supersaturation [154]. The intensity of 90° scattered light was recorded for the precipitated crystals. The experimental induction period was considered to be the time between the attainment of the required supersaturation and the detection of the increase in the intensity of scattered light. The time dependence factor of light scattering intensity for barite was investigated. He – Ne laser was used as an excitation power line. Beside the increase in supersaturation and its role in nucleation, the effect of the energy input on the induction time was also investigated, Figure 4-14. It was found that the induction time decreases with the increase of the input energy [155].

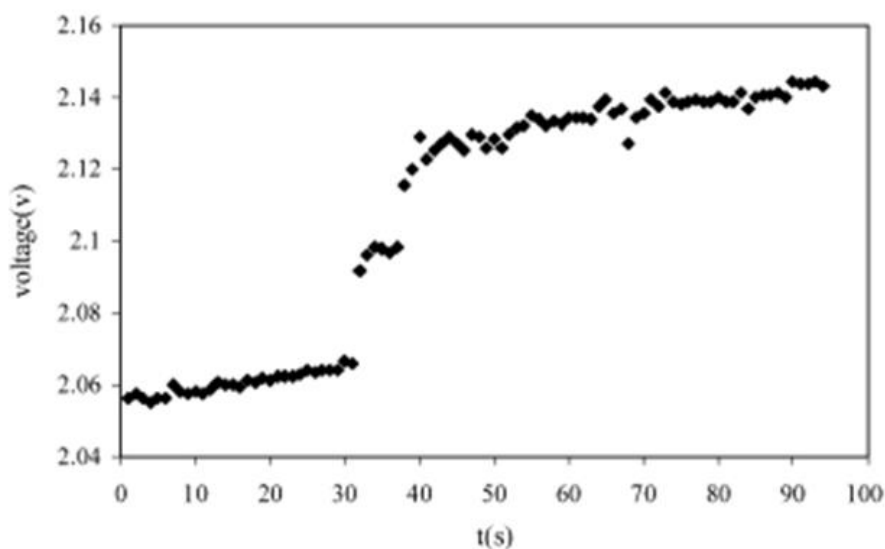


Figure 4-14 : Variation of output voltage (reflecting turbidity) vs time [155].

4.10.1. X-Ray Diffraction (XRD)

More than a decade ago (2002), a new flow cell technique was introduced to simulate the mix of different supersaturated brines in a petroleum reservoir. However, no complete description of barite nucleation and inhibition mechanisms have appeared to clearly and consistently explain in full all the observed effects of the different parameters on these processes. Crystal structure measurements of the a -axis deformation of the barite lattice were explained theoretically [156], and experimentally [91, 157].

As a matter of fact, the crystallization process is usually sensitive to the external physical conditions such as temperature, pressure, pH, mixing ratio and the incorporation of the foreign bodies inside the barite unit cell. Intensive studies were performed on the latest mentioned parameters in order to comprehensively understand the nucleation kinetics, unit cell parameters transformation and crystal morphological interest. At room temperature and extremely high pressure, an *ex-situ* X-Ray diffraction analytical technique was used in combination with Raman spectroscopic technique. The anisotropic compressibility of barite crystal lattice BaSO_4 along the three crystallographic axes was investigated [158] in which c shows the most compressible. Further increase in pressure beyond the phase transition

causes the distortion of -SO_4^{2-} tetrahedron, diamond anvils were used to allow the transparency and to handle the higher pressure applications.

On the other hand, and recently, a new dynamic flow cell was used to monitor the *in-situ* formation of mineral scale deposition using synchrotron angle-dispersive X-Ray diffraction. A flow cell diagram is shown in the coming experimental section. The technique allows the application of pressure and temperature prior to precipitation and data was collected in real time during crystallization. In 2001, the technique was used to monitor and investigate oilfield wax crystallization [159]. A year after, the cell was equipped with a single crystal silicon capillary to monitor *in-situ* barite deposition at non-ambient conditions of pressure using angle-dispersive XRD on beam line X17b1 [160].

Similarly, a wide angle X-Ray scattering (WAXS) was implemented for *in-situ* barite precipitation investigation supported by theoretical findings [161]. The *in-situ* measurement shows the potential of WAXS-synchrotron radiation to observe particle formation process of sparingly soluble substance in millisecond time scale. Recently, in 2008, the same technique (SXRD) was used to investigate the kinetics of barium sulphate formed on the stainless steel surface at two different temperatures at remarkably lower pressure (15 psi). The crystallographic nature of formed barite was examined in the presence of foreign bodies (for instance, Ca, Sr). The effect of poly phosphino carboxylic acid (PPCA, M.Wt.-3600 g/mol) on the barite crystal parameters was also investigated [8]. The *in-situ* synchrotron radiation grazing incidence X-Ray diffraction (SR-GIXRD) technique was used in combination with electrochemical impedance spectroscopy. It was actually used to investigate the electrochemical behaviour of the stainless steel and the influence of barium sulphate scaling and its inhibitions [162]. The study on stainless steel shows that different scaling inhibitors interact uniquely with the substrate when barium sulfate is precipitated on the electrode surface. Such techniques were also proven to be sensitive to study the *in-situ* structural chemistry of solid-liquid interfaces [163-165]. The environmentally friendly green polyelectrolyte-type additives, poly maleic acids for instance, were studied as scale deposit retarding agents. The experiments were carried out with a green additive, polymaleic acid, at a concentration of 1 and 4

ppm and with PPCA (phosphonate inhibitor at same two concentrations) used as inhibitor reference, Figure 4-15. The results show that polymaleic acid reduces the formation of scale by acting on the nucleation and growth process at a concentration of 4 ppm [166].

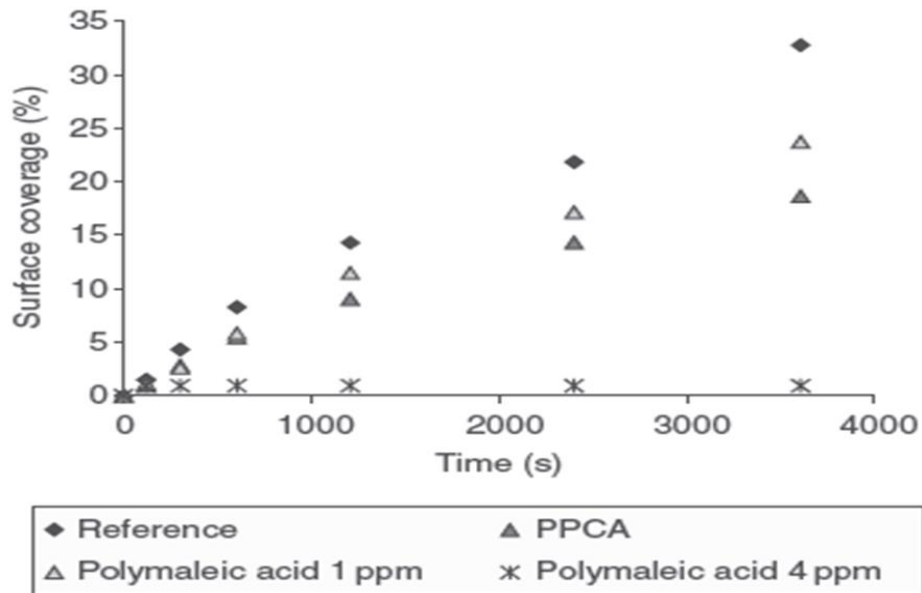


Figure 4-15 : The coverage % of the treated polarized steel metal surface [166].

4.11. LITERATURE CONTRIBUTION

The survey on the use of a similar flow dynamic technique shows clearly what this work has added to this area. It includes the last ten years. The earlier work was generally extended to include inhibitor ranking, scale kinetics in different environments, pre-scaled surfaces and surface crystals propagations in the presence and absence of additives. In the *in-situ* surface measurements, the test tubing is coupled with in-situ X-Ray incident [84] or optical spectroscopic techniques such as in-situ Raman for investigating Barium and strontium sulphate [80].

The applied setup in this work has an advantage to quantify the scale deposited from which further kinetic factors can be investigated. In terms of mixing of formation and sea water brines, it is obviously similar to the dynamic flow rigs set up which

were used by different authors. However, the difference becomes clear at capillary test cell compartment and implementing the differential pressure technique. This unique set up should facilitate more kinetic data. In this research study, a new upgraded setup with new replaceable cell dimensions (10 mm length x 1 mm ID) was introduced; it facilitates possible deposit quantification in a unit of time. It enables several experimental factors to be investigated such as the average rate of deposition, scale thickness development in a unit of time, total mass, surface crystallization pattern, surface condition, temperature and pressure during long duration test.

The dynamic technique statistics have shown the major use of conventional tube or capillaries over coils to explore different scale kinetics or inhibition studies. Using the former may lead to forming a uniform scale deposit by which the scale thickness propagation can be assessed.

On the other hand, longer duration scaling tests facilitate a valuable information about the surface nucleation period from zero time to the final blockage of the capillary. This period has never been explored the way it is in this work at three different temperatures and mixing ratios. This helps assess;

- The surface deposition pattern which could have an impact on surface gain.
- Steadiness/unsteadiness of surface deposition process.
- Surface induction periods based upon the above factors.

In addition, the inhibited surface nucleation period was also explored at different saturation levels from highest at room temperature to the lowest at 75 °C. Moreover, scale quantity (scale gained by capillary during testing), which is the amount of scale deposit gained in a time unit, provides information about the average mass gained, nature of scale and its arrangement in capillary, mass variations and its relation to the recorded induction time at the three applied temperatures.

Kinetically, it was concluded that by controlling the residence time, the location of crystal birth can be controlled if the bulk induction period determined. The effect of

Ba²⁺ ions on saturation ratio was predicted thermodynamically and experimentally proven at different barium contents. This was in good agreement between theory and surface assessments. This setup has proven that at lower SR, the surface crystal seem to adhere to the surface while at highest concentration, the crystals seem to deposit. Lighter capillary at higher barium content is assumed to be related to the deposit arrangement.

This study also focuses on the barite surface kinetics in the presence and absence of scale inhibitor (SI). In dynamic evaluations, a replaceable capillary facilitates the investigation of different parameters; longer duration tests exploring the surface filming nucleation period or surface induction period, quantifying the actual mass reveals some kinetic facts, and average deposition rate. All of these parameters were investigated at different experimental conditions and correlated with prediction and bulk data. Above all, reproducible data was collected with precise control of the parameters.

The ability of the DETPMP to retard the growth of barite scaling at the minimum concentration is investigated at three different temperatures of 25 °C, 50 °C and 75 °C. The investigation is extended to study the effect of heat compensation at 75 °C (the combination of both the inhibitor and higher temperature application), when the lower saturation ratio (SR) and higher solubility are predicted. Then later is compared with a range of temperature applications in terms of surface shape and coverage and possible deposit distribution/composition using different optical techniques [167].

4.12. SUMMARY OF LITERATURE REVIEW

First of all, a review of the dynamic flow test activity through the last decade was reviewed. Various aspect of surface crystallization were studied within different research groups. The outlines of this section was set to show most of the aspects which are dealt with throughout this research work, namely; effect of various

temperature condition, flow effect, different saturation condition, surface condition and inhibition.

The complex brines are known to have an effect of specific ions such as calcium and magnesium on scale crystallization processes, different related studies were reviewed. Although a small amount of work was done on inhibition, this chapter is constructed to include chemical inhibition using an anti-growth DETPMP product. Theories of the three inhibition mechanisms were explored and shown in schematic diagram. *Ex-situ* and *in-situ* scale surface crystallization using different optical techniques were reviewed. The temperature effect on both uninhibited and inhibited scale formation was revealed in different research work.

The contribution in the research work on surface scale kinetic using the dynamic flow system was included in this section and the main points on literature gap filling were shown.

Chapter 5. EXPERIMENTAL METHODOLOGY

5.1. INTRODUCTION

The experimental work in this research covers two main experimental techniques supported by thermodynamic model predictions. The dynamic flow and static bulk tests are the major components. Thermodynamic assessment was usually the first step to examine the scaling tendency and severity as well as the possible composition of scale. This was done with the Multiscale program.

5.1.1. Outlines

In this work, the experimental methodology follows the scheme below which is divided into two parts. The first part highlights the scale surface deposition observation methods, followed with bulk assessments, then finally explores the thermodynamic prediction used. The second part explores the surface deposit analysis. The following points show briefly (in sequence) the experimental plan layout and techniques in use:

A- First Part (Dynamic, Static & Prediction)

1. The major part of this work is related to inorganic mineral surface deposition kinetics and is actually done on stainless steel surfaces (SS 316L). The modified tube blocking rig was upgraded to facilitate a wide range of experimental parameters; temperature, pressure, scale mass, flow rate, cell dimensions, mixing ratio, surface material and inhibition. In addition, there are also some other parameters related to the solution properties such as the saturations of the reacting species in brine mixture. Apart from pressure which was ambient most of the time, all other mentioned parameters are considered in this work.

All of the surface tests were done with a laminar flow regime, Figure 5-1 shows the important parts of surface deposition apparatus.

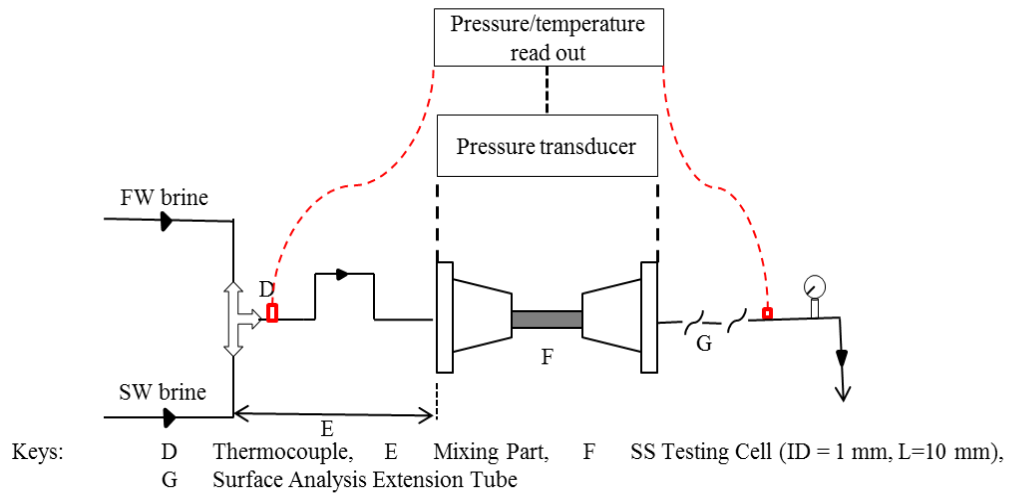


Figure 5-1 : Surface deposition components.

2. Static bulk assessment: This is done in parallel with surface assessments; the bulk tests support the surface tests which reveal the scale crystal status in a time unit using the light scattering techniques. The common NACE coded turbidity measurements; Hack turbidity meter in Figure 5-2, conductivity and ion selective for barium were used. This is because of the closed dynamic system during the surface deposition process and the cell is non transparent.

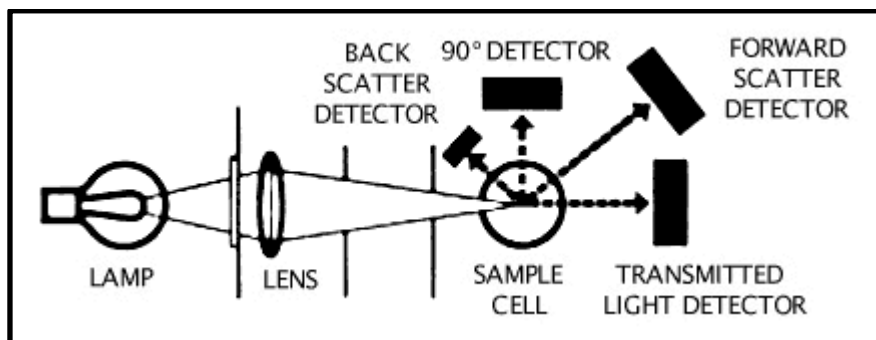


Figure 5-2 : Schematic diagram of the turbidity measurements [168].

3. Prediction method: Theoretical approach using mathematical software was used to assess the thermodynamic properties of brine solution mixtures at different reaction conditions. These conditions include concentrations, temperatures, and

saturation ratios. The theoretical calculation is most likely representing the bulk reaction rather than the surface reaction.

The outcome result file contains valuable figures such as supersaturation ratio (SR) levels at equilibrium, saturation index (SI), precipitated mass, predicted pH. All these reaction parameters are considered important before any experimental setup. The experimental assessments were subdivided into two forms: Static bulk jar precipitation and dynamic flow surface deposition, these methods were set to simulate the real field conditions in terms of brine compositions, flow rate temperature and the mixing ratios.

B- Second Part (Surface deposit assessment)

The second part of this investigation actually focuses on assessment of crystallites on steel surfaces. It is either surface multiphase crystallites of deposited scale, scale deposited in bulk or complex divalent ions with applied scale inhibitor. These surface investigations were carried out by different surface integration techniques such as scanning electron microscope (SEM), electronic microscope (EM), energy dispersive X-Ray (EDX), X-Ray diffraction apparatus, Raman spectroscopy and FT-IR. These techniques were used to help assess the effect of different parameters on surface crystallization.

5.1.2. Brines Composition

The brine formulations were chosen to simulate oil field conditions in terms of multi active ions content and their variable concentrations. The formation water brines contain mild barium ions concentration (64 ppm) as maximum and 16 ppm as minimum in the final brine mixtures. These concentrations are produced through five mixing ratios. They facilitate a range of barium content from mild to less to trace amount. So the calculated saturation ratio (SR) varies within each temperature application (25 °C, 50 °C and 75 °C) at smaller differences. These calculated figures are clearly noticed in the results (SR and SI). The calculated SR values are bigger at different temperatures compared with their values due to the mixing within each temperature. In the other brine formulations, apart from barium ions, all other ions

are kept constant at constant mixing ratio of 50 : 50 sea water to formation water. In these applications, at mixing, the concentration of barium free species were at 150 ppm as a maximum and at 20 ppm as a minimum. This should practically cover a wide real field practise (reservoir conditions). The synthetic formation and sea water used are shown in Table 5-1.

Table 5-1 : Synthetic formation and sea water used in this part.

Salt (ion)	Concentration (ppm)	
	FW	SW
KCl (K ⁺)	1906	380
CaCl ₂ . 6H ₂ O, (Ca ⁺²)	2033	405
MgCl ₂ . 6H ₂ O, (Mg ⁺²)	547	1300
BaCl ₂ . 6H ₂ O, (Ba ⁺²)	64 - 16	0
SrCl ₂ . 6H ₂ O, (Sr ⁺²)	417	0
Na ₂ SO ₄ , (SO ₄ ⁻²)	0	2780
NaCl, (Na ⁺)	13570	17978
Cl ⁻	38475	29636

5.2. DYNAMIC FLOW TEST

The dynamic flow rig/condition (for scale kinetic studies) represents part of an oil field flow mixing condition. It is vital to accurately calculate the flow rate (Q) and understand the nature of the flow in terms of the condition (Laminar or turbulent). So the following shows the flow rate calculation and residence time in the mixing part and testing cell.

5.2.1. Hydraulic design and flow calculation

The scale crystallization kinetic assessment on surfaces is principally based on determining the time, location and at what rate. It was necessary to determine the appropriate flow rates (Q) through the capillary tube and the mixing part. The appropriate determination of a mixture residence time is very important and that is governed by the following:

- Volumetric flow rate, Q (m³/s).
- Fluid volume is calculated from the volume of a cylinder = $\pi r^2 \times L$ (m)
- The residence time, T(s), in capillary is the ratio of fluid volume, (m³), to the volumetric flow rate.

At two different flow rates (5ml/min & 10 ml/min), the residence time was calculated at constant test capillary ID. The length and ID of the mixing part was also constant, Table 5-2 shows the calculated figures.

Table 5-2 : Calculated residence time at the two selected flow rates (5 ml/min and 10 ml/min).

Flow rate	Residence time (s)	
	Test Capillary L = 10 mm, ID = 1mm	Mixing Part L = 110 mm, ID = 3 mm
5 ml/min	0.10	37.32
10 ml/min	0.05	18.66

5.2.2. Flow Rig Description

Besides bulk jar techniques, one other reliable technique which is used to investigate both calcite and barite surface deposition is the tube blocking test. This technique, by the nature of the setup where scale deposits on the wall of the flow cell, offers complementary information to the scaling kinetics investigations.

In this study, a flow rig was used to simulate aspects of the flow in a typical industrial system. The scale rig's image and its schematic diagram is shown in Figure 5-3 and Figure 5-3 respectively. The rig was equipped with a differential pressure measurement tool to measure the pressure difference across the capillary cell. Two reservoirs hold the formation water and seawater separately. Gilson pumps (type, 100 SC) were used to inject the brines into the steel coils which are immersed in a heated water bath to provide the required temperature of reaction. After leaving the bath, the heated brines entered the mixing chamber followed by the capillary test tube of either 1 mm or 2 mm, depending on the diameter required. The test cell was located 110 mm away from the mixing chamber. The temperature of the brines was controlled by the thermostat connected to the lab view data acquisition system. The Omega (PX80D0-030-5T type) differential pressure sensor, with a sensitivity as low as 30 psid, was fitted on the cell compartment. The compartment held the cell between two well-sealed removable caps.

The rig was equipped with a spool pipe that contains a flat steel surface, on which the deposition took place, for surface analysis and observations. Surface scale deposits were characterized using scanning electron microscope (SEM), energy dispersive X-Ray (EDX) and *ex-situ* X-Ray. The rig was also equipped with a cooling system followed by the pressure column leading to the waste. A pressure regulator was fitted to control the line pressure as required. Moreover, the pressure relief valves were located before and after the cell compartment for safety reasons. At the end of each test, the rig was properly cleaned with specified cleaning solution (NaOH + EDTA at pH =10) for half an hour followed by two hours with distilled water. Each test, the cell was replaced with a new one providing a new and clean surface.



Figure 5-3 : Dynamic flow rig in use for surface deposition.

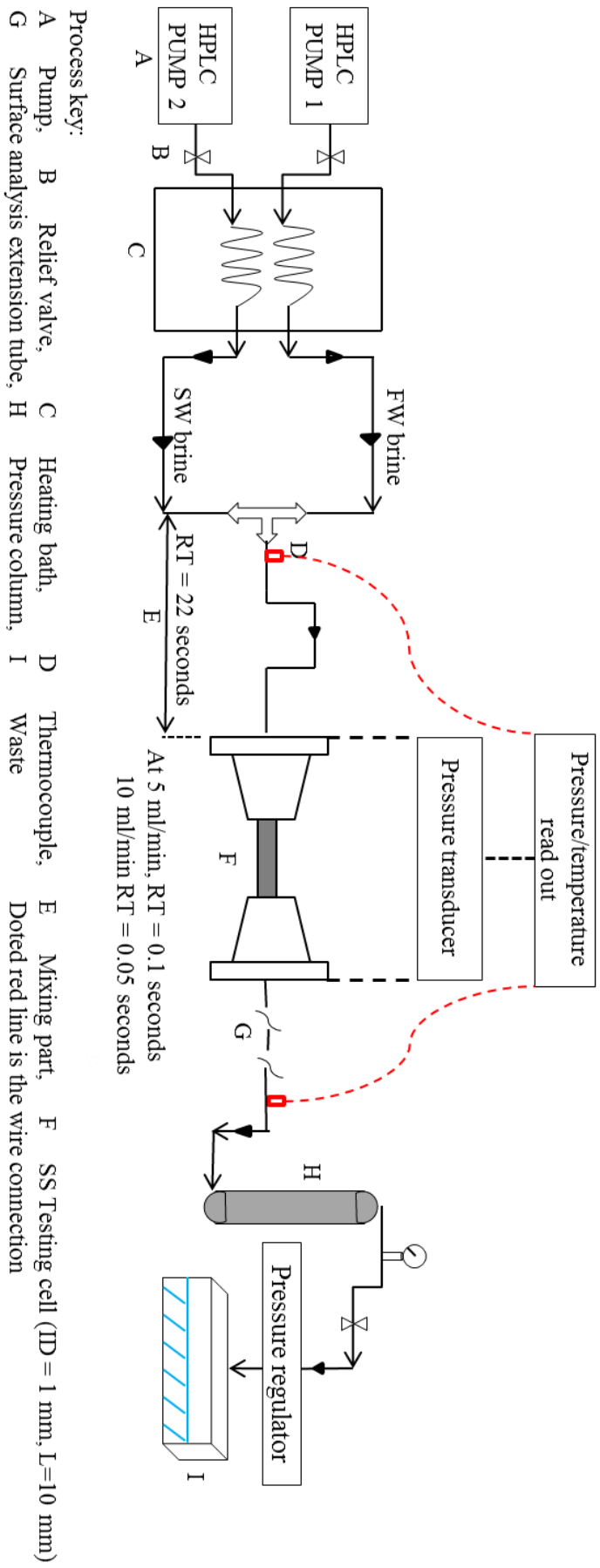


Figure 5-4 : Dynamic flow scale rig in use for surface deposition.

In this work, a new approach is taken. The testing cell dimension is reduced from the conventional 1 m coil to a capillary tube of SS 316L with dimensions of 10 mm length and 1 or 2 mm bore size. At this dimension of cell capillary, the residence time for a volumetric flow rate of $8.333 \times 10^{-11} \text{ mm}^3/\text{sec}$ was calculated to be 0.10 sec. The differential pressure is recorded across the testing cell as the scale develops on the internal surface of the cell. For this purpose, a sensitive Omega differential pressure sensor (PX80D0-030-5T type) was used. The sensor was the most sensitive provided by Omega. It was chosen for accuracy with a sensitivity of 30 psid.

The advantage of having such a capillary cell is to enable the quantification of the average scale deposited within the testing cell as the initial and final weight are recorded. The trend of mass deposited according to different process conditions based on saturation will highlight some important kinetic terms. These are represented in crystal-crystal and crystal surface stability during flow, scale thickness development vs time, average rate of deposition, and the surface nucleation pattern at early nucleation stage.

The series of long period dynamic flow system experiments were performed to assess the barite surface kinetics using the flow rig by means of differential pressure measurements across the capillary.

5.2.3. Capillary Cell Design

The stainless steel (SS 316L) capillary cells were fabricated locally at desired dimensions. The steel rod is supplied in a cylindrical shape at about 6.3 mm of external diameter (OD). The cell dimension is fitted to a cone like chamber which is tied to the two steel caps that hold the cell compartment. The steel cone chamber is considered the mixing part on its own (short residence time), or it can also be considered part of the extended mixing part (longer residence time). It depends on the experiment design used. These two capes are designed to hold the capillary cells firmly between them. The caps then are brought tightly together by four long screws so no pressure/water leaks is possible as the pressure increases due to capillary

scaling. The cells are cut to be 10 mm in length and this is fixed throughout the study, see Figure 5-5.

In order to get the desired internal hole dimension (the surface to be scaled), these cells are transferred to a special drill and carefully holed. In this work, the cell dimension varies from 1 to 2 mm internal diameter but most work was done with 1 mm capillaries.

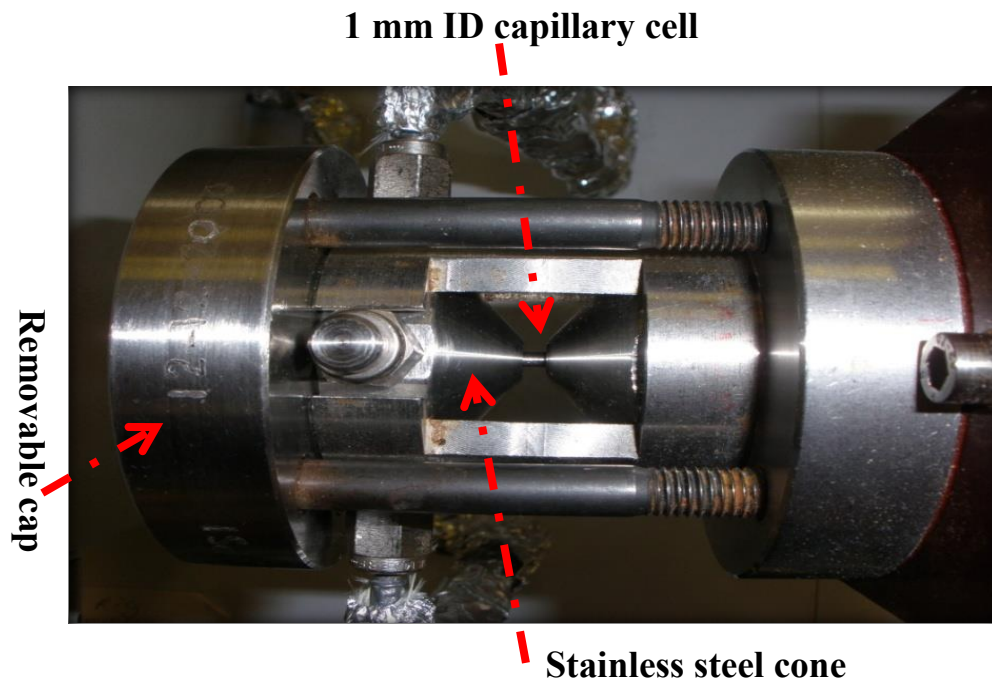


Figure 5-5 : The scale rig's cell compartment including the capillary cell.

The purpose was to examine the barite surface kinetics with the same brine composition at different solution and experimental parameters.

5.2.4. Specimen Surface Scaling for Optical Analysis

Due to the nature of the capillary cell design, as it is a closed system, it is hard to investigate the surface deposition using the optical surface tools after the surface is scaled. A suitable flat stainless steel surface for characterizing the scale crystals alignment and surface topography was designed from similar cell material. This was to investigate the effects of different variables on dynamic surface deposition e.g

saturation ratio (SR), variable temperature, surface condition, flow rate, chemical effect, barium contents and the surface materials.

Although the internal scaled curved surface were analysed with some optical techniques, a flat surface is immensely important when *ex-situ* X-Ray diffraction analysis is required. It is also suitable in the case of SEM or EDX analyses.

In order to overcome such problems, a flat plate having similar material specifications which is used in designing the capillary cell was fabricated. Its dimensions are set to be able to get into the ¼” spool extension pipe. The specimen dimensions are; 4 mm in width, 1.5 mm in thickness and ~ 25 mm in length. The specimen is positioned very close to the cell to exhibit what is taking place on the internal surface of the capillary. The surface sample is usually positioned flat in the downstream of the solid particles solution. The direction of the flow was also marked on the outside of the spool pipe.

Immediately after the surface crystallization process ending by a cell blockage, the specimen is dried in the oven along with cell. The cell is then weighed to find the scale net mass, the image the extension plate is shown later.

5.2.5. Sampling During Flow Test

In both bulk and surface tests, samples were taken for the mother brines before mixing in order to determine the actual initial ions concentrations. These samples are not quenched using quenching solution (KCl/PPCA) to eliminate any further reactions. The solutions resulted from the mixed brines were treated and quenched in the same as the bulk or flow tests.

In this test, the effluent water was collected for ICP analysis to determine the divalent cations left after deposition. This takes place differently depending on the condition and aim of the test. The samples are taken immediately after the deposition from sampling point close to testing cell. Some samples are taken from the scale rig's dump drain line for comparison. The use of quenching solution is similar to

that mentioned earlier. The mixture was not quenched only in the case of treatment with DETPMP, when 10 ml was taken from the treated mixture and analysed straight.

5.2.6. Inductively Coupled Plasma (ICP)

Inductively coupled plasma (ICP) is a well-known technique for finding trace metal ions usually present in water. This gives the technique an advantage when used to track the concentration of the leftover species after mixing process. In the case of scale kinetics study, the change or the attenuation of metal ion concentration gives rise to scale forming and it is possible to recognise the severity of preprecipitation. ICP apparatus (Type ULTIMA HoribaJobin YVON), see Figure 5-6 for the ICP image, is used to analyse the effluent water from the synchrotron scale rig. The sample analysis is performed by injecting the subjected brine mixture into a plasma chamber after mixing it with a carrier (usually argon gas) to get the mixture into spray form. The plasma excitation is followed by ionization and emission processes of the alkali earth metal atoms, the concentration of each cation is detected and recoded by attached computer software.

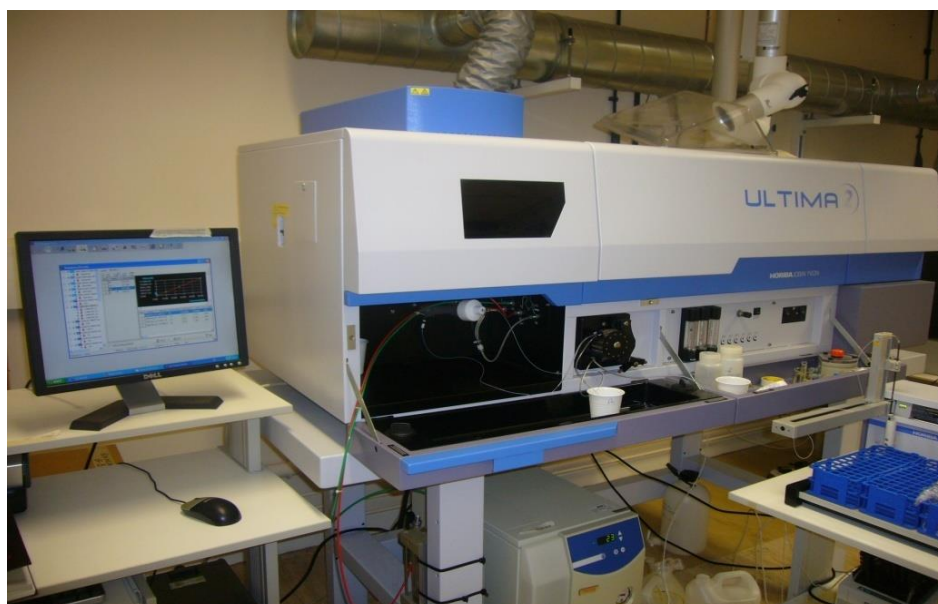


Figure 5-6 : ICP unit used for water analysis.

The effluent water sample was collected at the same time interval from the start of each experiment, an hour after commencing the test. 1 ml of the brine mixture or the waste is taken to a new sampling bottle. Thereafter, 9 ml of quenching solution (mixture of PPCA and KCl solution) was added to the contents of the bottle. The ICP instrument was standardized to the specified range of concentration of each analyte (Ba^{2+} , Sr^{2+} , Ca^{2+} and Mg^{2+}).

5.2.7. Scale Surface Kinetic (Barium Varies 20 – 150 ppm)

These surface investigations at different barium concentrations were actually done following the earlier tests, which were performed at three temperature conditions and five mixing ratios. The aim was to control the variables to spot their effect on the scale surface deposition kinetic. This time, the barium content was the only variable at constant flow rate of 10 ml/min and constant temperature of 75 °C. Real complex sea water and formation brines are used, the brine formulation is in Table 5-1. The barium concentrations (20 ppm, 50 ppm, 80 ppm, 100 ppm and 150 ppm) are varied in the final mix at constant 50:50 mixing ratios. The surface material specifications (316L stainless steel substrate) were the same throughout the tests as well as the ambient pressure. The collected results are shown in terms of a change of the differential pressure versus time.

5.2.8. Dynamic Test – Flow Effect

The tube blocking tests (TBT) are widely used for assessing the inorganic scale/barite and calcite scale measurement since the testing rig is equipped with highly sensitive differential pressure device. Unlike using coils in one or two meter length, the scale/barite deposition kinetics on the internal surface of a capillary tube (1 – 2 mm ID & 10 mm length) was investigated. The resulting long duration test enables minute by minute surface scale monitoring in the early surface nucleation and growth regions. Experimentally, two flow rate were used to investigate the effect of flow at different resident time and shear. In the testing capillary, the resident was calculated to be 0.05 s at 10 ml/min flow while at 5 ml/min flow, it was

0.1 s. The same flow rates were used during the chemical treatment of brine mixtures.

In this part of the study, a higher flow rate of 10 ml/min was implemented in order to investigate its effectiveness, in terms of reproducibility and consistency, on both the observed induction period and final growth crystals morphology. Bearing in mind, such a setup has never been used before. The results are discussed in the result and discussion sections.

5.3. CHEMICAL TREATMENT (DYNAMIC)

The chemical treatment was carried out to investigate the effect of anti-growth products at different residence times (at different flow rates) and temperatures. DETPMP was used at different concentrations. This was suggested when scale crystal growth was confirmed in the flow stream within the mixing part – correlated to conductivity measurements. Moreover, It is also important to find out the effect of the anti-growth retardant on the observed surface crystallization pattern. The sensitivity of the pressure tool could probe the change in differential pressure at lower levels, this will help assess the inhibition efficiency at different saturations due to temperatures

5.3.1. Barite Scaling Treatment Test

In this part, an anti-nucleation chemical product (DETPMP scale inhibitor) was tested at lower dynamic flow rate conditions to minimize the flow effect. The DETPMP surface nucleation inhibition efficiency and its effect on final crystal orientation on the surface were tested at two different concentrations (10 ppm and 5 ppm). The inhibition tests were done at 5 ml/min flow rate, fixed 50:50 mixing ratio and the three temperature conditions.

5.3.4. Physical and Chemical Properties

DETPMP is a pale yellow acidic liquid, it does easily chelate with di- and trivalent ions such as Mg^{2+} , Ca^{2+} , Ba^{2+} , and Sr^{2+} etc. It can be prepared by the reaction between diethylene tri amine, formaldehyde, and phosphorus tri chloride.

5.3.5. DETPMP Applications

Aqueous diethylene tri amine penta(methylene phosphonic acid) (DETPMP) is used as a scale inhibitor, deflocculant, sequestrant, water stabilizer in cooling water, boiler, oil-drilling, detergent under high pH (10 ~ 11). The DETPMP scaling inhibitor specifications are very important in the practical use of such products and are listed below in Table 5-3.

Table 5-3 : DETPMP specification

Items	Specification
Appearance	Amber liquid
DTPMP Content	50±2%
Phosphorous Acid (as PO_3)	3.0% max
Chlorides (as Cl)	10.0% max
Iron (as Fe)	35ppm max
pH Value (1% aqueous)	2.0 max
Density(20 °C), g/cm^3	1.30~1.40
Ca Sequestration (as $CaCO_3$ mg/g)	450 min

5.3.6. Inhibitor Preparation and Treatment

DEQUEST 2066 type is supplied as stock solution with an activity of 25 – 30%, the 27 % activity (as average) was used to calculate the required volume from chemical stock. Initially, 3000 ppm stock solution was prepared from supplied DETPMP, 8.6 ml of the supplied product was transferred to a standard 1000 ml measuring flask. Then deionized water was added to top up to the mark to get 1000 ml of 3000 ppm inhibitor solution. The amount required to prepare 1000 ppm active inhibitor was

carefully prepared. In order to prepare 1000 ppm active DETPMP, 2.9 ml of 3000 ppm stock solution was transferred to an empty clean standard flask and topped up with deionized water as required. The required amount for inhibition is then calculated based on the minimum inhibitor concentration (MIC) required, 5 ml of 1000 ppm inhibitor solution was added to 1000 ml of brine. The prepared diluted inhibitor is then added to the anionic seawater brine. No solution haziness or any form of precipitations was observed when the inhibitor was added to the sea water (SW plus required DETPMP results in clear solutions).

The scale inhibitor was used in two concentrations starting with 10 ppm then followed by 5 ppm at 5 ml/min flow rate. The differential pressure vs. time graphs were obtained and assessed. The weight of scale-inhibitor complex gained in the capillary tubes were obtained. The physical mass gained in the capillary was measured for both treated and untreated scales. The mass was plotted vs. temperature, more details are in the results and discussion sections.

The purpose was to examine the barite surface kinetics with the same brine composition at 50:50 mixing ratio and different temperatures (consequently different SR). The scale deposited in the testing cells was quantified based on the initial and final weights. Thereafter, the comparison was made between the masses of treated and untreated cell deposits. The question here is that – is it possible to probe or observe any trace of scale inside the capillary after treatment? What about the surface crystal morphology and orientation?

Furthermore, the ICP analysis was done on the effluent waste brine mixture. In the case of the treated test, the concentration of both Ba and P were evaluated. The sampling process is explained elsewhere earlier. The treated samples were not quenched using quenching solution. Tabulated result of the conductively coupled plasma show very helpful results. It shows the behaviour of the Ba^{2+} cation species in the presence of the anti-scaling agent immediately after addition and after longer durations.

5.3.7. Surface Pre-treatment (chemically pre - coated)

The chemically pre-coated surface was designed to investigate the deposition kinetics of scale/barite on such surfaces. Anti-nucleation Diethylene tri amine penta (methylene Phosphonic Acid), DETPMP was used to coat the surface at 1000 ppm for 1 hrs. The DETPMP product has three nitrogen groups in its structural formula by which it is able to bind to the stainless steel surface. Later on, infrared (IR) surface analysis was done to characterize and confirm DETPMP existence on the surface. There is a strong probability that the phosphonate branches of DETPMP bind to the metal scale particles to form a ligand, while the whole molecule is bonded to the steel surface through N atoms (ionic bonding).

The question was, would this product be able to retard the scaling deposition process and extend the surface induction period? Or would those smaller complex aggregates work as a scale initiator and speed up the surface deposition process kinetics. After surface treatment with 1000 ppm DETPMP for one hour, brine mixtures at different Ba^{2+} were tested at 50:50 mixing ratio and 10 ml/min flow rate. The same steel surface grade SS 316L and 75 °C were used. It is worth mentioning that this test was done initially on an untreated surface in order to compare and find the effect of surface changes.

5.3.8. Surface Pre-scaling (surface seeding)

The kinetics of the scale formation on different surface conditions is part of this research work. In this section, the earlier surface nucleation pattern, a result of different brine mixtures at different temperature and flow, have shown the impact of surface condition. Using the capillary cell shows remarkably longer surface scaling and surface induction periods. The effect of surface pre crystallization on the scaling kinetics was vital to investigate the effect of surface condition.

The questions were - would the surface seeding affect the surface scale kinetics? Would the effect of pre-scaling be noticed on the final surface induction period (longer or shorter)? In addition to its effect on the growth period. It seemed that pre-scaled/nucleated has a major effect on the surface kinetic and the results are discussed in a later section.

5.3.9. Surface Pre-scaling Steps

The higher sensitivity of the Omega differential pressure sensor gives an indication of a micron scale thickness nucleation layer. This is clear when the surface nucleation pattern is examined during the scale layer's failure/detachment, or in the case of its rebuilding on the surface. This enables interpretations of a very important period in the whole surface crystallization process, which is the early nucleation period.

The surface seeding or surface nucleation experiment is started with a new cleaned surface. The surface is cleaned with solvent (acetone) to remove any probability of organics being stuck to the surface. The surface was then cleaned thoroughly with distilled water for an hour. The surface was nucleated based on a slight change in the recorded differential pressure. The surface seeding lasted for nine hours at a mixing ratio of 70:30 FW: SW. The increase of the pressure was observed to be 0.08 psid. In order for the early formed crystal layer to stick firmly to the capillary internal surface, the system was shut down for exactly 12 ½ hours at 0.08 psid. Thereafter, the system is resumed (from 0.08 psid differential pressure) to complete the experiment (till the final cell blockage). The complete blockage had taken place after five hours. This figure is then compared to unseeded surfaces at higher saturation brines (90:10 FW:SW). These series of experiments were performed at three different mixing ratios named 50:50, 70:30 and 90:10 SW: FW and the flow rate were adjusted to 10 ml/min. The scaling of pre – scaled surface took place at 70:30 mixing ratio and 5 ml/min flow rate. The flow rate was decreased to minimize the flow effect on nucleated surfaces and increase the residence time. The entire test was performed at ambient temperature and pressure.

5.4. BULK PRECIPITATION TEST

After the thermodynamic prediction, the experimental bulk measurements were conducted using different techniques; turbidity measurements at three different temperatures at the five mixing ratios earlier mentioned (25 °C, 50 °C, and 75 °C), conductivity and ion selectivity for barium measurements at one temperature (75

°C). It was done to support both the kinetic investigations on surface kinetic measurements and approve the prediction findings. It was important to highlight the correlation between the three techniques combined.

5.4.1. Turbidity Measurements

A turbidity meter was used as a light scattering technique to assess the precipitation kinetics of the BaSO₄ in the bulk phase. It reveals the concentrations of formed barite/scale suspensions in the brine mixture. Although neither rate of deposition nor the kinetics of the process in terms of quantity were measured using this technique, the technique is still valid to follow the scale formation versus time. Moreover the technique allows the detection of the induction time even in the case of scale/BaSO₄ when the phase change occurs very quickly.



Figure 5-8 : HACH colorimeter DR/890 turbidity meter [168].

Apart from NaCl, all of the chemical salts (KCl, CaCl₂. 6H₂O, MgCl₂. 6H₂O, Na₂SO₄, SrCl₂. 6H₂O, BaCl₂. 6H₂O), which were used to prepare brines, were Sigma-Aldrich's research grade salts. Highly purified deionised water was also used to prepare the solutions.

It is known that it is a challenge to detect the induction period for barite precipitation in the bulk as it normally happens relatively quickly especially at higher temperature. In this work, the induction time is evaluated experimentally based on the phase change [169]. At room temperature (25 °C), for instance, it is clear other factors may play a role in barite solubility such as the molar concentration of NaCl in the mixture. A typical turbidity graph in a bulk using a turbidity meter at room temperature is shown in the Figure 5-9.

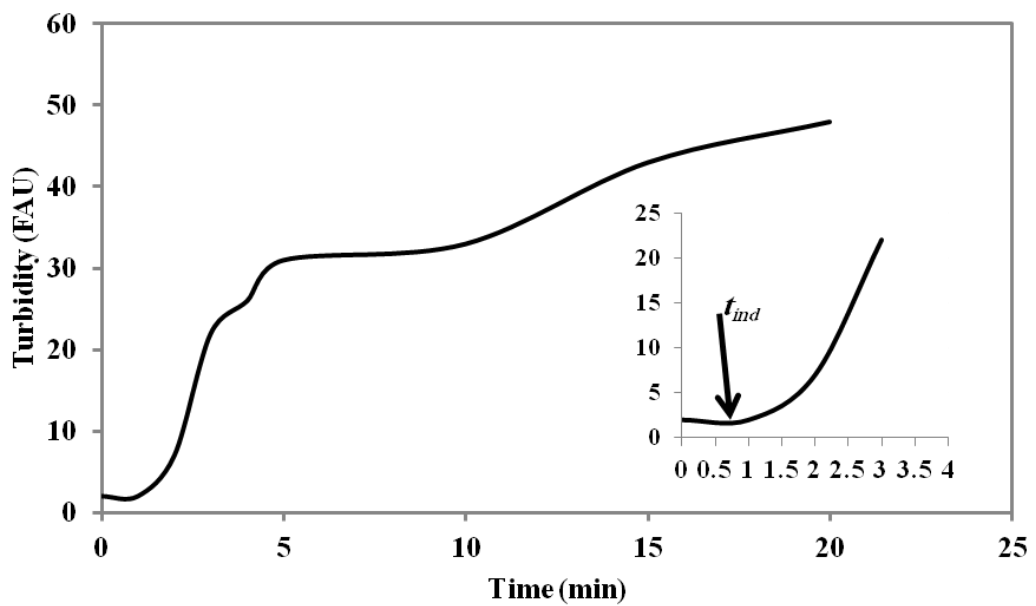


Figure 5-9 : A typical bulk measurement using the turbidity with phase change assigned (t_{ind}) at 25 °C and 50:50 SW:FW mixing ratio.

This turbidity test, using a HACH colorimeter DR/890, Figure 5-8, was conducted in a bulk jar test for a mixture of the synthetic seawater and formation waters at three different temperatures (25°C, 50°C and 75°C). The test was done at ambient pressure conditions and five mixing ratios of 20:80, 40:60, 50:50, 60:40 and 80:20 (FW: SW), see figures in the results section.

The formation and seawater were prepared in two different measuring flasks. This was for accuracy and to avoid any possible contamination. Then the distilled water

was added just below the flask standard volume's mark, the salt solutions were stirred until the salts completely dissolved. The resulted mixture was topped up with distilled water to get 1 litre of brine. The test was done at room temperature and 50:50 SW:FW mixing ratio, in this case, 500 ml of the formation water brines were transferred to a 1000 ml beaker. 500 ml of seawater was transferred to another 500 ml flask, the brines were at the same temperature level prior to mixing. The magnetic stirrer was set at 450 rpm in the formation water to provide good mixing and avoid local supersaturation changes.

Before addition, although barite scale formation is not a pH dependant, the actual pH values were taken and used for scale prediction calculations using Multiscale software. The pH of the mother brines (FW pH = 5.91, SW pH = 5.88) and the mixture were measured. This enables the determination of the actual pH at equilibrium which was pH = 6.04.

Immediately after mixing, as it is a time dependent test, the first turbidity measurement were usually taken between 0 - 10 seconds to catch any possible phase change in the mixture during the precipitation reaction. The result of the initial turbidity test, which were collected at shorter duration of 20 minutes, at the three temperatures and 50:50 mixing ratio, were used as a reference throughout this work. The reading time interval was set to be; immediately after mixing <10 seconds, 1 min, 2 min, 3 min, 4 min, 5 min, 10 min, 15 min, 20 min, 25 min, 30 min, 40 min, 50 min and 60 min. The reason for the longer time was to monitor the crystal clusters behaviour after ripening in terms of growth/re-dissolving processes.

The bulk precipitation test was extended to include four more mixing ratios and extended to 1 hour to properly assess the effect of different mixing ratios and SR.

At the end of the tests, the actual barite mass precipitated in the bulk solution was filtered with a 0.45 μ m membrane filter to compare the barite actual mass precipitated with predicted data from Multiscale software. Later, in the case of surface deposition, it helps to assess the total amount of the deposited scale passed through the capillary cell and its actual percentage deposited on the surface.

5.4.2. Sampling During Bulk Test

In this test, the samples used throughout the one hour test were intended to cover certain times; the first few seconds, then one minute, two minute, 3 minute, and four minutes. The following five samples were taken every 5 minutes (minutes 10, 15, 20, 25 and 30). Finally, in the final half an hour, the samples were taken every 10 minutes (minutes 40, 50 and 60. At each sampling occasion, 1 ml of mixed brine (scaling mixture) is transferred to a cleaned and dried plastic sample tube. 9 ml of quenching solution is added immediately to control and possibly stop any further reactions taking place. All the samples are well-sealed, marked and then sent to the ICP unit for analysis.

5.4.3. Conductivity Measurements

Conductivity is another technique which is used to assess the scaling of a system and the precipitation of solids from a brine mixture. As scaling progresses, the number of free conducting ions drops, the solution mixture becomes more turbid and the conductivity also drops. This test was performed to assess what happens to the barium ions in the bulk solutions (in a time unit) before reaching a targeted surface (capillary surface) on which they are deposited in a scale form. In this work, the conductivity was measured in micro Siemens per centimetre ($\mu\text{S}/\text{cm}$). An S70 METTLER TOLEDO meter was used, Figure 5-10, equipped with an ion selective probe for barium ion measurement. The bulk test provides details of when the system was thermodynamically stabilized and no more reactions are taking place. Kinetically, the assessment of time and location of crystal formation in bulk helps in designing and modelling the mixing parts in the surface deposition. Bulk pH measurements were also made while the conductivity was measured, and the $\text{pH}_{(e)}$ at equilibrium was determined. A sensitive pH meter from Thermo Scientific (Orion Star A 111) was used. The pH of both mother brines was measured before, during and after deposition.

Note: For accuracy and consistency, the surface and bulk tests were carried out on the same brine, Table 5-4. The brines used in bulk were taken from those already prepared to investigate surface deposition.



Figure 5-10 : The Mettler Toledo combined conductivity/ion selectivity probe setup used in the bulk measurements and pH meter.

In bulk measurements, 150 ml of formation water was transferred to a 500 ml clean beaker and heated to the desired temperature ($50\text{ }^{\circ}\text{C}$) and stirred, while the same amount of seawater is transferred to another beaker to be heated to $50\text{ }^{\circ}\text{C}$. For both brines, an ionic strength adjustment buffer (ISAB) was prepared by dissolving 300 g of KCl in 1000 ml distilled water. Addition of 1 ml of ISAB per 100 ml of any brine was used. The standard concentration slope was collected prior to the test to prove the system accuracy and sensitivity.

The above system was connected to software for data collection of both conductivity and barium ions at the same time interval. The time interval was set to 5 seconds and to take a total of 6 readings within 30 seconds.

Table 5-4 : Formation and sea water brines formulation used.

Salt (ion)	Concentration (ppm)	
	FW	SW
KCl (K ⁺)	1906	380
CaCl ₂ . 6H ₂ O, (Ca ⁺²)	2033	405
MgCl ₂ . 6H ₂ O, (Mg ⁺²)	547	1300
BaCl ₂ . 6H ₂ O, (Ba ⁺²)	20, 50, 80, 100 & 150	0
SrCl ₂ . 6H ₂ O, (Sr ⁺²)	417	0
Na ₂ SO ₄ , (SO ₄ ⁻²)	0	2780
NaCl, (Na ⁺)	26535	10900

5.4.4. Ion Selectivity for Barium as a Main Variable

The bulk investigations were extended to assess/confirm the barium ion behaviour in the complex brine using the ion selectivity probe for barium in combination with the conductivity probe. A S70 METTLER TOLEDO meter was used which facilitates the connection of different probes at the same time. The purpose was to determine Ba²⁺ ions concentrations in time units. It helps the prediction of constant SR at a specified time. This is applicable in the case of surface deposition as this measurement is not possible during an accessible flow test. The setup is combined with the above conductivity test in Figure 5-10, this probe measures the barium content at the same interval as the conductivity probe - every 5 seconds using software.

It was expected to provide information about the attenuation of barium ions as the barite formation reaction proceeds. Theoretical calculations are done for the bulk solution. The experimental parameters are as follows: Complex sea water and

formation water brines were prepared. Before mixing, both brines were buffered with the concentrated KCl solution (300 g in 1 litre distilled water). Barium concentrations were varied from 20 – 150 ppm in the final mixture at 50:50 mixing ratio and 50 °C. The temperature was chosen due to a probe operating with a temperature limitation of 58 °C. As mentioned earlier, no inhibitor was applied in any tests at this stage. This work was published in NACE recently.

An Ion-Selective Electrode (ISE) produces a potential that is related to the concentration of an analyzed ion. The ion measurement using an ISE is therefore a form of potentiometry. The pH electrode is the most common ISE widely used. It simply contains a thin glass membrane that responds to the H⁺ concentration in a solution. ISEs for other ions must have an appropriate membrane that is sensitive to the ion of interest, but it should not be sensitive to interfering ions. This membrane in many commercial ion selective electrodes use a polymer membrane to embed ion-sensitive species that are sensitive to the common ions Ba²⁺, Ca²⁺, NO₃⁻, NH₄⁺, or other ions. In mixtures, ISEs are susceptible and sensitive to several interferences. In this case, samples and standards are to be diluted 1:1 with total ionic strength adjuster and buffer (TISAB). In this work, a buffer solution of 300 g KCl in 1000 ml was used. In some cases, The TISAB consists of 1 M NaCl to adjust the ionic strength, acetic acid/acetate buffer to control pH, and a metal complexing agent [170].

5.4.5. Turbidity Measurements for Scale Particles

Both the bulk precipitation and surface deposition plots at low saturation (20 ppm) are clearly distinguished from those at highly saturated solutions (50 ppm, 80 ppm, 100 ppm and 150 ppm). This also supports the reliability of conductivity/ion selective bulk measurements compared to turbidity measurements as bulk measurements take into account the active ions in the environment. The conductivity measurements clearly show the metastable or unstable period of time (15 – 20 s) before a crystal reaches its final form. The optical turbidity measurements using the turbidity meter confirms the detection of particles at 22 seconds at different

temperatures of 50 °C and 75 °C, the former was the probe system limitation and the latter is the targeted experimental temperature.

5.5. THERMODYNAMIC SCALE PREDICTION

Thermodynamic predictions represent the theoretical part of scale study, and it is very important to initially find out that there is a tendency of brine mixture to form a scale. The scaling solution which is thermodynamically evaluated to have excessive free ions of reactants causing instantaneous precipitation. The calculation is done to determine the level of saturations with the free ions, then the saturation index can be determined.

The other valuable information includes the pH at equilibrium and predicted mass. However, kinetic data is extremely important which describes when (timing) the scale is likely to form and at what rate either in bulk or on surfaces. Simple indices are widely used in the field of water treatment in order to assess and predict the formation of scale. They provide an indicator of scale potential, but the lack of accuracy arises as these software consider that every ion (in the solution) is active. So the use of reactant's total analytical values and neglect the inactive or bound ions mislead the evaluation. Such inactive ions do not actually participate in reactions such as calcium associated with sulphate [171]. In fact, in the past, and even after the computer software was introduced, different simple indices have been used to assess the scaling systems. Simple indices include the Langelier Saturation index, Ryznar Stability index [172], Stiff-Davis Saturation scale index and Oddo -Tomson index [173] for calcium carbonate. Indices have also been developed for other common scales such as calcium sulphate and calcium phosphate.

There are different modern software packages available to theoretically calculate the activity-based supersaturation for any brine mixture [174]. In this work, most of the theoretical approximation and predictions were performed using the Multiscale software version. The scale Softpitzer scale prediction software was also used for confirmation and comparison.

The Multiscale prediction method was used on four different occasions to assess and predict the SR and SI as detailed below and later in the result section:

Initially, the maximum supersaturation ratios and mass deposited were determined at three different temperatures (25 °C, 50 °C and 75 °C), and five mixing ratios within each temperature. Later, the maximum supersaturation ratios were also predicted as they vary based on barium ion contents;

- Determination of the SR for the barite single brine.
- Determination of the SR for the barite complex brine.
- Assess the SR at zero barium concentration.

The saturation index for barite scale is defined as the logarithm of the saturation ratio (SR) as following;



$$SR = \frac{[\text{Ba}^{2+}][\text{SO}_4^{2-}]}{[\text{BaSO}_4]} \quad \text{Equation 5-2}$$

$$SI = \log \left(\frac{a_{\text{Ba}^{2+}} \cdot a_{\text{SO}_4^{2-}}}{K_{sp}} \right) \quad \text{Equation 5-3}$$

$$a_i = \gamma_i C_i \quad \text{Equation 5-4}$$

When a_i , γ_i and C_i are the activity, activity coefficient and the concentration of i^{th} species respectively. K_{sp} is the solubility product.

5.5.1. Predicted SR at Different Temperature/Mixing Ratios

In this work, real field brine compositions are used to represent real seawater and formation water with mild Ba^{2+} (subjected ions) content in the formation water. At three different temperatures (five mixing ratios at each temperature), the maximum supersaturation ratios and predicted scale mass were calculated based on the targeted mixing profile. The sea water percentage was set to be 20%, 40%, 50%, 60% and 80% for sulphate ions (SO_4^{2-}) content ranges from 556 ppm to 2224 ppm at 20% and 80% of sea water respectively.

On the other hand, the barium species concentration (Ba^{2+}) ranges from 64 ppm at 80% as the highest to 16 ppm at 20% as the lowest. Prior to calculation, additional chloride and sodium ions concentration, which were resulted from the dissociations of chloride salts, were taken into account for prediction accuracy. The brine compositions used throughout this study were shown earlier in Table 6-1. The saturation ratio (SR) and the associated mass of precipitates at each mixing ratio were predicted for the selected brines. The bulk thermodynamic assessments were correlated to kinetic data of observed static and dynamic tests. The data includes the observed induction periods and surface growth.

5.5.2. Scale Prediction at 25 °C, 50 °C and 75 °C

In this case, the predicted scale/barium sulphate supersaturation ratio values are plotted with respect to sea water percentage at the three different temperatures. It is clear that the saturation ratio (SR) decreases with the increase of temperature from ambient at 25 °C through mild at 50 °C and finally to 75 °C. The predicted graph is presented in the result section. The predicted barite mass precipitated is given in mmol/Kg solvent. The maximum saturation ratios are shown at 50 % and 60 % of seawater (40 & 48 ppm Ba^{2+} contents respectively). Regardless of the temperature, the maximum masses are precipitated at about 20 % sea water, this is expected to be true as the number of moles of reacted species are at maximum at highest formation water of 80% (64 ppm Ba^{2+}).

In this work, the Multiscale software considers the activity based supersaturation instead of the total concentration, which is more accurate. At 50:50 mixing ratio, the maximum SR was predicted between 40% to 60% seawater. The values of SR at 25 °C, 50 °C and 75 °C were predicted to be 383.8, 191.4 and 115.7 respectively and the predicted saturation indices for previous saturation ratios are 2.58, 2.28, and 2.06 respectively. At 50:50 mixing ratio, the barium species concentration (Ba^{2+}) was about 40 ppm while the sulphate (SO_4^{2-}) content was 1390 ppm at the moment of mixing. See Table 5-1 shows brine compositions.

5.6. SURFACE ANALYSIS

In general, surface analysis is very important to explain the surface morphology which reveals an effect of certain process conditions. The effect of different experimental parameters on surface crystals growth and alignment can be investigated. There are a wide range of surface characterization techniques, which were used in this study namely; Environmental scanning electron microscope (ESEM), energy dispersive X-Ray (EDX), *e-situ* X-Ray diffraction, Raman spectroscopy and Fourier transform infrared (FT-IR) spectroscopy. Energy dispersive X-Ray diffraction (EDX) is combined with scanning electron microscope for surface investigation. It is used as a quantitative elemental analysis technique.

5.6.1. Scanning Electron Microscope (SEM)

As a complementary surface topographic analysis technique, SEM was used to characterize the surface scale/barium sulphate BaSO_4 crystals deposited on the stainless surface (SS 316L). The Philips XL30 SEM instrument was used in the first part of this study, later, a new Carl Zeiss EVO MA15 SEM was provided.

In comparison with Philips XL30, EVO MA 15 SEM facilitates better functions for material analysis using a broader range of sample dimensions. This new generation of surface imaging techniques has a wide range of applications vary from surface integration, geology, forensics, and failure analysis.

EVO MA 15 includes a motorised Z movement of 50 mm, X and Y both 125 mm, the maximum specimen height is about 145 mm. It has a port for wavelength-dispersive spectroscopy (WDS) instrumentation.

The sources or the filaments are made of tungsten, the two SEM systems are shown in Figure 5-11 respectively. During the surface analysis test, The SEM was used in high vacuum mode of about 3.2×10^{-5} mbar, at accelerating voltage of 10 KV and approx. 10 mm working distance (WD). Secondary electron (SE) mode was used for surface imaging. The magnification varies between 100x to 5000x depends on the resolution and the purpose. The scan rate is usually between 5 – 6.

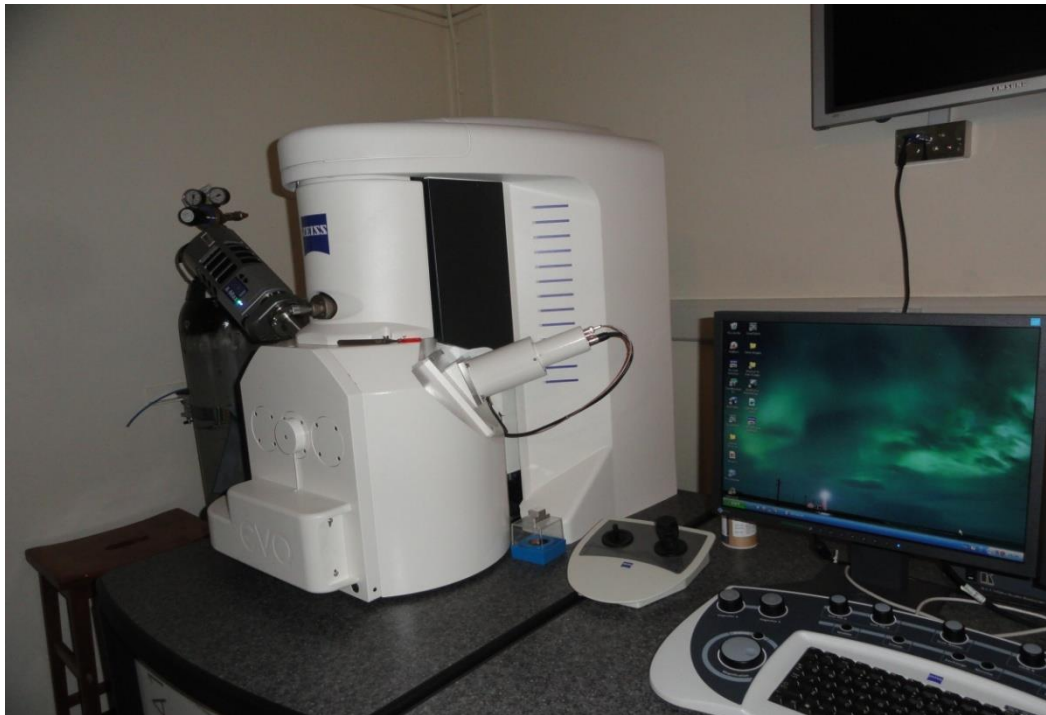


Figure 5-11 : New Carl Zeiss EVO MA15 SEM apparatus

5.6.1.1. Samples surface preparation and design

It appears from the test capillary design that the *in-situ* analysis of the surface scaling propagation is impossible during scaling process unless synchrotron X-Ray apparatus is used. So in this case, the design of a suitable surface was a must and this surface, once scaled, is analysed by different non-destructive test techniques mentioned earlier. This means the deposited scale crystals should not be exposed to any physical deteriorations before testing.

The surface steel sample, on which the scale is deposited, is designed before the experiment setup. It is a stainless steel 316L plate (capillary material) of 4 mm in width and about 25 mm in length. The plate is free of any contaminations such as scratches, organic, inorganic remains or any dust particles that could work as a scale initiator of a heterogeneous crystallization. So it is cleaned with acetone as a solvent followed by distilled water before it is positioned inside $\frac{1}{4}$ " stainless steel SS 316L extension tube, Figure 5-12. The flow direction is marked outside the extension tube.

After the experiment is completed, the scaled plate is taken to a dryer and it is now ready to be analysed. The first test was done using *ex-situ* X-Ray diffraction followed by other surface analysis techniques (minimize interferences). The reason that some techniques require a coating application to the deposited scale samples.

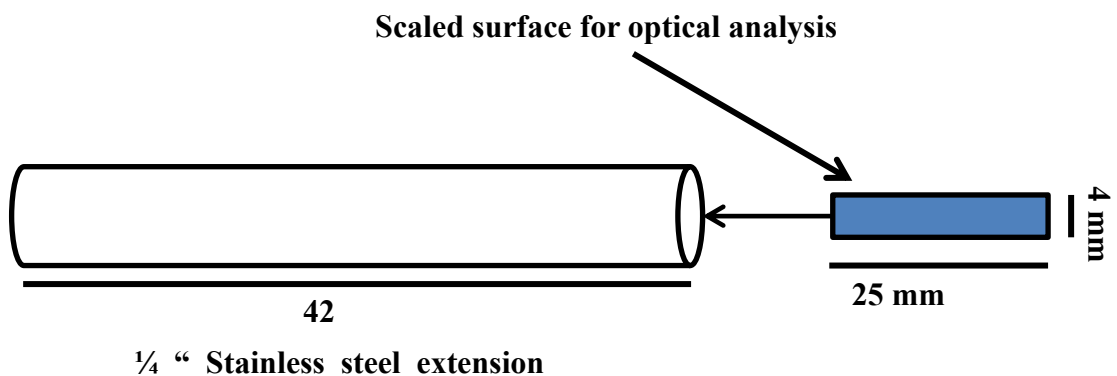


Figure 5-12 : The $\frac{1}{4}$ " stainless extension tube and the plate for the surface analysis.

5.6.1.2. Surface preparation for SEM and EDX test

Due to working under a vacuum, the scaled steel sample must be stabilized on the provided studs using special glue and a sticky rubber surface. Then the sample is secured on the stud by using extra glue, the applied sticky glue was left to dry out before it is positioned in a sputtering unit for gold coating. It is to minimize the charging surface and improve the image resolution.

Scaled surfaces behave differently when they are exposed to photonic radiation with higher energy, some are charged such as barite scale and others are less likely to be charged. The charging surface counts against the resolution of SEM images. In order to minimize the surface charging, certain steps are taken into consideration; first, the sample is coated with nanometre layers of gold using sputtering. Secondly, or some air is deliberately induced from surrounding atmosphere. But in this case, the image will lose part of its sharpness and resolution and becomes blurrish. Technically, the thicker the gold coat the lower the surface charges. The samples were coated with a longer coating time (4 min for three times) and good surface imaging was successfully analysed.

After the surface dynamic tests, the surface investigation of deposited scale was done. Surface topography, crystal size, crystal shape, scale film thickness, uniform and non-uniform scale aggregates were investigated. The complete surface integration helps to determine the effect of different variables applied during the surface deposition process. The imaged surface deposit using scanning electron microscope (SEM) is then analysed quantitatively using energy dispersive x – Ray (EDX) apparatus for alkaline earth minerals such as Ba, Sr, Ca, Mg. It was done by loading the SEM images to project software, which controls the energy dispersive x – Ray (EDX) system.

5.6.2. Energy Dispersive X – Ray (EDX) Analysis

Energy dispersive X – Ray is another valuable surface analysis technique. It is used throughout this work to quantitatively investigate the surface chemical composition (elemental analysis) at different surface scaling conditions in dynamic flow test. The sample preparation is similar to the previous section for surface characterization with (SEM) as the two systems work in parallel.

5.6.3. Surface Deposit Analysis Using EDX

The energy dispersive X-Ray analysis usually starts by loading the subjected image from the SEM to the project software which operates using the EDX system. This system is based on the unique energy of excitation of each element. The expected result is given as energy in electron volt (eV) versus the percentage % of the different element existing in the sample. Once the image is loaded to the project and given a name, then the site of interest is selected with the cursor. The system immediately starts to acquire the spectrum of surface composition of the top deposit layer. For the sake of repeatability and confirmation, which is difficult so far with this system as the mineral concentrations at different aggregates differ, two or three spots are usually chosen. The average of the collected quantities is usually considered. The gold coating has no effect apart from being seen in the final analysis. The data are tabulated and interpreted later in the results and discussion chapters.

5.6.4. X-Ray Diffraction Analysis

The X-Ray surface analysis technique is a well - known sophisticated system for data extraction from surfaces of inorganic deposits. The X-Ray investigations on precipitated scale in bulk and/or deposited on surfaces were carried out using a Philips PanAlytical X'pert PRO diffractometer. This upgraded system is used to analyse the single and multiphase scale crystals. The High ScorePlus software is used to acquire the data and analyse the samples using a build in data bank. The goniometer which represents the mechanical assembly that makes up the sample holder, detector arm and associated gearing is also shown in Figure 5-13.

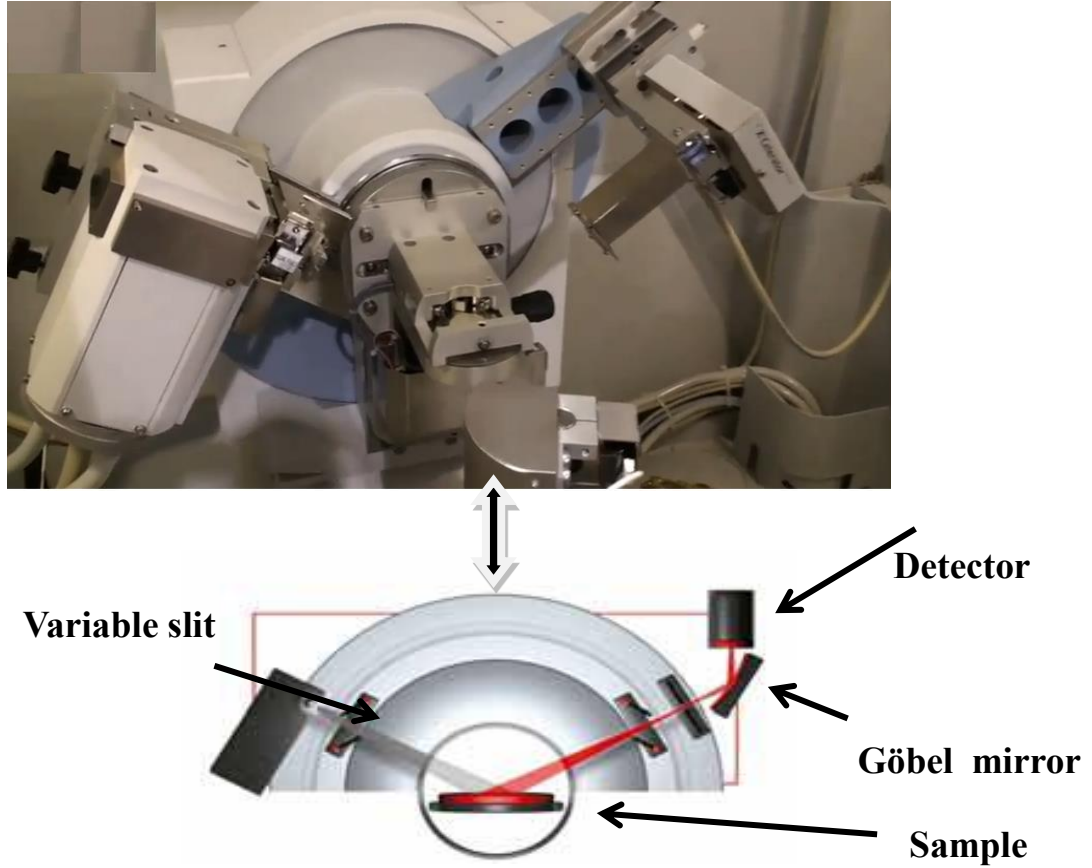


Figure 5-13 : The simple goniometer image shows details of the Philips Analytical diffractometer [175].

5.6.4.1. Philips PanAnalytical X’pert PRO X-Ray System

The Philips PanAnalytical X’pert PRO MPD has the ability to perform a full range of applications, from qualitative and quantitative phase identification, under ambient or non-ambient conditions, to crystal structure solution from powder samples, crystallite size determination, micro strain analysis, residual stress analysis, and preferred orientation.

Philips PanAnalytical X'pert PRO was manufacturer by PANalytical. The source is copper long fine focus with 60 kV, 2.2 kW. The goniometer specification is; Theta-theta, horizontal, and stationary sample mount. The apparatus's incident optics and receiving optics are controlled by software.

5.6.4.2. Sample Preparation and Analysis

X-Ray diffraction (XRD) patterns of powder and surface samples were collected using a PANalytical X'Pert Pro MPD goniometer with Cu-K radiation. Fixed slit incidence specification (0.5 deg. divergence, 1.0 degree anti-scatter, surface specimen length 20 mm) and diffracted (0.5 deg anti-scatter, 0.02 mm nickel filter) optics were implemented.

The surface specification and properties are important to get sensible and accurate X-Ray diffraction data. The improper surface mount would have an impact on the collected figures and mislead the interpretations. So in this case, the curvature surface, which is a result of the ¼” extension pipe, on which the scale is deposited, affects negatively the diffraction angles. Figure 5-12 shows the alternative design to have a flat surface with non-distractive or mechanical damage when it is prepared for a test.

5.6.4.3. Powder Diffraction Sample Preparation

This X-Ray powder diffraction analyses were done on scale powder produced from the bulk precipitation test at different temperatures and mixing ratios. The sample holder, Figure 5-14, is a cell designed to hold a powder and shows no absorption or interference in the X-Ray region. The test cell surface was cleaned using acetone as a solvent, thereafter; the cell is firmly rinsed with distilled water. 1 – 2 mg of filtered/dried scale powder was then collected and smoothed on a properly cleaned and dried portable cell compartment.

The powder samples were prepared by the back-loading method in which a 1 – 2 g scale powder sample is pressed onto the cavity of a dark quartz low-background

support. Data was collected using a point detector in scanning mode with a power spectral density (PSD) length of about 3.35 degree for 15 minutes duration time.

The first step is to chose where the acquired data is to be stored, then the required angle range, the scanning rate or the accumulation are also set at this stage. The more accumulations will increase the spectral resolution and minimize the signal noise ratio in the collected spectra.



Figure 5-14 : Sample holders for XRD powder diffraction [175].

Ex – situ X-Ray diffraction patterns of the collected barite (BaSO_4) scale powders were analysed with 45 kV power (40 mA) and angle of $2\theta = 10 - 80^\circ$ at a 5° min^{-1} scanning rate. The accumulation time is about 5 - 10 min based on the collected spectra's resolution. The pure barite single crystal spectrum was taken as a background or reference before proceeding to the multiphase scale precipitation analysis.

5.6.4.4. Surface scale sample preparation

The $\frac{1}{4}$ " scale spool pipe, which accommodates the stainless steel plate for the surface *ex-situ* XRD analysis, is already fitted into the scale rig system earlier. This idea will facilitate examining and technically analysing the scale barite crystals binding/or adherent to the steel surface in flow conditions. The X-Ray surface analysis technique is to analyse the final crystals faces and their alignment on the subjected surface.

The surface analysis is more difficult compared with the powder analysis as it is more likely that the fluorescence (from substrate) would affect the spectra's resolution. More accumulations will increase the resolution and minimize the noise to signal ratio in the collected spectra. So, there is a difference in the experimental setup.

Similar to the powder, surface *Ex – situ* X-Ray diffraction of the deposited scale/barite (BaSO_4) on stainless steel (SS 316L) was collected at $2\theta = 10 - 80^\circ$ at a 5° min^{-1} scanning rate. The accumulation time is about 15 - 30 min based on the collected spectra's resolution. The XRD spectrum of a scale free steel surface was collected to eliminate any interference from the background. A pure barite single crystal spectrum on steel was taken as a background or reference before proceeding to surface scale analysis to eliminate any interferences.

The untreated scale/barite deposit on the stainless steel surface was also prepared as a background or reference. The *ex – situ* XRD spectrum of untreated scale/barite (blank or reference) was collected without the addition of scale inhibitor (DETPMP). Then, it was compared with treated/surface pre-treated figures and literature to conclude the effect of additive and pre-treated surface on crystal's surface alignment. In addition, the shape and orientation of scale-inhibitor complex crystal were investigated.

5.6.5. Raman Surface Analysis and Observation

Raman spectroscopy is another surface scattering technique tool for surface analysis. Raman sensitivity arises from a wide range of power lines and their intensities. The surface signals are enhanced by rough surfaces. This is governed by other factors such as; surface nature, adsorbate surface alignment, power percentage used and others. As a complementary surface analysis technique, Raman scattering spectra of barite crystal were collected using Rainshaw Raman apparatus equipped with 780 nm laser excitation line. It is supported by software for data analysis.

5.6.5.1. Raman experiment aim and setup

It was mentioned earlier that the barite single crystal (as powder) has been identified by Griffith in 1970. So the purpose of this study was not only to identify its existence on the surface but also to reach its reactivity with the scale retardant. Since the chemical products are well known to form a soluble complex compound, it is very important to investigate (after treatment) if the barite can or cannot be probed on surface at relatively high Ba^{2+} concentration. The chemisorption of chemical products on metal surfaces affect the Raman shift?

In this part, supersaturated real field brine at a saturation index of $SI = 2.6$ was used to deposit the scale/barium sulphate on the internal surface of the stainless steel test tube.

The surface deposition takes place at room temperature and pressure at 50:50 mixing ratio. A new tube capillary is installed for each experiment to provide a new clean surface. The untreated deposit of barium sulphate/scale crystals (additives free) were exposed to 0.1 % power of 780 nm excitation line to determine the finger prints of barite on surface. The Raman scattering spectrum was identified for the scale deposit on surface.

5.6.6. Fourier Transform Infrared (FT-IR) Surface Analysis

In the external reflection spectroscopy (ERS), the sample often consists of a film on a metal surface. The films are usually formed and applied to the surface by different ways e.g., spinning, casting from solvent and deposition. The incident angle is usually high (between $70 - 89^\circ$) in such infrared test. The use of P-polarization increases the spectral sensitivity at this angle. The external reflection process is shown in the figure below, Figure 5-15.

In this work, the anti-growth Diethylene triamine penta methylene Phosphonic Acid (DETPMP) was used to coat a steel surface using the flow dynamic system. In order to have a better understanding of the DETPMP adsorption on stainless steel surfaces, 1000 ppm active concentration of the product solution was used to coat the

steel surface. The DETPMP solution was used in dynamic flow to pass on the 316L stainless steel surface for an hour, the specimen was left to dry. The collected spectrum was used to interpret the DETPMP binding to steel surface for pre-treatment. The question was ‘could the DETPMP chemically manipulate the steel surfaces prior to surface deposition’? Could it affect the surface deposition kinetic process on those surfaces? What about the crystal shape and conformations? The prepared sample was placed under the infrared microscope and exposed to the FT-IR beam, the spectra of the DETPMP organic molecule was collected and the phosphonate group was detected.

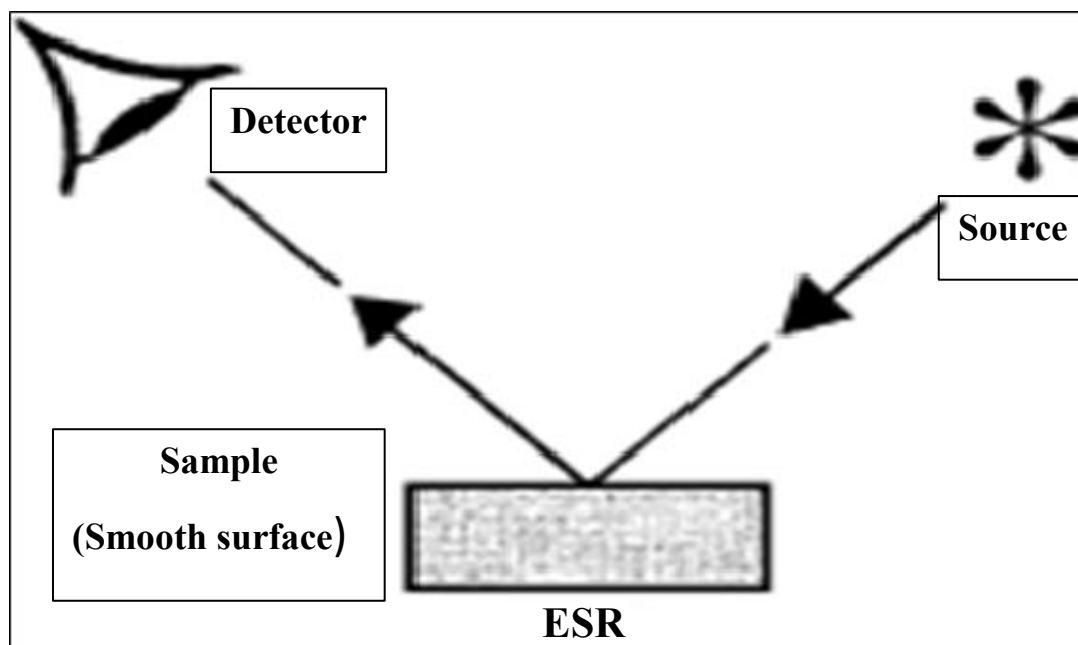


Figure 5-15 : Diagram of the external reflection spectroscopy.

Chapter 6. RESULTS: THEORETICAL, BULK AND DYNAMIC TESTS (PART 1)

6.1. INTRODUCTION

The results section is divided into two chapters; the first one includes the results that deal with the thermodynamic model, the static bulk precipitation tests and the surface deposition tests using the dynamic flow conditions. The new upgraded flow rig system allows control of different experimental parameters on which the collected results rely. This design maintains a constant SR across the capillary and so gives a good understanding of the surface kinetics of deposition as a function of saturation ratio (SR).

The scaling kinetics investigation of different saturated brine compositions show that the SR, the combination of the nature of precipitates and the surface condition, play an important role on scale surface crystal alignment and topography. The focus is given to the surface deposition using dynamic tests. The data which resulted from the three techniques (bulk, surface and theory) are plotted in this section and interpreted later in the discussion section.

The second part of the results are presented in a separate chapter; there are mainly related to the scale crystals surface analysis using different surface analysis techniques. These surface techniques are as follows; Environmental Scanning Electron ESEM, Energy Dispersive X-Ray (EDX), Raman spectroscopy, FT-IR and *ex - situ* X-Ray Diffraction (XRD). The surface samples are designed to be flat to enable adequate surface measurements. These samples are taken from the cell extension after dynamic surface deposition tests.

The brine formulations were kept the same throughout this work at the three temperatures and five mixing ratios. It was subjected to change only when the

saturation ratio (SR) varied based on the barium content in the brine composition. Almost all of the bulk and surface tests were started by determining the theoretical amount of scale. The scaling process parameters were changed throughout the research study from three parameters to two parameters and later to one when barium content was varied.

6.1.1. Result Outlines

The results in this research work are divided into two parts; firstly, there will be three different results which were collected from the three different techniques explained earlier. The results collected from these techniques are put in sequence in this chapter, namely; the thermodynamic theoretical approximations, followed by the bulk tests (turbidity, conductivity and ion selective for barium) and finally the dynamic flow surface tests at different experimental conditions. At the beginning, theoretical scale prediction of the real oilfield complex brine mixture should show the tendency of such brines to form complex deposits at different temperatures. The other experimental parameters are mixing ratio, flow rate and variable saturation ratios. The scaling evaluation was extended to include different barium content at specified temperature of 75 °C.

6.2. MODEL PREDICTIONS

6.2.1. Thermodynamic Scale Predictions

Normally, in real oilfield practice, the prediction of scale is one of the most important steps to understand the system tendency to scale formation. In this work, the Multiscale software was used as scale prediction model. The result files usually contains the pH at equilibrium, saturation ratio (SR), mineral scale precipitates and the masses. Most common ions, which are in the used brine, exist in real field of sea and formation brines. These will form the sparingly soluble scales of sulphates (Barite BaSO_4 , strontium sulphate SrSO_4 , Hydrated $\text{CaSO}_4 \cdot 2\text{H}_2\text{O}$, a hydrated calcium sulphate CaSO_4) and carbonates (calcium carbonate CaCO_3). The focus is

given to the barite formation in both bulk and surface and its thermodynamic and kinetic effect on the whole deposition and precipitation processes. The theoretical prediction method gives only the bulk approximation which is used to assess the surface kinetics.

Generally, the theoretical work study includes thermodynamic assessments of brine mixtures at different temperatures and mixing ratios, different barium contents, brine composition, single brine and at zero barium content in the formation water.

6.2.2. Scale Prediction at 25 °C, 50 °C and 75 °C

Firstly, the aim was to investigate the effect of a wide range of temperatures (25 °C, 50 °C and 75 °C) on surface scale kinetics at different mixing ratios of sea water and formation brines. Table 6-1 shows the formulation of both sea water and formation water brines. These figures were used to predict the scaling tendency of the brine mixtures. The predicted scale/barium sulphate supersaturation ratio values are plotted with respect to sea water percentage at the three different temperatures. The precipitated barite mass (in mmol/Kg of solvent) was predicted using Multiscale software. The barite scale (as a major precipitant) mass was compared with the actual measured mass of scale/barite precipitated in bulk experiment (in g/Kg of water as a solvent).

Table 6-1 : Formation and sea water brines formulation used.

Salt (ion)	Concentration (ppm)	
	FW	SW
KCl (K ⁺)	1906	380
CaCl ₂ . 6H ₂ O, (Ca ⁺²)	2033	405
MgCl ₂ . 6H ₂ O, (Mg ⁺²)	547	1300
BaCl ₂ . 6H ₂ O, (Ba ⁺²)	80	0
SrCl ₂ . 6H ₂ O, (Sr ⁺²)	417	0
Na ₂ SO ₄ , (SO ₄ ⁻²)	0	2780
NaCl, (Na ⁺)	26535	10900

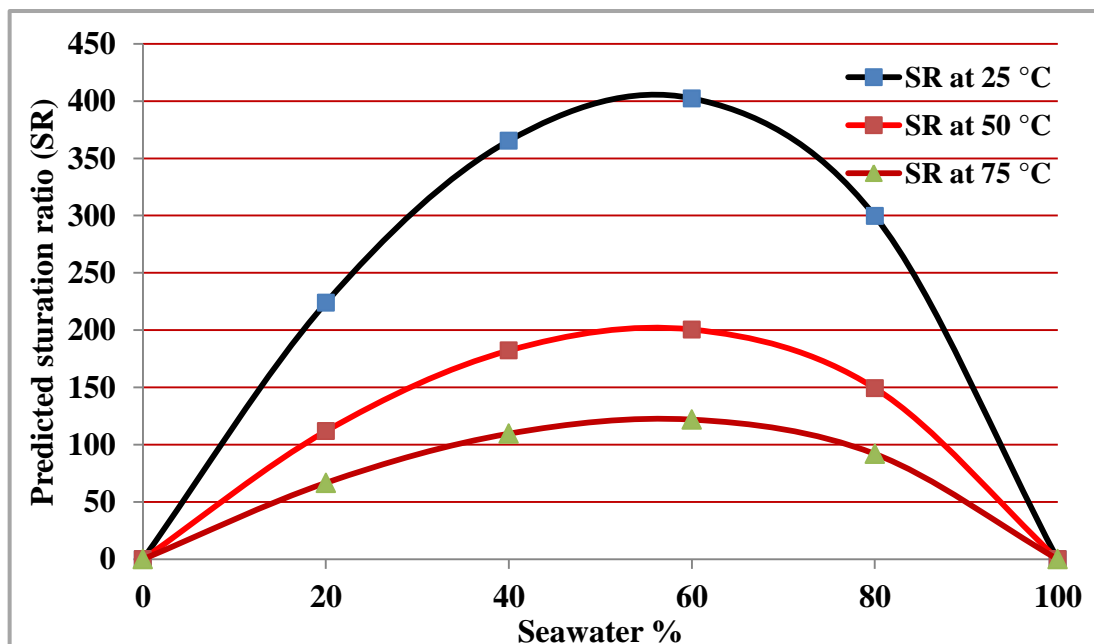


Figure 6-1 : Predicted supersaturation ratio (SR) at different temperature sea water % values.

The predicted scale/barium sulphate supersaturation ratio (SR) values are plotted with respect to sea water percentage at the three different temperatures. It is clear that the saturation ratio (SR) decreases with the increase in temperature from ambient at 25 °C through to 50 °C and to 75 °C. The predicted graph is presented in Figure 6-1. The scale predicted and actually measured masses in bulk are presented in Figure 6-2 and Figure 6-3 respectively. The maximum saturation ratios are shown at 50 % to 60 % of seawater (40 & 48 ppm Ba²⁺ contents respectively) at different temperatures. Regardless of the temperature, the maximum masses are precipitated at about 20 % sea water. This is expected as the number of moles of reacted Ba²⁺ species are mainly controlled by the mixing ratios, this is provided by 80 % formation water (64 ppm Ba²⁺) at the three applied temperatures.

6.2.3. Actual Mass Precipitated in Bulk

The static test was done in the bulk at the same mixing ratios and temperatures at 450 rpm agitation. The purpose was to confirm the prediction plot collected. 500 ml of each brine (formation water and sea water) was transferred to a beaker and heated to a required temperature (if needed). This forms a kilogram of solvent with solute, and the brines were stirred during heating and mixing. Then the mixture was left to cool and settle, it was filtered with a pre-weighed 0.45 microns cellulose filter paper. The formed scale crystals were then dried on filter paper prior to reweight. The net collected scale mass is then plotted with respect to the sea water fraction similar to the prediction results. The collected graphs in both (prediction and experimental) are identical in shape when compared.

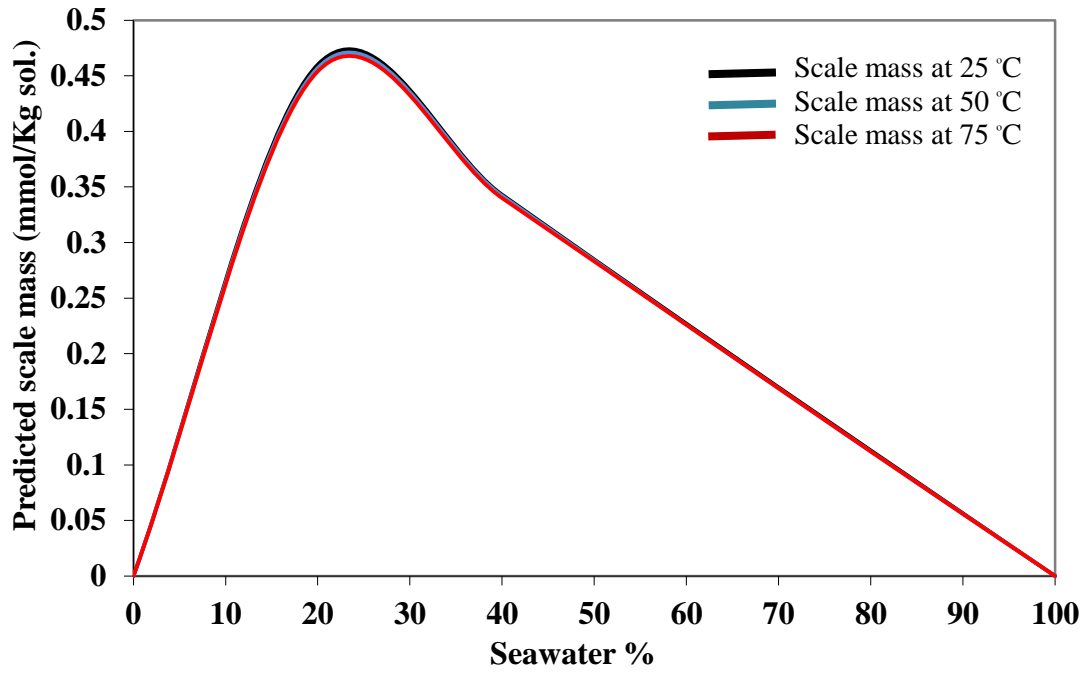


Figure 6-2 : The barite mass predicted at different temperature versus sea water %.

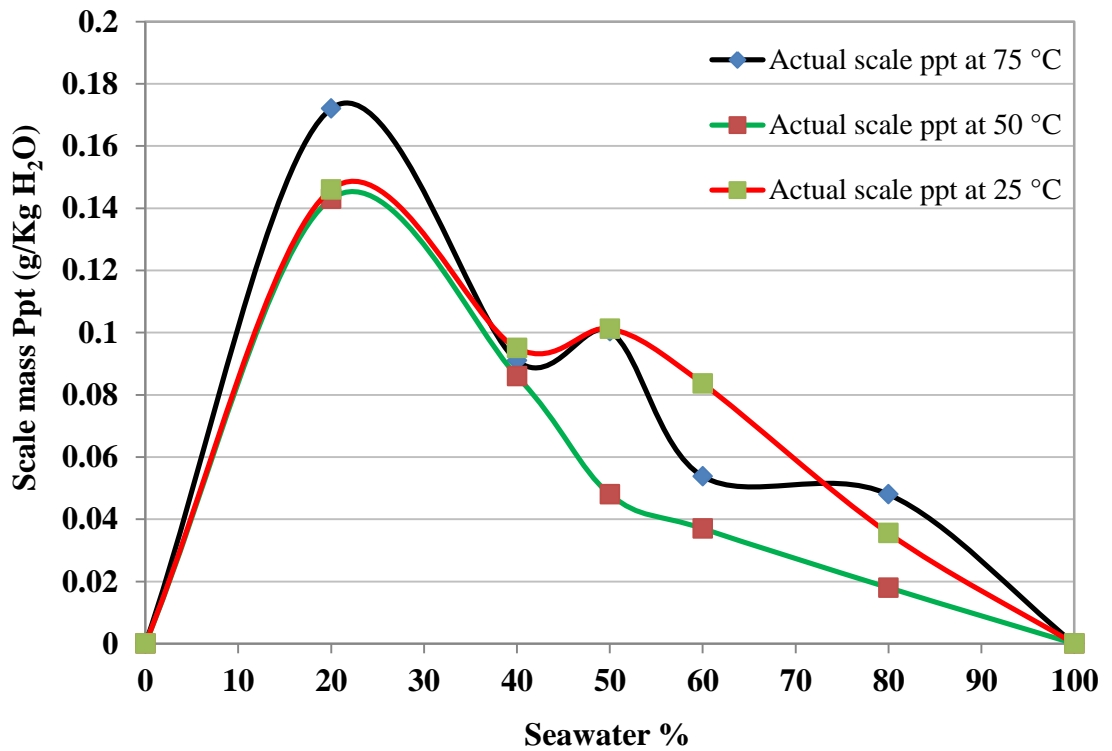


Figure 6-3 : The actual scale mass precipitated during bulk jar tests at 25 °C, 50 °C & 75 °C.

At a specified mixing ratio, the change of temperature has no effect on the number of moles of barium species that were taking part in the reaction. The similarity between the predicted and observed mass graphs has shown a good agreement between the predicted and the experimentally collected masses. This agreement may lead to assume that the bulk precipitation is most probably controlled thermodynamically.

It should be noted that the Multiscale mass assessment does not seem to take the effect of the temperatures into account on the mass predicted as the Figure 6-2 shows. The maximum scale precipitation at 20 % sea water shows a good agreement between the predicted and actual mass precipitated in bulk.

6.2.4. Thermodynamic Predictions at Different Ba²⁺ Contents

Thermodynamic predictions represent a theoretical assessment of whether scale tends to form or not through an indicator of excessive free ions, which describes the instantaneous precipitation/dissolution required to bring the mixture to equilibrium. If supported with kinetic data which will explain when the scale is likely to form and at what rate, either in bulk or on surfaces, a complete understanding of the scaling kinetic process can be achieved.

This calculation was done at one elevated temperature of 75 °C and the resulted plot is shown in Figure 6-4. The saturation ratios of the mixed brines were calculated based on the targeted mixing of 50 % sea water, 10 ml/min flow and a range of barium concentrations (20 ppm, 50 ppm, 80 ppm, 100 ppm and 150 ppm). As expected, the maximum SR was predicted at the highest barium content of 150 ppm Ba²⁺ and the minimum SR at 20 ppm Ba²⁺. But the question was; could that clearly be proven kinetically in terms of dynamic surface deposition (surface scaling film to final growth) and supported/confirmed by bulk measurements?

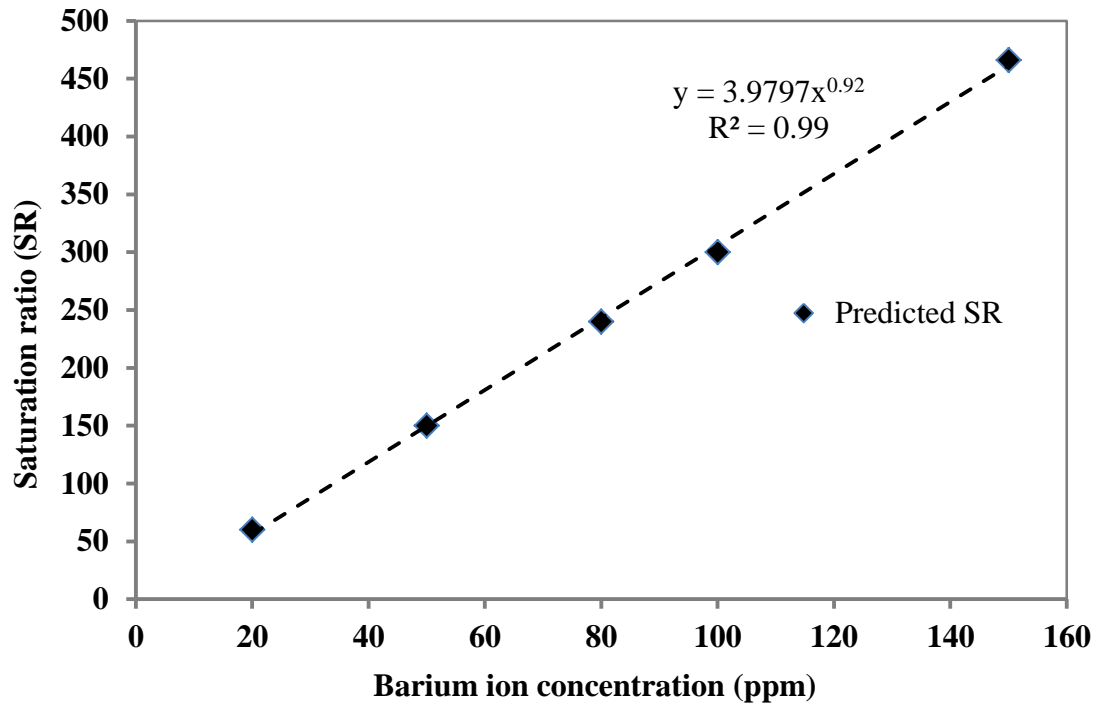


Figure 6-4 : The linear increase of the SR versus the actual Ba^{2+} (at 75 °C) in the final mix at equilibrium.

6.3. BULK SCALING ASSESSMENT

6.3.1. Turbidity Bulk Assessments

In this part of thesis, the bulk tests were done at five mixing ratios and three temperatures. In this case the SR varies within each temperature due to mixing ratios and as a result of temperature differences. The idea was to investigate the kinetics of the scale precipitation resulting from the above complex brine in static bulk conditions at one variable (SR). The saturation ratio, in this case, varies only due to the temperature applied at a constant mixing ratio of 50:50. The barite bulk test is time dependent, it was also a challenge to detect the bulk induction time in thermodynamically very fast reactions especially at elevated temperature. The accurate assessment of bulk induction time will lately be used to evaluate the surface deposition kinetic process. Precise bulk kinetic measurements are also used to design and model the mixing part in dynamic flow assessments.

At the beginning, the test was simply started with a constant (50:50) mixing ratio and variable temperature (25 °C, 50 °C and 75 °C). The static bulk precipitation result is shown in Figure 6-5. From initial static test data, it was noticed that the increase in temperature decreases the induction period in the case of bulk precipitations at 50 °C. The enhanced solubility of barium sulphate/scale in the solution, due to elevated temperature, promotes or accelerates the nucleation rate as the surface tension between the formed barite crystals and the solution decreases.

The bulk test was extended to 1 hour to reveal the state of formed scale crystals/clusters in the long term. Based on the initial bulk precipitation, the test was extended to include five different mixing ratios (20:80 FW: SW, 40:60 FW: SW, 50:50 FW: SW, 60:40 FW: SW and 80:20 FW: SW) at each temperature. The collected data at 25 °C, 50 °C and 75 °C is shown in Figure 6-6, Figure 6-7 and Figure 6-8.

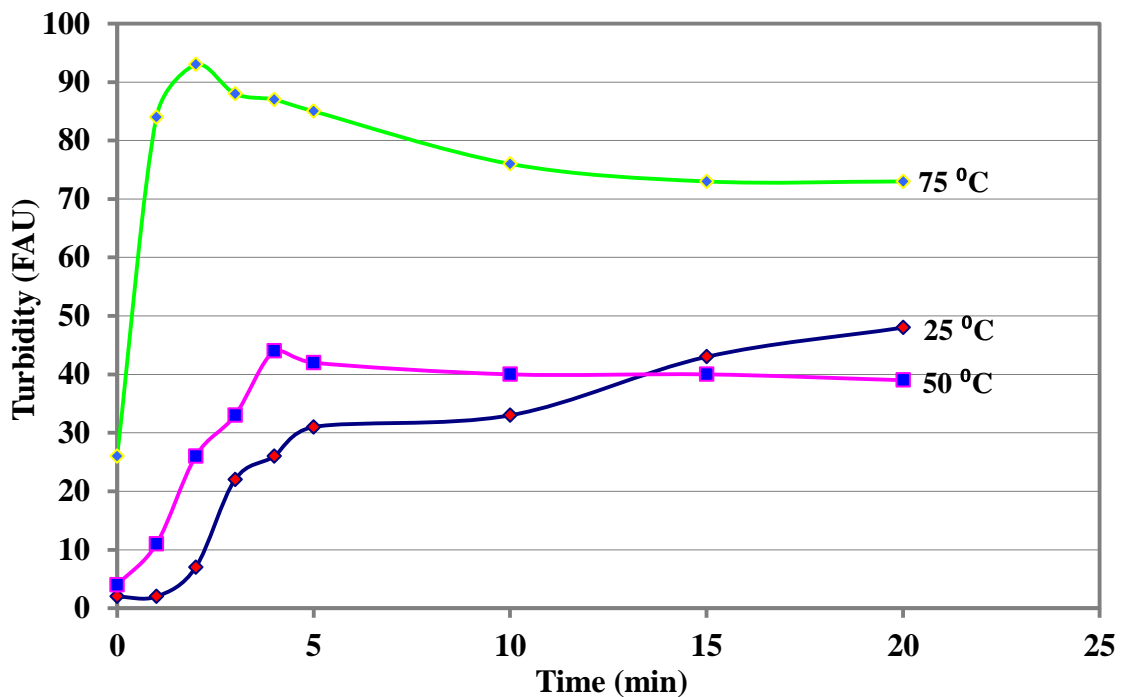


Figure 6-5 : Turbidity of formed scale vs. time at 50:50 mixing ratio at three temperatures (25 °C, 50 °C and 75 °C).

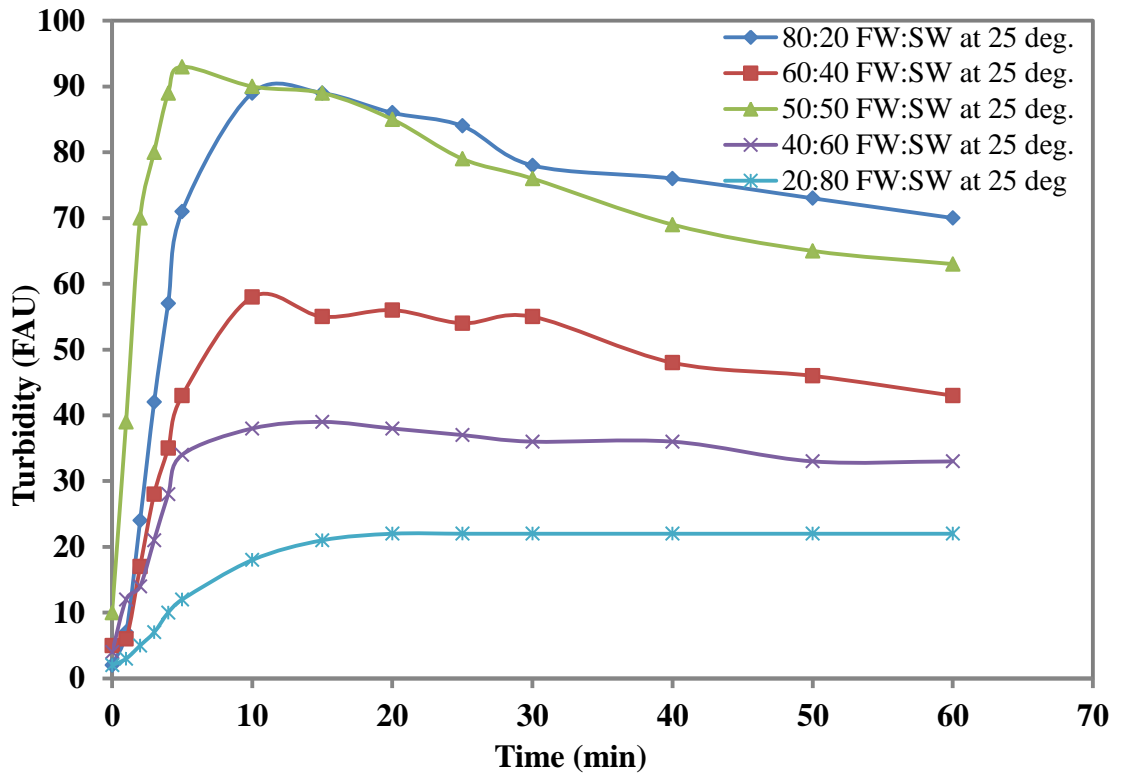


Figure 6-6 : Scale bulk precipitation tests – turbidity versus time at 25 °C.

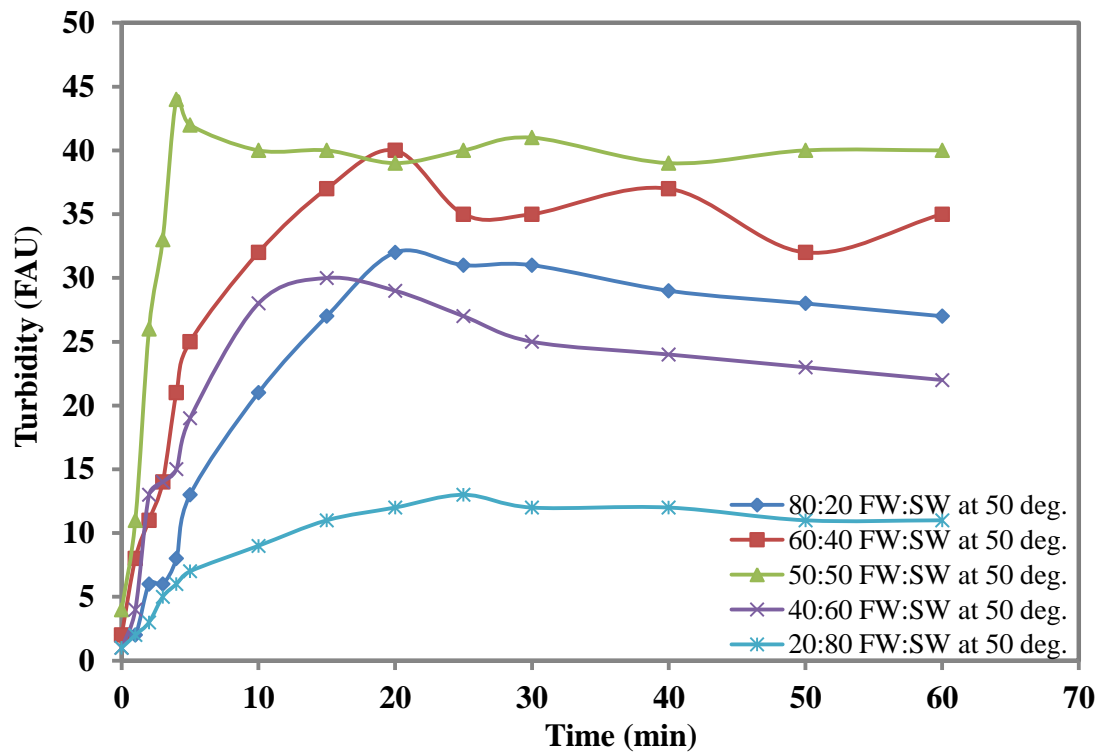


Figure 6-7 : Scale bulk precipitation tests – turbidity versus time at 50 °C.

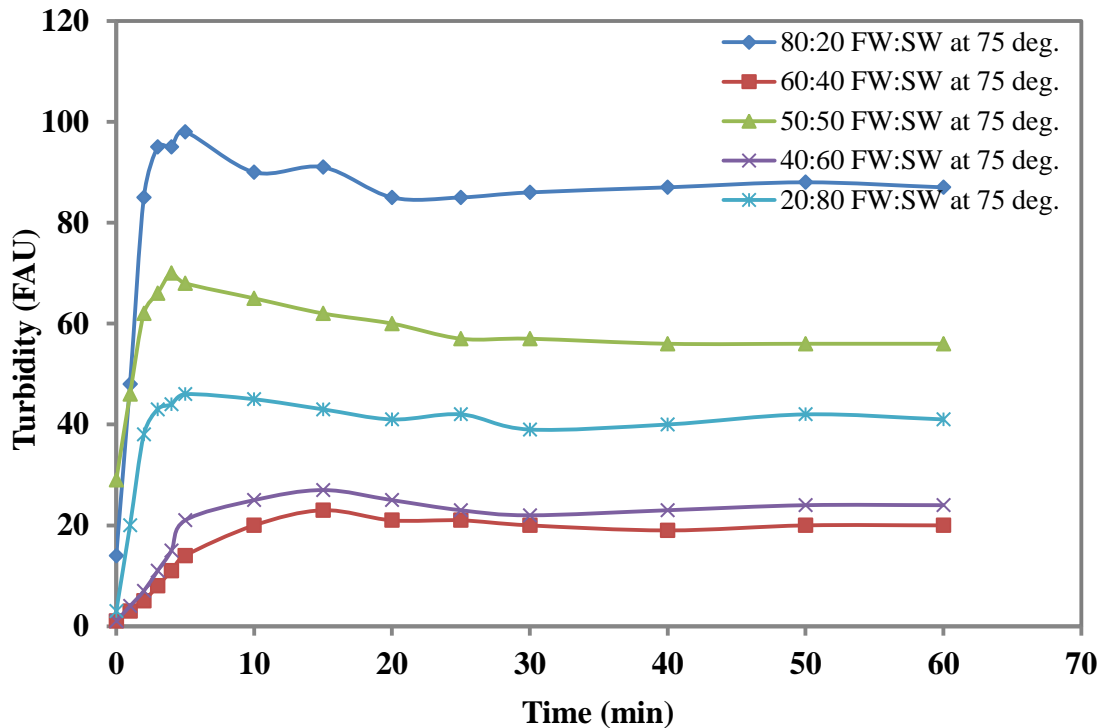


Figure 6-8 : Scale bulk precipitation tests – turbidity versus time at 75 °C.

Apart from 75 °C, the results show that the mixing ratios at which the maximum turbidity was predicted do seem to control the maximum turbidity in bulk. As the temperature increases, it is hard to detect the induction period due to the nature of fast reaction. Most of the extended plateaus show the state of the bigger formed aggregate and their re-dissolution back in the brine mixture with time due to heat.

6.3.2. Effect of Barium Content on Bulk Kinetic

In this part, the state of formed crystallites was the target in terms of the induction time and the growth. At this point, the bulk and surface techniques overlap to assess the whole kinetic process. So the bulk induction time is very important as it is used for assessing a close dynamic system. Moreover, it is used to verify the assumed location where the crystals are formed and their states at specific time. The location and time helps assess the scale kinetics on surface using flow dynamic test.

6.3.3. Conductivity at Different Ba²⁺ Content (75 °C)

The bulk conductivity measurements were done to interpret the bulk precipitation kinetics with surface observations (surface/bulk overlaps mentioned above). The barium content is used as a main factor for variable SR in the test. This was also to find what actually happens to the barium ions in the flow stream from the moment of mixing until the crystal reaches a detectable size. The success is to correlate the bulk observation to the surface figures in terms of time and location in the system. The bulk test was done using two methods to track the ions through and after mixing. Combined conductivity and ion selective electrodes in complex brines were used. In order to find the correlation between surface and bulk processes, the collected bulk data are used to interpret the kinetics of surface deposition (in terms of time). So what happens in the bulk stream before surface deposition takes place in the capillary cell?

The collected bulk figures which represent the conductivity and ion selective measurements are shown in Figure 6-9 and Figure 6-10, respectively. The targeted time of 22 seconds from mixing is marked on the conductivity graph. On the surface, this is associated with calculated residence time prior to deposition in capillary cell a 10 ml/min flow rate.

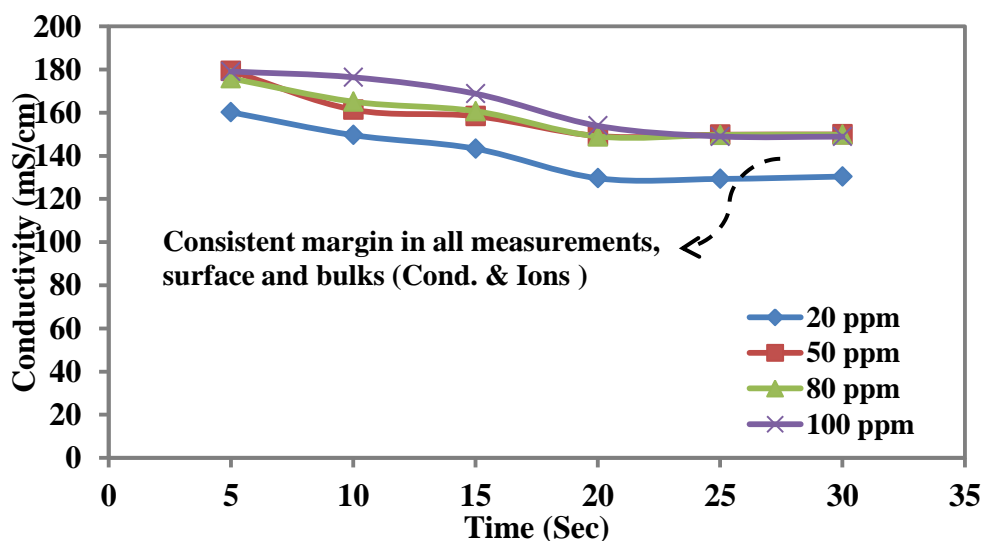


Figure 6-9 : Barium Ions Conductivity Measurements at 50 °C.

At higher barium contents at 100 ppm and 50 ppm, the conductivity drops from about 179 mS/cm to about 149 mS/cm after about 22 seconds respectively. This would then give an impression about the massive ion consumption from the highly supersaturated brine mixture (but not all ions). Using the selective electrode confirms that free barium ions are still detected at lower conductivity measured at the capillary surface – at 22 seconds.

6.3.4. Ion Selective for Ba²⁺ Concentrations at 50 °C

It is vital to use other techniques to confirm the data collected from bulk measurements. Conductivity assessment in such a complex brine (more than one conductive ion) is not enough alone to reveal the role of one species in bulk precipitation. So, the use of an ion selective electrode for barium was vital. The time elapsed (after mixing) for free ions or ions participating in forming crystals was not enough to bring the conductivity to its minimum. This means the sulphate – barium ions reaction continues even beyond the targeted cell (in case of surface). Due to the temperature limitation of ion selective electrode apparatus of 58 °C, the data was collected at 50 °C, see Figure 6-10.

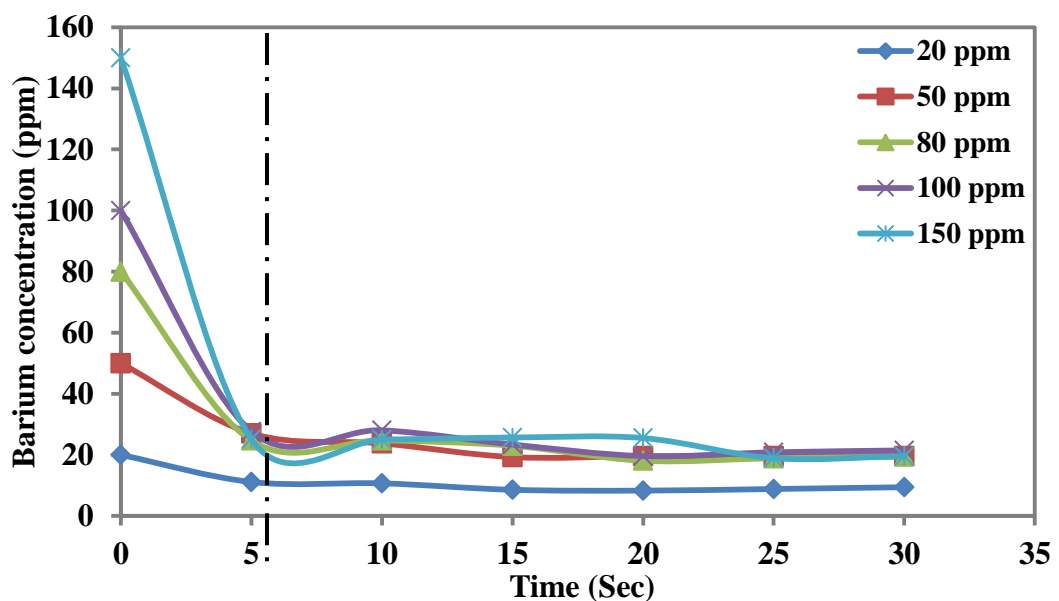


Figure 6-10 : Barium Ions Selectivity Measurements at 50 °C and the Induction Period Marked at About Five Seconds.

6.3.5. Turbidity Assessments at Different Barium Contents

The turbidity measurement was planned to confirm/support the previously mentioned bulk precipitation methods. In order to confirm it, the turbidity measurement was done at the same experimental temperature level of 75 °C and 50 °C; the 50 °C temperature test was done due to the probe's temperature limitation.

Kinetically, two turbidity tests were done to assess the bulk crystallization at 22 seconds elapsed time. It is the time at which a ripened scale crystal should reach a detectable size according to conductivity figures. These two tests were done in parallel. Five hot plates were used to heat the formation and sea water brines (two each) to the desired temperatures. Sea and formation water were heated up to 50 °C in 1000 ml beaker and other sea and formation water were heated up to 75 °C. An additional hot plate was used to heat the brine mixture (at the mixing time) to keep constant temperatures after mixing. After 22 seconds of mixing, 10 ml of the brine mixture was taken to the turbidity (mentioned earlier) meter and the whole results were tabulated. The results are shown in Figure 6-11, more explanations are in the discussion chapter.

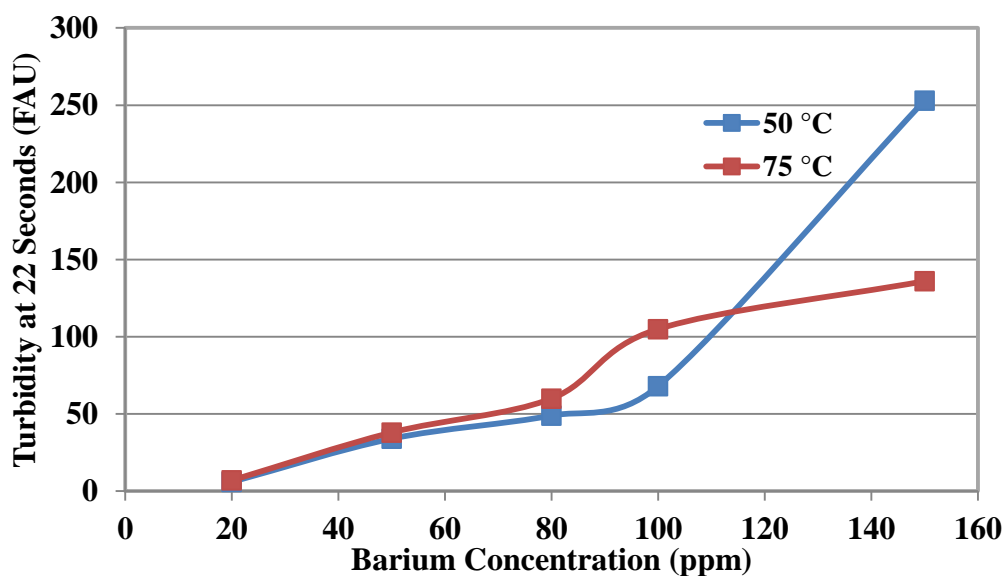


Figure 6-11 : The Observed Turbidity Using Bulk Measurements at 50 °C and 75 °C at 22 Seconds.

6.4. DYNAMIC FLOW: SURFACE SCALING KINETIC ASSESSMENT

The surface kinetic assessments were carried out using the flow scale rig. Different experimental parameters were investigated such as different temperature, mixing ratio, flow rate, barium contents, chemical treatment and surface condition.

6.4.1. Effect of Different Temperature and Mixing Ratios

The surface kinetic measurements were conducted at the same mixing conditions and at the same three temperatures of 25 °C, 50 °C and 75 °C applied in bulk measurements. As this work is based on bridging the three techniques (prediction, bulk and surface measurements), the collected data from the theoretical thermodynamic approach, bulk and dynamic tests are tabulated. The aim is to properly evaluate the kinetics of barite (multiphase scale but mainly barium sulphate) scaling on stainless steel surface SS 316L, which results from the mixing of the chosen brine compositions.

When the actual scale precipitate mass in Kg of water (solvent) is experimentally determined, then the total brine mixture volume (litre) used for any experiment will give the actual mass of scale particles formed. Thereafter, quantitatively, the scale deposit percentage which is actually stuck to the internal surface of the capillary cell from the total mass passed through is obtained. The actual weight deposited in the capillary does not only give the average weight and estimated rate of deposition in a time unit but also helps to assess the kinetics on bare steel and pre-scaled surfaces.

The new set up (unlike coils) facilitates the quantification of mass deposited at different temperatures. The scale deposited mass was found to differ with applied temperature regardless of the constant inner volume dimension of the capillary. The question is why this fluctuation in mass, induction time and the final blockage time? The latter is explained in detail below at different temperatures. At this stage of the research, 5 ml/min flow rate was implemented using a 100 SC Gilson head. At each

experiment, the volume of the mixture was physically measured in a time unit using a measuring cylinder.

6.4.2. Scale Surface Deposition Kinetics at 25 °C

The barite surface deposition kinetics were monitored by measuring the differential pressure across a capillary. Most of the theoretically predicted barite mass and experimentally deposited on the capillary's internal surface (columns 7 & 8 in Table 6-2) show a good agreement in terms of the direct increase of scale mass gained from lower to higher barium contents. The surface kinetic investigation tests are shown as a recorded differential pressure (psid) versus time in hours, as in Figure 6-12.

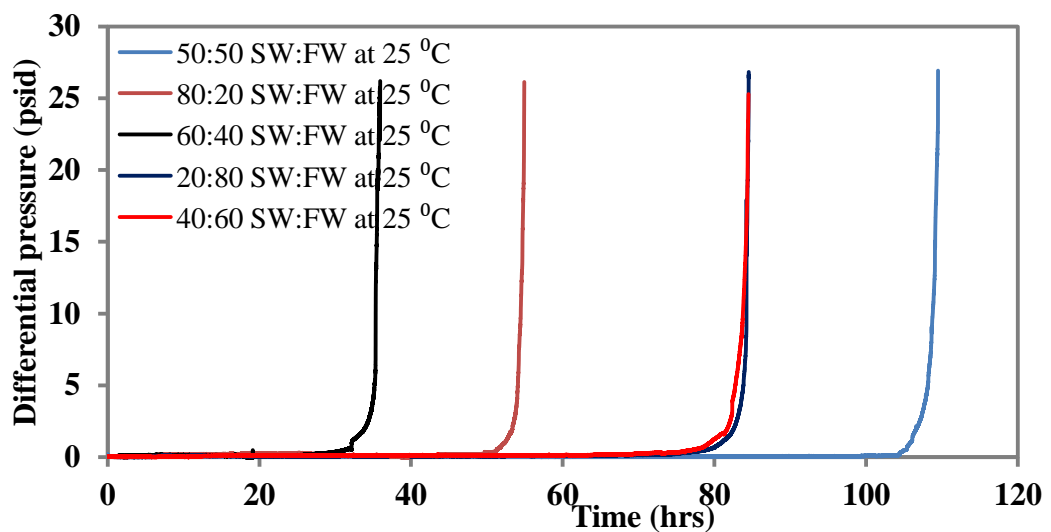


Figure 6-12 : Shows differential pressure as a function of time at 25 °C at five mixing ratios.

Table 6-2 : Bulk precipitation and dynamic surface deposition data at 25 °C.

Mixing ratio FW:SW	Total brine mixture volume used (litre)	Ind. time (Hrs) (flow test)	Total time (Hrs)	Actual Wt. through test cell (g)	Measured Ppt in bulk (g) per Kg H ₂ O	Multiscale predicted (mmol/Kg H ₂ O)	Measured Wt in test cell (g)	% Wt. deposited in test cell	Avg. rate of deposition x 10 ⁻⁸ g/sec
20:80	16.5	43.6	55	0.55	0.0335	0.113	0.0046	0.83	2.31
40:60	10.8	23.7	36	0.9	0.0836	0.227	0.012	1.32	9.23
50:50	32.8	99	109	3.32	0.1012	0.285	0.0115	0.35	2.92
60:40	25.4	63	84.5	2.4	0.0950	0.343	0.0195	0.81	6.44
80:20	25.3	52	84.5	3.7	0.1460	0.46	0.0284	0.76	9.33

6.4.3. Scale Surface Deposition Kinetics at 50 °C

This test was done at a mild temperature condition of 50 °C at the same five mixing ratios. One mixing ratio, 60:40 FW: SW, was reserved to investigate the surface nucleation period and the test was not completed to the final blockage of the capillary. This is also noticed from the plotted graph in Figure 6-13. The kinetic interpretation is given in the discussion part of this work. The resulted scale weight percentage stuck in the testing cell from the total mass deposited, surface scale filming induction time, average rate of deposition, the total blockage time and some relevant figure to understand the two scaling processes are tabulated in one table, see Table 6-3.

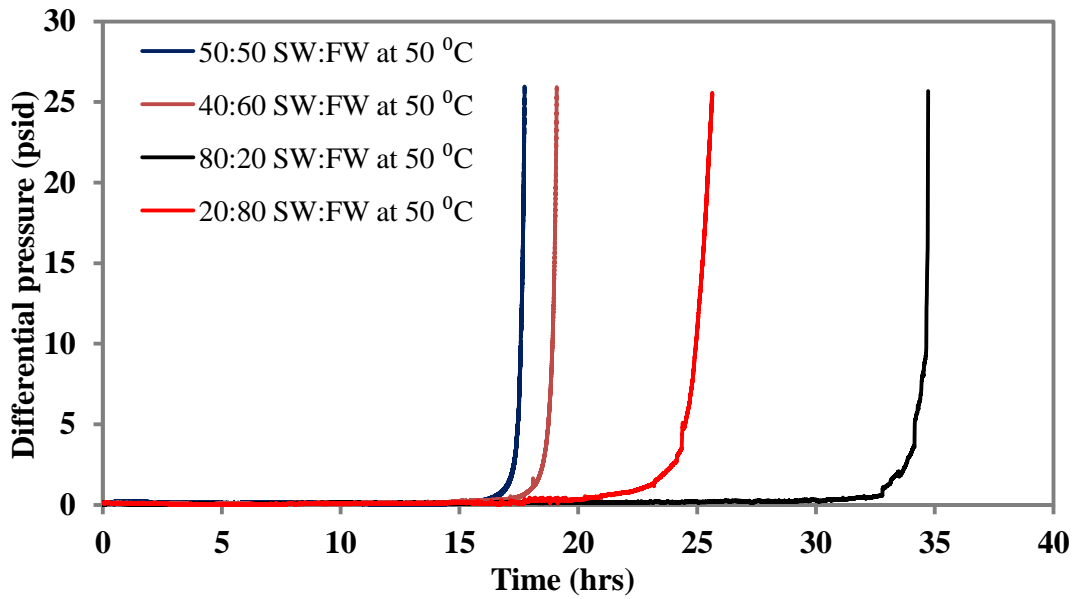


Figure 6-13 : Shows scale surface deposition at different mixing ratios at 50 °C.

It is known that the scale/barite's solubility is expected to increase with temperature and the deposition kinetics rate also increases. At this moderate temperature (50 °C), the main figures from different techniques were tabulated below. At 50 °C, the observed surface scaling induction period (before scale film final growth) was recorded at lowest Ba²⁺ content at 16 ppm in the final brine mixture (20:80 FW: SW). At 50 °C and 20 % formation water, the longest surface scaling induction time was observed at the lower predicted mass and SR.

The resulting scale weight percentage stuck in the cell, from the total mass precipitates, shows some agreement with most of the figures resulting from different mixing profiles. Exceptionally, the weight percent was dropped to 1.47 % at 80:20 FW: SW, this confirms the ability of bigger particles (highly populated stream with suspended solids) to disturb the surface nucleation and growth.

At a moderate temperature of 50 °C, the recorded shorter surface scale filming induction times was obvious at 40 % and 50 % sea water at maximum predicted saturation ratio (SR). At 20 % sea water (64 ppm Ba²⁺ content), 1.1011 g of scale is

the total mass deposited from 7.7 litre of mixed brine consumed. It was the highest mass precipitated in bulk, and it was also the highest in the case of surface deposition by 0.01621 g.

Table 6-3 : Bulk precipitation and dynamic surface deposition data at 50 °C.

Mixing ratio FW:SW	Total brine mixture volume used (lit)	Ind. time (Hrs) (flow test)	Total time (Hrs)	Actual Wt. through test cell (g)	Measured Ppt in bulk (g) per Kg H ₂ O	Multiscale predicted (mmol/Kg H ₂ O)	Measured Wt in test cell (g)	% Wt. deposit - ed in test cell	Avg. rate of deposit - ion x 10 ⁻⁸ g/sec
20:80	10.4	16.5	34.7	0.1875	0.018	0.112	0.0075	3.98	0.55
40:60	3.6	--	12*	0.1332	0.037	0.226	0.0033	2.47	0.76
50:50	5.3	14	17.7	0.2544	0.048	0.284	0.0115	4.5	1.8
60:40	5.7	14.3	19	0.493	0.086	0.342	0.0158	3.2	2.5
80:20	7.7	17.7	25.6	1.1011	0.143	0.457	0.0162	1.47	1.9

* Surface pre-scaled.

6.4.4. Scale Surface Deposition Kinetics at 75 °C

The dynamic test at elevated temperature (75 °C) was created to imitate the barite deposition kinetics on the downhole equipment surfaces in the oilfield. At this higher temperature, all the predicted and the experimental bulk/surface data were also tabulated in Table 6-4. Comprehensive information on scaling kinetics on scaling on steel surfaces is revealed. The figures are supported by thermodynamic predictions and bulk assessments. Figure 6-14 shows the observed scale film induction time of scale surface deposition at the targeted five different mixing ratios (20:80, 40:60, 50:50, 60:40, 80:20 FW: SW) at 75 °C. Relevant information for kinetic interpretation of deposition at elevated temperature of 75 °C is collected in Table 7-4.

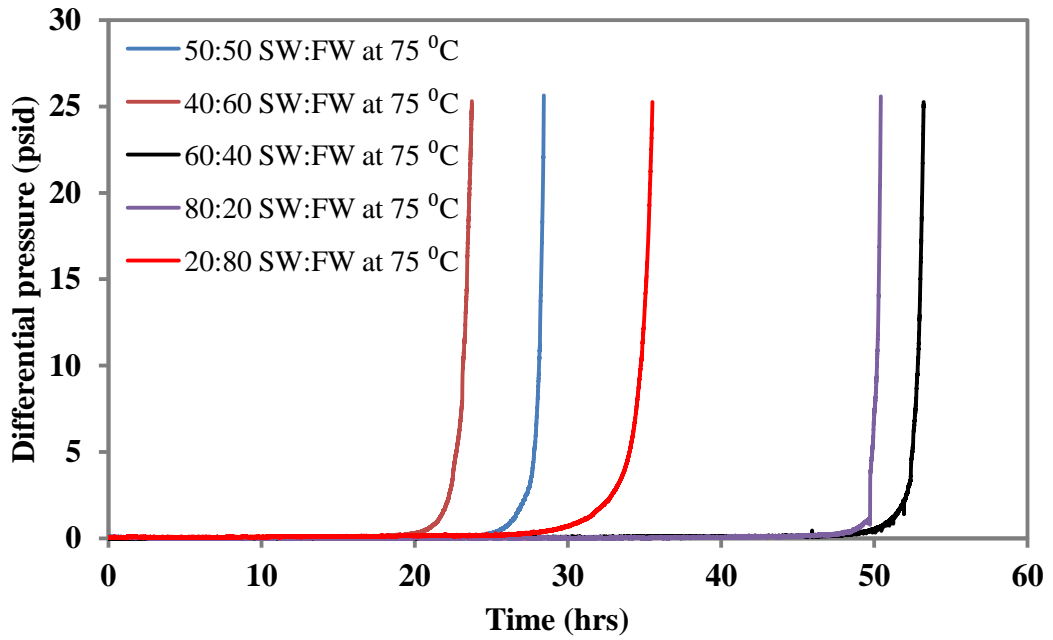


Figure 6-14 : The observed surface scaling film induction time at different mixing ratios and 75 °C.

Table 6-4 : Bulk precipitation and dynamic surface deposition data at 75 °C.

Mixing ratio FW:SW	Total brine mixture volume used (lit)	Ind. time (Hrs) (flow test)	Total time (Hrs)	Actual Wt. through test cell (g)	Measured Ppt in bulk (g) per Kg H ₂ O	Multiscale predicted (mmol/Kg H ₂ O)	Measure-d Wt in test cell (g)	% Wt. deposit - ed in test cell	Avg. rate of deposit - ion x 10 ⁻⁸ g/sec
20:80	15.1	40.3	50.4	0.73	0.04826	0.112	0.0076	1.046	4.21
40:60	15.1	40.5	53.2	0.812	0.05381	0.226	0.0164	2.016	8.58
50:50	7.9	23.3	28.4	1.183	0.14923	0.284	0.0112	0.949	0.11
60:40	6.3	17.2	23.7	0.574	0.09118	0.343	0.0118	2.047	0.14
80:20	9.3	23.3	35.5	1.597	0.17196	0.454	0.0231	1.445	0.18

Theoretically, at 75 °C, the supersaturation ratios at the different mixing ratios were decreased dramatically compared with at 25 °C and 50 °C. The SR ranges between 66.6 (80:20 SW: FW) as the lowest and 121.9 as the highest (40:60 SW: FW). Accordingly, the saturation index (SI) will range between 1.82 and 2.08 respectively. Generally, the observed surface scale film induction times (at 75 °C and different mixing conditions) show that most of the induction time values are lower than those observed at 25 °C and higher than those recorded at 50 °C. It is noticed that, at the highest predicted saturation ratio (at 60 % SW), the induction period was higher (40.5 hrs). It can be referred to the higher scale crystals solubility due to the combination of flow and surface temperatures.

In addition, it can also be explained by the possible failures of the nucleation layers at any stages due to flow/surface high temperature, and the size of barite particles formed as suspensions. This argument can be supported by the bulk result tests at 75 °C in which the induction period was not even observable. The turbidity units were at a maximum due to massive light scattering (high absorbance) by possible bigger scale/barite formed clusters at 80:20 FW: SW. The tabulated bulk and surface figures at 75 °C show the net scale weight gained in the testing cell, and the percentage of scale weight deposited in the capillary. This percentage was calculated from the total scale mass actually precipitated. It explains the discrepancies of the possible detachments of surface crystallites during the early stage of crystallizations or even at the growth levels. The temperature effect on the surface scaling are compared and analysed in terms of observed surface kinetics.

For easy comparison between the observed induction periods which were recorded at different temperature applications, the values are collected in Table 6-5.

Table 6-5 : The observed surface deposition induction time using tube capillary at 25 °C, 50 °C & 75 °C.

Sea water %	Observed induction time per hrs (dynamic test) at:		
	25 °C	50 °C	75 °C
0	0	0	0
20	52	17.7	23.3
40	63	14.3	17.2
50	99	14	23.3
60	23.7	**	40.5
80	43.6	16.5	40.3
100	0	0	0

** Chosen for surface pre-scaling.

6.4.5. Surface Kinetic Data Versus Prediction

Useful data can be extracted from the previous surface observation results. This would help clarify/highlight some kinetic concepts and physical quantities in the dynamic scaling systems such as; the rate of surface deposition, mass quantity variations, and surface scaling film induction period. These figures are correlated to the predicted saturation ratios (SRs) or saturation indices (SIs). In this regard, the figures were not dealt with as a single mixing profile but the idea was to treat the whole five mixing profile within each temperature as one data set. The comparison was done between the three applied temperatures.

6.4.6. Prediction Versus Observed Induction Period

At 25 °C, 50 °C, and 75 °C, the observed surface scale filming induction period was extracted for every mixing profile. The recorded time was plotted with respect to the predicted saturation ratio which drops as a function of temperature. Figure 6-15 shows the resulting relations between the predicted saturation ratio and experimental surface scale filming induction time of barite/scale system.

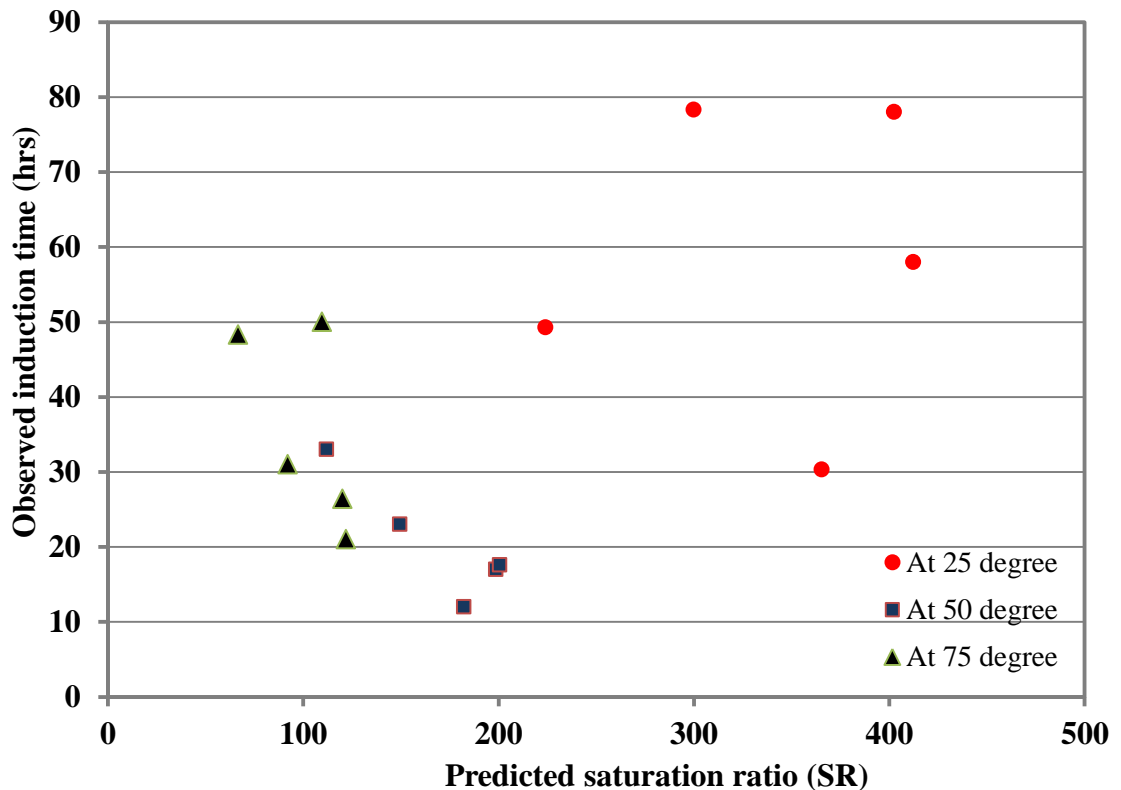


Figure 6-15 : Observed surface scale filming induction times vs. predicted saturation ratios at different SW: FW mixing ratios.

6.4.7. Average Rate of Deposition and Seawater Fraction

The rate of deposition varies based on surface conditions which could be a bare steel surface at the beginning of crystallization process or later as pre-crystallized surface (crystal-crystal contact). So, in this case, the rate of surface deposition will definitely change with time and the best term to use is the average rate of surface deposition. Figure 6-16 shows the measured average surface deposition rate with respect to the seawater fractions at 25 °C, 50 °C & 75 °C and five mixing ratios. The saturation ratios variation with the mixing ratios can be recalled for comparison.

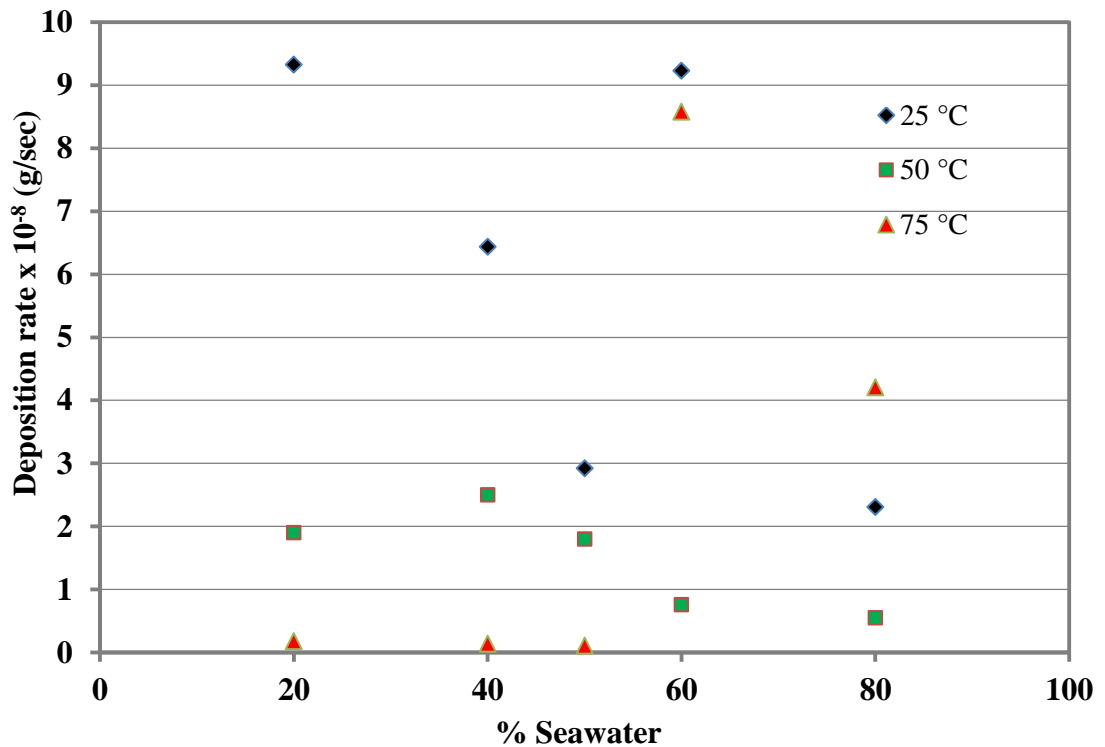


Figure 6-16 : Measured average surface deposition rate at 25 °C, 50 °C & 75 °C and five mixing ratios.

6.4.8. Mass Percentage Deposited on Surface

It is worth mentioning here that the capillary cell volume which is used throughout this work was similar. However, the final deposit weight varies based on different experimental parameters (seawater percentage, temperature and SR for instance). This alone gives an indication about different scaling mechanisms which may have an effect on the surface filming induction period, the particle arrangement in a capillary and their surface adhesion/deposition.

In addition, using the same volume of cylindrical capillaries should end up with a constant mass no matter what was the saturation, rate of flow, temperature or mixing ratios, but in fact that was not the case experimentally. The weight percentage of deposited barite on the internal surface from the total precipitated barite/scale mass, at different temperatures and seawater percentage, was estimated and plotted. Figure

6-17 shows the scale mass % deposited on the capillary surface from the total mass precipitated at different temperatures and sea water percentage. It is an additional advantage of using the capillary cell in terms of better understanding of surface crystallization kinetics. It reveals the effect of possible different arrangements of formed crystallites at different thermodynamic and kinetic conditions (temperature and SR).

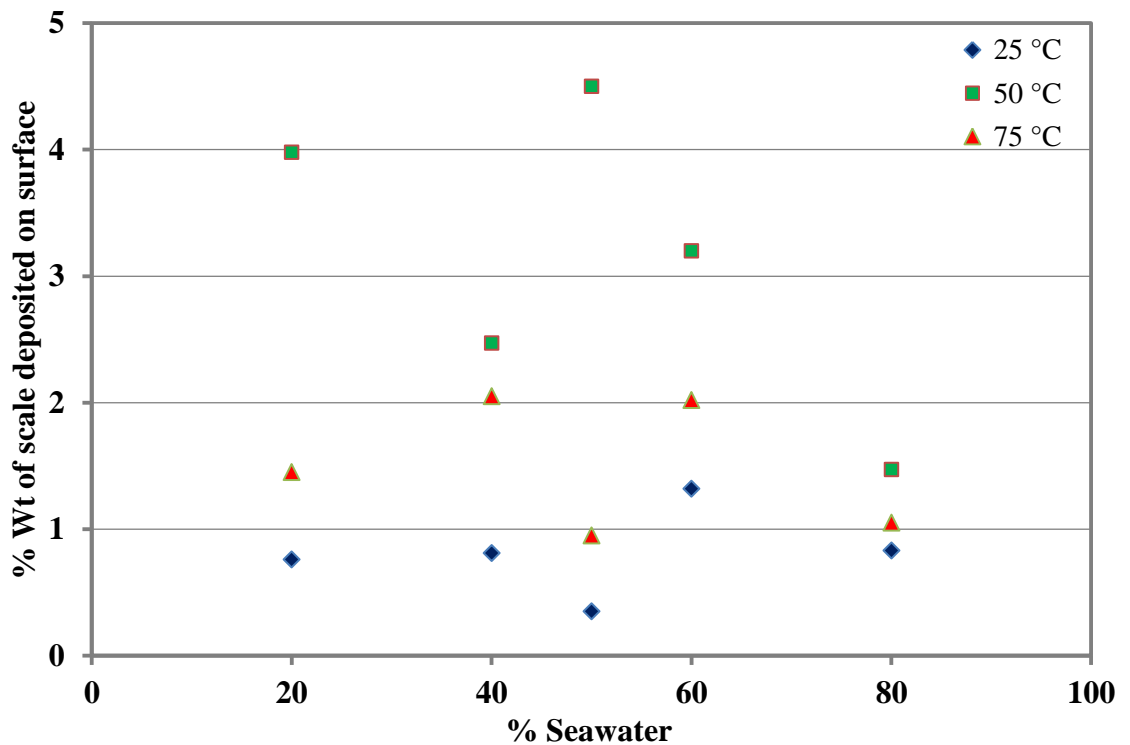


Figure 6-17 : The mass % deposited on the capillary surface from the total mass precipitated at different temperatures and sea water percentage.

6.4.9. Total Scale Mass Deposited in Capillary

This is an additional concept for scale surface kinetic investigations which is different from the previously highlighted term (mass percentage). These results, in both mass and mass percentage on the surfaces, are presented as five figures from different mixing ratios (at each temperature). But these figures are considered to represent a one set of data when it is compared across different temperatures. So the

variation with the temperature applied becomes clear unlike when individual figure (at different mixing ratio) is dealt with separately.

6.4.10. Total Surface Mass Gained at Different Saturations

It was proven earlier that the mass predicted to precipitate and actually precipitated in the bulk jar are in good agreement. However, the situation on the surface appears to be different.

Apart from at room temperature, none of the other two temperatures applied (50 °C & 75 °C) show a linear relationship of deposited mass with respect to the seawater fractions. Figure 6-18 shows the total barite mass deposited in the steel capillaries at different temperatures and seawater percentage. There is a linear relation between the mass and sea water percentage when the temperatures were not applied. The scale quantities, which are scattered, shows also an agreement between the other two cases when temperature was applied. The only factor at this stage is temperature that makes a difference. Interestingly, all of the three masses deposited at 50:50 mixing are similar.

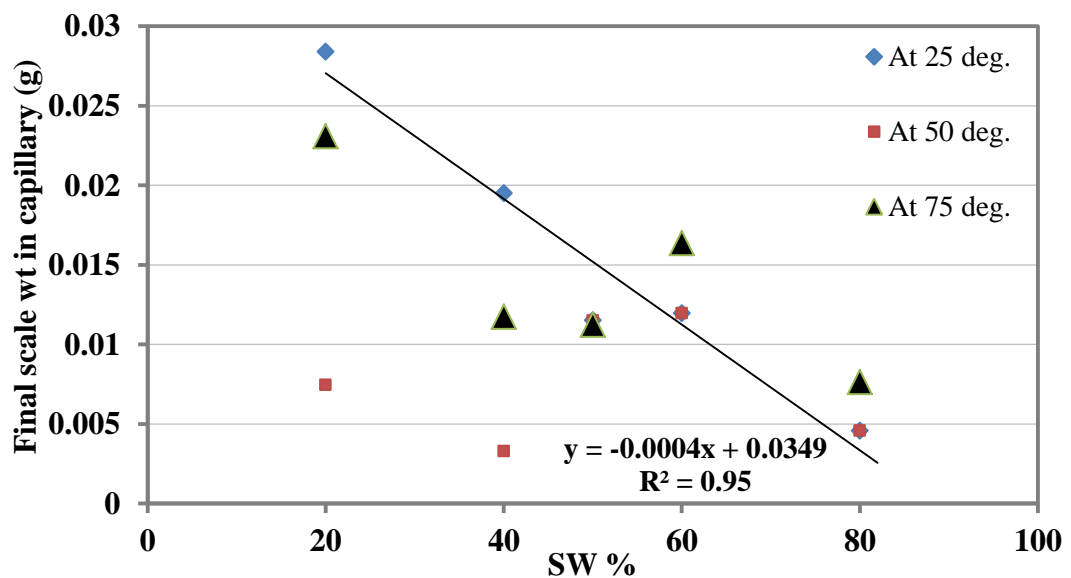


Figure 6-18 : Total barite mass deposited in capillaries at different temperatures and seawater percentage.

6.4.11. ICP Analysis of Rig Waste During Surface Deposition

Practically, the ion measurement gives the actual concentration after surface deposition. It also reveals a change in the saturation ratio in brine mixture (waste water). The question was whether the surface deposition continues after the saturation ratio drops resulting in a drop of saturation index (SI) as well. The suggestion is related to the scale particles formed in the bulk stream then transferred to the surface to continue growing.

The ICP data, which was collected from the effluent brine mixture from dynamic flow scaling rig, shows the expected reduction of the concentration of the reacted species. A flow test at 20:80 FW: SW and 50 °C is taken as an example. Figure 6-19 shows that 75 % of barium ions were consumed to form BaSO₄ (the precipitant). Ca²⁺ precipitates/deposits as sulphate. CaSO₄ is predicted to precipitate in three different salts but no significant ion change observed in ICP figures. This may be related to the lower pH of 6.05 at 50 °C, however, Ba²⁺, Mg²⁺ and Sr²⁺ contents after deposition show a significant change.

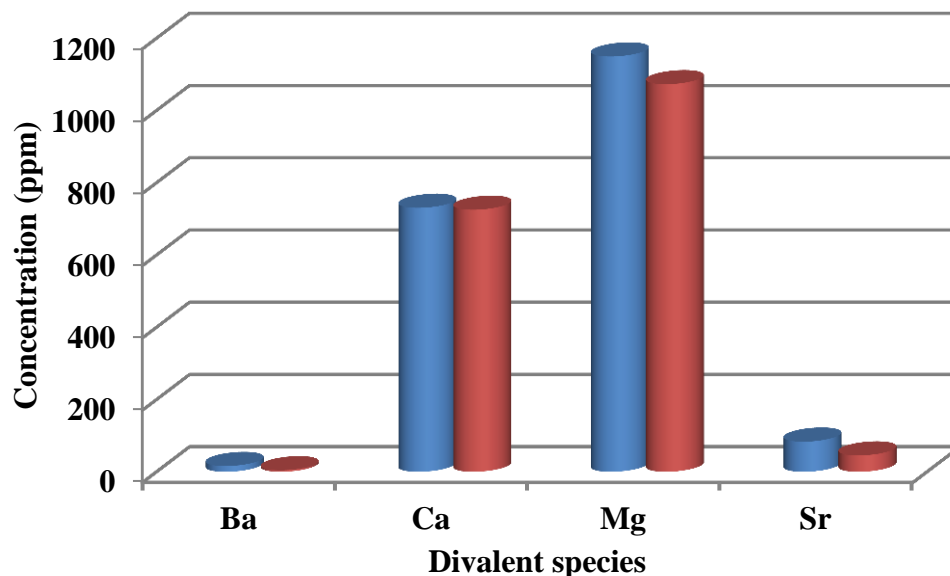


Figure 6-19 : The ICP elemental analysis of the brine mixture waste at 20:80 FW: SW and 50 °C.

6.4.12. Scale Surface Kinetics at Fixed Mixing Ratio (50:50)

In this part, typical surface deposition experiments at a 50:50 mixing ratio were carried out. The differential pressure versus time at different temperatures across testing capillaries was recorded. Raw data is given in Figure 6-20. The variation of induction period with respect to the temperature application was observed.

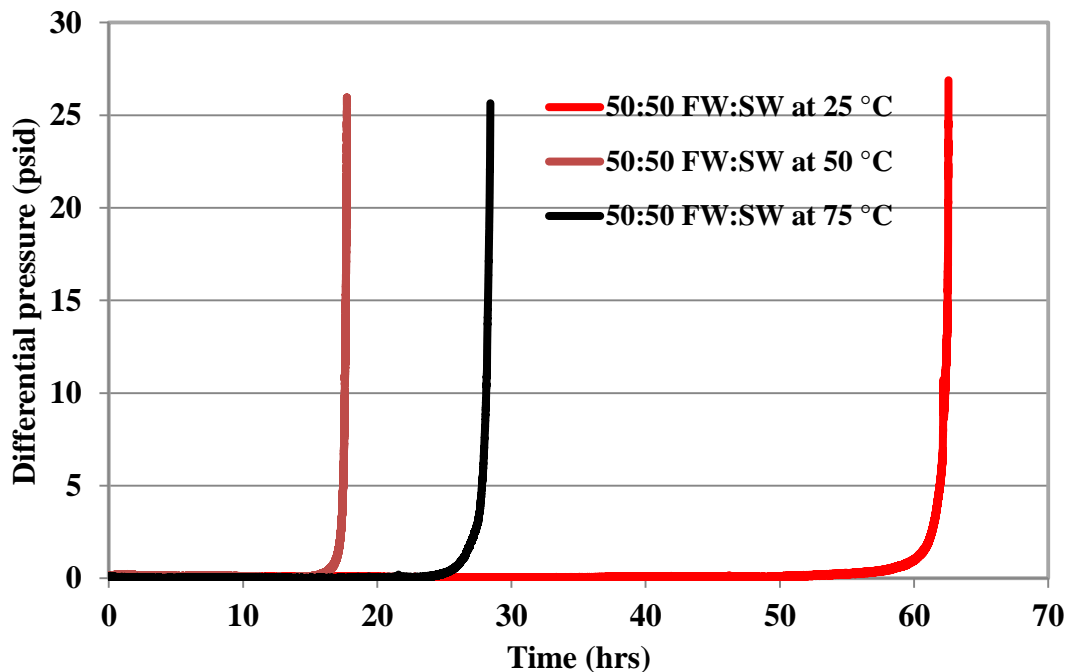


Figure 6-20 : Observed differential pressure values vs. time at 50:50 mixing ratio and 25 °C, 50 °C and 75 °C.

6.4.13. Effect of Flow Rate on Surface Deposition

In the earlier dynamic flow tests, the effect of temperature and the saturation ratio changes at different mixing ratios were examined. The other dynamic test factor, which is related to scale surface kinetics in dynamic flow, is the flow rate. The effect of flow on the surface crystallization kinetics and the final scale surface topography was investigated.

The earlier investigations were done at a lower flow rate of 5 ml/min, so it is vital to try a different flow conditions to get a comprehensive view about the surface deposition. This test was done at 10 ml/min flow rate at a constant mixing ratio of 50:50 and the three temperatures (25 °C, 50 °C & 75 °C). The barium ion concentration was 40 ppm at the targeted mixing ratio. It is obvious that the higher the flow the shorter the residence time, and the chance of bigger size crystals aggregate is less likely to disturb the nucleated surface. The surface growth seems steadier and a shorter surface filming induction period is likely. During surface deposition, the formed crystals or aggregates are exposed to two possible surface conditions with different energy. The crystals are started with surface – crystal contact and lately crystal – crystal arrangements (impingent or diffusion).

Generally, the effect of flow study reveals the effect of two aspects in this series of investigations; first, the effect of residence time, and the effect of the formed scale particles on a scale film being in growing progress in the capillary.

Consistent reproducible data were collected. The test was carried out in atmospheric pressure using a similar upgraded scale rig for the tube blocking test. It was used to investigate the kinetics of barium sulphate formed on the stainless steel surface, at two different temperatures in atmospheric pressure [8].

The same brine formulations were used and predicted barium sulphate/scale supersaturation values with respect to sea water percentage at the three different temperatures recalled from previous assessment. The surface tests which were carried out at 5 ml/min flow (collected earlier at three temperatures of 25 °C 50 °C, 75 °C and 50:50 mixing ratio) were also recalled for comparison, Figure 6-20.

6.4.14. Surface Deposition at 10 ml/min Flow Rate

At 10 ml/min, the recorded differential pressure versus time plots were very consistent and reproducible, see Figure 6-21. The observed surface filming induction time was collected at 10 ml/min flow and different temperatures. Similar to those figures collected at 5 ml/min flow, a higher saturation ratio at 25 °C shows longer induction period followed by 50 °C and the shortest at 75 °C. The comparison and interpretation were expanded in the discussion part. For the sake of reproducibility, these tests were done twice and the collected data (e.g induction period, weight % precipitated from the total mixture, scale mass in cell, and the total blockage time) were tabulated below, see Table 6-6.

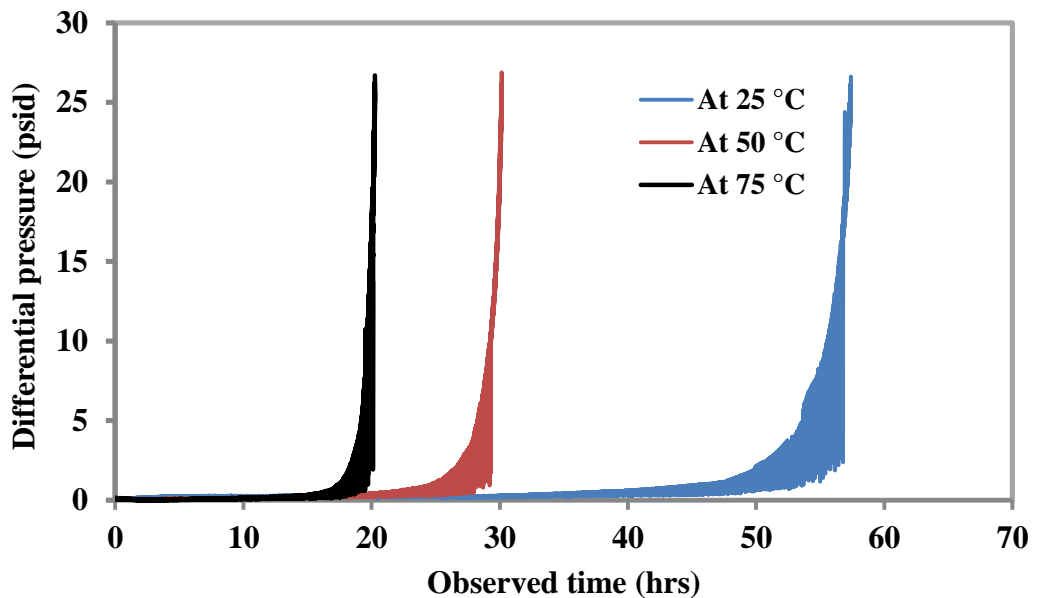


Figure 6-21 : The reproducible recoded differential pressure versus time at 10 ml/min flow rate.

Table 6-6 : Reproducibility of dynamic surface deposition data of barite at 25 °C, 50 °C & 75 °C at 10 ml/min flow rate.

Temperature (°C)	Total brine mixture volume used (lit)	Induction time (hrs) (dynamic test)	Total blockage time (hrs)	Actual Wt. through tube capillary (g)	Measured Ppt in bulk (g) per Kg H ₂ O	Measured Wt. in capillary cell (g)	Wt. % deposited in capillary
25	34.38	32	57.3	5.7	0.1012	0.0159	0.278
25	33.48	34	55.8	5.65	0.1012	0.0098	0.173
50	18.12	12.3	30.2	0.869	0.048	0.0135	1.55
50	18.06	12.3	30.1	0.867	0.048	0.0125	1.42
75	12.12	10.7	20.3	1.806	0.149	0.0122	0.675
75	15.18	15	25.3	2.262	0.149	0.0175	0.774

The differential pressures versus time graphs were successfully obtained for the barite scale surface deposition. At the higher (10 ml/min) flow rate, the logical sequence of the plotted differential pressure figures from high temperature to the lower temperature or vice versa is confirmed. This is also supported not only by the reproducible data but also the observed scale film induction time durations, total blockage time and the net scale mass adhered to the cell's internal surface, all these figures are tabulated in Table 6-6. Similar to the surface deposition at 5 ml/min flow rate, the scale surface film induction time at 25 °C is observed the longest. So at 25°C, no matter what the rate of flow (5 or 10 ml/min) was, the surface deposition was of a longer duration.

At the 10 ml/min flow, broader lines at growth periods were observed, these actually are a sum of spikes heading down and appear to be one thick line, it was not the case at 5 ml/min flow rate. This is due to the velocity of the formed barite/scale particles, which appear to fracture and destabilize the surface growth sites. It causes unsteady scale film growth; pressure keeps dropping/rebuilding very frequently. These

approaches are supported by the fact that the width of the graph at the area in question (growth area) decreases with temperature. Statistically, the less mass gained in the tube capillary at room temperature confirms the early results at lower flow conditions. Figure 6-22 shows the barite mass deposited in the capillary at 10 ml/min flow rate.

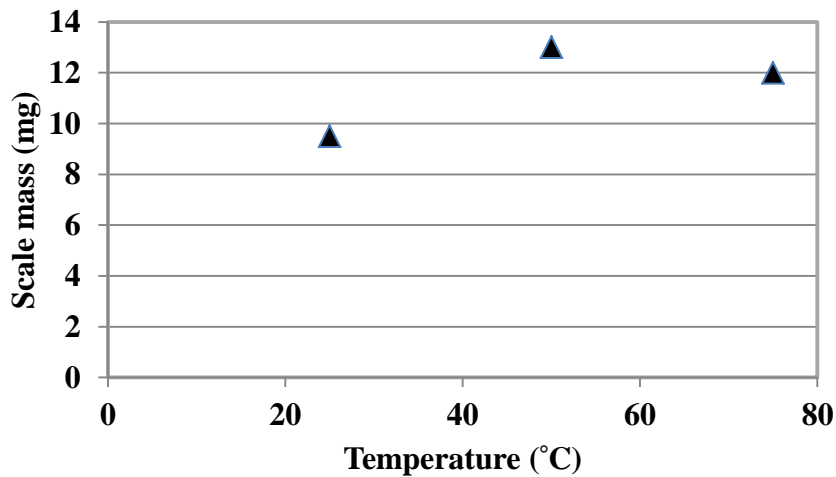


Figure 6-22 : Barite scale mass deposited in capillary at 10 ml/min flow and 50:50 mixing ratio.

The differential pressure versus time graph at 5 ml/min flow rate was collected earlier and brought here for comparison. At this lower flow rate, it was found that the observed induction time varies broadly at different applied temperatures. At 5 ml/min, although the highest saturation ratio (SR) is predicted at 25 °C and 50: 50 mixing ratio, the induction time was observed to be the longest (at 50.3 hours). On the other hand, the test, which was performed at a higher flow rate of 10 ml/min, shows a lower surface scaling film induction period at 32 hours. The observed induction periods at the two flow rates of 5 & 10 ml/min was plotted in Figure 6-23.

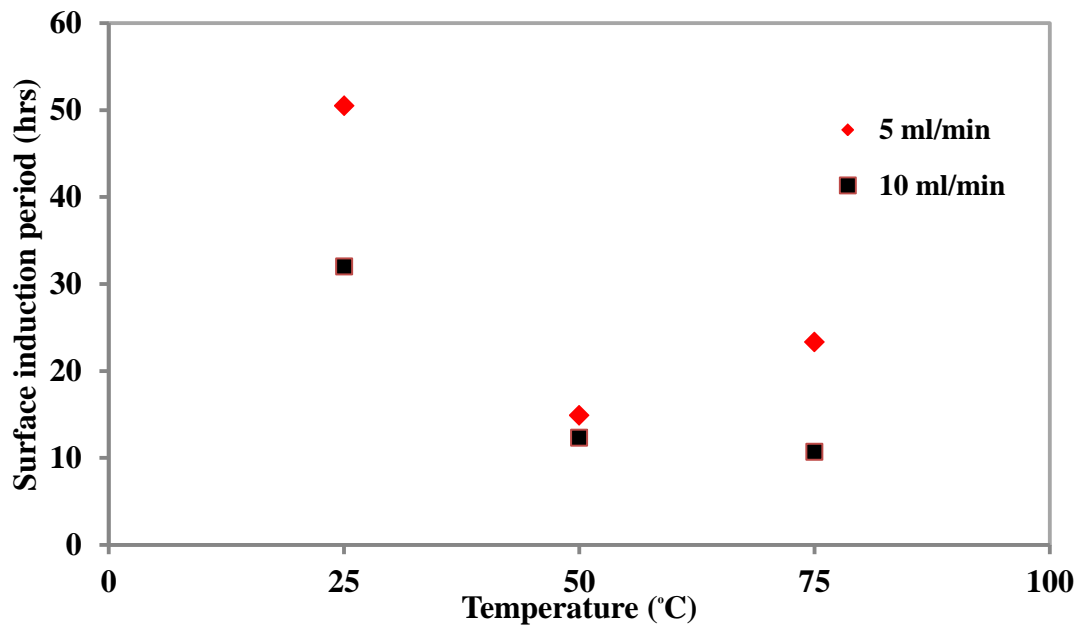


Figure 6-23 : The relation between the 5 & 10 ml/min flow rate and the recorded induction time (hrs).

6.5. EFFECT OF Ba²⁺ CONTENT ON SURFACE DEPOSITION

In this part, the saturation ratio (SR) was the only variant in the final mixture. The barium concentration ranged from 20 ppm as the lowest to 150 ppm as the highest. The targeted concentrations also included 50 ppm, 80 ppm and 100 ppm. The test conditions were explained in the experimental and methodology part. The dynamic flow graph was successfully collected to clearly show the effect of the dominant lowest solubility of barite formation on the whole deposition process.

6.5.1. Scale Surface Kinetics at Different SR and Barium Contents

For the first time, using the flow test cell to represent a typical industrial system, the effect of barium ion content as a main variant was clarified. The differential pressure versus time was measured using the sensitive pressure sensor across a capillary tube of 1 mm internal diameter (ID). The brine formation and seawater compositions were given earlier and the only difference was the barium concentrations. The flow rate was 10 ml/min at 50:50 mixing ratio and 75 °C.

The difference between the surface scaling film induction period for the lower barium content brine (20 ppm) and the higher barium content brine (150 ppm) is found to be huge (1.34 to 22.6 hrs respectively). This is in stark contrast to the surface scaling induction time difference between highly supersaturated brines at 50 and 80 ppm. This reproducible data confirm that the existence of barium ions at any concentration has a significant effect on scale surface deposition. From this data, the surface scaling induction time was determined. The dynamic flow results below, Figure 6-24, show a huge effect of the supersaturation ratio that varies according to the barium contents.

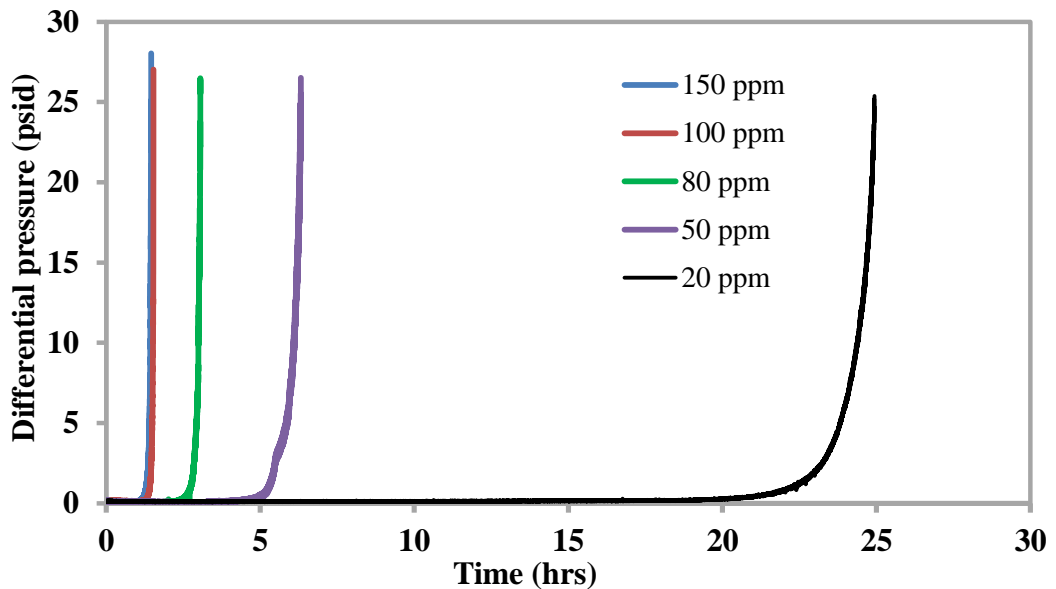


Figure 6-24 : The surface dynamic flow test at different barium contents.

6.5.2. Observed t_{ind} and Predicted Saturation Ratios

This investigations attempts to establish a clear link between the theoretical predicted saturation ratio and the observed surface scaling induction period. Bearing in mind that predicted saturation ratios are actually considered in bulk, in this case the three techniques are bridged to explore the variation in barium content. Figure 6-25 shows the relation between the predicted saturation ratio and experimentally

observed surface scaling induction time figures along with the actual concentration. The model prediction shows a linear increase of saturation ratio with respect to the increase of barium content; the test graph is shown in Figure 6-4 earlier. The calculated pH seems to decrease with the increase of barium concentration. The surface scale film induction time as a function of both SR and the actual barium concentration was confirmed in Figure 6-25, and the trend was consistent.

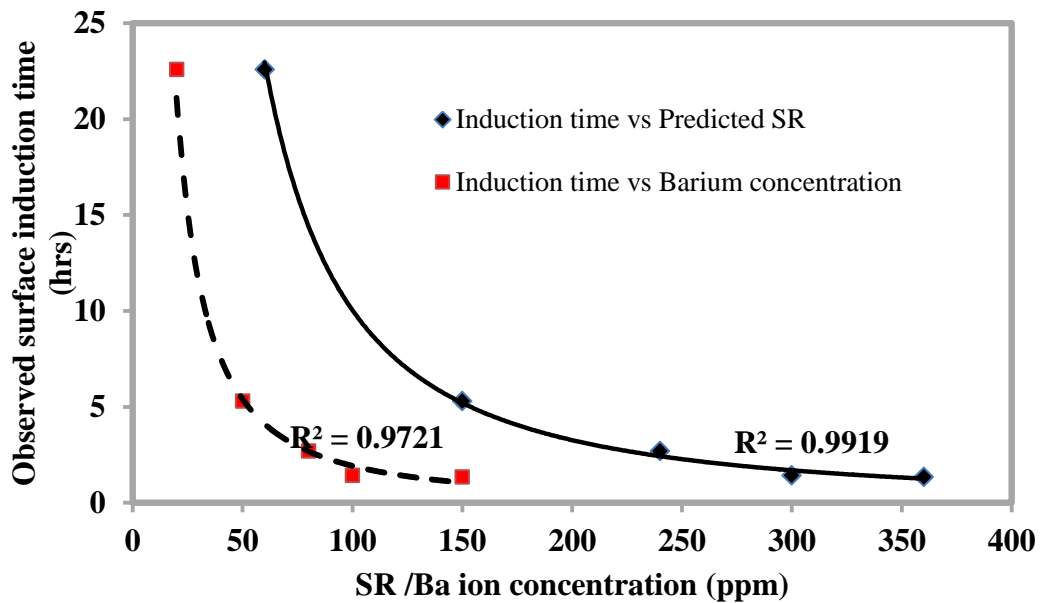


Figure 6-25 : The relation between the predicted saturation ratios, actual Ba^{2+} concentration and experimentally observed surface scaling induction time (hrs).

6.5.3. Surface Scale Growth Period at Different Barium Content

Once the surface scaling induction period was verified, the kinetic investigation was extended to include an important period of the surface crystallization process. The propagation of the scaling film growth period rate as a function of barium content was also investigated. The growth was monitored in terms of the phase change following the surface nucleation time as the capillary cell inner diameter reduces. One example (at 150 ppm) of such scale film growth was chosen at the highest barium content (Figure 6-26). The surface growth typically starts at less than 1 psid on the time axis at highest SR (150 ppm) while it takes hours as the supersaturation

ratio (SR) of the mixture drops to 20 ppm. A clear phase change in the surface scale filming plot represents a scale surface growth. The scale film phase change was started from 0.11 psid at 0.95 hrs and the growth proceeds to reach 1.7 psid. Excel software was used to evaluate the surface film growth period. The exponential growth factors were plotted against the barium concentrations, it shows a polynomial increase from lower to the highest barium contents, see Figure 6-27. The slope shows the effect of barium on the scale film growth period.

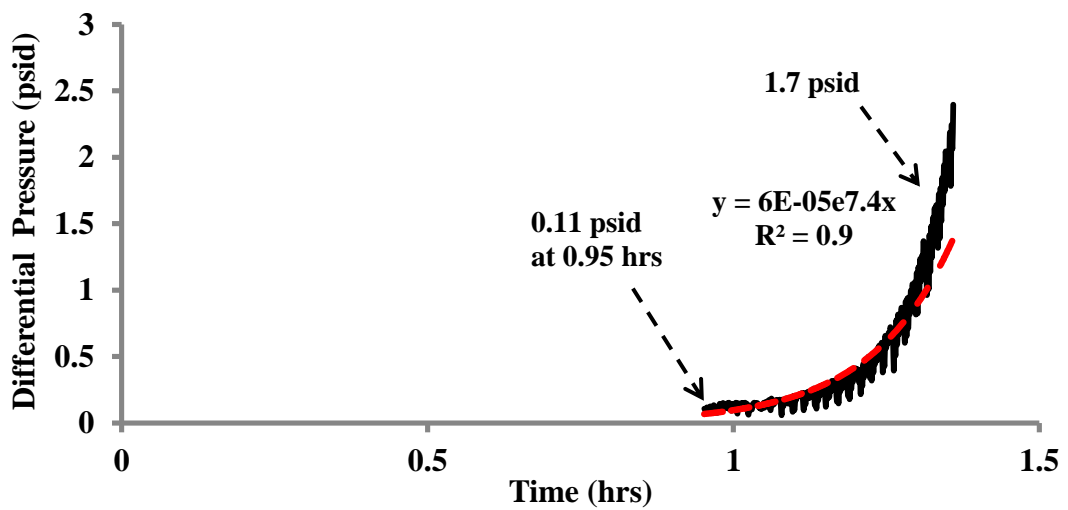


Figure 6-26 : The Growth period on surface at 150 ppm barium concentration at 75 °C.

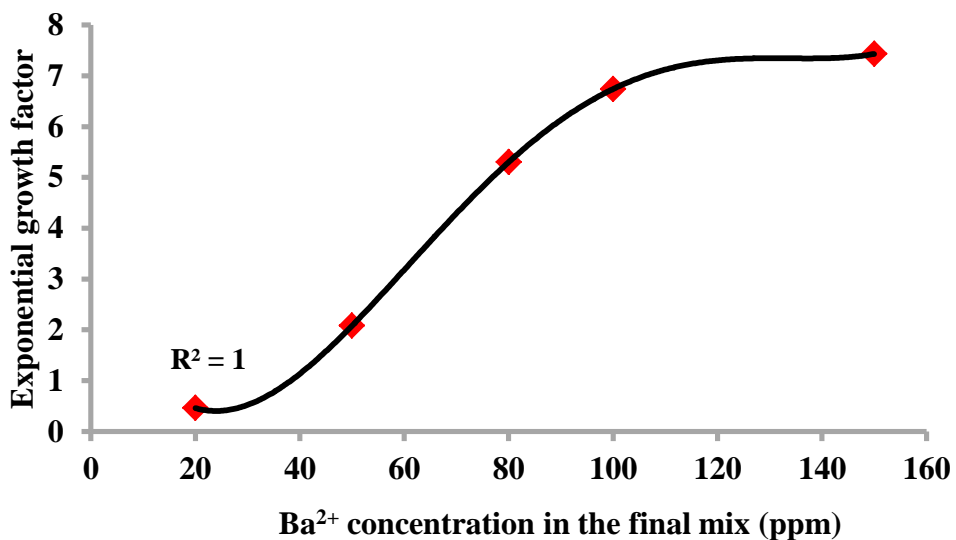


Figure 6-27 : The growth factor increases as a function of the barium content increase.

6.5.4. Scale Mass Deposited at Different Barium Contents

The deposited mass is an additional physical parameter to investigate the effect of barium content on the whole scale surface kinetic process. This is only available if a replaceable capillary is used to quantify the resulted mass. The net scale mass, which was gained in a capillary, results from the weight difference between unscaled and scaled capillary before and after scaling process respectively. Interestingly, the resulted scale mass appears to be proportional to the barium contents and saturation ratios (SRs), see Figure 6-28. The highly saturated brine mixtures show lower mass in the capillary while the lower saturated show higher mass gained in capillaries.

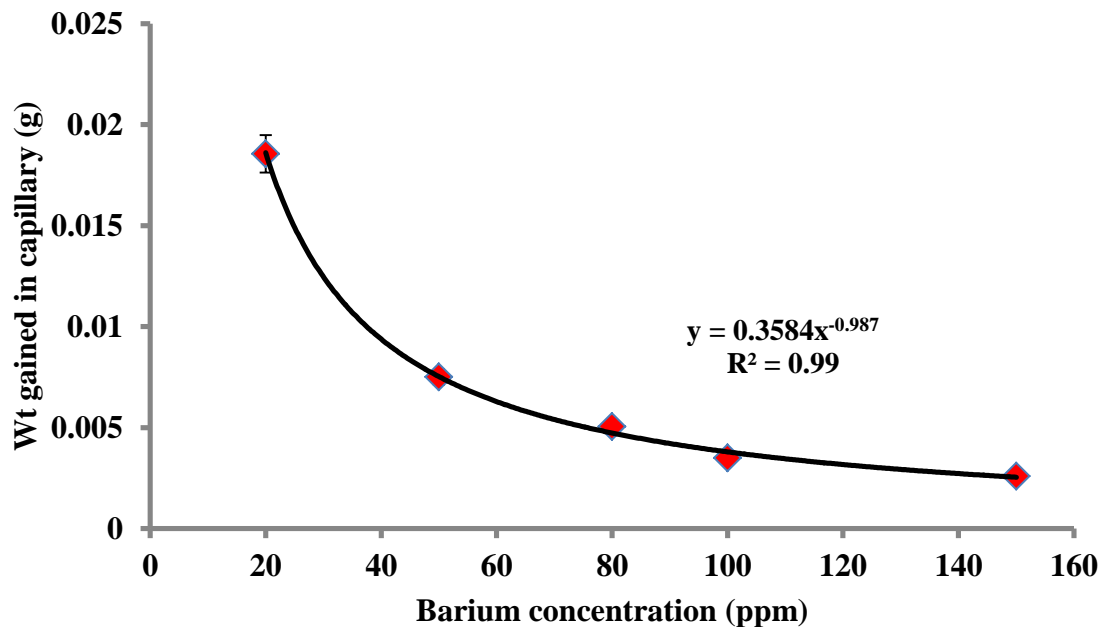


Figure 6-28 : The scale deposited in the capillary cell with respect to the barium concentrations.

6.5.5. Surface Mass gained Correlation to Observed t_{ind}

In the previous section, the correlation between the mass gained and the barium concentration/saturation ratio was exhibited. In this part, another kinetic factor,

which is the surface induction period, is added to enrich the discussion. It is obvious that the surface scaling induction period decreased with the increase of barium concentration and the saturation ratio. On the other hand, the scale mass quantity drops at the higher Ba^{+2} free ion and saturation values, Figure 6-29. So in practice, the slower the surface scaling the higher the mass gained. It could be related to the particle size and distribution.

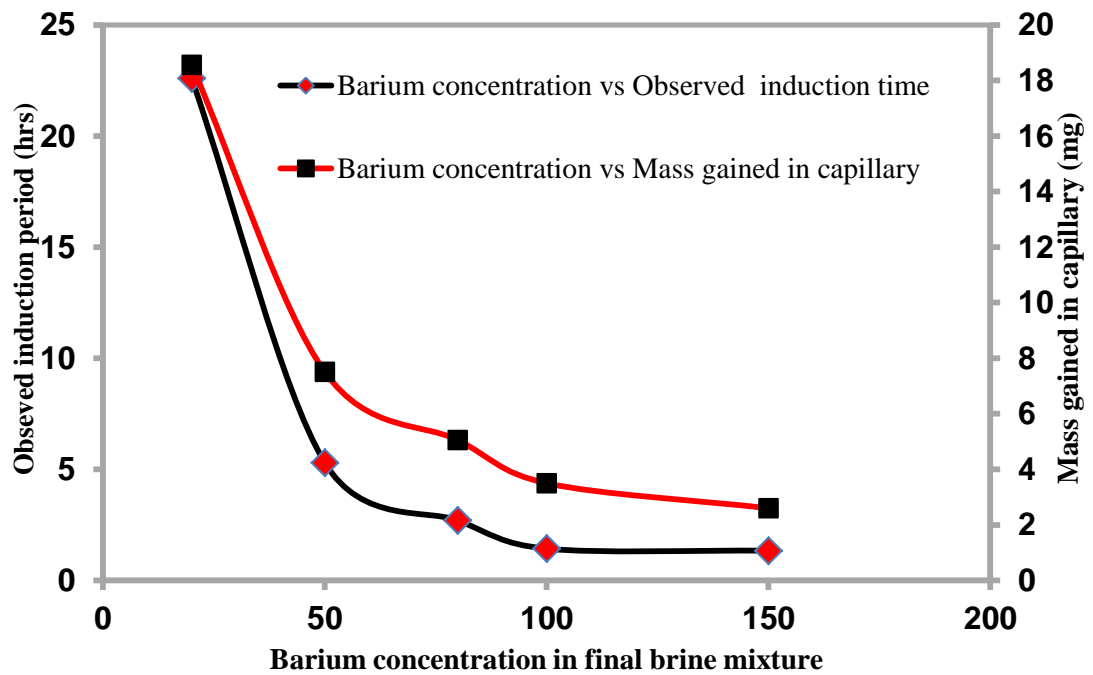


Figure 6-29 : The relation between barium concentrations and both the surface induction period and the gained scale mass as a function of the barium content.

6.5.6. Scale Thickness growth with Time

The Hagen–Poiseuille equation relates the pressure drop Δp across a circular pipe of length (L) to the average flow velocity in the pipe Q and other parameters according to:

$$Q = \frac{\pi r^4 \Delta p}{8 \mu L} \quad \text{Equation 6-1}$$

When Q is the volumetric flow.

r , mm, is the radius.

Δp is the pressure drop along length of pipe (psid).

L , mm, is the length of line.

μ is dynamic viscosity.

The resulted radius through scaling can be assessed by the change in pressure from initial to a time t (ΔP_i , ΔP_t).

$$\text{So the radius (r) is } r = R \left(\frac{\Delta p_i}{\Delta p_t} \right)^{0.25} \quad \text{Equation 6-2}$$

Then the thickness, mm, is represented as;

$$\tau = \frac{\Delta p \cdot r}{2L} \quad \text{Equation 6-3}$$

In this work, the scale thickness along the circular capillary was evaluated for different field brine mixtures at different saturation ratios resulting from different barium species concentration levels, Figure 6-30.

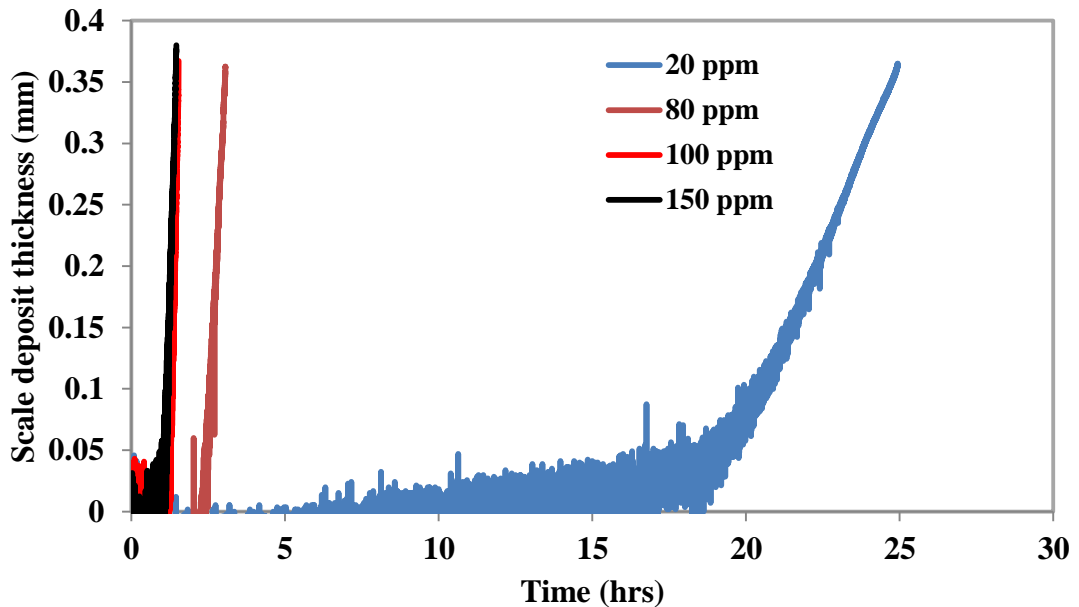


Figure 6-30 : Surface scale thickness (mm) development with time at different barium content and SR values.

This fact can also be presented in the form of capillary radius reduction with respect to time. One case was chosen (20 ppm). It was observed that the internal ID was reduced slowly for a long period of time (20 hrs) before the scale thickness starts to increase rapidly, Figure 6-31. The reduction becomes faster from 0.4 mm ID to 0.1 mm ID left to the final blockage.

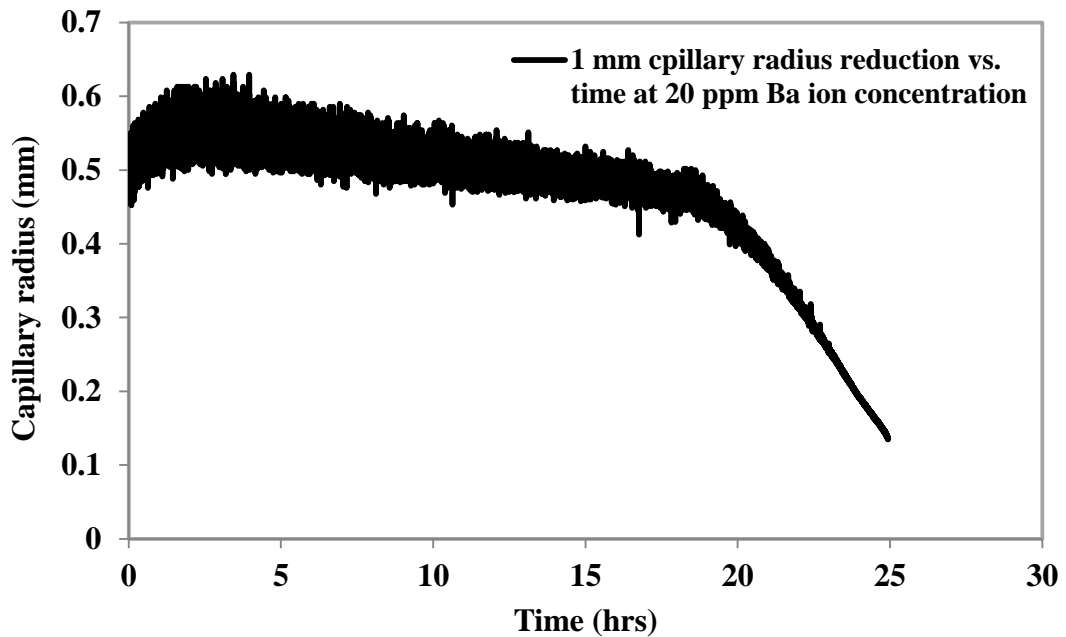


Figure 6-31 : Capillary radius reduction with respect to time.

6.5.7. Surface Deposition at Zero Barium Content at

As part of the scheme (since the previous investigations show a remarkable effect of barium content at any concentration), it is worth investigating the effect of an absence of barium species has on the scale surface deposition. The under saturation was predicted at zero barium content and the scaling was unlikely. However, could that be experimentally observed and confirmed? The other question was how the barium affects the surface kinetics in terms of the rate of surface deposition and the shape of differential pressure vs. time graphs.

In fact, thermodynamically, the system is left with the second lowest solubility species (strontium Sr) to control the whole process. It could also be based on how the resulting scale deposit responds to heat of flow and existence of other species such as Mg, Ca and even sodium as a co – deposit. The surface deposition plot was successfully collected with a huge difference in the recorded surface scaling induction period and the total blockage (growth period). A slow film growth was observed when it is compared with the brine formulation in which the barium ion species exists, see Figure 6-32.

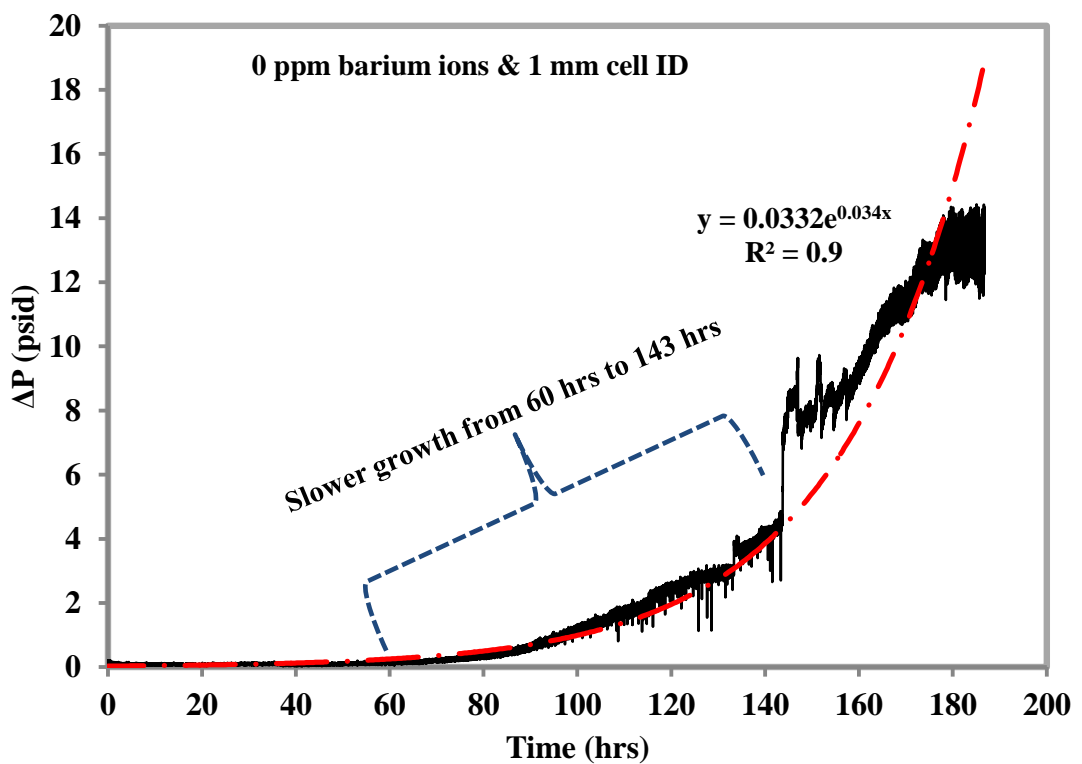


Figure 6-32 : Surface deposition at zero barium content at 75 °C and 10 ml/min flow.

6.6. RESIDENCE TIME IN DYNAMIC SYSTEM

6.6.1. Modified Mixing Part (Shorter Residence Time)

In this part, the mixing part was redesigned to shorten the flow residence time; it was based on the observed surface scaling induction time in the bulk solution using conductivity measurements. The assumed capillary cell in dynamic flow tests was positioned accordingly. This design allows only 2 - 3 seconds residence time at 5 ml/min flow rate. At this stage and based on the bulk kinetics, could the crystal birth location be predicted on surface using the bulk observed induction time. This may also lead to proper inhibitor selection for a dynamic system as the crystal nucleation and growth stages are defined. The 50 ppm barium concentration in the final mixture was chosen at the above mentioned flow and 75 °C. It was an eight day surface flow test. The aim was to investigate the surface scaling induction period in a very short residence time between the mixing chamber and the testing capillary. The aim of this design is also to investigate the possible crystal *birth* on the surface of the testing tube rather than in the bulk stream then transferred to the surface as a deposit. Below, some facts are listed to support the data acquired using data acquisition software.

After an eight day test, the mixing cone chamber (where brines first meet) was scale free, and no sign of any deposit was noticed. This gives the impression that the crystal does not have time to reach to the detectable size in the first second, and it was most probably created on the internal surface of the capillary. The *evidence* was that the scale was formed inside the capillary and not in the mixing chamber. The capillary was not completely blocked. The weight gained on the surface capillary was confirmed by mass evaluation.

The data acquisition, without doubt, shows scale formation within this long duration test with a difference in the differential pressure from 0.05 psid to 0.35 psi. Although it was not a steady surface crystallization process, the graph was collected and the trend shows a direct slow increase in differential pressure, Figure 6-33.

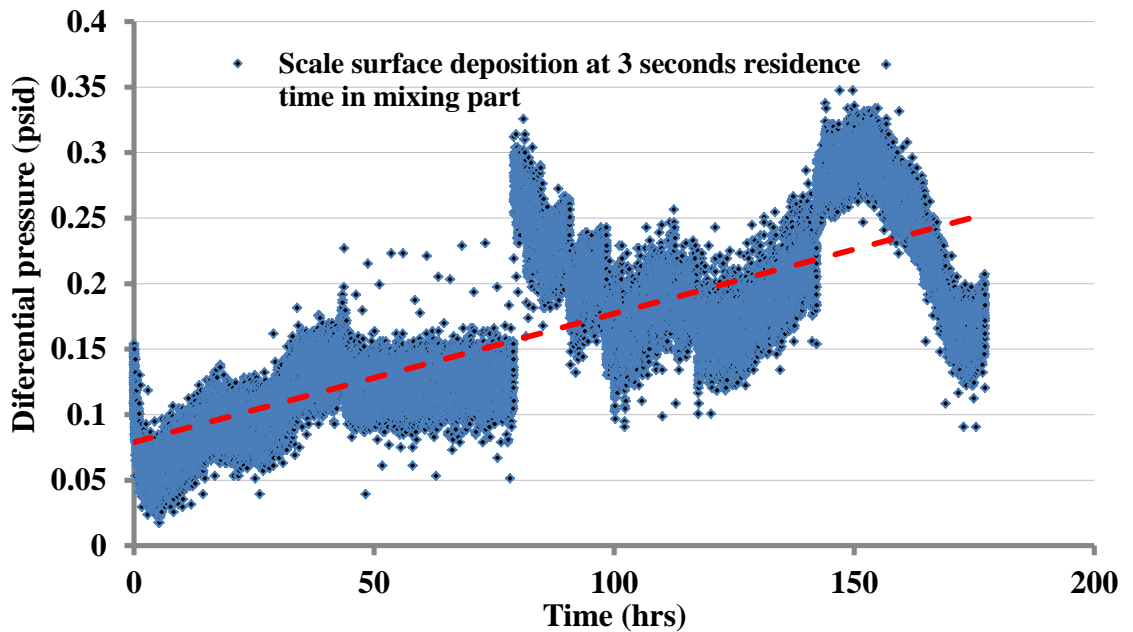


Figure 6-33 : Scale/barite surface deposition at 50 ppm barium in the final mixture at 2 – 3 seconds residence time.

6.7. INHIBITION OF GROWTH STAGE (DYNAMIC)

This study focuses on the first step of scale/barite kinetics on the surface in the presence of anti-growth scale inhibitor (SI). The new dynamic setup enables the investigation of the inhibited nucleation and growth periods. The ability of the DETPMP to retard barite scaling at minimum concentration is investigated at three different temperatures of 25 °C, 50 °C and 75 °C.

The study is extended to look at the effect of the combination of both the inhibitor and higher temperature application, when the lower saturation ratio (SR) and higher solubility are predicted. The results are later compared with a range of temperature applications in terms of surface coverage and deposit distribution/composition using different optical techniques.

6.7.1. Surface Deposition Treatment with DETPMP

The mixing and inhibition processes are explained elsewhere in the experimental methodology. At both (10 ppm and 5 ppm) inhibitor concentrations, the same steps were followed to inhibit the crystal nuclei growth in the flow stream or onsite. The differential pressure versus time plots were successfully collected. The recorded pressure shows no significant increase with respect to time. The observed surface nucleation inhibition at the two mentioned DETPMP concentrations are shown below; see Figure 6-34 and Figure 6-35 respectively. The quantitative measurement of the complex barite scale, which is formed inside the tube capillary, shows a fluctuating amount depending on temperature. It is the only changeable factor. Figure 6-36 shows the treated scale mass formed inside the capillary is at a minimum, this plot is in good agreement with the untreated case in terms of the maximum and minimum amounts. This means in both cases, regardless of the mass, the maximum mass was recorded at a mild temperature of 50 °C and due to the fluid and surface heat, the minimum was recorded at 75 °C.

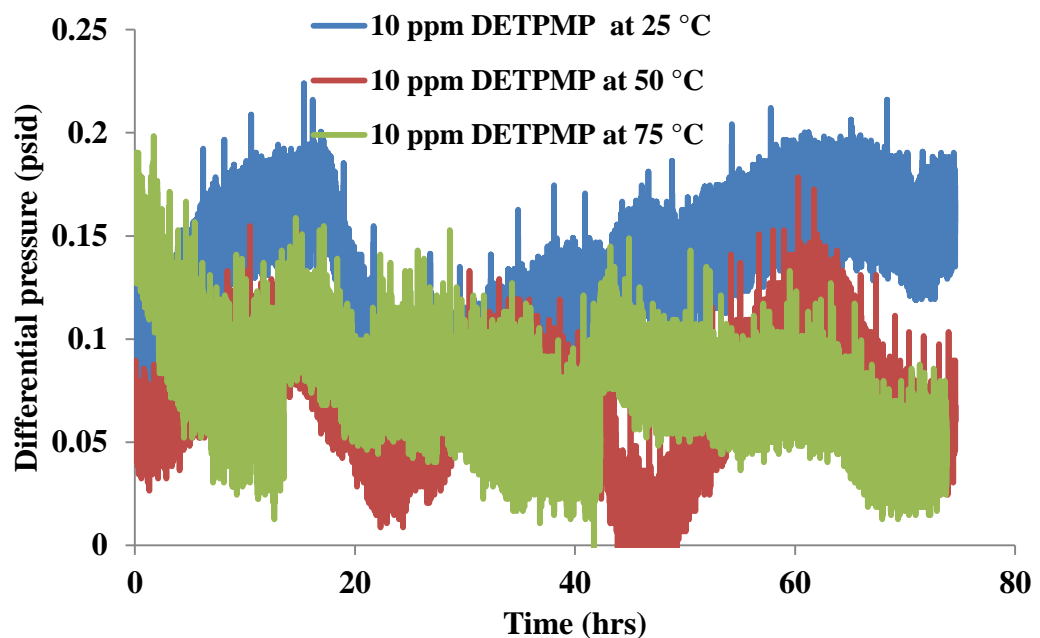


Figure 6-34 : Differential pressure versus time for surface deposition treatments with 10 ppm DETPMP at 25 °C, 50 °C & 75 °C and 50:50 mixing ratio.

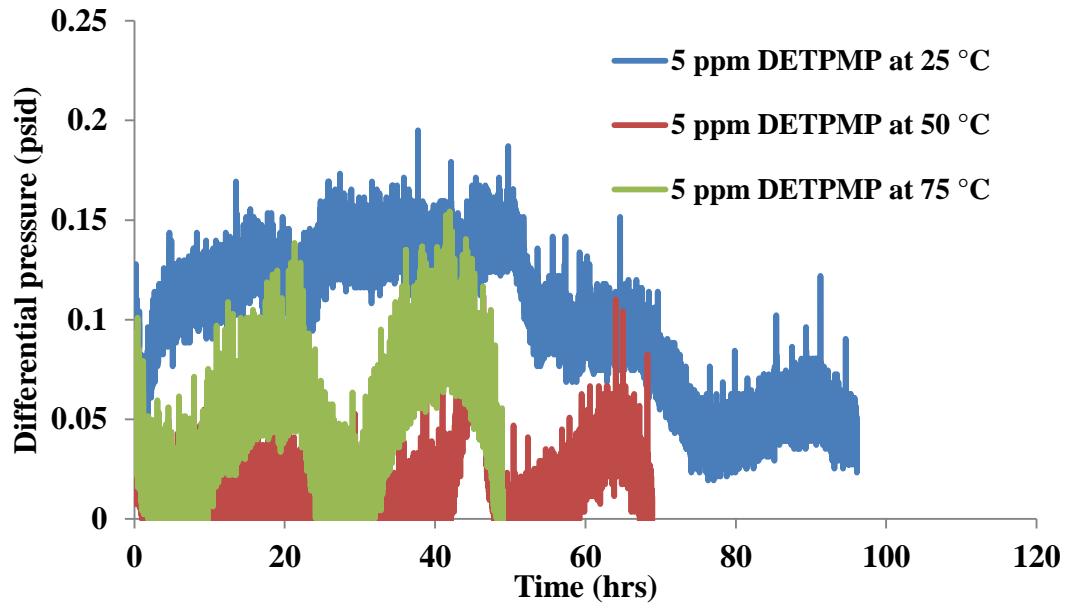


Figure 6-35 : Differential pressure versus time for surface deposition treatments with 5 ppm DETPMP at 25 °C, 50 °C & 75 °C and 50:50 mixing ratio.

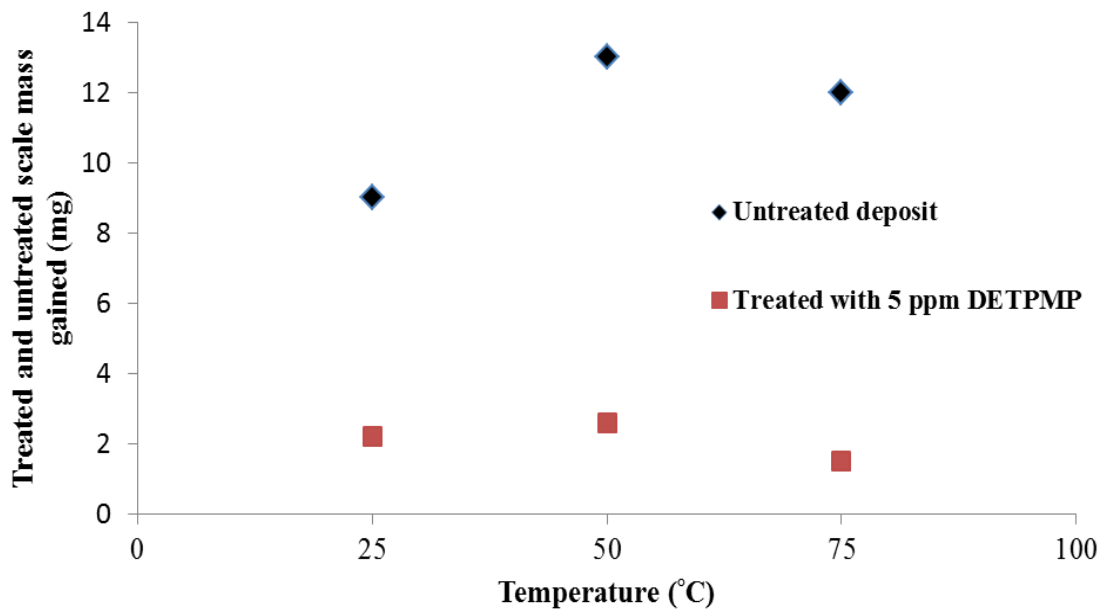


Figure 6-36 : Scale and scale – DETPMP complex mass deposited in capillary during treatments with 5 ppm DETPMP.

During the surface deposition tests, it is worth determining the concentrations of the major ions in the stream. Their behaviour during a deposition/treatment process reveals valuable information. In this regard, the focus is given to the residual ions of barium and phosphorus species. In order to assess the residual barium and phosphorus concentrations in the rig effluent brine mixture, ICP samples were collected from two sampling points. One sample was immediately taken after the brine mixture comes into contact with the scale inhibitor (SI). The other point is positioned at the end of the scale rig tail loop. The collected figures are tabulated in Table 6-7.

It was found that the 5 ppm phosphorus (P) original concentration, which represents the concentration of the active species in the DETPMP, drops by about 94 %. This scale inhibitor (DETPMP) concentration consumption takes place in less than 25 seconds. This is the time that the inhibited brine mixture takes to reach the sampling point (A), which was immediately positioned after capillary cell . This is, of course, after passing the mixing part, cell capillary and the extension spool. The sampling position (A) in the table represents immediate sampling after mixing while position (B) is the rig waste water end line. This fast drop in the scale inhibitor (SI) concentration could be referred to two reasons; first is that the SI has a higher reactivity and makes weaker bonds with all other divalent cations in the seawater brine. The second reason is that the additive could chemisorb to the surface (bare steel surface) as the DETPMP molecular structure has three nitrogen active groups. The dehydrogenated phosphonate group ($-\text{PO}_3^{2-}$) will definitely bond to barium as a radical in the early stage of the complex formation. On the other hand, barium ion concentrations approximately drop by 92% immediately after mixing and 96% at the end of the rig waste line.

The 4% of free barium ions are able to generate new sites on the stainless steel surface (on internal surface of 1 mm capillary) at very early stages once bonded to the sulphate species. These sites face either a detachment due to the flow shear/weaker binding to steel surface or slower growth to form bigger aggregates.

Table 6-7 : ICP analysis of the treated brine mixture waste for Ba & P residuals

Sample Name	Ba	P
25 °C A	1.36	0.336
25 °C B	1.15	0.341
50 °C A	2.66	0.276
50 °C B	1.89	0.311
75 °C A	3.68	0.354
75 °C B	2.80	0.367

6.8. EFFECT OF SURFACE CONDITION ON SURFACE DEPOSITION

During the surface scale deposition, the surface condition is considered one of the most important factors to study surface scale kinetics. So in this part of this research study, surface manipulations or condition either as pre – scaled or pre – inhibited are considered.

6.8.1. Surface Pre-Scaling

Surface scaling, by definition, is seeding a surface with the same deposited crystal or a crystal from different ion compositions. There are many different kinetic study approaches in seeded media, most of them were performed in bulk. The seeding is implemented to speed up the crystallization process or design a yielded crystal product – shape and size control.

In this work, the internal surface of a stainless steel SS 316L tube capillary was pre – scaled or pre-seeded prior to surface deposition. An odd mixing profile was used to nucleate and deposit a multiphase (mainly barite) scale on the subjected surface.

The experimental procedure is described in the experiment section. The graph was plotted and the effect of the surface pre – scaling also noticed, see Figure 6-37. The shorter surface induction period, shape of growth region and speed of final blockage time were affected in the case of pre-scaling. More details are in the discussion chapter.

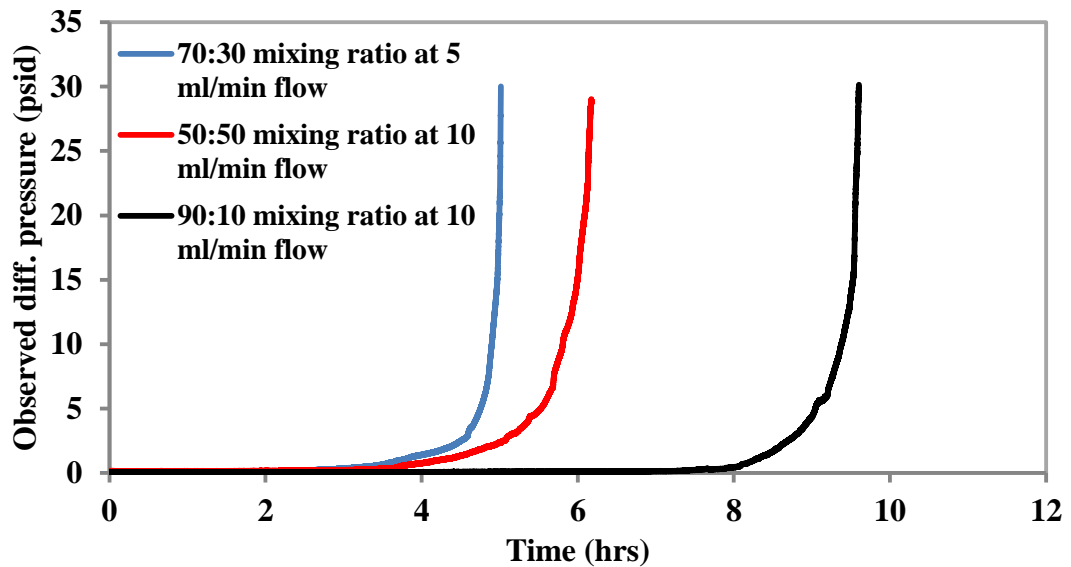


Figure 6-37 : The pre-scaling surface effect on surface deposition.

6.8.2. Surface Pre-Treatment

Surface treatment prior to surface deposition is a surface condition that is given attention as the crystallization is taking place on chemically treated surfaces. If the chemical product has an ability to bind chemisorbedly to the surface, could the adsorbed molecular species orientation affect the surface deposition process? Earlier, the effects of different parameters on surface scaling or crystallization were explored. This test was done on the same real brine mixture in which the barium species vary (50 ppm, 80 ppm, 100 ppm and 150 ppm). The observed surface scaling induction time (hrs) versus the differential pressure results were then compared with the surface deposition results on bare steel surfaces (no surface modifications or alterations by chemical products). Figure 6-38 and Figure 6-39

below show unique comparison observations in presence and absence of DETPMP on the stainless steel surface. The first compares the effect of chemical treatment on surface deposition with the recorded induction time and the second compares it with total blockage time.

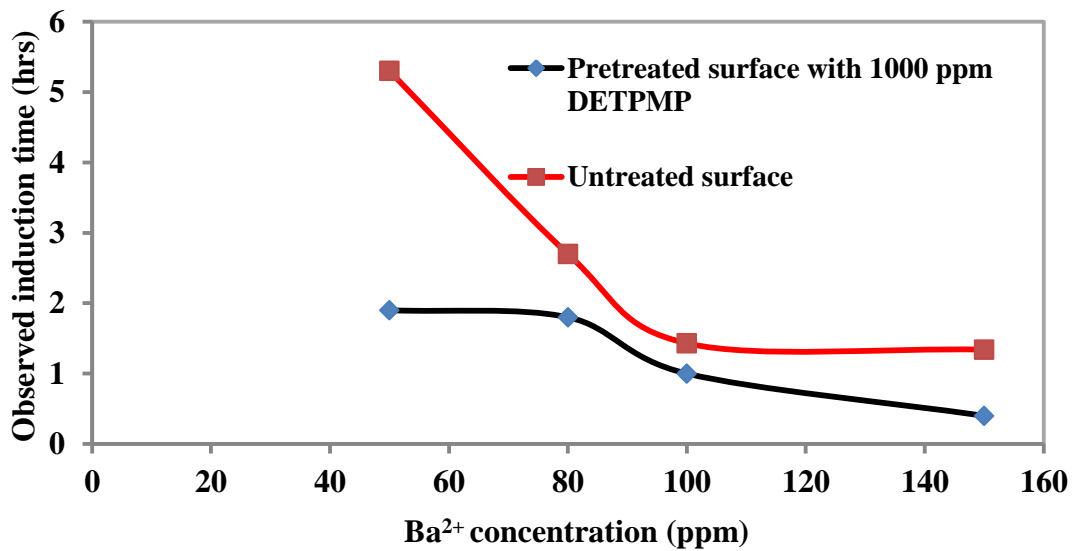


Figure 6-38 : The effect of surface pre-treatment using 1000 ppm DETPMP on surface scaling film induction time.

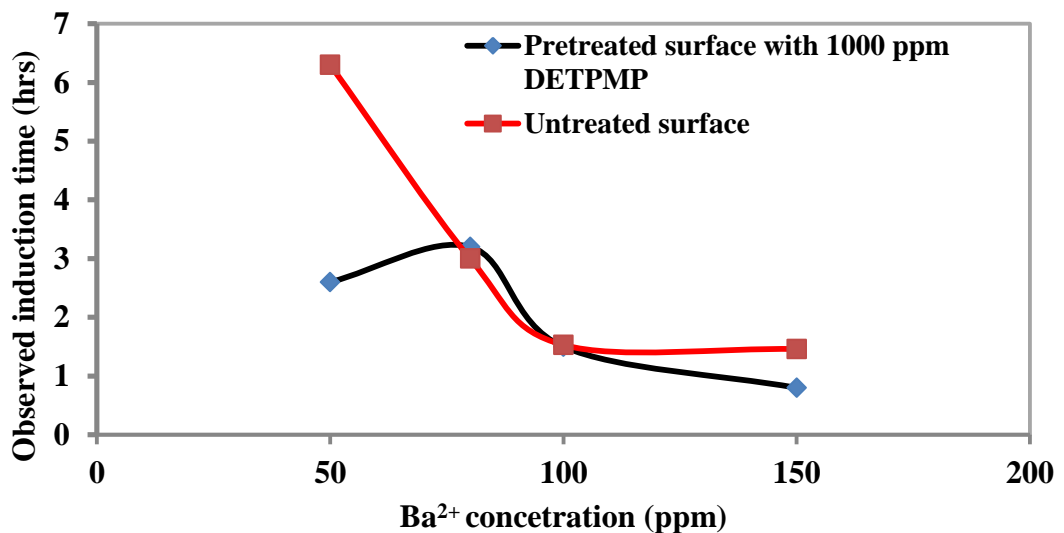


Figure 6-39 : The comparison between the total blockage time during pre-treatment using 1000 ppm DETPMP and no treatment.

6.9. SUMMARY OF RESULTS

This chapter focuses on the results which were collected from different techniques. The results starts with the thermodynamic assessment of the used brines to confirm its tendency to scale formation. The results covers dynamic and bulk kinetic evaluations of the complex brine. Different flow, surfaces and brine compositions were used. This part was divided into three categories:

- Thermodynamic evaluation using prediction method.
- Bulk assessments.
- Dynamic flow assessments.

Chapter 7. SURFACE ANALYSIS RESULTS (PART 2)

7.1. INTRODUCTION

This chapter mainly focuses on the surface analysis following surface deposition from the dynamic flow tests. The surface investigations were carried out to characterize the deposits on the surface in terms of composition, shape and alignment.

This work is based on the change of different experimental parameters and their effects on scale/barite surface kinetics. The surface techniques enable the understanding of these effects from a different perspective. So, in this regard, different complementary surface analysis techniques were used e.g. the environmental scanning electron microscope (ESEM), energy dispersive X-Ray (EDX), Raman spectroscopy, FT-IR and *ex - situ* X-Ray diffraction (XRD).

7.2. SURFACE ANALYSIS

The surface imaging and characterization techniques are widely used to analyse materials on surfaces such as deposited mineral scale on stainless steel surfaces. Some other techniques were to determine the composition of the deposit. The aim was to investigate the effect of thermodynamic and kinetic conditions on surface morphology and composition. Different parameters such as saturation ratio (SR), temperature, mixing ratio, barium content and the flow on the surface scale. If the surface structure is to vary according to the above parameters, what is the major factor to show an effect? This is especially when the difference between the saturation ratios is small according to the five mixing ratio (slight changes, 20:80 SW: FW, 40:60 SW: FW, 50:50 SW: FW, 60:40 SW: FW and 80:20 SW: FW).

The surface composition and crystal alignment were to confirm the effect of the main precipitant which shows the lowest solubility (BaSO_4). This is overlapped with the surface flow results to give a better view of what was actually happening during surface deposition. The other interesting point is the ability of surface chemical adsorbate on ions or growth crystal in the flow stream.

7.2.1. Surface Analysis at Different Variables

The first data were collected at three levels of temperature (at 25 °C, 50 °C and 75 °C), and the mixing ratio by which the saturation ratio varies as well. The numbers of the parameters depend upon the mixing ratios within each of the applied temperatures or the three temperature applications.

7.2.2. The Surface Scale Topography - Effect of Early Surface Nucleation

The nucleation of barite on surface, which is the first stage during the surface scaling induction period, is very important to understand the surface kinetics from the very early to final growth stages. Using a high sensitivity differential pressure sensor also allows the investigation of a challenging surface nucleation period. Different nucleation patterns were noticed at different temperature, this was the reason to bring the some examples of dynamic flow in this section. This finding may support a thought, and possibility that the early observed surface nucleation patterns affect the final crystal surface confirmation. In this study, three different mixing ratios were chosen as examples to show different nucleation patterns at 25 °C, 50 °C and 75 °C, as presented in Figure 7-1, Figure 7-2, and Figure 7-3 respectively.

It is clear that the surface barite formation, at early stages of the surface nucleation or even during the whole induction time, was not steady. This was noticed even at 25 °C when the barite formation is enhanced due to the very low solubility. At room temperature, it can be seen that the surface nucleation failure (unsteady scale build

up) occurs almost every 20 hours. It was more frequent than the other two tested temperatures especially between 40th and 80th hour as marked on the figure. This surface nucleation failures appear to be less intensive with elevated temperature at 50 °C (see Figure 7-2). At the highest temperature of 75 °C, the surface nucleation and film growth tends to be more stable (steady) with fewer failures. It shows a more clear trend of increase of the differential pressure readings.

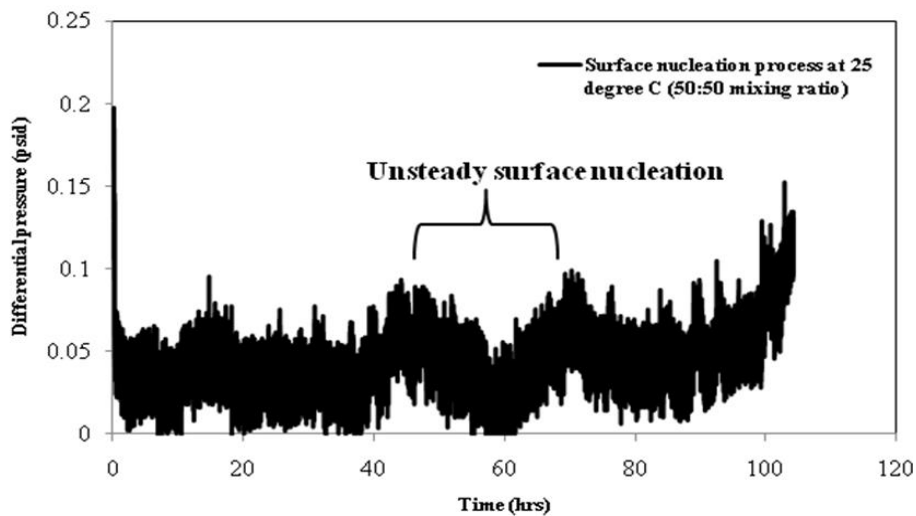


Figure 7-1 : Surface nucleation period at 50:50 mixing ratio and 25 °C.

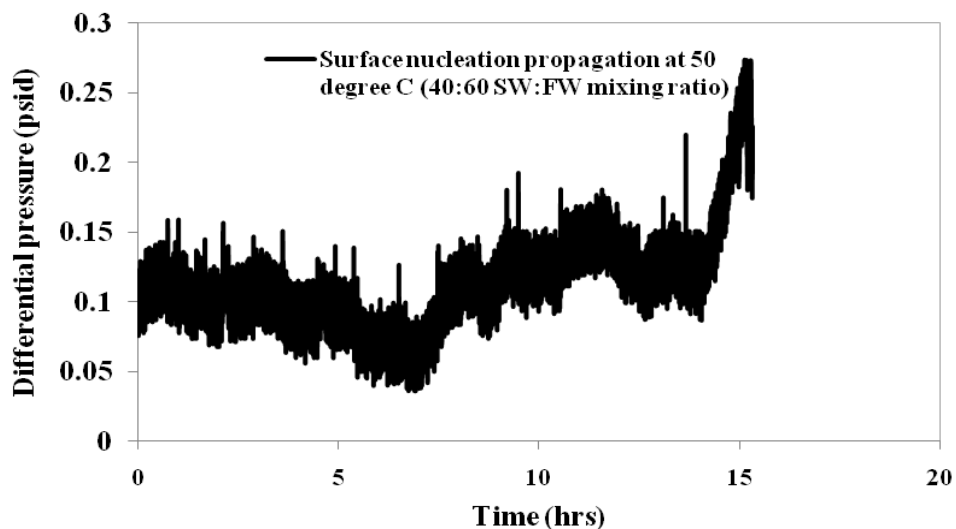


Figure 7-2 : Surface nucleation period at 40:60 SW: FW mixing ratio and 50 °C.

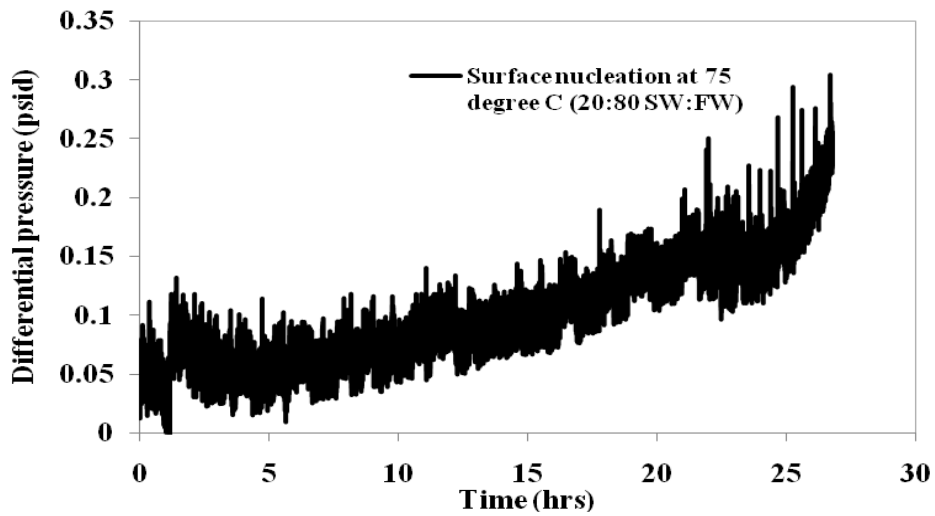


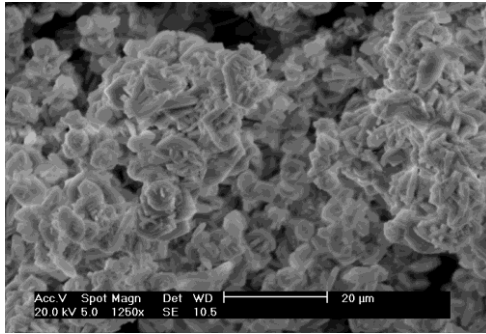
Figure 7-3 : Surface nucleation period at 20:80 SW: FW mixing ratio and 75 °C.

7.2.3. Scanning Electron Microscope Analysis at Different Temperatures & Mixing Ratio

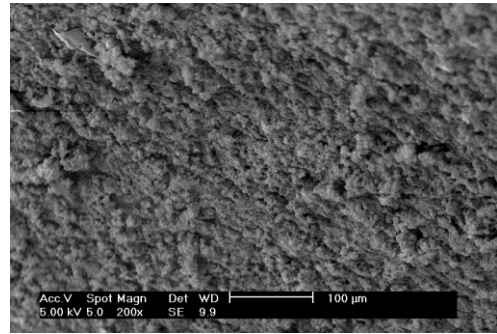
These results were collected from the ¼” extension tube with a curved pipe surface, the natural appearance of scale deposit on the internal surface of the extension (oilfield pipe system) was successfully done. The only SEM surface imaging analysis was done on these half tubes. However, the curved surface is not suitable for X-Ray diffraction (XRD) analysis. The surface topography images below of the scaled surfaces show the obvious temperature effect rather than the resulting saturation due to mixing ratio at each temperature. A replaceable stainless steel spool pipe extension is installed as part of the test cell. The surface deposited scale/barite ($BaSO_4$), which was observed with SEM, is presented in Figure 7-4..

Scanning electron microscope SEM of barite surface deposits at:

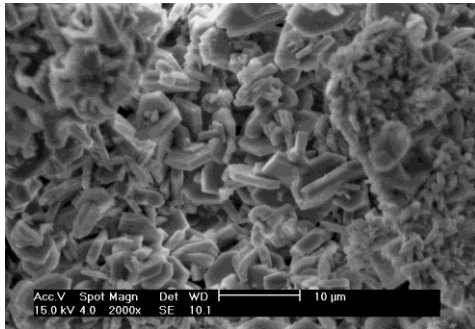
25 °C



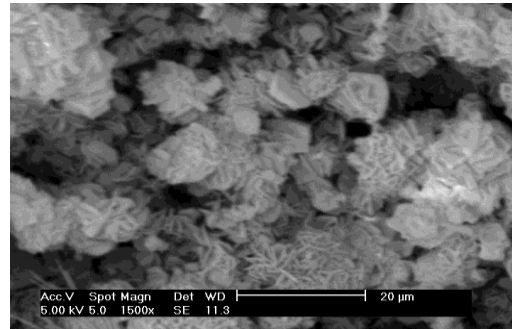
50 °C



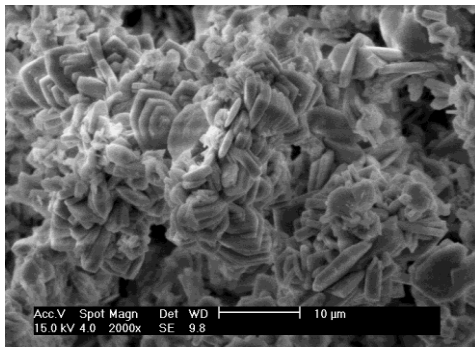
50:50 SW: FW



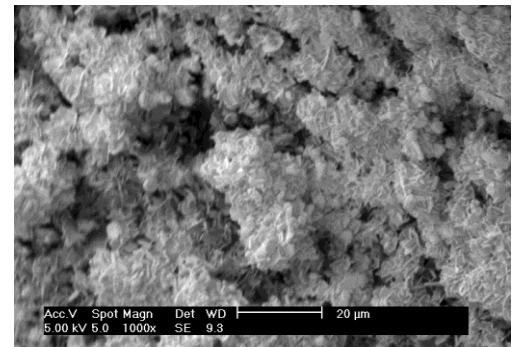
50:50 SW:FW



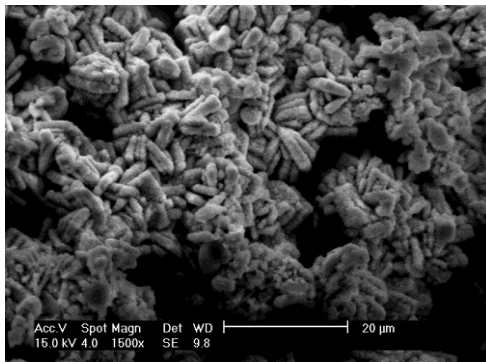
20:80 SW: FW



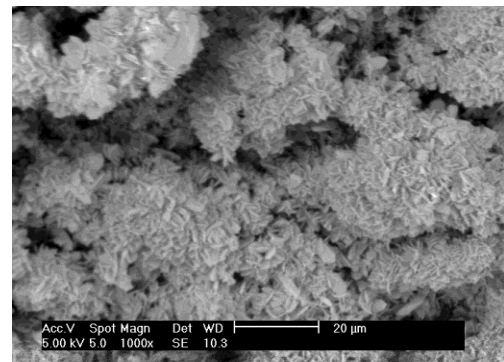
20:80 SW: FW



40:60 SW: FW

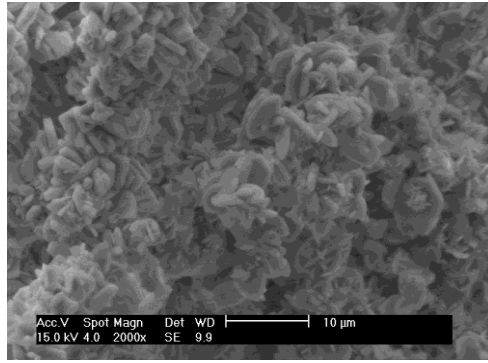


40:60 SW: FW

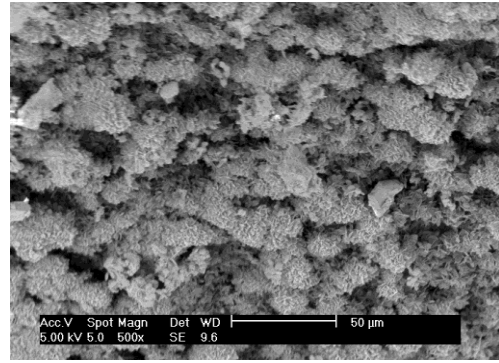


80:20 SW: FW

80:20 SW: FW



60:40 SW: FW



60:40 SW: FW

Figure 7-4 : SEM images of final barite deposit surface growth at 25 °C & 50 °C.

This was to investigate the effect of different experimental conditions on the morphology of deposited scale/barite. There is no impact of the change of saturation ratio due to mixing ratio within same temperature. It appears that the temperature difference has the major effect on the surface deposition rather than the mixing ratio. Most of the crystallites, which were deposited at 25 °C, look similar at different mixing ratios except at the highest sea water percentage (80% or minimum saturation at lowest barium concentration). At 50 °C, the surface morphologies are also similar at different mixing ratios.

7.2.4. Scanning Electron Microscope Analysis - Surface Pre-Scaling (Seeding)

The pre-scaling involves pre-scaling or nucleation of a surface prior to scaling, this was to assess the scaling propagations and kinetic rates on different surface conditions . In this work, the sensitive differential pressure sensor facilitates the measurements of tiny scale layer formation. The interest is given to the shape of these final growth scale deposits at different surface conditions and flow rates. The surface seeding or nucleation steps are explained in detail in the experimental section.

7.2.5. SEM Analysis of the Pre-scaled Surface with Odd Mixing Ratio

In this part, three mixing ratios were used at 25 °C. The odd mixing ratios were implemented as follows; 50:50, 70:30 and 90:10 SW: FW. In principle, the surface induction period at 50:50 SW:FW, at the highest predicted saturation ratio, should be shorter. It was expected to be longer at lower barium content at 90:10 SW: FW. Owing to the surface pre- scaled condition, the surface scaling at 70:30 SW: FW (at about 56 ppm Ba²⁺) shows a remarkably low surface induction and final blockage time. It was not only the observed surface induction time or the change in the surface kinetics noticed with surface pre -scaling, but also the surface topography. The resulting SEM surface analyses of pre – scaled and non pre – scaled surfaces were compared. Figure 7-5 shows the surface crystal shape and alignment at each mixing ratio. Interestingly, the pre – scaled steel surface test was done at 30% formation water. The surface crystal image shows that the scale/barite is tend to crystallize in a single crystal with well-defined shapes.

The surface chemical composition of the deposited scale/barite was analysed using energy dispersive X-Ray (EDX) technique, see Figure 7-6. The mixture with lower barium content was targeted, it is resulted from 90:10 SW: FW mixing ratio. In the final mixture at 90:10 SW: FW, the Ba²⁺ concentration was 12.5 ppm. At lower concentration, the deposited barium sulphate with the lowest solubility dominates the surface deposited minerals. In dynamic flow condition, the whole three previous mixing ratios were carried out at the same experimental parameters e.g. flow rate of 10 ml/min, stainless steel surface, cell dimension of 1 mm internal diameter, and at 25 °C. Moreover, the flow rate was changed 5 ml/min in the case of deposition on pre - scaled surface.

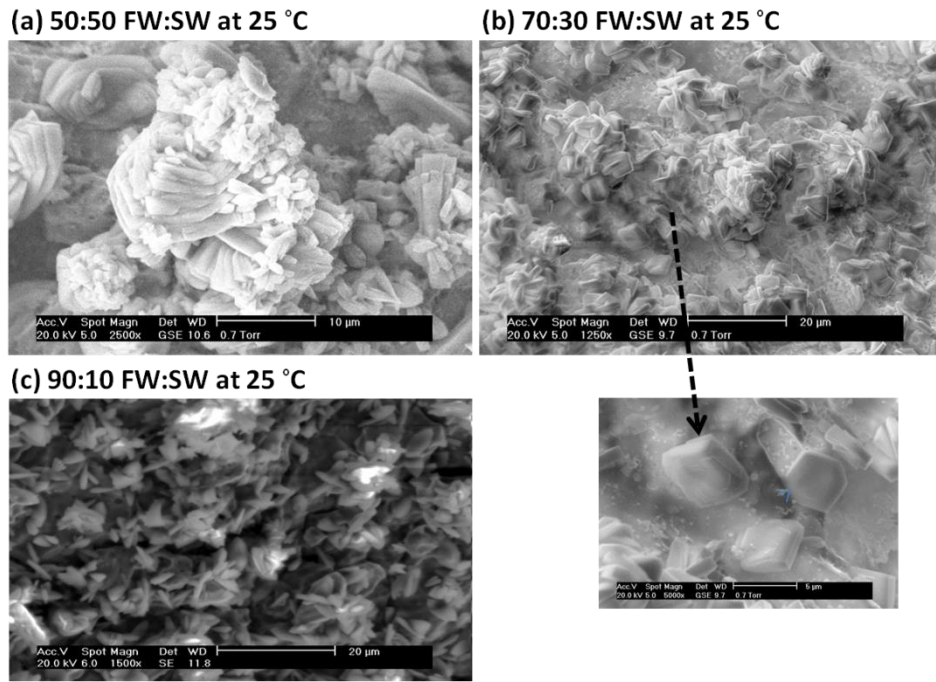


Figure 7-5 : SEM images of deposited barite at 25 °C (a) 50:50, (b) 70:30 and (c) 90:10.

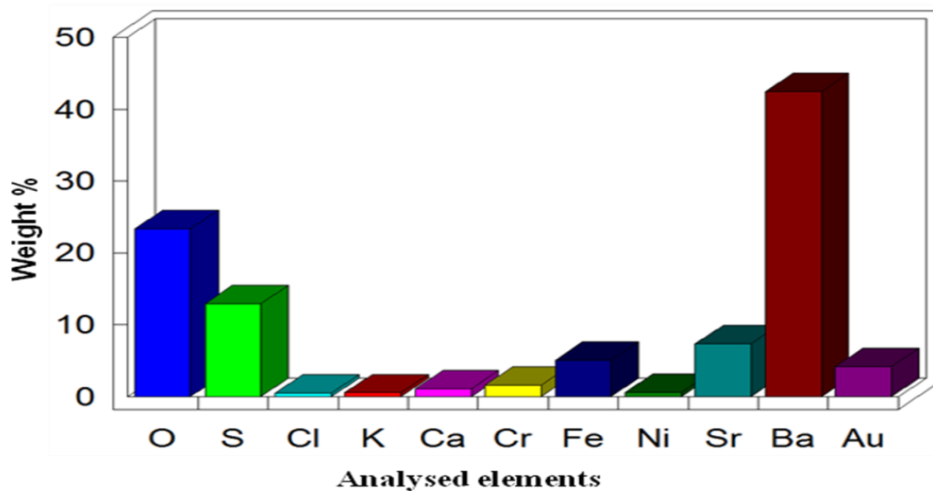


Figure 7-6 : EDX quantitative analysis of barite deposited at 90:10 FW:SW at 25 °C.

7.2.6. SEM Surface Analysis of Treated Deposit in Dynamic Condition

It is now known that the scale flow rig is a close system, and in order to track the surface crystals morphology (shape/size), surface optical measurements were implemented. The surface crystallization is found to vary based on different parameters and experimental conditions. It was not possible to probe the early surface nucleation *in – situ* or in real time. Alternatively, the idea was to investigate the final growth layer(s) which was resulted from the dynamic flow test. In this part, the focus is on the effect of chemical treatment by adding DETPMP as anti-scaling agents. The final surface crystal growth of deposited scale was analyzed with range of surface assessment techniques namely; scanning electron microscope (SEM), EDAX and Raman spectroscopy.

The analyzed scale surfaces are coated twice to three times with gold using sputtering techniques to minimize surface charge and increase the image resolution. Typically, there are two ways of treatment in a flow system; continuous treatment when the scale retardant is directly injected into the system just before or during mixing. The other way, which was applied in this work, is to add the scale inhibitor to the sea water brine mixture as a batch treatment. The inhibitor is soluble and dissociates in water to become reactive species with phosphonate negative charges. This may also result in complex formation between the added inhibitor and the existing ions in the sea water even before mixing. The flow is partially fed with two pumps, the final inhibitor concentration in the final mixture is carefully calculated. The wet crystallized surface is usually taken from the cell compartment extension to dry out in a moderate temperature. For the sake of comparison between treated and untreated surface sites, the previous untreated surface crystals were brought to support the surface interpretations.

The first treatment was carried out at 10 ppm DETPMP. Figure 7-7 shows the SEM images of the scale-DETPMP complex final growth for treated and untreated brine

mixture. The comparison between treated and untreated surface sites is made in order to investigate the effect of DETPMP. The barite scale surface deposit treated at the minimum inhibitor concentration (MIC) of 5 ppm in flow regime is shown in Figure 7-8.

The deposited complex is clearly observed at lower magnification at room and moderate temperature of 50 °C, but that was not the case at 75 °C in which the surface background is clearly seen (surface free scaling). The thickness of the scale-DETPMP complex was determined, one example was selected at 50 °C. The thickness of treated deposit was about 14.3 microns, while the untreated deposit thickness reaches 42 microns. In advance, surface analysis was expanded to include the energy dispersive X-Ray analysis (EDX). The surface deposit samples, which were treated with 5 ppm DETPMP at 75 °C, were chosen for EDX analysis. The elemental analysis is usually done at three different spot for confirmations. Interestingly, no phosphorous (P) or barium (Ba) were probed at 75 °C and 10 ppm DETPMP. The determined surface elements are tabulated in Table 7-1.

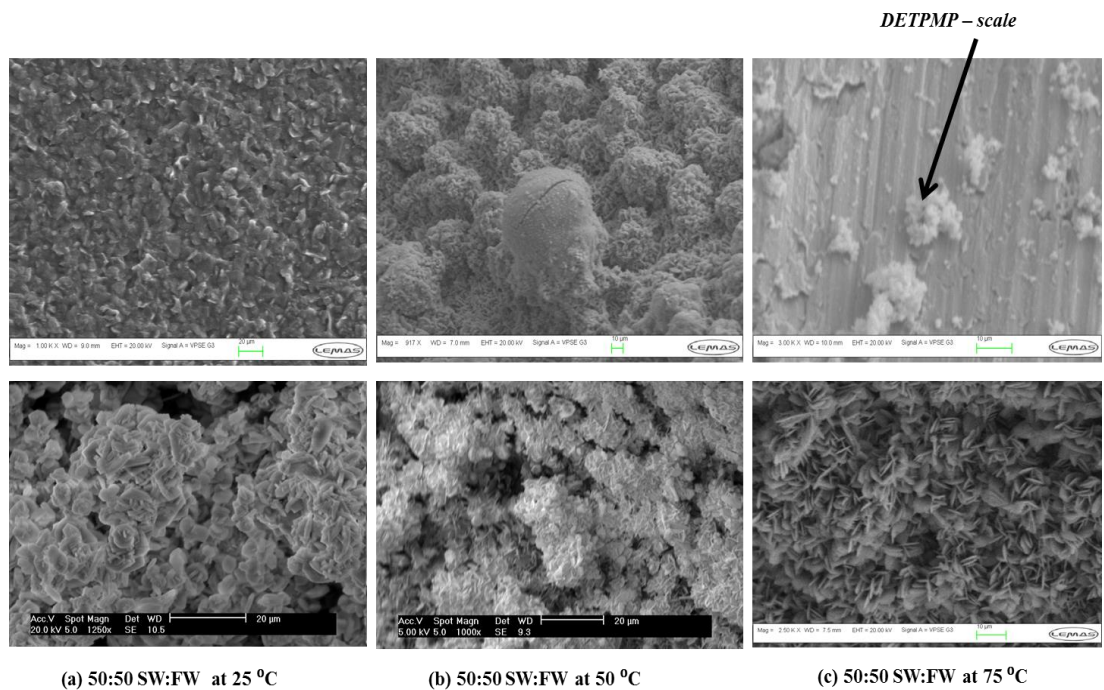


Figure 7-7 : SEM images of untreated barite deposit at 5 ml/min flow (bottom row) and treated barite deposit with 10 ppm DETPMP (top row) at specified temperatures and mixing.

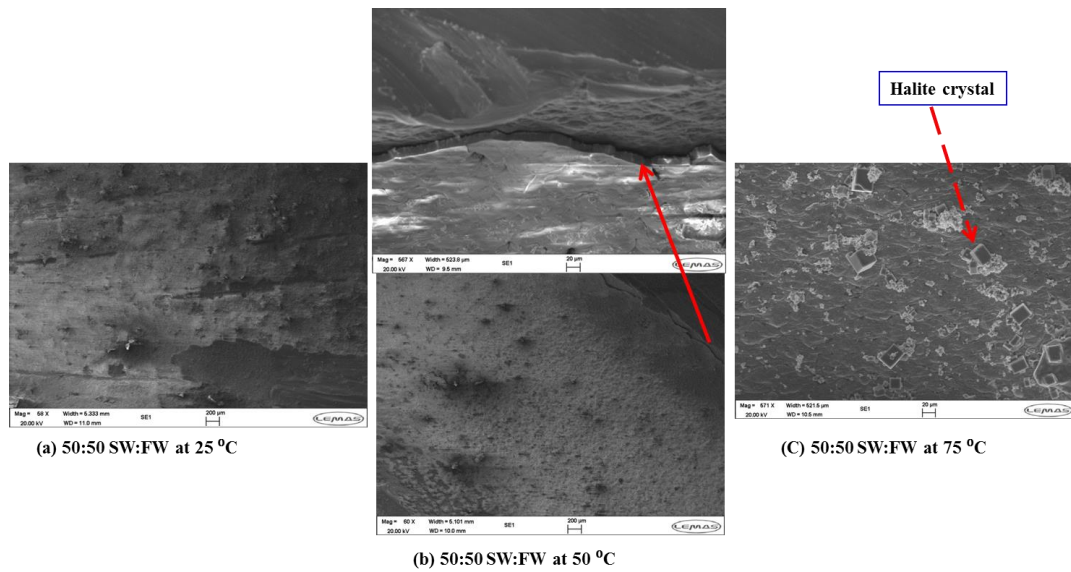


Figure 7-8 : SEM images of treated barite surface with 5 ppm DETPMP at specified temperatures and mixing.

7.2.7. Raman Analysis

The surface investigation was extended to include other sensitive surface analysis technique called Raman spectroscopy. This technique was used to confirm EDX analysis especially at 75 °C. A lower energy laser line in far infrared region was used (780 nm wavelength). As this line has a lower energy, 100% power was used to overcome the possible fading or weak spectrum peaks. A higher spectrum resolution was increased with higher accumulation mode. The surface deposited barium sulphate spectrum was confirmed at room and moderate temperatures (25 °C, 50 °C), but that was not the case when the barium sulphate is deposited at higher temperature (75 °C), see Raman Figure 7-9. As it was mentioned earlier, three locations are usually probed in each case for result confirmation. The Raman figures at 75 °C was confirmed using EDX at three random locations, no barium was detected, see Table 7-1.

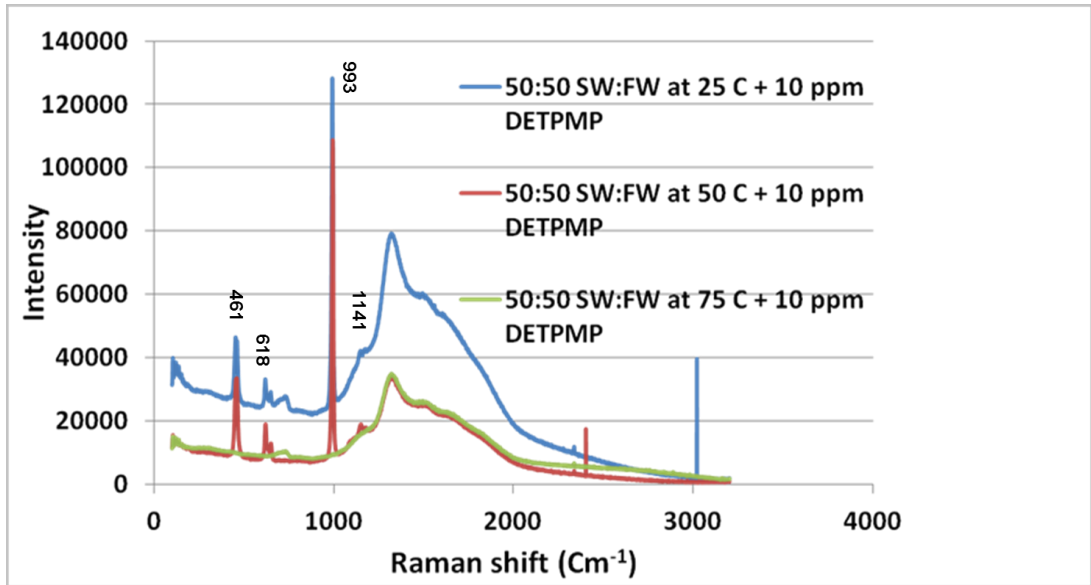


Figure 7-9 : Raman spectra of treated barite with 10 ppm DETPMP deposit on steel surface at 25 °C, 50 °C and 75 °C.

Table 7-1 : EDX analysis of the surface complex deposit treated with 5 ppm DETPMP at 75 °C in Figure 7-7.

Element	Weight%	Atomic%
O	5.21	10.39
Na	27.15	37.68
Cl	52.69	47.41
Cr	1.29	0.79
Fe	3.69	2.11
Au	9.97	1.61

7.2.8. Effect of Flow Rate (10 ml/min) on Surface Alignment

In the above previous work, almost all of the flow dynamic tests were done with lower flow rate at 5 ml/min; some of the tests were done with chemical application and some without. The setup of this experiment facilitates the flow rate control to

investigate another experimental parameter. The test was done at 10 ml/min and constant 50:50 SW: FW mixing ratio at 25 °C, 50 °C and 75 °C.

At this stage, the number of experimental parameters are minimized or limited. In this case, the mixing ratio and temperature are fixed at 50:50 SW: FW at 75 °C respectively. Figure 7-10 shows the final barite/scale surface growth at 10 ml/min, this image is compared with the bottom row in Figure 7-7 image in which the surface deposition was done at 5 ml/min flow rate. The comparison between these two images gives a clear idea about the effectiveness of the flow rate on surface crystal conformation. The shape and rose like crystal growth at 10 ml/min flow rate are not seen when lower flow rate (5 ml/min) was applied. The residence time could have a role to play in this case, and more explanation will be in the discussion section..

The untreated barite scale deposit at higher rate of 10 ml/min appears to crystallize similarly with little differences of shape at constant mixing ratio. The images background are similar at both 50 °C and 75 °C. In general, the surface crystals alignment seems differ with temperatures especially at room temperature, see the below figure.

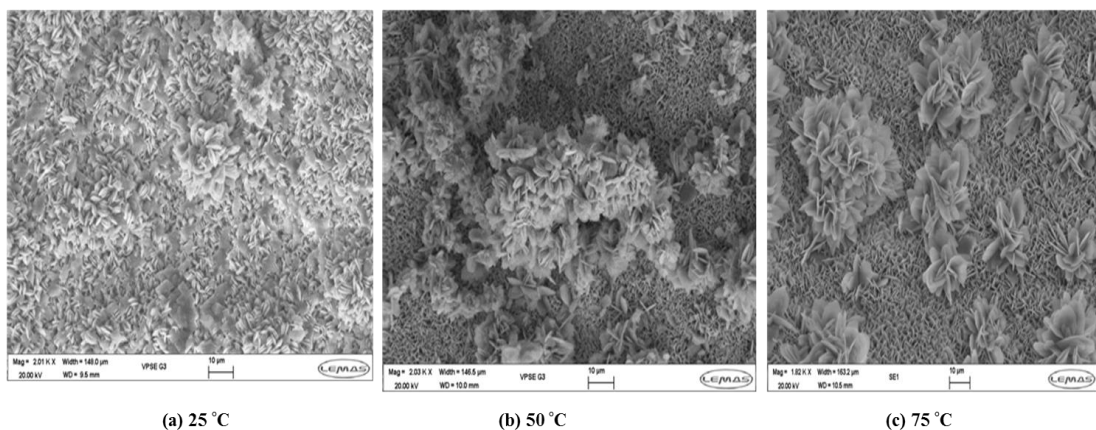


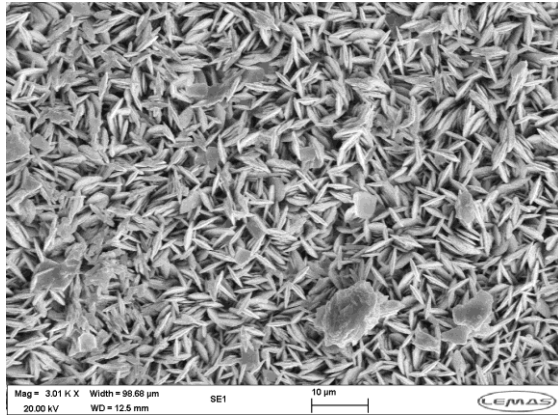
Figure 7-10 : Barite crystallization on steel surface at 10 ml/min flow and 50:50 mixing ratio (temperatures from left to right 25 °C, 50 °C & 75 °C) – no treatment.

7.2.9. Crystal Morphology on SS 316L Substrate at 20 – 150 ppm Ba²⁺ and 75 °C

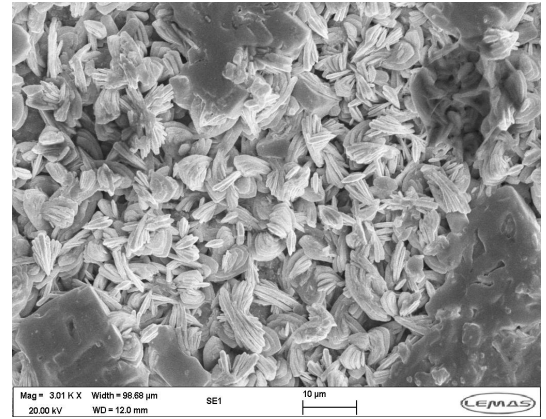
Technically, these tests were done at two different surface conditions; firstly, the deposition which was taken place on bare 316L steel surface substrate based on different barium content. Secondly, the same tests were performed on a pre-treated surface at exactly similar experimental conditions. These conditions are temperature (75 °C), saturation ratios, flow condition and the concentration of ions in sea and formation water. As a matter of fact, in the second case, the surfaces were treated or coated with highly concentrated DETPMP at 1000 ppm dissolved in distilled water. The experimental details are explained elsewhere, and the focus here is on the effect of surface condition on the scale crystals surface alignment and topography. These conditions are taken in steps in the following sections.

In this test condition, the system was actually left with only one kinetic factor namely the supersaturation ratio (SR) which was resulted from different barium content. The significant effect of barium contents, which is observed in the flow dynamic test, encourages tracking and investigating the barium finger prints onto the surface crystals.

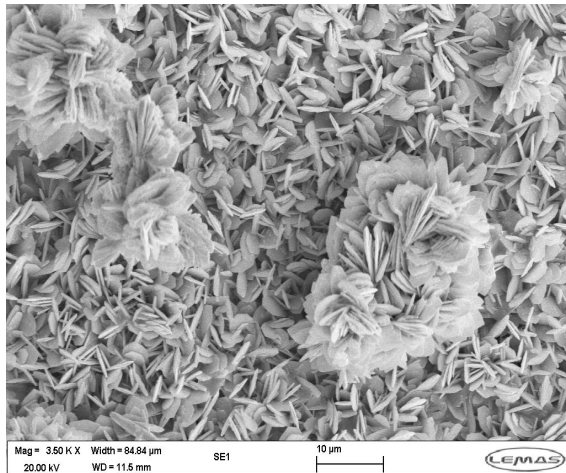
In fact, this test helps in two ways once it was done at 75 °C, one is already mentioned previously, and the other one is a confirmation of earlier claim of the effect of temperature when a wide range of mixing ratios were used within each temperature application. Figure 7-11 shows the surface crystals final growth at 75 °C and different barium contents (50 ppm, 80 ppm, 100 ppm and 150 ppm). The surface morphology which was resulted from the lowest barium content is excluded as the surface coverage is at minimum with few crystal clusters scattered on stainless steel background, See Figure 7-12.



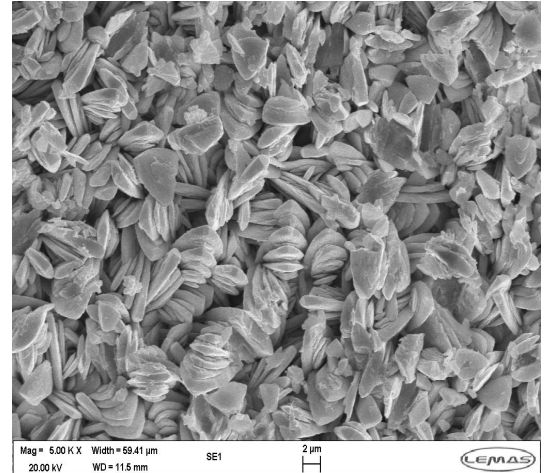
at 50 ppm



at 80 ppm



at 100 ppm



at 150 ppm

Figure 7-11 : Scale barite deposition on a bare 316L steel surface substrate at 50 – 150 ppm Ba²⁺ and 75 °C.

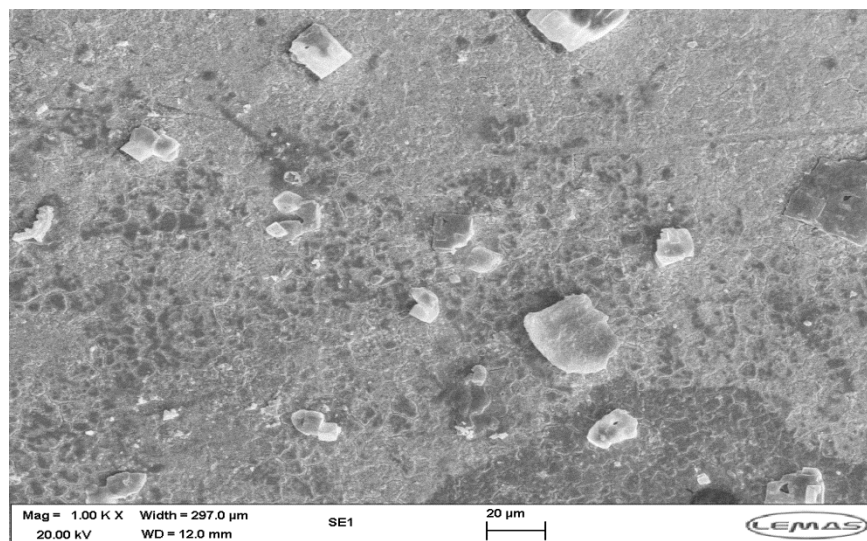


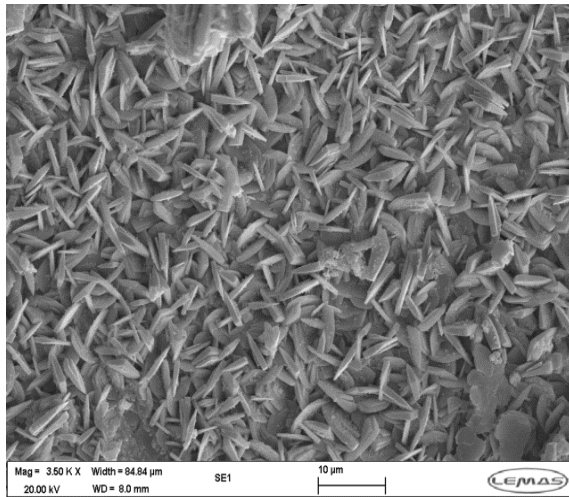
Figure 7-12 : Scale barite deposition on bare 316L steel surface substrate at the lowest 20 ppm Ba²⁺ and 75 °C.

7.2.10. Scale Deposition on Pre-treated Steel 316L Surface

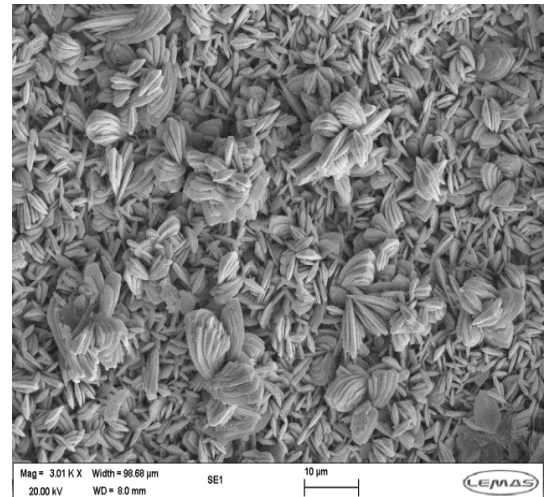
Substrate

The idea was to investigate the effect of chemically treated surface on the kinetics of complex scale in terms of induction time and the final surface crystal morphology/alignment. The DETPMP chemical product was used to treat/coat the surface with 1000 ppm in dynamic flow for three hours prior to surface deposition. The longer time duration for treating steel surface and the higher concentration were to ensure the surface binding or reaction between the anti-scaling agent and the surface. The key for this factor effect (surface pre-treatment) is the surface orientation of the adsorbed DETPMP on steel before deposition. Once the molecule is bonded to the surface, there is a probability to have the highly reactive phosphonate functional groups ($-\text{PO}_3^{2-}$ groups in DETPMP) aligned perpendicularly to the steel substrate. The three nitrogen atoms bind and hold the molecule to the steel surface through an ionic bond. This proposed molecular surface alignment was confirmed with the Fourier transform infrared FT-IR technique using external reflection (ER) mode.

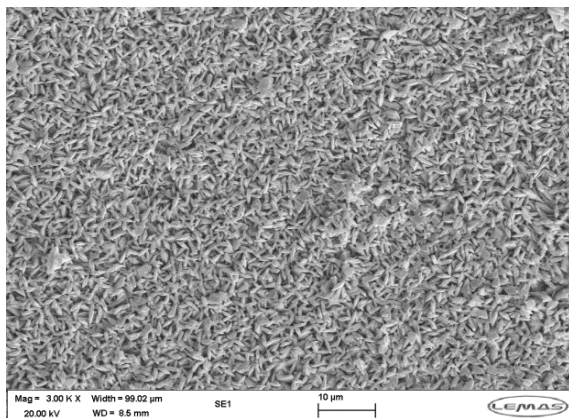
The pre – chemically coated stainless steel surfaces were prepared to deposit the scale/barite from same formation and sea water brine mixtures, which were based on the barium content in the formation water. So in this case, free divalent barium species in the saturated brines at different concentrations (50 ppm, 80 ppm, 100 ppm and 150 ppm Ba^{2+}) will have a chance to react with the treated surfaces. In fact, the rest of the divalent cations (Sr^{2+} , Ca^{2+} , and Mg^{2+}) are not excluded in this process, but the attention is given to the dominant one. The scanning electron microscope (SEM) images of surface deposit on a pre-treated steel surface with the DETPMP are shown in Figure 7-13.



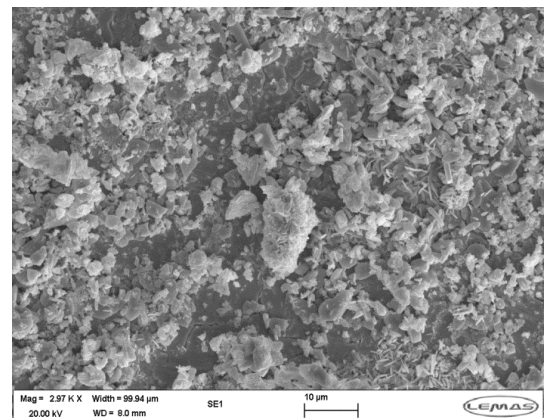
at 50 ppm



at 80 ppm



at 100 ppm



at 150 ppm

Figure 7-13 : SEM image of scale barite deposition morphology on pre – treated SS 316L in dynamic flow system at 75 °C.

7.2.11. EDX Elemental Analysis of Scale/Barite Deposited on a Pre – Chemically Treated Stainless Steel 316L Substrate

During surface crystallization, the surface morphology can be affected by different parameters and the co-existence of organic surface adsorbate is one of them. The argument here is “would it be possible to notice an effect of organic adsorbate on surface scale kinetics when inorganic minerals are deposited on an organic film in the dynamic flow system?” It is actually well – known that most of the scale inhibitors are water soluble. So the scale inhibitors dissociate easily to give free radical active groups and the possibility to bind to the surface with nitrogen groups

(chemisorption) is high. The free phosphonates could bind to the divalent species in the mixture flow stream forming nuclei that grow to form a deposit. In addition, it was expected that the early ions in the mixture stream may come in the direct contact with the scale inhibitor on the surface. It may have an impact on the surface nucleation stage in terms of its stability and shape of the final crystal growth.

Once the early surface nucleation is affected, the whole surface scale kinetics may also be affected. The observed surface induction period under this surface condition was successfully obtained. The collected results are compared with surface scaling kinetics on untreated surface, unlike the surface morphology assessments, no major effect was noticed on the observed surface induction time. Figure 7-14 shows the morphology and the selected area for energy dispersive X-Ray (EDX) elemental analyses of the scale/barite deposit on the pre-treated surface. Bearing in mind that the surface deposit was carried out at different barium concentrations and fixed temperature of 75 °C. The final surface deposit can possibly be affected by the early surface nucleation pattern. The earlier surface nuclei are first to be in direct contact with the nucleophilic organic phosphonate groups on the treated surface. Consequently, the scaling film crystals grow starts from those phosphonate – divalent ions complex sites to reach the final shape and sizes.

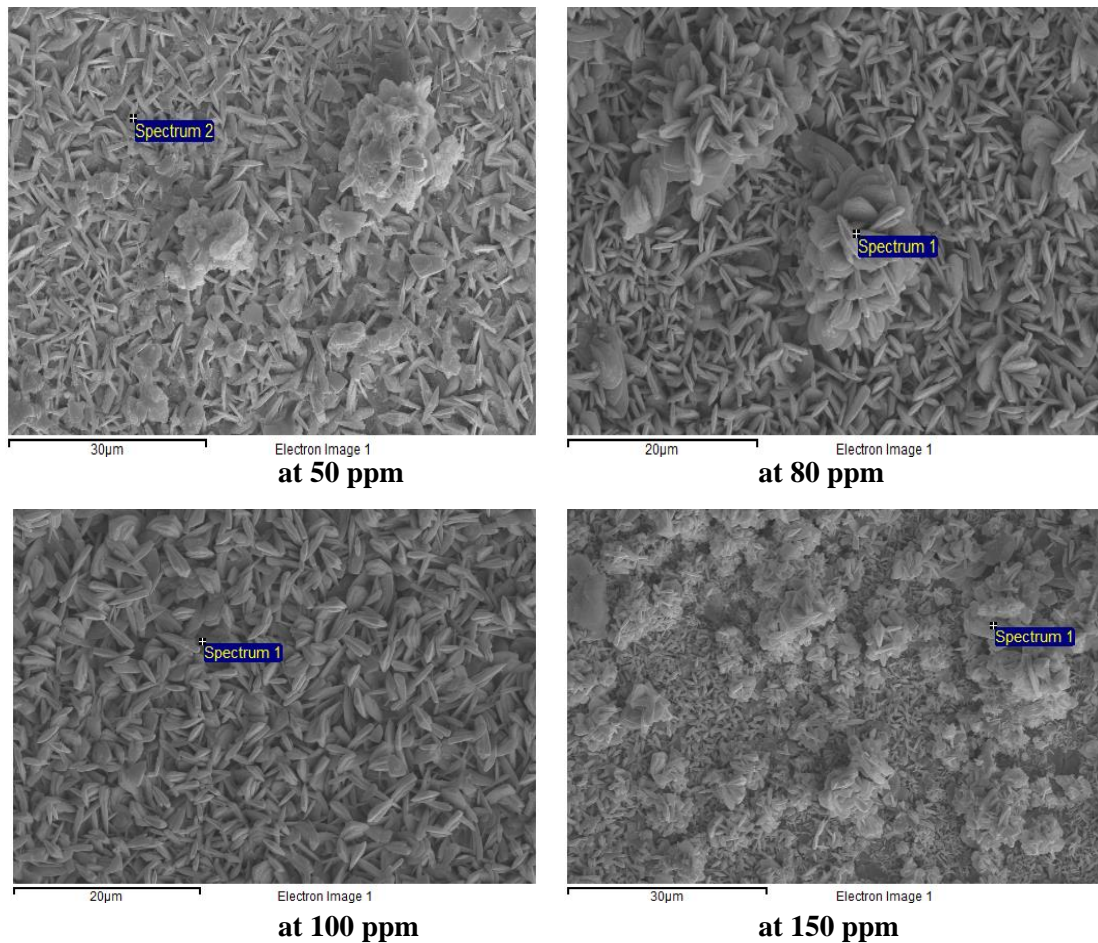


Figure 7-14 : EDX elemental analyses (selected area) of scale barite deposit on the pre-treated surface at different barium concentration and 75 °C.

The previously mentioned surface figures show the spots from which the EDX elemental analysis was taken, although it seems only one spot per image, but in fact, the average of three analysed spot is considered.

The EDX analysis was mainly to investigate the barium ions behaviour, strontium and calcium and their variation in barite controlled environments. The attention is also given to the phosphorous weight percentage and its variation in the final growth sites. The possible trace amount of the remaining phosphorous on the surface is related to the surface scale coverage percentage, and its ability to suppress and

conceal the DETPMP on surface. The phosphonate group surface reactivity with scaling species should also be considered.

The tabulated, Table 7-2, figures of barium, strontium and the phosphorous are based on average of three readings at three different surface areas. The collected figures are plotted in Figure 7-15. The results are investigated in more details in the discussion chapter.

Table 7-2 : The elemental analysis of the main precipitant at different Ba²⁺ contents.

Element	Wt. % at 50 ppm Ba ²⁺	Wt. % at 80 ppm Ba ²⁺	Wt. % at 100 ppm Ba ²⁺	Wt. % at 150 ppm Ba ²⁺
Ba	13.35	15.75	15.89	18.61
Sr	3.63	3.10	2.25	2.31
Ca	0.56	0.52	0.56	0.58
P	0	0	0	0

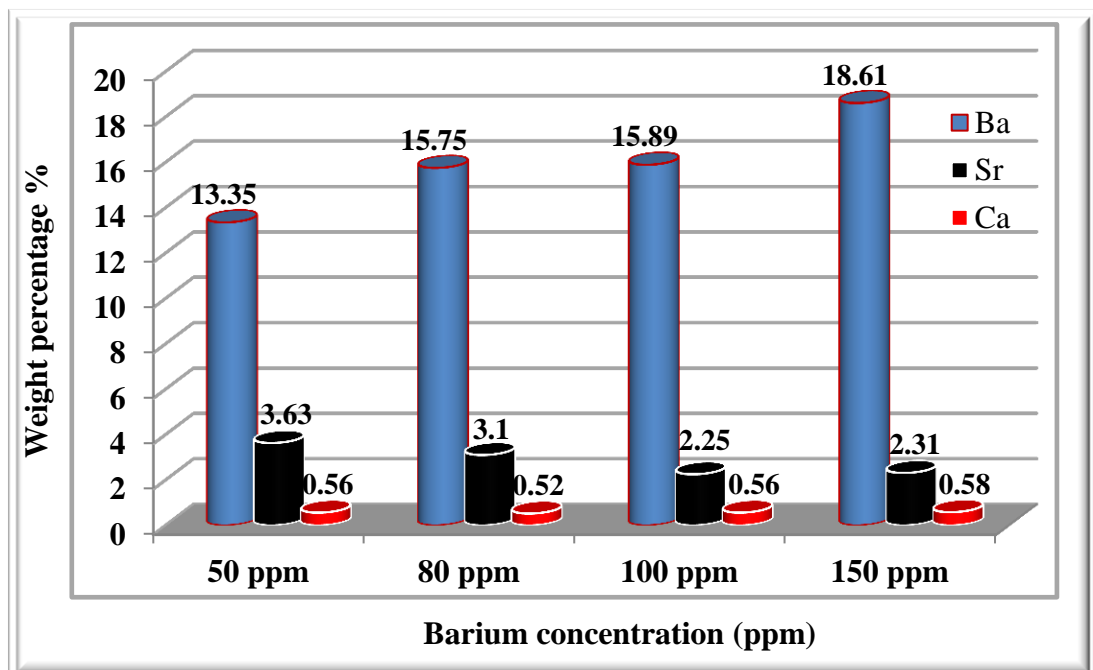


Figure 7-15 : EDX elemental analyses of complex scale barite deposit on pre-treated surface at different barium concentration 50 – 150 ppm at 75 °C.

7.2.12. *Ex – Situ* X-Ray Diffraction Analysis

As part of this research work on a scale deposited on surfaces, *ex-situ* X-Ray techniques is used to analyse the deposit crystal phases on surface. The aim was to investigate the effect of both thermodynamic and kinetic factors on these phases. The thermodynamic factor is represented in the saturation variations due to the free barium content. The kinetic factor is related to the effect of different surface condition on the final crystal shape and alignment. As predicted in advance that the barite is the main precipitant with the lowest solubility. In this case, the X-Ray spectrum of barium sulphate (as background for further analysis) is vital. It is also known that the barium and strontium in a complex brine mixture deposit as Celestine or Barian. The barium and strontium sulphates are existed at different ratios in these scale complexes. The back ground spectra was collected from a pure barium sulphate deposited on steel surface to get a BaSO₄ single phase on 316L steel surface.

7.2.13. Single Phase Barite Crystal on SS 316L Substrate – Surface Background

The *Ex – situ* X-Ray analysis of the barite single phase crystal diffraction was carried on flat stainless steel substrate samples. The single phase barium sulphate crystallization on surface was deposited at 50 ppm and 100 ppm Ba²⁺ concentrations in dynamic flow regime. The flow rate was 10 ml/min at 50:50 mixing ratio, and 75 °C on 316L stainless steel substrate.

The aim was to get a reference or background of BaSO₄ X-Ray spectrum on specific surface as a dominant single phase. So later, the collected spectrum is used as a reference to investigate/assign the crystal faces which was deposited from the real complex brine mixture in dynamic flow. The test was done on crystals formed from the complex brines in which the saturation ratio varies according to barium content. For this reason, the barite single crystals resulted from 50 and 100 ppm Ba²⁺ solution mixtures were chosen to collect reference barite surface spectrum, it was

meant to be two concentration cases - instead of one - for the sake of confirmation and reliability. Figure 7-16 shows the background reference agreement between the two spectra at different barium concentrations. This was done just to confirm the backgrounds.

The surface deposit composition, crystal phases and orientation were characterized by using the built-in crystal data base software called HighscorePlus. The observed crystal phases were assigned between 10° to 80° diffraction angles. The focus is given to the angles ranged from 20° to 60° . The barium sulphate assigned crystal phases were (200), (210), (201), (211), (112), (221), (122), (113), (401), and (104).

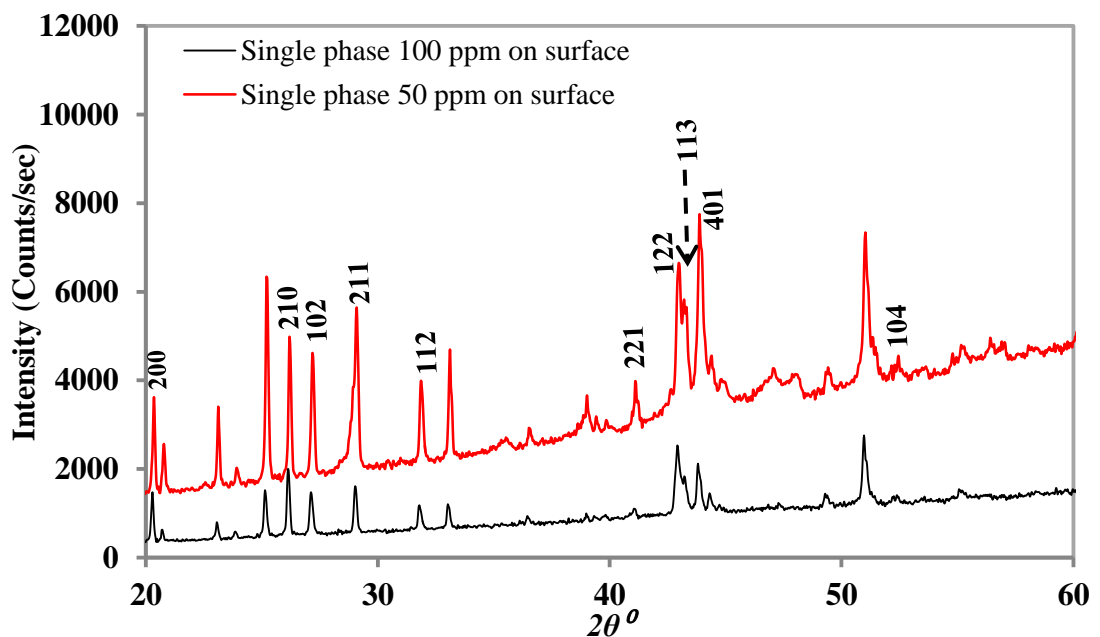


Figure 7-16 : *Ex – situ* X-Ray spectrum of single barite crystal deposited on steel surface used as a background.

7.2.14. *Ex –Situ* X-Ray Analysis of Multiphase Scale/Barite Crystals

In general, the multiphase crystal analysis is a complicated issue especially when one component is found in many phases at different ratios such as Celestine and Barian. In such formed complexes, the percentage between barium and strontium vary from 50:50, 25:75 or 75:25 Ba:Sr. It is possible to find some other percentage such as 40:60 Ba:Sr 40:60. The problem arises when each of these complexes has its own crystal phases and orientations and these phases are found to overlap.

The multiphase scale crystals are expected to deposit from a complex brine mixture when all the alkaline earth minerals are existed as soluble ions. In this work, the barite is deposited as the main precipitant in addition to hydrated and anhydrous calcium sulphate, magnesium oxide ($Mg(OH)_2$) and sodium chloride (NaOH). An attention is given to the behaviour of some crystal phases in barite as a function of barium content, the co-deposition from other existed ions, and effect of surface chemical treatment prior to deposition on the steel surfaces.

7.2.15. Multiphase Scale Deposited on Untreated SS 316L Substrates as a Function of Barium Content (flow)

The *ex – situ* X-Ray analysis tests were done on the specimens fabricated to investigate the barium concentration (20 ppm, 50 ppm, 80 ppm, 100 ppm and 150 ppm) effect on the deposited surface crystal orientation. This also was done to support the surface deposition findings in dynamic test as a function of barium variations. The question was not only how that effect takes place in terms of the observed induction period, but also how the effect can be assessed in terms of the final surface topography and orientations in flow systems. There is no need to repeat the test description conditions here as it was described in the first part of the experimental work. The collected X-Ray spectrum in Figure 7-17 shows the effect of the barium content on multiphase crystal system. It is compared with the single phase barium sulphate spectrum on the similar steel substrate and test condition. The

most interesting area was chosen at diffraction angles ($40^{\circ} - 50^{\circ}$) and enlarged in Figure 7-18 in order to properly assess the affected phases. The effect was noticed on (122), (113), and (401) crystal faces in terms of the orientation and positions; this is detailed in the discussion section.

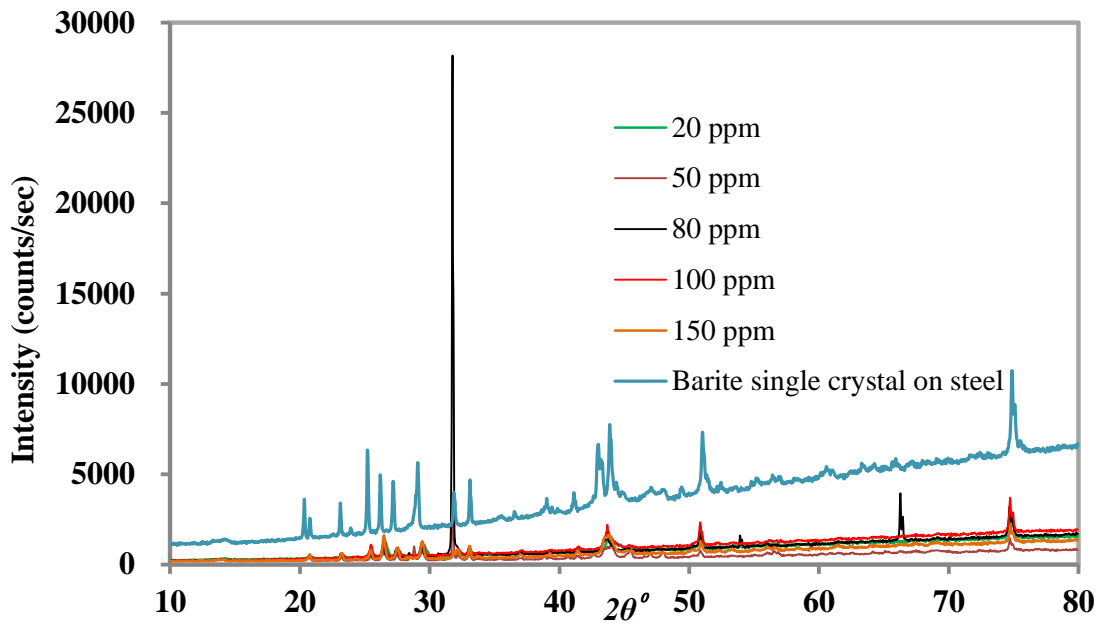


Figure 7-17 : The multiphase X-Ray spectrum of scale/barite deposition on SS 316 substrate.

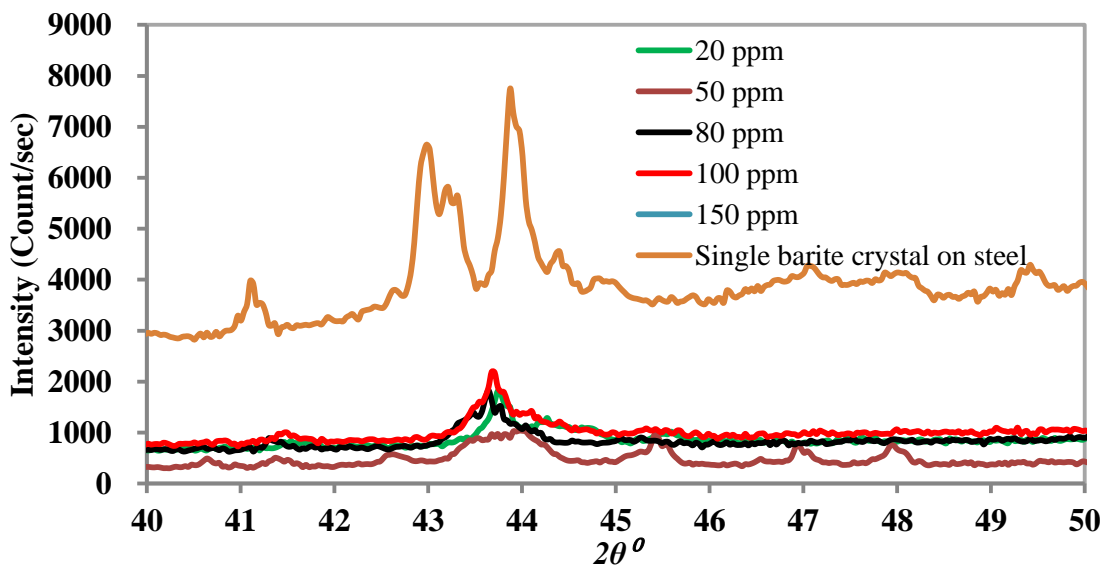


Figure 7-18 : The effect of barium content on (122), (113), and (401) crystal faces in terms of the orientation and positions.

7.2.16. Phase Analysis of Multiphase Crystal Deposit

Phase analysis of the multiphase scale deposit is immensely important to identify the composition and the percentage of each component, the percentage is related the different ions incorporation in one crystal matrix. The incorporation is also taken place due to the co-deposition of multi ions from complex brine mixtures. In this research work, most of the thermodynamically predicted components using the Multiscale software were detected in the formed scale/barite crystal deposits. These phases were characterized and defined using bunch of softwares e.g. HighscorePlus to analyse the peaks and most possible components. This software is designed to contain a huge number of built-crystals configuration data base as references. Origin 8 and excel were also used in data interpretations.

In this part, due to the vast number of data were collected from multiphase crystal at different barium concentrations (20 ppm to 150 ppm), the deposition which was resulted from the lowest barium content mixture was chosen for phase analysis. Figure 7-19 shows the phase component analysis of the multiphase scale /barite deposit at 20 ppm Ba²⁺ content.

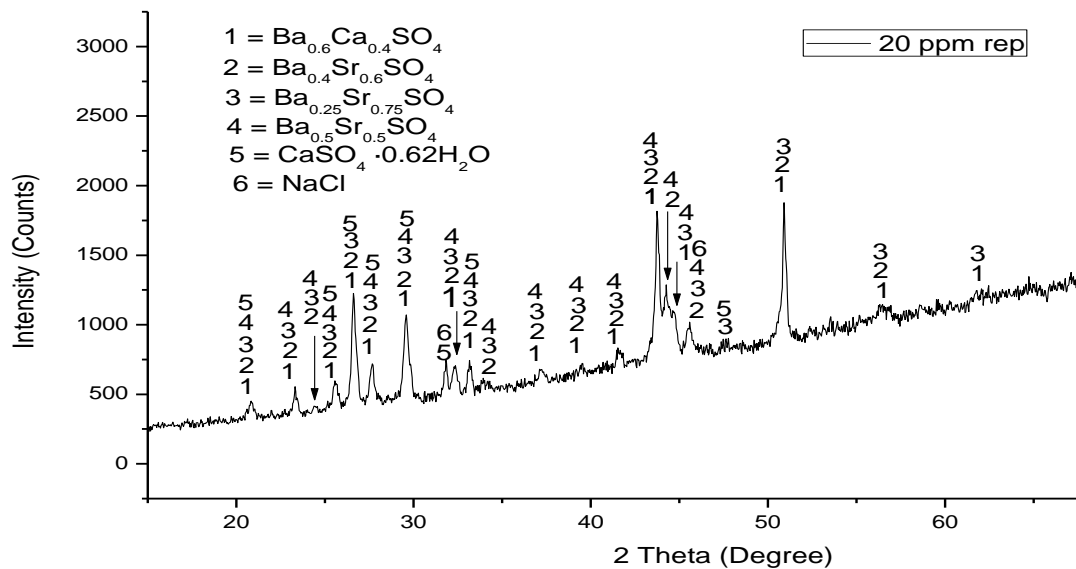


Figure 7-19 : The phase analysis of the multiphase scale deposit at 20 ppm Ba²⁺ content.

7.2.17. Multiphase Scale Deposited on Treated SS 316L Substrates (Flow).

The effect of surface condition is one of the parameters which are investigated in this work. In this case, the steel surface was chemically manipulated using anti-scaling DETPMP. The chemical pre-treatment or coating process was lasted for one hour in flow system at 10 ml/min. The DETPMP concentration was 1000 ppm in order to grantee the scale inhibitor film formation prior to deposition at different barium contents (similar to the previous section). It is known that the DETPMP has three nitrogen atoms in the backbone of its chemical formula. These rich electron nitrogen atoms are able to bind chemisorbedly to the steel surface. The organic surface adsorbents were characterized using Fourier Transform Infra Red FT-IR surface technique using External Reflection mode. The pre – treated surface was scaled using the same conditions that was described in the previous section when the bare steel surface was scaled at different barium content (no surface modifications).

7.2.18. FT-IR Surface Characterization of DETPMP

DETPMP organic film was used to chemically modify the stainless steel surfaces prior to scaling. The aim was to investigate the effectiveness of the scale retardant on the scale/barite kinetics. Firstly, in terms of its impact on the observed induction time and secondly, it is role to affect scale crystals arrangement and shape on surface.

The chemically coated surface was initially analysed using FT-IR to confirm the film binding to surface and possible DETPMP orientation. Figure 7-20 shows the FT- IR spectrum of DETPMP on SS 316 surface substrate. The phosphonate group – PO_3^{2-} absorption band was assigned at 1016 Cm^{-1} wavenumber, the region in which it is expected ($950 - 1100 \text{ Cm}^{-1}$). The disappearance of absorption bands between $1250 - 2350 \text{ Cm}^{-1}$ does not mean they do not exist. Their appearance is related to the molecule's surface orientation/alignment and whether the mode is IR active or not and its intensity or strength.

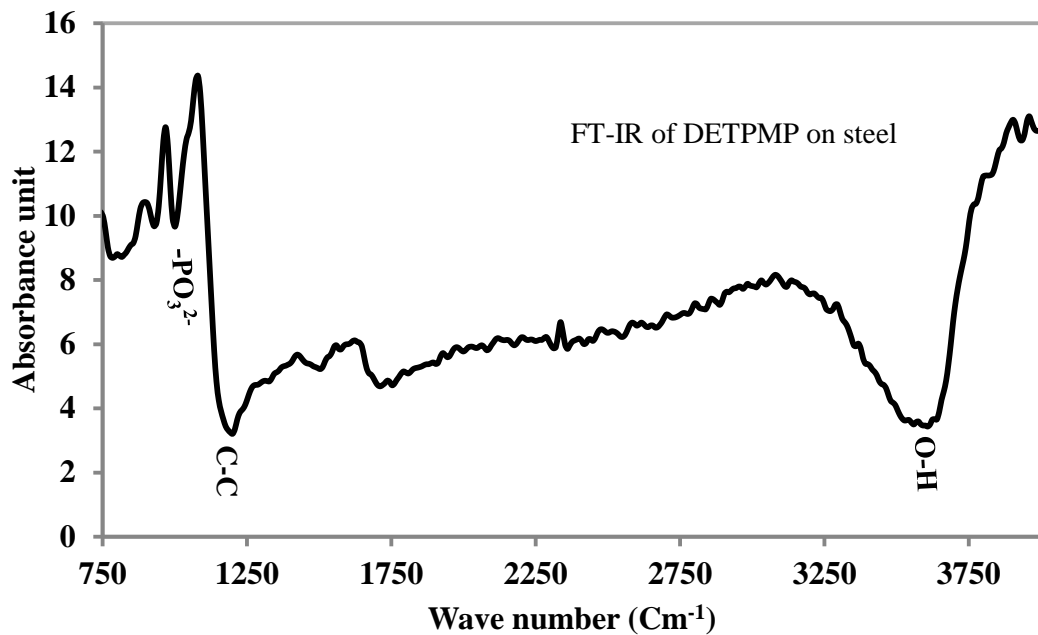


Figure 7-20 : FT- IR spectrum of DETPMP on SS 316 surface substrate.

The *ex – situ* X-Ray analyses were done under similar testing parameters, which were applied when the test was performed on the scaled specimens without surface treatments. A similar diffraction pattern noticed in the case of treated surface when it is compared to none treated one. The focus is given to the most interesting area, which was chosen in the above at $40^{\circ} - 50^{\circ}$ diffraction angles. The effect was noticed on (122), (113), and (401) crystal faces in terms of the merge of these faces and forming a broad band, the preferential orientation is also highlighted. Moreover, the phases overlapping is also considered. Figure 7-21 shows the *ex – situ* X – Ray analysis of multiphase crystallization on pre - treated steel surfaces with DETPMP for three hours. In order to properly investigate the effect of treated surface (the only variable parameter here) on deposited crystals on it, Figure 7-22 shows the *ex – situ* X – Ray analysis of multiphase scale/barite surface crystals deposited at 50 ppm barium content on both treated and untreated stainless steel surfaces. This is also detailed in the discussion section.

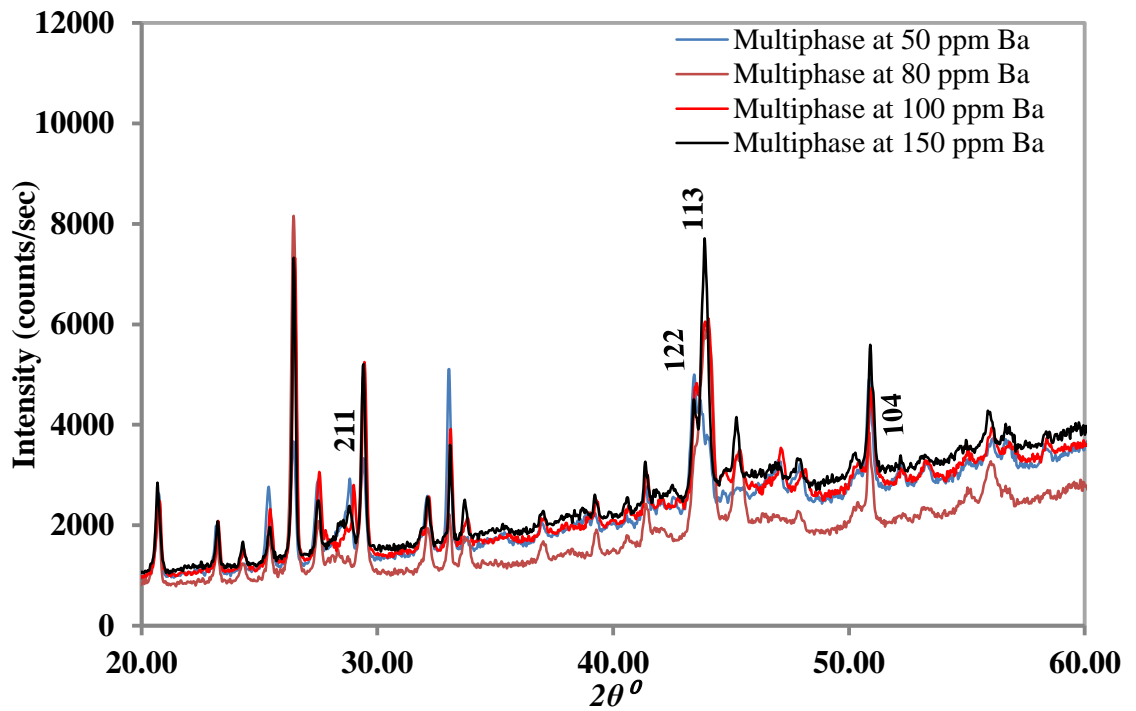


Figure 7-21 : *Ex – situ* X – Ray analysis of multiphase crystallization on pre - treated steel surfaces.

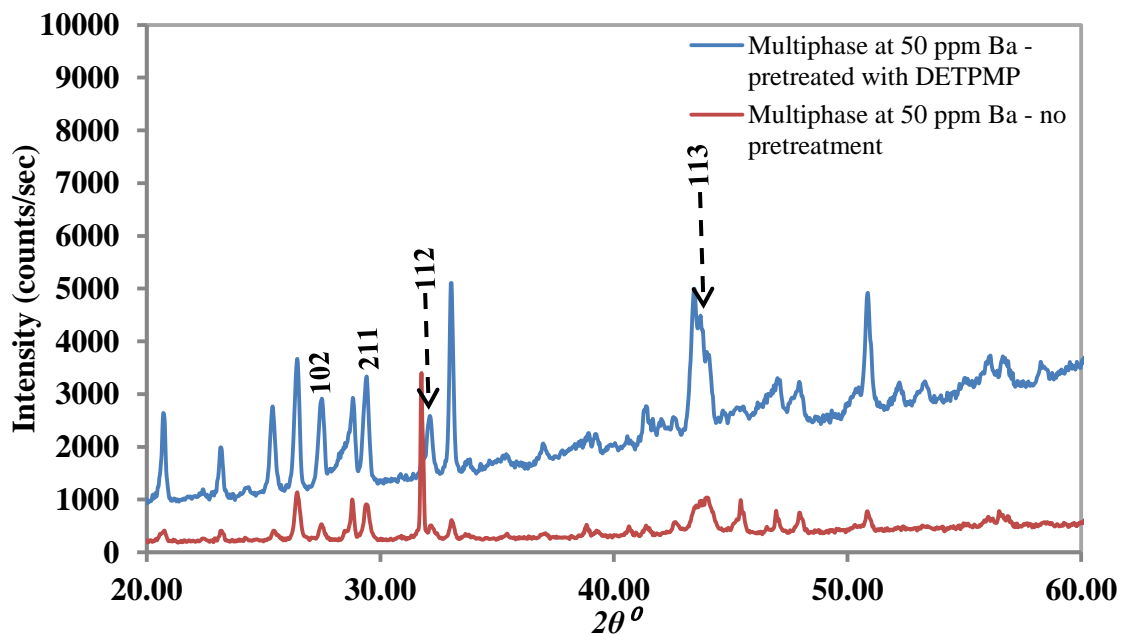


Figure 7-22 : *Ex – situ* X – Ray analysis of multiphase crystallization on pre - treated steel surfaces.

Chapter 8. DISCUSSION

8.1. INTRODUCTION

This part of this research work is set to provide a comprehensive conclusion about the bulk and surface crystallization kinetics of barite in multiphase complex brine systems. The kinetics were investigated at different experimental conditions varying parameters such as temperature, mixing ratio, saturation ratios (SR), flow rate, surface condition and the free Ba^{2+} ion concentrations. The discussion focuses on the following main issues:

- 1- Thermodynamic predicted saturation ratio and surface deposition (bulk precipitation versus surface deposition at different temperatures).
- 2- Scale surface growth and Δp measurements.
- 3- Scale inhibition.
- 4- Effect of saturation ratio on scale crystals' shape and its impact on surface packing.

8.2. PREDICTED SATURATION RATIO – BULK PRECIPITATION VERSUS SURFACE DEPOSITION

The application of different temperatures and mixing ratios are to simulate different oilfield mixing conditions at different temperatures from the down hole to the topside surface production facilities. Once the scale is predicted, the effect of these variables is considered in both bulk and surface and where the three techniques overlapped.

Bulk kinetics shows that the increase of temperature decreases the induction period in the case of bulk precipitations at 50 °C (this is also noticeable in the case of surface deposition). It seems that the enhanced solubility of barium sulphate/scale in the solution, due to elevated temperature, promotes or accelerates the nucleation rate as the surface tension between the formed barite crystals and the solution decreases. This finding is in good agreement with earlier investigations [169]. It is also worth mentioning that the induction period is solution component dependent as it decreases with the increase of the concentrated species.

The plateau of the turbidity graph at various temperatures shows the state of formed crystals growth in the solution mixture. It is explained according to the Ostwald ripening principle, where small crystals dissolve in favour of the bigger crystals due to the dependence of solubility on the surface curvature [57]. In previous work on CaCO₃ systems, the instability of the plateau in an under saturated mixture (after attainment of supersaturation) was referred to as a secondary growth. At higher temperature, this late growth seems independent of the saturation ratio after time elapsed. This explains the bulk observations at high temperatures in this work as when the temperature is high it also becomes a dominating factor of crystallization and the saturation ratio is no longer critical [176]. See Figure 8-1.

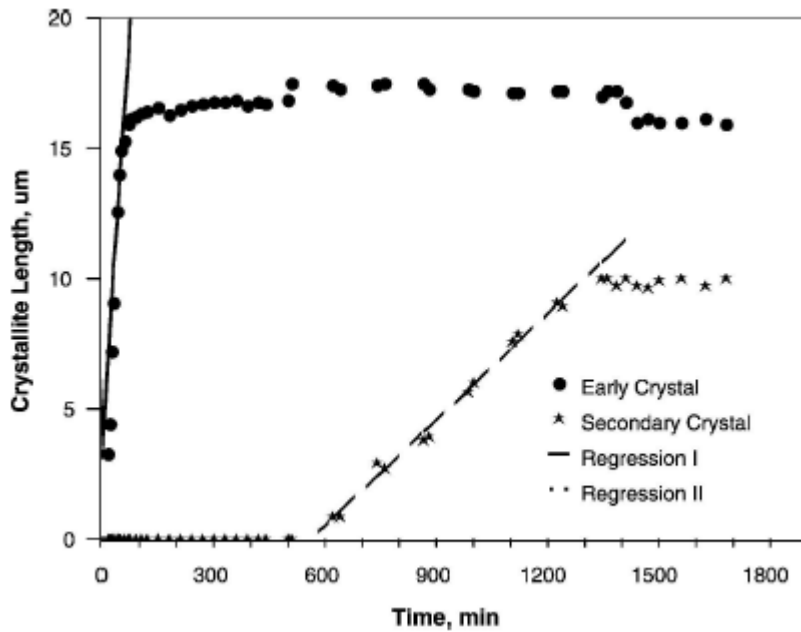


Figure 8-1 : The early and secondary crystal growth and induction time at high temperature [176].

Various research works have been done when it was proven that the bulk and surface scaling kinetics are two different processes. Tao and co-workers [96] have proven this approach in bulk and on surfaces. On surfaces the evaluation was based on the surface scale coverage percentage and quantification of the deposited elements, and in bulk on change of residual ions through a time intervals. In this work, this in fact was approached differently based on predicted saturation ratios and actual mass deposited across different temperatures and mixing ratios. In addition, the current initial estimation of surface kinetics involves a new evaluation of early surface nucleation. Generally, the instability of surface nucleation during surface induction period seems to have no major impact on the final surface growth at constant temperature. The failure of the early formed scale layers was more intensive at room temperature while it becomes less intensive at moderate temperature of 50 °C. At higher temperature of 75 °C, the surface scaling build up looks much steadier throughout the deposition process. The unique early nucleation pattern may be one of factors of the unique final growth on surfaces, but it is not the main factor.

The prediction figures represent mostly the thermodynamics of the bulk test rather than the surface. No matter what the temperature was, model prediction was in good agreement with and bulk precipitation in terms of the systematic variation of the observed induction period of the formed crystals at lower, mild and higher temperatures. This also confirms that barite system is a heat sensitive system regardless the level of the supersaturation saturation predicted. So the static experimental induction period was found to be proportional to the applied temperature which decreases as the temperature increases and the saturation ratios decreases. This has a remarkable effect on the surface kinetics. The predicted mass does agree with actually precipitated masses in bulk and deposited on surface regardless within each temperature. Figure 8-2 shows the predicted mass with respect to the predicted SR. The higher mass is related to the barium content while the SR is related to the actual free species and not all of them active.

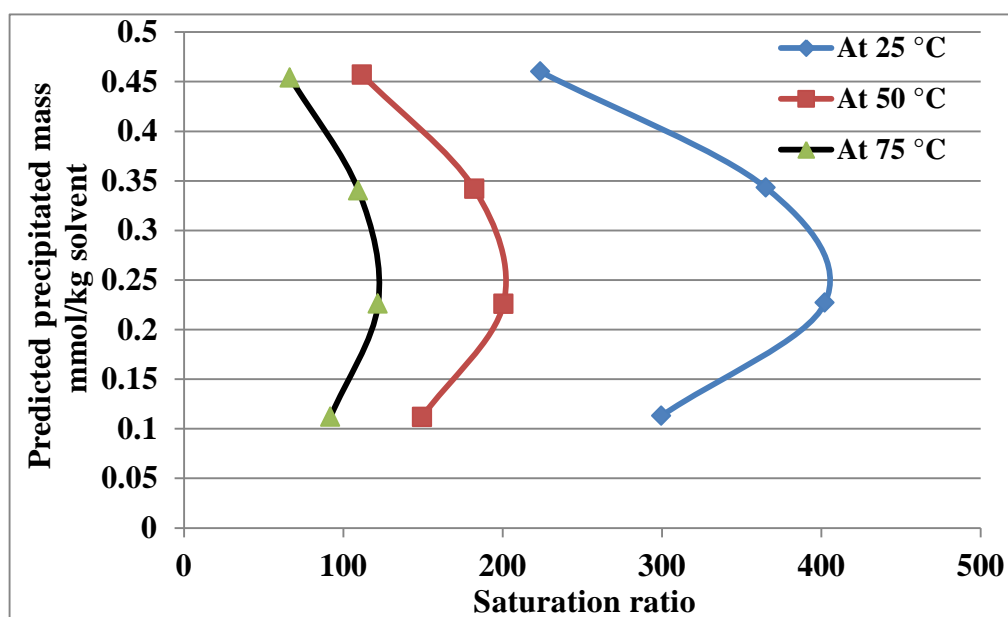


Figure 8-2 : Predicted masses with respect to the predicted SR.

On the surface, initially, the assessment of the crystals' induction period was determined by conductivity measurements in bulk. It was the first step to finalize the surface crystallization mechanism, the induction period was estimated to be 2 – 3

seconds. This assessment of barite scaling system was in good agreement with previous work using the same technique in which the system response was 2 seconds [59], in comparison; the response of the used system in current study is 3 second. Taguchi in Figure 8-3 shows a very rapid decline in barium ions concentration which is in agreement with the bulk scaling trends in this work using conductivity measurements.

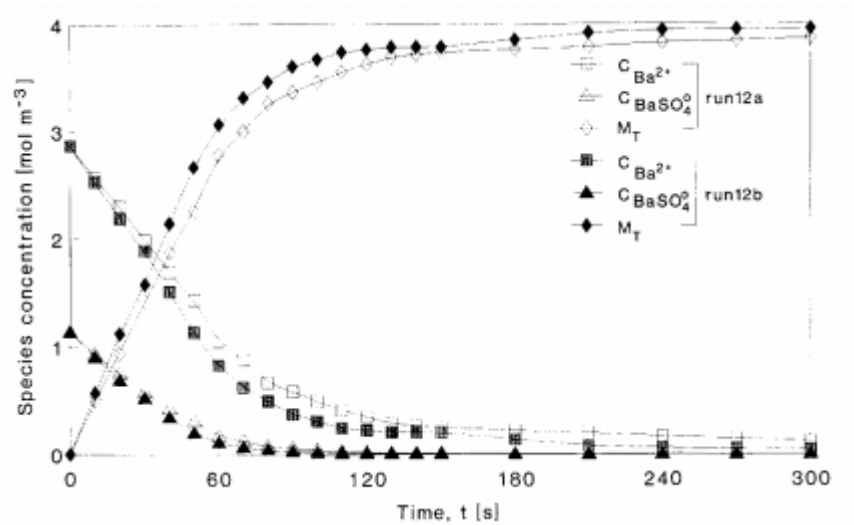


Figure 8-3 : The rapid variation of barium species concentration with time in a non-nucleated system [59].

8.3. SCALE SURFACE GROWTH AND ΔP MEASUREMENTS

Surface scaling rate determination can be assessed using the dynamic system coupled with a differential pressure sensor across the test section to monitor tube blockage. A back pressure regulator is used to maintain the system pressure for accuracy.

Previously, in dynamic systems, scaling rate determination was considered from the time required to block the tube and the thickness of the scale. In this case, the time required to block the tube should include the combined time for nucleation, crystal

growth and scaling film growth. The surface nucleation time and, of course, the total blockage can be minimised by using pre-scaled tubes.

The upgraded dynamic flow setup used has an additional advantage that it facilitates a precise investigation and following up of the initial surface nucleation period of scale deposition on surfaces. Unlike using a coil [177] when it is used as a surface, in smaller cell dimensions, scale deposit is most likely to propagate in uniform layers through growth to the final cell blockage during a long duration test.

Yuping and co-workers [81] have evaluated the scale thickness along one meter tube and 0.285 ID using a kinetic model for calcium carbonate single brine, Figure 8-4. It was assumed that the scale was uniform on the capillary wall. It sounds far from reality at such capillary length and high supersaturation. The upgraded system in this research work with smaller dimension cell capillary is most likely to present the scale uniform claims (1mm ID and 10 mm length). Surface scale porosity is less intensive with thinnest particle at higher temperature and it is possible for a uniform surface scale to gain more weight (due to the well arrangement of crystals on surface). The average of overall weight gained was calculated on the average of weight gained [178].

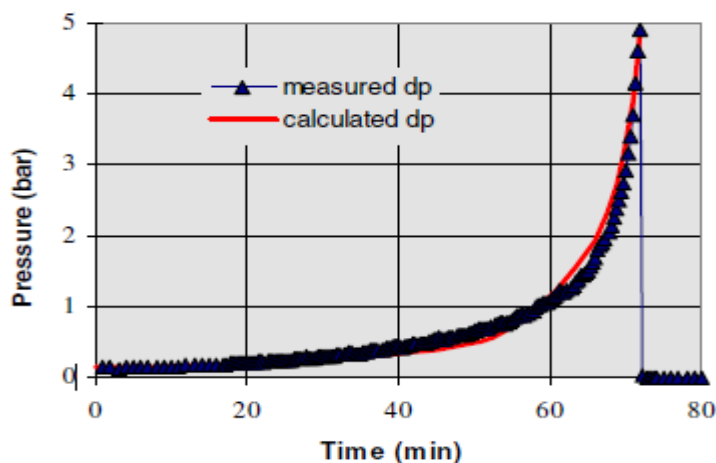


Figure 8-4 : Measured and calculated ΔP between the inlet and outlet of a one meter long tube, 3.04 mm ID tube at same flow rate used in this work (10 ml/min) [81].

In this work, the Hagen-Poiseuille equation was used to assess the development of scale wall thickness. It relates the pressure drop Δp across a circular pipe of length (L) to the average flow velocity in the pipe (Q). It was applied on different testing cell diameters and length. This approach gives a precise radius reduction in a unit of time under the effect of saturation ratios due to barium concentration in the final brine mixture.

Using asphaltene as a colloidal precipitant in solvents, the hydrodynamic thickness of deposited material on surface was assumed to propagate homogeneously by different researchers [111, 179, 180]. The surface deposition rate was investigated in terms of pressure, temperature and different fluid compositions by measuring the pressure drop over the length of a stainless steel capillary. The impact of porous media was also evaluated.

Latter, the surface homogeneity of the deposit was criticized when different flow condition was used. It was confirmed by the visualization of surface profile estimation of deposited asphaltene by image analysis [181].

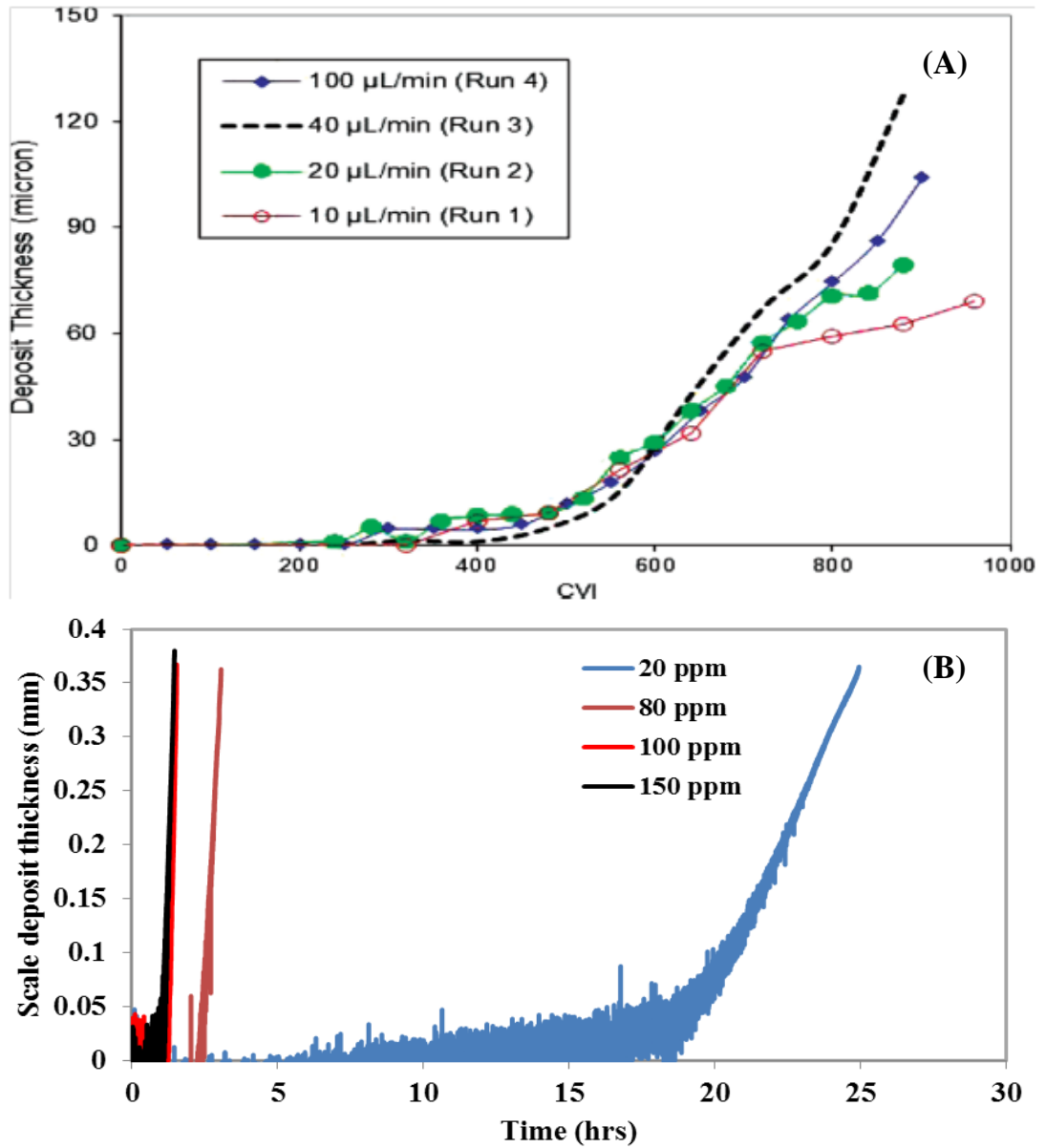


Figure 8-5 : (a) Effect of flow rate on deposition with respect to the capillary-volume injected (CVI) as a measure of the elapsed time, Lawal [180], and (b) the effect of SR, this work.

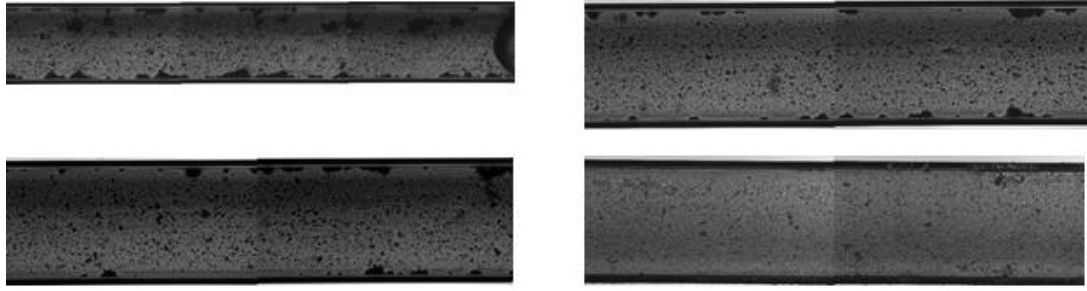


Figure 8-6 : The effect of flow rate on the uniformity of surface deposit (no homogeneity [181]).

So what is new? Unlike previous approaches, this work investigates the different nature of material which was solvent free solid minerals with different densities. The variation of saturation ratio is the most important factor to approach the surface rate of deposition using the Hagen-Poiseuille relation. Figure 8-5 shows the comparison between the effect of both the flow rate in Lawal's work [180] and the effect of the saturation ratio at different barium contents in this work. The gap between the film growths as a result of flow is clearly seen apart from the lowest flow at 10 $\mu\text{l}/\text{min}$, whereas in this work, the surface film growth is clearly distinguished. The effect of flow on scale surface homogeneity is clearly proven in Figure 8-6.

8.3.1. Theoretical Calculation and Surface Kinetic Agreement

In this work, based on the barium free ions content in the final brine mixture, the differential pressure technique was used to extend and expand the investigation on the effect of such species on scale surface kinetics. Earlier, published experimental data shows that the $\log t_{ind}$ vs. $(\log SR)^2$ relation at constant temperature was linear for a large number of substances. These data vary based on crystallites' solubility. As a readily soluble compound, the potassium dihydrogen orthophosphate's (KDP) rate of nucleation in supersaturated aqueous solution was investigated [92], see Figure 8-7. It was found that the nucleation rate increases with supersaturation, temperature and agitation. Moreover, these investigations were extended to include sparingly soluble minerals, e.g. BaSO_4 , SrSO_4 , BaCO_3 and PbSO_4 , when homogeneous nucleation followed by diffusion was assumed to control the crystal

growth. The induction period and the number of particles per cm^3 were found to increase with increasing concentration [94, 95].

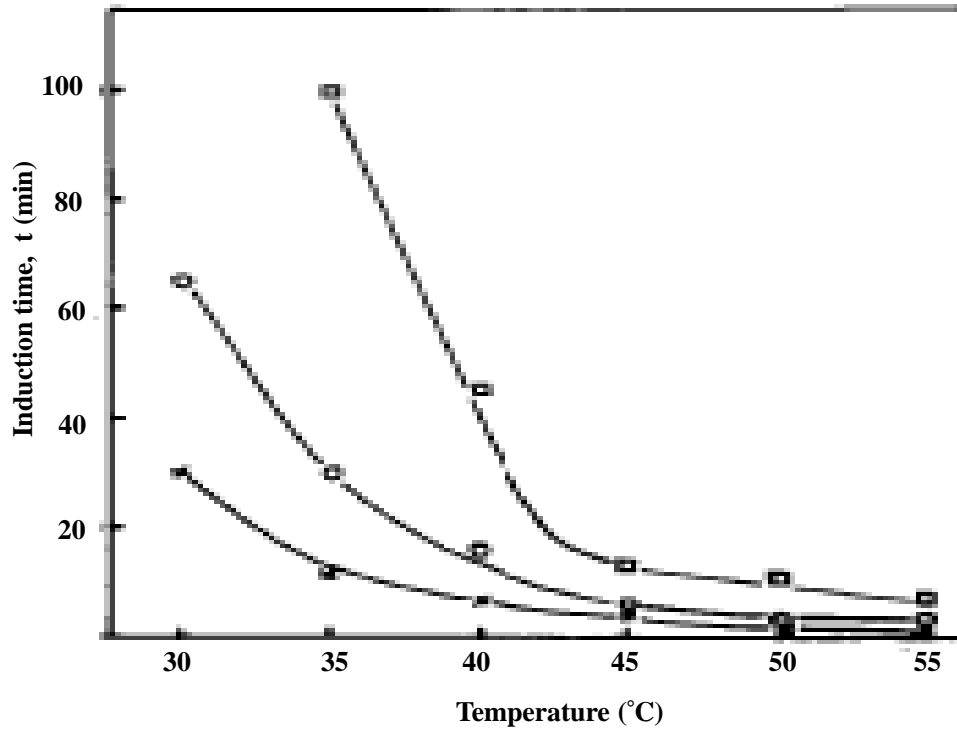


Figure 8-7 : Effect of temperature on the induction period at different supersaturations [92].

Currently, the previous relation was approached differently when variable barium concentrations (20 ppm, 50 ppm, 80 ppm, 100 ppm and 150 ppm) were used. The saturation ratios of the mixed brines were calculated based on 50:50 % mixing ratio of sea water to formation water brines at 75 °C. The maximum SR was predicted at the highest barium content of 150 ppm Ba^{2+} and minimum for 20 ppm Ba^{2+} . It was confirmed that the saturation ratios are increased with the increase of the barium contents, but the question was; could that clearly be proven kinetically on surface. It was in terms of scaling rate and final cell blockage while most the previous work was done in bulk precipitations. The calculated saturation ratio (SR) values and the saturation indices are shown in Table 8-1.

Table 8-1 : Calculated saturation ratios (SR) and the saturation indices of the brine mixture.

Barium Ions Concentration ppm (Final mix)	Predicted Saturation Ratio (SR)	Predicted Saturation Index (SI)
	75 °C	75 °C
20	60	1.8
50	150	2.2
80	240	2.4
100	300	2.5
150	466	2.6

The predicted saturation ratios appear to be in good agreement and increases with barium concentrations (thermodynamic value), and is proportional to the reproducible (kinetic value). On the surface, the SR shows an inverse relation to surface scaling film induction time and final capillary blockage. This was found in good agreement with earlier findings by Joshi and Antony using potassium dihydrogen orthophosphate KH_2PO_4 system. The interfacial energy for growth of KDP crystals in mild temperature range shows a decrease with the increase in temperature [92]. This reveals a fact that the existence of barium ions at any concentration has a significant effect on surface deposition. The induction time as a function of both SR and the actual barium concentration was confirmed. A wide range of field criterion in terms of barium range is covered.

8.4. SURFACE PRE – TREATMENT – INHIBITION OR CRYSTALLIZATION INITIATOR

The conventional scale treatments are well-known which range from batch/squeeze treatment, continuous treatment and surface engineering. The phosphonates dissociate in water to form electrophilic groups by which they coordinate with divalent cations. The process is called the anchoring of Phosphonate and their derivatives and coupling them with metals particles. Previous example was implemented on the titanium oxide particles which were treated using organophosphorus compounds [142, 143]. The ability of these coupling molecules to modify the metal surface of the TiO₂ particles was demonstrated by elemental analysis, and the bonding modes on the surface were investigated by means of diffuse reflectance IR Fourier transform (DRIFT).

Similarly in this research work, on steel surface, phosphonate scale inhibitor (DETPMP) molecules were anchored through the nitrogen atoms to the steel surface and was characterized using FT-IR. This chemical inhibitor has previously been described to work via two mechanisms: nucleation inhibition, which disrupts the thermodynamic stability of the growing nucleons [182], and retardation of crystal growth [122].

Although the processes are similar, the main targets of the two investigations were different. In the previous work, the surface photo degradation of the surface adsorbed species was investigated. This work focuses on the surface reactivity and ability of DETPMP to bind to the capillary cell surface and cations in the flow stream. Furthermore, in the case when the surface adsorbate acts as a centre of crystallization, it could have an impact on surface kinetics and accelerate the surface deposition process. Moreover, the effect of the chemical film on the formed crystallites would impose a crystallization regime which may have on the alignment and the packing of the formed crystals on surface.

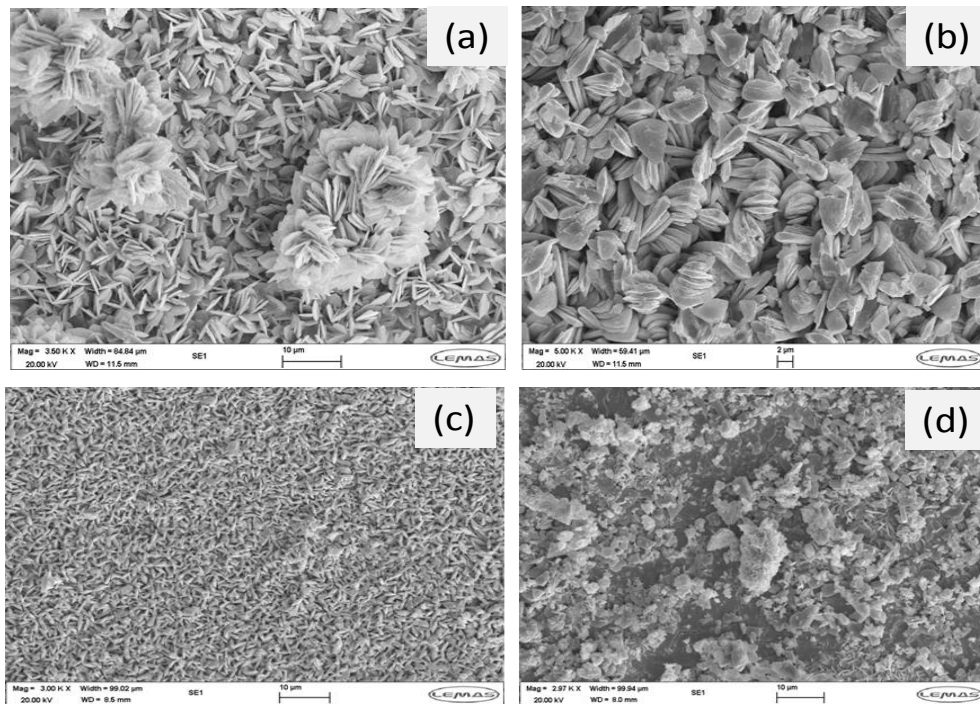


Figure 8-8 : The untreated barite scale crystals at 100 and 150 ppm (a,b) and effect of the surface pre-treatment on crystal morphology (c,d) at 75 °C.

It is known that the solubility of the DETPMP in water produces the phosphonate radical groups ($-\text{PO}_3^{2-}$) with negative charges. The surface orientation of the adsorbed DETPMP on 316 steel before deposition is highly important, and the most important is the orientation of the phosphonate groups, Figure 8-8. So it is the key factor for the scaling kinetics on the pre-treated surface in terms of both the induction time recorded or the crystals surface conformation or orientation. According Van der Leeden, the additives behave as active centres for nucleation and do not alter the surface free energy and edge free energy of the nuclei by adsorption on them, because of the short lifetime of the nuclei and/or their small surface area [183].

Once the molecule is bonded to the steel surface through the nitrogen atoms, Figure 8-9, there is a probability of some highly reactive functional groups (five $-\text{PO}_3^{2-}$ groups in the case of DETPMP) to freely move perpendicular to the substrate, while the three nitrogen atoms bind and hold the molecule to the steel surface.

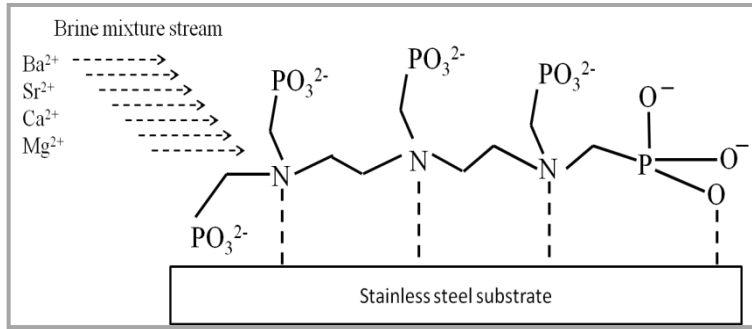


Figure 8-9 : The DETPMP expected alignment on steel surface prior to scaling.

It was suggested that the DETPMP adsorption on barium sulphate reagent powder shows that its adsorption continuously increases as temperature rises. It was also suggested that the adsorption level of DETPMP on barium sulphate surface may not be the key factor in the nucleation inhibition or crystal growth retardation, when temperature is a variable [152].

Chapter 9. CONCLUSIONS

The barite/scale surface kinetics in dynamic flow and bulk systems was assessed using the known complementary techniques – thermodynamic prediction, dynamic flow test and static bulk jar – at 25 °C, 50 °C and 75 °C. It is thought that this range of temperatures covers a significant range of field temperature applications. Although the supersaturation ratio is the main driving force for crystallization, also theoretically predicted, the supersaturation ratio decreases with temperature increase and in this case the barite solubility increases.

Experimentally, barite induction time was evaluated in bulk at specified temperatures, it shows that the bulk is thermodynamically controlled as the t_{ind} is undetectable at highest temperature and lowest saturation ratio. The Ba^{2+} residual in the system shows that its concentration drops in no time. At this stage it was necessary to use the prediction and bulk data to investigate the surface depositions. On surface, as in the case of bulk, the observed induction period decreases with elevated temperature when the saturation is lower and the solubility is higher. It was found that, on surface, the SR is not the only or main factor but also how the formed crystal particles arrange themselves on the surface through the early stages of surface scaling. The size and mobility of the late formed scale on the early formed nucleation layers play a role not only in induction period but also in the final growth shape and mass gained in the capillary cell.

The combination of surface/fluid heat and the massive increase in solubility has a major effect on surface deposition rate at higher temperatures of 75 °C. The thinner produced scale particles would provide a regular systematic surface nucleation and/or surface growth (crystallization regime). It is mentioned elsewhere in the literature that the induction period is a solution component dependent as it decreases with the increase of the concentrated species, but on the surface, this is not always right and depends on the surface condition in terms of heat, existing of foreign bodies, flow rate, Reynolds number...etc.

In general, apart from room temperature, the increase of temperature decreases the induction period in the case of surface deposition and bulk precipitation at 50 °C and 75 °C. So, the barium sulphate/scale solubility which is resulted at mild and higher temperature respectively is found to generate earlier nuclei and accelerates the nucleation rate followed by growth. In this case, the interfacial surface energy changes, due to temperature, between the formed scale/barite crystals and the solution decreases, this allows the crystals to aggregate before it starts to redissolve under heat effect.

The saturation ratio resulted from the change of mixing ratio has a minor impact on the final surface growth morphology, while the major effect comes from the saturation ratio (SR) which is resulted from temperature changes. In addition, the instability of surface nucleation during surface induction period seems to have no impact on the final surface growth. The surface crystal topography varies according to the temperature application and not the smaller saturation variation due to mixing within each temperatures.

According to the plot of the early stages of surface nucleation, the failure of the early formed scale layer was noticed to be more intensive at room temperature (lowest solubility). On the other hand, it becomes less intensive at moderate temperature of 50 °C. At the highest temperature of 75 °C, the surface scaling propagation looks much steadier, this could be the reason to observe the lower induction period and final blockage. In this regard, the size of produced scale crystal in combination with the flow may have an impact on continuous building of the surface deposit. The surface analysis of the barium species, diluted to as low as 1 ppm in the final mixture at 10 ml/min flow rate, shows that the barite is still dominant as predicted followed by strontium.

9.1. EFFECT OF THE FLOW RATE ON MASS AND SURFACE MORPHOLOGY

Since the barium sulphate deposition/precipitation process is a temperature dependant, it can be concluded that the deposition process is highly affected at only higher or lower temperature 25 °C when the solubility of the formed crystal clusters is either high or low respectively. At moderate temperature, the deposition regime unexpectedly varies especially at lower flow rate, but the surface leans to gain more mass out of the solution mixture, unlike at higher flow rate when the residence time is shorter. It was noticed that the higher flow provides more reproducible data. It was confirmed that the crystals morphologies change with the wider change of supersaturation ratios due to temperature, theoretically predicted using Multiscale, rather than the SR minor changes due to mixing within each temperature applications.

At different temperature within one flow rate (10 ml/min), the untreated barite scale deposit at higher flow rate appears to crystallize similarly with little differences in shape and size. The rose like growth is common in all the cases regardless the temperature. But this final interesting flakes shape are clearly vary in terms of the thickness as temperatures arises, the higher the temperature the thinner the observed surface deposited crystals. The surface crystals alignment seems differ with temperature as well, and this comparison is noticed when the figures were compared which were collected at lower flow rate of 5 ml/min. The effect is clearly observed when the comparison at this stage involves the two flow rates application within on temperature.

The combination of both temperature and inhibitor has an impact on the surface coverage percentage especially elevated temperature at 75 °C. The three growth profiles were affected by addition of the scale retardant and the well-defined crystal in the case 25 °C was deformed and that goes for the other two temperature applications of 50 °C and 75 °C.

9.2. EFFECT OF BARIUM CONTENTS IN COMPLEX BRINE

The effect of barium concentration on the complex process of scaling precipitation and deposition was clearly revealed using complementary techniques (prediction by modelling, bulk conductivity, concentration measurement and the surface flow tests). On the surface, the collected figures were reproducible, and the observed surface induction time was found to be inversely proportional to the barium content as lower barium brine contents (lower SR) shows higher and extended induction period. The trend of the surface growth periods at each concentration was analyzed, and it appears to be in a very good agreement with that found in induction time versus barium concentration figures.

The observed surface growth constant is found to increase exponentially with the increase of free barium species in brine mixtures (20 ppm to 150 ppm). The relation between the growth and barium concentrations/saturation ratio was extracted, the higher the supersaturation ratios (due to barium level), the faster and sharper the growth. It highlights the role that the barium ions play in both the bulk precipitations and surface depositions forming the lowest solubility compound of BaSO₄ among the ion species in the brine mixture.

9.3. BULK PRECIPITATION IN FAVOUR OF SURFACE DEPOSITION

The bulk conductivity test provides information on the individual scale crystals and crystal aggregates during the unstable stage of scale formation. This enables the assessment of the induction time of the formed scale crystals which are already present (or reached the detectable level) at the time of surface deposition. This may also give the precise location of crystal birth whether in the mixing part or on the targeted capillary cell surface.

Based on the used mixing part design, it is clear that crystals ripened or grown in the bulk flow before adhering to the capillary surface, where further growth and

aggregation occur. These figures could help to improve the design of the mixing chamber for surface deposition in terms of time and position of the capillary. Plots at the low concentration of 20 ppm for all surface and bulk measurements are clearly distinguished from the rest of observed data. It indicates the consistency across both types of measurement and shows the actual time and growth stage at which the crystal reaches the capillary.

9.4. PREDICTED SATURATION RATIOS AND BULK KINETICS CORRELATION

Once the prediction figures represent mostly the thermodynamics property of a BaSO_4 solution mixture represented in the level of the saturation ratio, the bulk kinetics of this mixture may show a reverse relation once temperature is introduced to the system. In terms of the consistent variations of bulk induction time (from higher to lower temperature applications or vice versa), the predicted figures are in a very good agreement with the observed bulk kinetics assessment figures. This also confirms that barite system is a heat sensitive system regardless the level of the supersaturation saturation predicted. So the static experimental induction is inversely proportional temperature applications which decrease as the temperature increases and the saturation ratios decreases.

Note: How the surface kinetics data will correlate to predicted and bulk data at this stage?

9.5. TECHNIQUES OVERLAP (THEORETICAL, BULK AND SURFACE)

As the heat was the key factor on both theoretical and bulk kinetic assessments and proven a reverse relation, this would have a remarkable effect on the surface kinetics assessment as the surface kinetic cannot correlate with both.

It is clearly observed that the observed surface kinetic data was mostly correlated to the bulk kinetic rather than to the thermodynamic property of the solution, this was noticed as the surface induction period becomes lower with increase of temperature and decrease of the supersaturation ratio (SR). It was not impossible to find a correlation between predicted and surface kinetic data, it was one of this research work challenges, it was finalized by limiting the variables to minimum (one variable).

9.6. THE FINGER PRINTS OF INITIAL NUCLEATION AND ITS EFFECT ON SURFACE MORPHOLOGY

As the barite solubility varies with temperature, it would be expected that different surface filming nucleation patterns may take place during crystallization noticed at different temperature; this could be one of the reasons for of different surface crystal alignment. This was confirmed by examining the roots or the back ground of surface deposits. Most of the surface crystallizations do take a constant shape and conformation on steel surfaces as long as the experiment condition is kept constant.

The minimum solubility of barite in the system is related to instability of surface filming plot due to the mobility of bigger aggregates on a submicron or nano film thickness. In this case, bigger crystal clusters are likely to disturb the propagation to growth stage. This surface nucleation failures appear to be less intensive with mild/moderate temperature at 50 °C and at the higher temperature of 75 °C. This explains the long and short surface nucleation with respect to temperature applied, let alone the effect of temperature on lowering the crystal's surface energy.

9.7. THE CORRELATION BETWEEN PREDICTED AND SURFACE DATA

Theoretically, it was confirmed that the saturation ratios are increased with the increase of the barium contents, but the challenge and the novelty if this approach

were to correlate the predicted figures to what happen on surface (in dynamic flow) when other parameters are involved. In addition, once the predicted method representing the bulk thermodynamic the most, it is well known that the bulk precipitation and surface deposition have two different mechanisms.

Kinetically, in terms of surface deposition, (surface scaling film induction period to scale film final growth), the predicted saturation ratios were found to be in a very good agreement with barium concentrations/SR (thermodynamic value). The predicted figures were also found to be in a good agreement with the reproducible surface scaling film induction time (kinetic value). As a single variable when the rest of other cations concentrations were kept constant in brine mixture, it can be concluded that barium ions species at any concentration have a significant effect on surface deposition.

Surface condition is another factor which was investigated in this study, The remarkable differences in treated/untreated surface crystallizations (in terms of shape, size and conformation) were taken place as a result of one factor, which is the inexistence/existence of phosphonates groups on surface. The surface orientation of these multiphase crystals was investigated by using the *ex-situ* X-Ray diffraction technique.

The analysis shows a crystal face deformation based on the barium content in the scaling stream of solid solution when deposited on a chemically pre-treated surface. This could conclude that the surface pre-treatment affects the lower barium contents brine more that the higher contents. This may be referred to the DETPMP population in the stream's front and its ability to manipulate the scaling environment on the surface especially at the nucleation level. On the hand, in higher the concentration of barium, it is a possibility that the DETPMP active sites are suppressed by the fast crystallization on surface.

Chapter 10. FUTURE WORK

The reproducible surface kinetic results in this work has provided a data base for this dynamic surface crystallization to go much further and investigate different concepts in surface scale kinetics. Future work is listed below in points:

- The instability of the surface nucleation periods, which were reported in this work, is vital to be further investigated using an electrochemically polarized cell. This capillary testing cell can be insulated to be used as a working electrode.
- The reproducible flow dynamic surface deposition process can be used as data base for further investigations. For instance, the nature of the flow is known as a factor in crystallization process, and the turbulent flow may be used with upgraded scaling system to replace the existing laminar flow. This may have a major effect on induction period as well as the crystals shape and size.
- The *ex – situ* X-Ray analysis on the fully scaled capillary could reveal more information about the dehydrated surface scale on the initial stage by focusing the beam on the first layer of the internal surface deposit and on the final layer in the middle of the capillary. This will give any differences between the crystallization pattern from start to the end and its consistency/fluctuation. Compare the observation with SEM as it shows the pattern does not change when the sample background is visible.
- Using similar experimental condition, could the former point applied with *in –situ* X-Ray measurements to explore the effect (if any) of the hydrated media at variable temperature conditions.
- The upgraded scaling system is equipped with pressure regulator. So using similar experimental condition or higher harsh reservoir temperature and pressure conditions, this may not only show its effect on the crystal

parameters, shape or size on surface, but also the effect on the whole surface scaling process.

- In the case of longer duration flow test, surface induced crystals effect as a function of different supersaturation ratios (SRs) prior to surface deposition (seeding) can be examined; this may induce different surface condition based on the SR which may affect the surface induction period and even the shape of the topography of the crystallized surface.

- Unconventional addition of anti-nucleation (PPCA) or anti-growth (PETPMP) inhibitors based on bulk assessments of the crystal induction period; this will enable evaluation of the anti-growth retardants and compare it with other inhibitors for efficiency. Moreover, would it be possible to observe any shift in observed induction time in bulk and on surface.
Note: the chemical injection point position (after mixing) is based upon the observed bulk induction period. It is a continuous injection in surface flow deposition and drop-wise in bulk precipitations to reach the targeted MIC.

Introduce another scale inhibitor possibly green to investigate its effectiveness on the early nucleation stage and induction period using (TBT) and surface observations, comparing the efficiency.

REFERENCES

1. SNF-FLOERGER. *SNF - Manufacturer of Polymers for EOR, Oil division (Online)*. 2014.
2. Cowan, J.C. and D.J. Weintritt, *Water-Formed Scale Deposits*. 1976, Houston Texas: Gulf Publication Company, Book Division.
3. Chang, L.Y., R.A. Howie, and J. Zussman, *Rock-Forming Minerals*. 5B, 2nd ed. 1996: Longman.
4. Patnaik, P., *Handbook of Inorganic Chemistry*. 2003: McGraw-Hill,.
5. Ymcichem. *Barium Sulfate Crystal Structure, Online*. 2014.
6. Rendo'n-Angeles, J.C., et al., *Journal of Material Science*, 2008. **43**: p. 2189 - 2197.
7. Weintritt, D.J. and J.C. Cowan, *Unique Characteristics of Barium Sulfate Scale Deposition*, in *Society of Petroleum Engineers, SPE - 15231967*, Society of Petroleum Engineers. p. 1,381 - 1,394.
8. Mavredaki, E., A. Neville, and K.S. Sorbie, *Study of BaSO₄ Formation Kinetics and Inhibition Effect of Polyphosphino-Carboxylic Acid (PPCA) on Barite Formation with Synchrotron X-Ray Diffraction (SXR)*, in *SPE International Oilfield Scale Conference 2008*, Society of Petroleum Engineers: Aberdeen, UK.
9. Spiegler, K.S., *Salt Water Purification*. 1962, New York: John Wiley and Sons.
10. Boerlage, S.F.E., et al., *The Scaling Potential of Barium Sulphate in Reverse Osmosis Systems*. *Journal of Membrane Science*, 2002. **197**(1-2): p. 251-268.
11. Langelier, W.G., *The Analytical Control of Anti-corrosion Water Treatment*. *Journal of American Water Works Association*, 1936. **28**: p. 1500.
12. Stiff, H.A. and L.E. Davis, *A Method for Predicting the Tendency of Oilfield Water to Deposit Calcium Carbonate*. *Petroleum Trans. AMIE*, 1952. **195**: p. 213.

13. Jones, L.W., *Corrosion and Water Technology for Petroleum Producers*. 1987, Tulsa: Oil & Gas Consultants International.
14. Vetter, O.J.G., *How Barium Sulfate is Formed: an Interpretation*. *Journal of Petroleum Technology*, 1975. **27**: p. 1515.
15. Templeton C. C., *Solubility of Barium Sulphate in Sodium Chloride Solutions From 25 °C to 95 °C*. *Journal of Chemical Engineering Data*, 1960. **5**: p. 514.
16. Ostroff, A.G., *Introduction to Oilfield Water Technology*. 2nd ed. 1979, Huston, Texas: NACE.
17. Bovington, C.H. and A.L. Jones, *Trans. Faraday Soc.*, 1970. **64**: p. 764.
18. Liu, S.T. and G.H. Nancollas, *J. Colloid Interface Sci*, 1975. **52**: p. 593.
19. Kirk-Othmer, *Crystallization*, in *Encyclopedia of Chemical Technology* 1965. p. 482-515.
20. Ushasree, P.M., et al., *Journal of Crystal Growth*, 2000. **210**: p. 741 - 745.
21. Monnin, C.A., *Thermodynamic Model for the Solubility of Barite and Celestite in Electrolyte Solutions and Seawater to 200 °C and to 1 kbar*. *Chemical Geology*, 1999. **153**: p. 187-209.
22. Berry, C.R., *Photographic Science and Engineering*, 1976. **20**: p. 1.
23. Nielsen, A.E., *Kinetic of Precipitation*. 1964, Oxford, England: Pergamon press.
24. Karpinski, P.H. and J.S. Wey, *Handbook of Industrial Crystallization*. 2nd ed. 2002. 141 - 160.
25. Preben, R. and O. Terje, *Prediction and Kinetics of Carbonate Scaling from Oil Field Waters*, 2002, NACE International.
26. Young, S.W., *Mechanical Stimulus to Crystallization in Supercooled Liquids*. *Journal of the American Chemical Society*, 1911. **33**: p. 148-162.
27. Khamskii, E.V., *Crystallization from Solutions*. 1969, New York: Consultants Bureau.

28. Vonnegut, B., *Variation with Temperature of the Nucleation Rate of Supercooled Tin and Water Drops*. Journal of Colloid Science, 1948. **3**: p. 563-569.
29. Nancollas, G.H. and N. Purdie, *The kinetics of crystal growth*. Quarterly Reviews of the Chemical Society, 1964. **18**: p. 1 - 20.
30. Walton, A.G., *The Formation and Properties of Precipitates*. 1967, New York: Interscience.
31. Strickland-Constable, R.F., *Kinetics and Mechanism of Crystallization*. 1968, London: Academic Press.
32. Zettlemoyer, A.C., *Nucleation*. 1969, New York: Dekker.
33. Nyvlt, J., et al., *The Kinetics of Industrial Crystallization*. 1985, Prague.
34. Sohnel, O. and J. Garside, *Precipitation: Basic Principles and Industrial Applications*. 1992, Oxford: Butterworth-Heinemann.
35. Kashchiev, D., *Nucleation*. 2000, Oxford: Butterworth-Heinemann.
36. Mullin, J.W. and K.D. Raven, *Nucleation in Agitated Solutions*. Nature, 1961. **190**: p. 251.
37. Mullin, J.W. and K.D. Raven, *Influence of Mechanical Agitation on the Nucleation of Aqueous Salt Solutions*. 1962. **195**: p. 35-38.
38. <http://www.google.com/search?q=Heterogeneous+nucleation+model&nord>.
39. <http://www.eng.utah.edu/~ljang/images/lecture-12.pdf>.
40. McCabe, W.L., *The Enthalpy-Concentration Chart- a Useful Device for Chemical Engineering Calculations*. Transactions of the American Institute of Chemical Engineers, 1935. **31**: p. 129-164.
41. Gyulai, Z.B. and K. Kenntnis, *Zeitschrift far Physik*, 1948. **125**: p. 1 - 17.
42. Powers, H.E.C., *Nucleation and Early Crystal Growth*. The Industrial Chemist, 1963. **39**: p. 351-353.

43. Botsaris, G.D., *Secondary Nucleation: A Review in Industrial Crystallization*. 6th Symposium, Usti nad Labem, J. W. Mullin (ed.), 1976, 3 - 22, Plenum Press, New York.
44. Jong, E.J.D., *Nucleation: A Review in Industrial Crystallization*. 78 (7th Symposium, Warsaw), E.J. de Jong and S.J. Jancic (eds.), (1979), North-Holland, Amsterdam, 3 -17.
45. Sung, C.Y., J. Estrin, and G.R. Youngquist, *Secondary Nucleation of MgSO₄ by Fluid Shear*. AIChEJ, 1973. **19**: p. 957- 962.
46. Nienow, A.W., *The Effect of Agitation and Scale-up on Crystal Growth Rates and on Secondary Nucleation*. Transactions of the Institution of Chemical Engineers, 1976. **54**: p. 205 - 207.
47. Clontz, N.A. and W.L. McCabe, *Contact Nucleation of MgSO₄ 7H₂O*. Chemical Engineering Progress Symposium Series, 1971. **67**(110): p. 6 - 17.
48. Johnson, R.T., R.W. Rousseau, and W.L. McCabe, *Factors Affecting Contact Nucleation*. AIChE Symposium Series, 1972. **68**(121): p. 31 -41.
49. Becker, R. and W. DoSring, *Kinetische Behandlung der Keimbildung in iibers-ttigen Daimpfen*. Annalen der Physik,, 1935. **24**: p. 719 - 752.
50. Gibbs, J.W., *Collected Works*. Thermodynamics. Vol. I. 1948, New Haven: Yale University Press.
51. Mullin, J.W., *Crystallization*. 2001: Elsevier, Butterworth-Heinemann.
52. Ostwald, W., *Uber die vermeintliche Isomeric des roten und gelben Quecksilberoxyds und die Oberfliischen spannung fester KoSrper*. Zeitschrift ffr Physikalische Chemie, 1900. **34**: p. 495-503.
53. Freundlic, H., *Colloid and Capillary Chemistry*. 1926, London: Methuen.
54. Nielsen, A.E., *Homogeneous Nucleation in Barium Sulfate Precipitation*. Acta Chem Scan, 1961. **15**: p. 441-442.
55. Mohanty, R., et al., *Characterizing the Product Crystals from a Mixing Tee Process*. AIChE J, 1988. **34**: p. 2063-2068.

56. Roelands, C.P.M., et al., *Analysis of Nucleation Rate Measurements in Precipitation Processes*. Crystal Growth Design, 2006. **6**: p. 1380-1392.
57. Judat, B. and M. Kind, *Morphology and Internal Structure of Barium Sulphate - Derivation of a New Growth Mechanism*. Journal of Colloid and Interface Science, 2004. **269**: p. 341-353.
58. Mullin, J.W., *Crystallization*. 3rd ed. 1997, Oxford: Butterworth Heinemann.
59. Taguchi, K., J. Garside, and N.S. Tavaré, *Nucleation and Growth Kinetics of Barium Sulphate in Batch Precipitation*. Journal of Crystal Growth, 1996 **163**: p. 318-328
60. Dyer, S.J. and G.M. Graham, *The Effect of Temperature and Pressure on Oilfield Scale Formation*. Journal of Petroleum Science and Engineering, 2002. **35**(1-2): p. 95 -107.
61. NACE review, *Dynamic Scale Inhibitor Evaluation Apparatus and Procedures in Oil and Gas Production*. 2005: NACE Publication.
62. Pritchard, A.M., et al. *Test Methods for Calcium Carbonate Scale Inhibitors*. in *Proceedings of the RSC chemistry in the oil industry III*. 1988. Manchester, UK, April 19-20, 1988.
63. Jordan, M.M., et al., *The Correct Selection and Application Methods for Adsorption and Precipitation Scale Inhibitor for Squeeze Treatments in North Sea Fields*, in *Formation Damage Symposium 1996*, Society of Petroleum Engineering: Lafayette, LA, February, 14-15, 1996.
64. Yuan, M.D., P. Hammonds, and E. Jamieson, *Investigation of Scaling and Inhibition Mechanisms and the Influencing Factors in Static and Dynamic Inhibition Tests*, 1998, NACE International.
65. Graham, G.M., et al., *Scale Inhibitor Selection Criterion for Downhole (Squeeze) Application in Chalk Reservoir*, in *International Symposium on Oilfield Chemistry 2001*, Society of Petroleum Engineering: Houston, TX, Feb. 13 - 16, 2001.
66. Graham, G.M., et al., *The Importance of Appropriate Laboratory Procedures for the Determination of Scale Inhibitor Performance*, in *International*

Symposium on Oilfield Scale 2002, 2002,. Society of Petroleum Engineers Inc.: Aberdeen, United Kingdom.

67. NACE, *Laboratory Screening Test to Determine the Ability of Scale Inhibitors to Prevent the Precipitation of Barium Sulphate and/or Strontium Sulphate from Solution (for Oil and Gas Production Systems)*, in *Standards TM 0197-97* 1997, NACE International, Item No. 21228.
68. NACE, *Laboratory Screening Test to Determine the Ability of Scale Inhibitors to Prevent the Precipitation of Barium Sulfate or Strontium Sulphate, or Both, from Solution (for Oil and Gas Production Systems)*, 2010, NACE International, Standard TM0197-2010.
69. Melia, T.P. and W.P. Moffitt, *Secondary Nucleation from Aqueous Solution*. *Industrial and Engineering Chemistry Fundamentals*, 1964. **3**: p. 313 -317.
70. Graham, G.M., M.M. Jordan, and K.S. Sorbie. *How Scale Inhibitors Work and How This Affect Test Methodology*. in *Proceedings of the conference: Solving Oilfield Scaling*. 1997. Aberdeen, Jan. 22- 23, 1997: Organized by by IBC Technical Services Ltd.
71. Erling, N.H., et al., *New Method for Scale Inhibitor Testing*, 2009, Society of Petroleum Engineering, SPE 121663.
72. Wang, Q.-A., et al., *Large-Scale Preparation of Barium Sulphate Nanoparticles in a High-Throughput Tube-in-Tube Microchannel Reactor*. *Chemical Engineering Journal*, 2009. **149**(1-3): p. 473 - 478.
73. Brigitte, B., K. Norbert, and Z. Alain, *Some Insights into the Tube-Blocking-Test Method to Evaluate the Efficiency of Mineral Scale Inhibitors*, 2005, Society of Petroleum Engineers.
74. Moghadasi, J., et al., *Model Study on the Kinetics of Oil Field Formation Damage Due to Salt Precipitation From Injection*. *Journal Petroleum Science and Engineering*, 2004. **43**: p. 201- 217.
75. Kumar, T., S. Vishwanatham, and S.S. Kundu, *A laboratory Study on Pteroyl-l-Glutamic Acid as a Scale Prevention Inhibitor of Calcium*

Carbonate in Aqueous Solution of Synthetic Produced Water. Journal of Petroleum Science and Engineering, 2010. **71**(1-2): p. 1-7.

76. Fan, C., et al., *Barite Nucleation and Inhibition at 0 to 200 °C With and Without Thermodynamic Hydrate Inhibitors*, in *International Symposium on Oilfield Chemistry 2011*, Society of Petroleum Engineers, SPE 121559: Texas, US. p. 440 - 450.
77. Stamatakis, E., et al., *Study of Calcium Carbonate Precipitation in the Near-Well Region Using $^{47}\text{Ca}^{2+}$ as Tracer*, in *SPE International Symposium on Oilfield Scale 2004*, Society of Petroleum Engineers: Aberdeen, United Kingdom.
78. Chen, T., et al., *In-Situ Monitoring The Inhibiting Effect Of DETPMP On CaCO_3 Scale Formation By Synchrotron X-Ray Diffraction*, 2006, Society of Petroleum Engineering, SPE 100440: Aberdeen, UK.
79. Chen, T., et al., *Using Synchrotron Radiation Wide Angle X Ray Scattering (WAXS) to Study the Inhibiting Effect of Polyphosphonocarboxylic Acid (PPCA) on CaCO_3 Scale Formation*, 2006, NACE International.
80. Wylde, J.J., G.C. Allen, and I.R. Collins, *A Novel, Surface Sensitive Approach to Quantitatively Measure the Prediction and Inhibition of Scale Growth*, in *International Symposium on Oilfield Scale 2001*, Society of Petroleum Engineers, SPE 68299: Aberdeen, United Kingdom.
81. Zhang, Y. and R. Farquhar, *Laboratory Determination of Calcium Carbonate Scaling Rates for Oilfield Wellbore Environments*, in *International Symposium on Oilfield Scale 2001*, Society of Petroleum Engineers, SPE 68329: Aberdeen, United Kingdom.
82. Al-Nasser, F.H.A.S., *Scaling and Aggregation Kinetics Determination of Calcium Carbonate Using Inline Technique*. Chemical Engineering Science, 2013. **86**: p. 70-77.
83. Collins, I.R., *Predicting the Location of Barium Sulfate Scale Formation in Production Systems*, in *SPE International Symposium on Oilfield Scale*,

- SPE-943662005, Society of Petroleum Engineers: Aberdeen, United Kingdom.
84. Mavredaki, E., A. Neville, and K. Sorbie, *Assessment of Barium Sulphate Formation and Inhibition at Surfaces With Synchrotron X-Ray Diffraction (SXRD)*. Applied Surface Science, 2011. **257**(9): p. 4264 - 4271.
 85. Tolaieb, B., R. Bingham, and A. Neville, *Barium Sulfate Kinetics on Steel Surfaces at Different Supersaturation Ratios*, 2013, NACE International, 2751.
 86. Felmy, A.R., D. Rai, and D.A. Moore, *The Solubility of (Ba,Sr)SO₄ Precipitates: Thermodynamic Equilibrium and Reaction Path Analysis*. Geochimica et Cosmochimica Acta, 1993. **57**: p. 4345 - 4363.
 87. Chen, T., A. Neville, and M. Yuanb, *Assessing the effect of Mg²⁺ on CaCO₃ scale formation–bulk precipitation and surface deposition*. Journal of Crystal Growth, 2005. **275**(1 - 2): p. e1341-e1347.
 88. Chen, T., A. Neville, and M. Yuan, *Influence of Mg²⁺ on CaCO₃ Formation-Bulk Precipitation and Surface Deposition*. Chemical Engineering Science, 2006. **61**(16): p. 5318-5327.
 89. Folk, R.L., *The Natural History of Crystalline Calcium Carbonate: Effect of Magnesium Content and Salinity*. Journal of Sedimentary Petrology, 1974. **44**: p. 43 - 53.
 90. Jones, F., et al., *The Effect of Calcium Ions on the Precipitation of Barium Sulphate I: Calcium Ions in the Absence of Organic Additives*. Journal of Crystal Growth, 2004. **262**(1–4): p. 572-580.
 91. Hennessy, A.J.B. and G.M. Graham, *The Effect of Additives on the Co-crystallisation of Calcium with Barium Sulphate*. Journal of Crystal Growth, 2002. **237-239**(3): p. 2153-2159.
 92. Joshi, M.S. and A.V. Antony, *Nucleation in Supersaturated Potassium Dihydrogen Orthophosphate Solutions*. Journal of Crystal Growth, 1979. **46**(1): p. 7 - 9.

93. Kirkova, E. and M. Djarova, *Influence of Supersaturation on the Kinetics of Crystallisation of $ZnC_2O_4 \cdot 2H_2O$* . *Kristall und Technik*, 1971. **6**(5): p. 601-605.
94. Nielsen, A.E. and O. Söhnel, *Interfacial Tensions Electrolyte Crystal-Aqueous Solution, From Nucleation Data*. *Journal of Crystal Growth*, 1971. **11**(3): p. 233-242.
95. Nielsen, A.E., *Nucleation and Growth of Crystals at High Supersaturation*. *Kristall und Technik*, 1969. **4**(1): p. 17-38.
96. Chen, T., A. Neville, and M. Yuan, *Calcium Carbonate Scale Formation - Assessing the Initial Stages of Precipitation and Deposition*. *Journal of Petroleum Science and Engineering*, 2005. **46**(3): p. 185 -194.
97. Todd, A.C. and M.D. Yuan, *Barium and Strontium Sulfate Solid-Solution Scale Formation at Elevated Temperatures*. *Society of Petroleum Engineers, SPE - 19762*, 1992.
98. Lasaga, T., *Transition State Theory: Kinetics of Geochemical Process (eds. Lasaga & Kirkpatrick)*. *Review I Mineralogy, Min. Soc. Amer*, 1983. **8**: p. 135 - 169.
99. Yuan, M.D., M. Anderson, and E. Jamieson, *Investigation and Improvement of $BaSO_4$ Scale Inhibition Tests*, in *SPE International Symposium on Oilfield Chemistry 1997*, Society of Petroleum Engineers: Houston, TX.
100. Yuan, M., *Effect of Temperature on Barium Sulphate Scale Inhibition of Diethylenetriamine Penta (Methylene Phosphonic Acid)*, in *218th American chemical society national meeting 1999*: New Orleans, LA.
101. Walsh, M.P., et al., *Precipitation and Dissolution of Solids Attending Flow Through Porous Media*. *AIChE Journal*, 1984. **30**(2): p. 317-327.
102. Casey, W.H., *Heterogeneous Kinetics and Diffusion Boundary Layers: The Example of Reaction in a Fracture*. *Journal of Geophysical Research*, 1987. **92**(B8): p. 8007 - 8013.
103. Granbakken, D., et al., *Scale Formation in Reservoir and Production Equipment During Oil Recovery. III. A Kinetic Model for the*

- Precipitation/Dissolution Reactions*. Acta Chemica Scandinavica, 1991. **45**: p. 892-901.
104. Paraskeva, C.A., et al., *Sandbed Consolidation with Mineral Precipitation*. Journal of Colloid and Interface Science, 2000. **232**(2): p. 326-339.
 105. Johnston, C.J., W. Taylor, and L. Sutherland, *The Influence of Turbulence (or Hydrodynamic Effects) on Barium Sulphate Scale Formation and Inhibitor Performance*, in *Society of Petroleum Engineers, SPE-1640702013*, Society of Petroleum Engineers.
 106. Woods, A.W., T.E. Jupp, and C.N. Richardson, *The Interaction Of Flow And Reactions In Porous Media*, in *5th International Symposium of Oilfield Scale, SPE 803912003*: Society of Petroleum Engineering.
 107. Woods, A.W. and G. Harker, *Barium Sulphate Precipitation In Porous Rock Through Dispersive Mixing*, in *5th International Symposium of Oilfield Scale, SPE 804012003*, Society of Petroleum Engineering.
 108. Hasson, D., et al., *Influence of the Flow System on the Inhibitory Action of CaCO₃ Scale Prevention Additives*. Desalination, 1997. **108**(1-3): p. 67-79.
 109. Hasson, D. and S. Steinberg, *Continous-Flow Precipitation*. Desalination, 1983. **47** p. 129 -148.
 110. Lawal, K.A., et al., *Experimental Investigation of Asphaltene Deposition in Capillary Flow*. Energy fuels, 2012. **26**(4): p. 2145-2153.
 111. Broseta, D., et al., *Detection of Asphaltene Deposition by Capillary Flow Measurements*, in *Improved Oil Recovery Symposium*, 2000, SPE 59294: Tulsa, Oklahoma.
 112. Cayey, N.W. and J. Estrin, *Secondary Nucleation in Agitated MgSO₄ Solutions*. Industrial and Engineering Chemistry Fundamentals, 1967. **6**: p. 3 - 20.
 113. Rousseau, R.W., K.K. Li, and W.L. McCabe, *The Influence of Seed Crystal Size on Nucleation Rates*. AIChE Symposium Series,, 1976. **72**(153): p. 48 - 52.
 114. FAST#3, in *Progress Report 2, Section 2, 13.2007-2010*, HW University.

115. Nalco, O., *Controlling Inorganic Scale in Pulp Mills*, http://www.nalco.com/North_America/Industries-ph/Paper-Pulp-scale.html.
116. Rosenstein, L., *Process for Treating Water*, in *US patent*, 2, 038, 416.1936: US.
117. Yuana, P.-Q., et al., *Zeta Potential on the Anti-Scalant Modified Sub-Micro Calcite Surface*. *Colloids and Surfaces A: Physicochemical and Engineering Aspects*, 2008. **328**(1-3): p. 60 - 66.
118. Black, S.N., et al., *Interaction of Organic/Inorganic Interface: Binding Motifs for Phosphonates at the Surface of Barite Crystal*. *J. Chem. Soc., Faraday Trans*, 1991. **87**(20): p. 3409-3414.
119. Davey, R.J., et al., *The Molecular Design Based on Recognition at Inorganic Surfaces*. *Nature*, 1991. **353**: p. 540.
120. Sorbie, K.S. and N. Laing, *How Scale Inhibitors Work: Mechanisms of Selected Barium Sulphate Scale inhibitors Across a Wide Temperature Range*, in *International Symposium on Oilfield Scale*, SPE 87470, 2004, Society of Petroleum Engineers: Aberdeen, United Kingdom.
121. Chen, T., A. Neville, and M. Yuan, *Effect of PPCA and DETPMP Inhibitor Blends on CaCO₃ Scale Formation*, in *International Symposium on Oilfield Scale*, SPE 87442, 2004, Society of Petroleum Engineers: Aberdeen, United Kingdom.
122. Graham, G.M., L.S. Boak, and K.S. Sorbie, *The Influence of Formation Calcium and Magnesium on the Effectiveness of Generically Different Barium Sulphate Oilfield Scale Inhibitors*. *SPE Production & Operations*, 2003. **18**(1): p. 28-44.
123. *Laboratory Procedure Manual*, in *Oilfield Scale Research Group (OSRG)1995*: Heriot-Watt University.
124. Jones, F., et al., *Anomalous Behaviour within a Systematic Series of Barium Sulphate Growth Modifiers*. *CrystEngComm*, 2001. **40**: p. 1-3.

125. Coveney, P.V., et al., *A New Design Strategy for Molecular Recognition in Hetrogenous Systems: A Universal Crystal-Face Growth Inhibitor for Barium sulphate*. J. Am. Chem. Soc, 2000. **122**: p. 11557 - 11558.
126. Bromley, L.A., et al., *Interactions at Organic-Inorganic Interface-Molecular Design of Crystallization Inhibitor for Barite*. Langmuir, 1993. **9**: p. 3594-3599.
127. Volkmer, D., et al., CrystEngComm, 2002. **4**(52): p. 288-295.
128. Volkmer, D., et al., J. Chem. Soc., Dalton Trans, 2002: p. 4547-4554.
129. Volkmer, D., et al., J. Material Chemistry, 2004. **14**: p. 2249-2259.
130. Fricke, M., et al., Crystal Growth Design, 2006. **6**(5): p. 1120-1123.
131. Grassie, N. and G. Scott, *Polymer Degradation and Stabilization*. 1985, Cambridge: Cambridge University Press.
132. Fessenden, R.J. and J.S. Fessenden, *Organic Chemistry*. 1990: Cole Publishing, Pacific Cove.
133. Dyer, S.J. and G.M. Graham, *Thermal Stability of Generic Barium Sulphate Scale Inhibitor Species Under Static and Dynamic Conditions*. Journal of Petroleum Science and Engineering, 2003. **37**(3-4): p. 171-181.
134. Rajendran, S., B.V. Apparao, and N. Palaniswamy, *Corrosion Inhibition by Phosphonic acid-Zn²⁺ Systems for Mild Steel in Chloride Medium*. Anti-Corros. Methods Mater., 2000. **47**(6): p. 359-365.
135. Rajendran, S., et al., *The Role of Phosphonates as Transporters of Zn²⁺ Ions in the Inhibition of Carbon Steel in Neutral Solutions Containing Chlorides*. Anti-Corros. Methods Mater., 2002. **49**(3): p. 205-209.
136. Awad, H.S., *The effect of Zinc-to-HEDP Molar Ratio on the Effectiveness of Zinc-1, Hydroxyethylidene-1,1 Diphosphonic Acid in Inhibiting Corrosion of Carbon Steel in Neutral Solutions*. Anti-Corros. Methods Mater., 2005. **52**(1): p. 22-28.
137. Niess, R., et al., *Corrosion Inhibiting Rubber Compounds for Metal Surfaces*, in *German Patent DD2380601986*.

138. Raman, A., et al., *Formation of Self-Assembled Monolayers of Alkylphosphonic Acid on the Native Oxide Surface of SS 316L*. Langmuir, 2006. **22**: p. 6469-6472.
139. Gao, W., et al., *Self Assembled Monolayers of Alkylphosphonic Acids on Metal Oxides*. Langmuir, 1996. **12**: p. 6429-6435.
140. Textor, M., et al., *Structural Chemistry of Self-Assembled Monolayers of Octadecylphosphoric Acid on Tantalum Oxide Surfaces*. Langmuir, 2000. **16**(7): p. 3257-3271.
141. Pellerite, M.J., et al., *Effects of Fluorination on Self-Assembled Monolayer Formation From Alkanephosphonic Acids on Aluminum: Kinetics and Structure*. J. Phys. Chem. B, 2003. **107**(42): p. 11726 - 11736.
142. Schwartz, J., et al., *Cell Attachment and Spreading on Metal Implant Materials*. Mater. Sci. Eng., 2003. **23**(3): p. 395-400.
143. Guerrero, G., P.H. Mutin, and A. Vioux, *Anchoring of Phosphonate and Phosphinate Coupling Molecules on Titania Particles*. Chem. Mater. , 2001. **13**(11): p. 4367-4373.
144. Gouzman, I., et al., *Monolayer vs. Multilayer Self-Assembled Alkylphosphonate Films: X-Ray Photoelectron Spectroscopy Studies*. Surface Science, 2006. **600**: p. 773-781.
145. Fontes, G.N., et al., *Structural Investigations of Octadecyl Phosphonic Acid Multilayers*. Langmuir, 2003. **19**(8): p. 3345 -3349.
146. Hanson, E.L., et al., *Bonding, Self- Assembled, Compact Organophosphonate Monolayers to the Native Oxide Surface of Silicon*. J. Am. Chem. Soc, 2003. **125**(51): p. 16074-16080.
147. Nagayasu, T., et al., *Effects of Carboxyl Groups on the Adsorption Behaviour of Low-Molecular-Weight Substances on a Stainless Steel Surface*. Journal of Colloid and Interface Science, 2004. **279**: p. 296-306.
148. Stone, A.T., M.A. Knight, and B. Nowack, *Speciation and Chemical Reactions of Phosphonate Chelating Agents in Aqueous Media*. Chemicals in

- the environment: fate, impacts and remediation, ed. R.L. Lipnick, et al. 2001, Washington: American Chemical Society, ACS Symposium, Series No. 806.
149. Xyla, A.G., J. Mikroyannidis, and P.G. Koutsoukos, *The Inhibition of Calcium Carbonate Precipitation in Aqueous Media by Organophosphorous Compounds*. Journal Colloid Interface Science, 1992. **153**: p. 537-551.
 150. Jones, F., et al., *Investigation into the Effect of Phosphonate Inhibitors on Barium Sulfate Precipitation*. Journal of Crystal Growth, 2002. **237-239**: p. 424-429.
 151. Tantayakom, V., et al., *Scale Inhibition Study by Turbidity Measurement*. Journal of Colloid and Interface Science, 2005. **284**: p. 57- 65.
 152. Yuan, M., *Advances in Crystal Growth Inhibition Technologies*. Effect of Temperature on Barium Sulfate Scale Inhibition of Diethylene Triamine Penta (Methylene Phosphonic Acid). 2002, US: Springer.
 153. Couture, L., Annals of Physics, 1947. **2**(12): p. 5.
 154. Wojciechowski, K. and W. Kibalczyk, *Light Scattering Study of KH_2PO_4 and $BaSO_4$ Nucleation Process*. Journal of Crystal Growth, 1986. **76**: p. 379 - 382.
 155. Guo, Z., A.G. Jones, and N. Li, *Interpretation of the Ultrasonic Effect on Induction Time During $BaSO_4$ Homogeneous Nucleation by a Cluster Coagulation Model*. Journal of Colloid and Interface Science, 2006. **297**(1): p. 190 - 198.
 156. Putnis, A., *An Introduction to Mineral Science*. 1992, London: Cambridge University Press.
 157. Liang, N., *PhD Thesis*, in *Institute of Petroleum Engineering*2004, Heriot-Watt University.
 158. Lee, P.-L., H. Eugene, and Y. Shu-Cheng, *High-Pressure Raman and X-Ray Studies of Barite, $BaSO_4$* . High Pressure Research, 2003. **23**(4): p. 439 - 450.
 159. Hennessy, A.J.B., *PhD thesis*, 2001, Heriot-Watt University: Scotland.

160. Hennessy, A., et al., *New Pressure Flow Cell to Monitor BaSO₄ Precipitation Using Synchrotron in - Situ Angle-Dispersive X-Ray Diffraction*. Journal of Synchrotron Radiation, 2002. **9**(5): p. 323-324.
161. Kucher, M., T. Beierlein, and M. Kind, *In - Situ WAXS Synchrotron Radiation Study on Particle Formation of Precipitated Barium sulphate*. American Institute of Chemical Engineers, 2008. **54**(5): p. 1178 - 1188.
162. Jones, F., et al., *Understanding Barium Sulphate Precipitation onto Stainless Steel*. Applied surface science, 2008. **254**: p. 3459 - 3468.
163. Kautek, W., et al., *Multi-Method Analysis of the Metal-Electrolyte Interface: Scanning Force Microscopy (SFM), Quartz-Microbalance Measurements (QMB), Fourier-Transform Infrared Spectroscopy (FT-IR) and Grazing Incidence X-Ray Diffractometry (GIXD) at a Polycrystalline Copper Electrode*. Surface and Interface Analysis, 1997. **25**: p. 548.
164. Sathiyarayanan, S., M. Sahre, and W. Kautek, *In-Situ Grazing Incidence X-Ray Diffractometry Investigation of Phase Change Processes at the Silver/Aqueous-Halogenide Interface*. Electrochimica Acta, 1998. **43**(19-20): p. 2985-2989.
165. Sathiyarayanan, S., M. Sahre, and W. Kautek, *In-Situ Grazing Incidence X-Ray Diffractometry Observation of Pitting Corrosion of Copper in Chloride Solutions*. Corrosion Science, 1999. **41**(10): p. 1899-1909.
166. Martinod, A., et al., *Progressing the Understanding of Chemical Inhibition of Mineral Scale by Green Inhibitors*. Desalination, 2008. **220**(1-3): p. 345-352.
167. Benissa, T., M. Eleftheria, and N. Anne, *Barium Sulfate Formation in Bulk Phase and in a Modified Capillary Tube - Surface Kinetic Assessments*, 2011, FAST, HW University.
168. *Hack Company, Turbidity meter*. 2009 [cited 2014 08/04/2014]; Available from:
http://www.eoc.csiro.au/instrument/html/marine/marine_images/hack_diagram.gif.

169. He, S., J.E. Oddo, and M.B. Tomson, *The Nucleation Kinetics of Barium Sulphate in NaCl Solutions up to 6 m and 90 °C*. Journal of Colloid and Interface Science, 1995. **174**(2): p. 319 - 326.
170. <http://www.files.chem.vt.edu/chem-ed/echem/ise.html>.
171. Ferguson, R.J., *Computerized Ion Association Model Profiles Complete Range of Cooling System Parameters*, in *52nd Annual Meeting*, International Water Conference, PA, IWC-91- 47.: Pittsburgh.
172. Ryznar, J.W., *A new Index for Determining Amount of Calcium Carbonate Scale Formed by Water*. Journal of American Water Works Association, 1944. **36**.
173. Oddo, J.E. and M.B. Tomson, *Scale Control, Prediction and Treatment Or How Companies Evaluate A Scaling Problem and What They Do Wrong*, in *Corrosion/92, Paper No. 341992*, NACE International: Houston, TX.
174. OLI System, I., in *OLI Scalechem Software vs. 3.1.0.52002*.
175. <http://www.panalytical.com/Xray-diffractometers.htm>.
176. Kari, R., et al., *Predicting Carbonate Scale in Oil Producers from High Temperature Reservoirs*, 2005, Society of Petroleum Engineering, 87430
177. Fan, C., et al., *Barite Nucleation and Inhibition at 0 to 200 °C With and Without Thermodynamic Hydrate Inhibitors*, in *SPE Journal Paper - 1215592011*, Society of Petroleum Engineering: Aberdeen, UK.
178. Quddus, A. and I.M. Allam, *BaSO₄ Scale Deposition on Stainless Steel*. Desalination, 2000. **127**(3): p. 219 - 224.
179. Wang, J., J.S. Buckley, and J.L. Creek, *Asphaltene Deposition on Metallic Surfaces*. Journal of Dispersion Science and Technology, 2004. **25**(3): p. 287-298.
180. Lawal, K.A., V. Vesovic, and E.S. Boek, *Modeling Permeability Impairment in Porous Media due to Asphaltene Deposition under Dynamic Conditions*. Energy & Fuels, 2011. **25**: p. 5647-5659.

181. Seifried, C.M., et al., *Asphaltene Deposition in Capillary Flow*, 2001, Society of Petroleum Engineers, 166289.
182. Prieto, M., et al., *Nucleation, Growth, and Zoning Phenomena in Crystallizing (Ba,Sr)CO₃, Ba(SO₄,CrO₄), (Ba,Sr)SO₄, and (Cd,Ca)CO₃ Solid Solutions from Aqueous Solutions*. *Geochim. Cosmochim. Acta*, 1997. **61**((16): p. 3383-3397.
183. Leeden, M.C.v.d., D. Kashchiev, and G.M.v. Rosmalen, *Effect of Additives on Nucleation Rate, Crystal Growth Rate and Induction Time in Precipitation*. *Journal of Crystal Growth*, 1993. **130**(1–2): p. 221-232.